Dissertation

Characterizing Fuel Reactivity in Advanced Internal Combustion Engines

Submitted by

Marc E. Baumgardner

Department of Mechanical Engineering

In partial fulfillment of the requirements

For the Degree of Doctor of Philosophy

Colorado State University

Fort Collins, Colorado

Spring 2014

Doctoral Committee:

Advisor: Anthony J. Marchese

Ken Reardon
Daniel Olsen
Xinfeng Gao

Copyright by Marc Evan Baumgardner 2014

All Rights Reserved

Abstract

Characterizing Fuel Reactivity in Advanced Internal Combustion Engines

The urgent need to increase efficiency and reduce exhaust emissions from internal combustion engines has resulted in an increased interest in alternative combustion modes. Premixed or partially premixed compression ignition modes, such as homogeneous-charge compression ignition (HCCI), reactivity-controlled compression ignition (RCCI) and multi-zone stratified compression ignition (MSCI) have been a particular focus because of their potential to deliver enhanced fuel efficiency and meet exhaust emissions mandates without the addition of costly after-treatment technologies. For HCCI and other single fuel, partially premixed compression ignition schemes such as MSCI, many studies have shown that fuels with characteristics intermediate between gasoline and diesel fuel are necessary. Many researchers have shown, however, that existing industry metrics such as Octane Number and Cetane Number are insufficient to represent fuel ignition characteristics for advanced engine combustion modes. In light of the poor performance of traditional metrics, new methods have been proposed to try and better characterize, order, and rank fuels used in HCCI operation. However, studies have since shown that when a broad array of fuels are considered, these recent metrics fail to adequately define a characteristic HCCI fuel index.

Described in this work is an analysis of fuel reactivity in traditional and advanced internal combustion engines. Firstly, conventional engine regimes are broken down to their basic components, providing a framework for investigating the context of fuel reactivity. This analysis allows a novel equation to be formulated which links the historic metrics of Octane Number and Cetane Number. As part of this analysis a parameter, the knock length,

is developed which explains the underlying principles of the Research and Motor Octane Number scales and further shows why some fuels test differently in these two methods. The knock length is also used to investigate unusual behavior observed in Methane Number reference fuels data - behavior which traditional concepts such as ignition delay and flame speed are unable to explain on their own. Secondly, this work focuses on the application of fuels such as bio-derived alcohols (ethanol and butanol) and fatty acid methyl esters in traditional and advanced combustion applications. Reactivity differences between alcohol and petroleum fuels are described and explained. Lastly, a new metric, the HCCI Number, is developed which allows the prediction of combustion timing in HCCI engines, and is highly amenable toward the development of bench-top laboratory apparatuses to facilitate practical adoption by fuel manufactures. Data from 23 different fuel blends tested in Cooperative Fuel Research (CFR) engines, a Fuel Ignition Tester, and a HCCI engine provide the experimental support for the theory presented herein. Additionally, a new chemical-kinetic mechanism is developed and used to describe combustion of n-butanol/n-heptane fuel mixtures in both conventional and advanced combustion applications (HCCI). Computational modeling is also used to examine the experiments presented herein: single and multi-zone (CHEMKIN) as well as system-level (GT Power) and multi-dimensional (CONVERGE) modeling approaches are developed and discussed. For the HCCI experiments conducted herein, an engine test-bed that allows HCCI examination across a wide array of conditions was also designed and fabricated. In summary, it is hoped that with better understanding of how fuels react in current and future engines, researchers can achieve the control necessary to bring higher performance engines to market and help the world take one step closer to addressing some of the pressing environmental and humanitarian issues at hand.

Acknowledgements

My thanks go first of all to Prof. Marchese, who was the reason I came to Colorado State and without whose guidance I would not have come this far. Secondly, I thank the whole Marchese group for their incredible amount of help and advice along the way; Tim, Torben, and Jessica, Andrew & Andrew, Esteban, and Harrison, thank you! My committee, whose advice along the way helped me get to push beyond my abilities. Great thanks is also due to Aaron Gaylord, Michael Herder, Scott Salisbury, Ryan Farah, Ryan Peters, and Nathan Zeleski for their assistance in converting the John Deere 4024T engine to operate in HCCI mode, and David Llanos for his help in the FIT testing. Thanks also go to Kirk and Phil who have been a great help along the way in getting HCCI engine and RCM running; thanks guys! I would also like to thank the funding sources that made this work possible: the National Science Foundation (grant 0801707 an NSF IGERT Program in Multidisciplinary Approaches to Sustainable Bioenergy) and the Colorado Center for Biofuels and Biorefining (C2B2); Dr. Reardon and Barb, thank you so much for all you do for the IGERT students!

Lastly, my wife, Laura whose love and support made this all possible - thank you, this is for you.

Table of Contents

Abstract ii

Acknowledgements iv

List of Tables viii

List of Figures ix

Chapter 1. Introduction 1

1.1. Motivation 1

1.2. Advanced Combustion Engines 7

1.3. Rationale for Studying Fuel Reactivity 10

1.4. Reactivity in Traditional IC Engines 11

1.5. Reactivity in Advanced IC Engines 15

1.6. Organization of the Dissertation 27

Chapter 2. Experimental Methods 30

2.1. Liquid Fuels Examined 30

2.2. Fuel Ignition Tester 31

2.3. HCCI Engine 38

2.4. CFR Engine 49

2.5. Single and Multi-zone Chemical Kinetic Modeling of HCCI and FIT Experiments 51

Chapter 3. Traditional Metrics: Results and Discussion 56

3.1. Knock Length 56

3.2. Reference Fuels 60

3.3. Effect of Alcohols 64
3.4. Knock Length Approach to PRFs 69
3.5. Reference Methane Number Examination 73

Chapter 4. Future Metrics: Results and Discussion 78
4.1. FIT Experimental Results 78
4.2. HCCI Engine Experiments and Modeling 89
4.3. Impact of Low Temperature Heat Release on CA50 104
4.4. Relation Between fLTHR and CA50 106
4.5. Development of a Molar Octane Index 115
4.6. Development of the HCCI Number 122

Chapter 5. Other Modeling and Experimental Efforts 133
5.1. Control of Equivalence Ratio in the FIT 133
5.2. Heat Transfer Model Considerations in HCCI 139
5.3. GT Power HCCI Modeling 152
5.4. CONVERGE HCCI Modeling 159
5.5. CHEMKIN 1-D Flame Model 162

Chapter 6. Conclusions and Future Work 171
6.1. Future Work to be Considered 173

Bibliography 177

Appendix A. Synerject Fuel Injector 194

Appendix B. Single-Zone Ignition Delay Derivation 195

Appendix C. FIT Operating Conditions and Testing Procedure Summary 199

Appendix D. FIT Cleaning Procedure 202

Appendix E. CSU HCCI Engine Valve Profiles 211

List of Tables

1.1 ASTM Octane Testing Conditions 12

1.2 HCCI Index Coefficients from Shibata and Urushihara 23

2.1 Properties of Tested Fuels 31

2.2 Nominal Operating Parameters for the Waukesha FIT apparatus 32

2.3 Parameters for CSU HCCI Engine 39

2.4 Parameters for CSU CFR Engine 50

2.5 Chemical Kinetic Mechanisms for n-butanol/n-heptane considered herein. 55

3.1 CN-ON Equation Parameters for Tested Fuel Types 66

3.2 Reference Methane Number Data 74

4.1 Additional Fuels Tested in the FIT 87

4.2 Fuels Tested in HCCI Engine 90

4.3 Muli-Zone Model Parameters 96

4.4 HCCI Number Test Fuel Blends 129

5.1 Heat Transfer Coefficient Models 141

5.2 Default Heat Transfer Coefficient 146

5.3 Tuned Heat Transfer Coefficient 146

5.4 Location of Peak Heat Release Predicted by each Model 149

5.5 Evolved Wood-Gas Composition 166

E.1 CSU HCCI Engine Valve Profiles 211

List of Figures

1.1 Human Development Index versus Energy 2

1.2 World Oil Reserves 3

1.3 Life Cycle Emissions from Common Fuels 5

1.4 Emission Isopleths as a Function of Phi and T 9

1.5 IC Engine Regimes as a Function of Phi and T 9

1.6 Historical Data for CN versus ON 15

1.7 OI K values as a Function of T and P 19

1.8 RON and MON Referenced to an Ignition Delay versus Temperature 20

1.9 IQT Ignition Delay versus CA50 26

2.1 Schematic Diagram of Fuel Ignition Tester 33

2.2 Deviation Between FIT and IQT 34

2.3 HCCI-FIT Similarities 37

2.4 Schematic of HCCI Engine Layout 40

2.5 HCCI Intake Heater 41

2.6 HCCI Injector Cutaway 43

2.7 HCCI Intake 44

2.8 HCCI Fuel Controller 45

2.9 Picture of HCCI Piston 47

2.10 Cutaway View of the HCCI Piston 47

2.11 HCCI Piston Inserts 48

2.12 HCCI Piston Assembly Showing Install of the Inserts 48

2.13 CSU CFR Engine 50

3.1 Historical Data for CN versus ON 60

3.2 DCN versus RON for Reference Fuels 61

3.3 Example FIT Temperature and Pressure Trace 62

3.4 FIT %vPRF Results 63

3.5 FIT %vTRF Results 64

3.6 DCN versus ON for Alcohol Fuels 65

3.7 Butanol Isomers with Bond Strengths 67

3.8 Abstraction Rates for H from Fuels Considered 69

3.9 Laminar Knock Lengths for PRFs and n-Butanol Fuels. 70

3.10 Turbulent Knock Lengths for PRFs and n-Butanol Fuels. 71

3.11 Octane Requirement 73

3.12 Ignition Delay versus Temperature for Reference MN 76

3.13 Laminar Flame Speed for Reference MN 76

3.14 Laminar Knock Length for Reference MN 77

3.15 Square Root of Ignition Delay versus Methane Number 77

4.1 nBuOH FIT Results (vol) 80

4.2 nBuOH FIT Results (mol) 81

4.3 Example FIT Trace 82

4.4 Viscosity Effect on FIT-ϕ 83

4.5 FIT PRF Results 84
4.6 FIT nBuOH Results 85
4.7 Additional FIT Results:MD and Diesel Blends (vol) 88
4.8 Additional FIT Results:MD and Diesel Blends (mol) 89
4.9 HCCI Example 90
4.10 HCCI nBuOH40: Single Zone 93
4.11 HCCI PRF40: Single Zone 94
4.12 Illustrations of CHEMKIN Zone (Example) 96
4.13 HCCI Motored Pressure Trace 98
4.14 CHEMKIN Five-Zone Setup 100
4.15 CHEMKIN Five-Zone: n-Heptane 101
4.16 CHEMKIN Five-Zone: PRF40 101
4.17 CHEMKIN Five-Zone: PRF50 102
4.18 CHEMKIN Five-Zone: nBuOH40 102
4.19 CHEMKIN Five-Zone: nBuOH50 103
4.20 CHEMKIN Five-Zone: nBuOH60 103
4.21 CA50 versus fLTHR 106
4.22 Effects of LTHR on Ignition Delay for nBuOH60 108
4.23 HCCI-FIT Model 1 113
4.24 HCCI-FIT Model 2 113
4.25 HCCI-FIT Model 3 114

4.26 HCCI-FIT Simple Model 114

4.27 Norm-CA50 versus fLTHR 116

4.28 Norm-CA50 versus mRON 117

4.29 Original Kalghatgi OI Study 119

4.30 OI Data from Liu et al. 2009 119

4.31 CSU-HCCI versus RON and MON Tests 120

4.32 Volume Octane Index 121

4.33 Molar Octane Index 121

4.34 FIT Simple Model for FIT-DHN 125

4.35 The Colorado State University RCM 127

4.36 HCCI Number Example 130

4.37 RCM DHN Example 131

4.38 HCCI Number Computational Example 132

5.1 FIT Injector Unit 134

5.2 FIT: ϕ versus Viscosity 135

5.3 FIT: ϕ versus Density 135

5.4 FIT Injection Delay Knob 137

5.5 FIT Injection Delay Effect on ϕ 138

5.6 HCCI Example used in Heat Transfer Modeling 145

5.7 CHEMKIN Modeled Heat Transfer Coefficients 147

5.8 Pressure Traces with Heat Transfer 148

5.9 Zoomed-in Pressure Traces with Heat Transfer 149

5.10 Accumulated Net Heat Release 151

5.11 LTHR for Heat Transfer Simulations 152

5.12 GT-Power Block Diagram 154

5.13 GT-Power Simulations: Pressure 155

5.14 GT-Power Simulations: Low Temperature Heat Release 156

5.15 GT-Power Simulations: Speed Sweep 157

5.16 Temperature Dependence of Sensitive Fuels 158

5.17 Solidworks 3-D Model of the CSU HCCI Engine 161

5.18 3-D Cylinder Model in CONVERGE 162

5.19 Simplified 1-D Model of a Wood Flame 165

5.20 Temperature Profile in Simulated Chimney Stoves 168

5.21 Combustion Efficiency versus ϕ for the Stove Model 169

5.22 CO Formation for a Range of Equivalence Ratios and Temperatures 170

B.1 Modeled Ignition Delay for Ethanol 196

B.2 Modeled Arrhenius Plot for Ethanol and n-Butanol 196

C.1 Julabo Cooling System for FIT 199

C.2 Process Air for FIT 200

C.3 Combustion Air for FIT 200

C.4 Start Screen for FIT Program 201

CHAPTER 1

Introduction

1.1. Motivation

We as members of the human race have a staggering obstacle before us. Our increasing thirst for energy, the depletion of fossil fuel resources, and climate change from anthropogenic greenhouse gas emissions combine to create the first civilization-scale challenge we have ever faced[1, 2].

Addressing the first point, Figure 1.1 shows the Human Development Index (HDI) plotted against the annual per capita energy use. The HDI is a measure of the quality of one's life that takes into account prosperity, education, and life span/health[3]. What Figure 1.1 tells us is that humans need about 3000 kWhrs per year to live what is considered a high quality life. Many countries, including the U.S. and most of Europe (i.e. the developed world) are well past the inflection point in the curve and face diminishing returns on increased access to energy. Additionally, most of the world's population is well below the inflection point. For a moment though, let's focus on China. China's average HDI is nearing 0.8 HDI, but note that the top 500 million people in China are essentially at the same level as the U.S., while the bottom 800 million people are near 0.5 HDI. James Conca, former Director of the New Mexico State University Carslbad Environmental Monitoring and Research Center and co-author of "The GeoPolitics of Energy", argues that the stark contrast within China is due to recent meteoric rise of a middle class[3]. Conca further argues that most of China's current policies are geared toward raising the remaining 800 million above 0.8 HDI[3]. This need for energy in China as well as countries like Brazil and India means that the global need for energy is only going to increase dramatically in the next several decades.

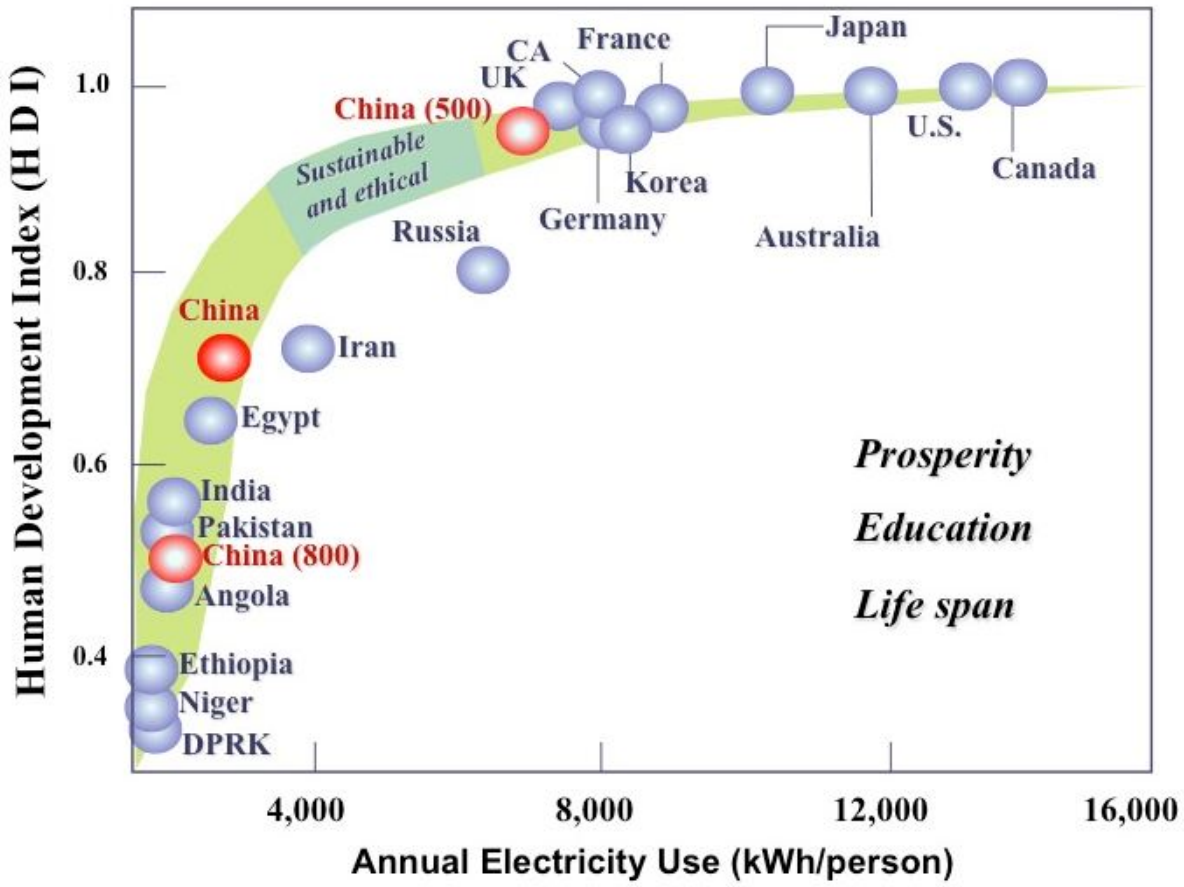


FIGURE 1.1. HDI vs. per capita annual electricity use for representative countries throughout the world. This figure is from[3], but is based on a DOE report from 2000[4]

To respond to the increased need for energy, the most immediate resource - and the one that we have infrastructure to currently support - is increased fossil fuel production. A recent study examined the existing reserves of fossil fuels and presented them in contrast to two main factors: (a) the cost of getting those resources, and (b) the total greenhouse gas (GHG) contribution of acquiring and consuming those resources - Figure 1.2. What can be seen in Figure 1.2 is that in comparison to the amount of fuel humanity has used thus far, there are potentially orders of magnitude more fuel within the earth waiting to be extracted. The potential economic, environmental, and humanitarian impact of rapidly releasing emissions

from these fossil fuel reserves into the atmosphere could be catastrophic without a unified technological approach to reducing emissions and increasing overall efficiency.

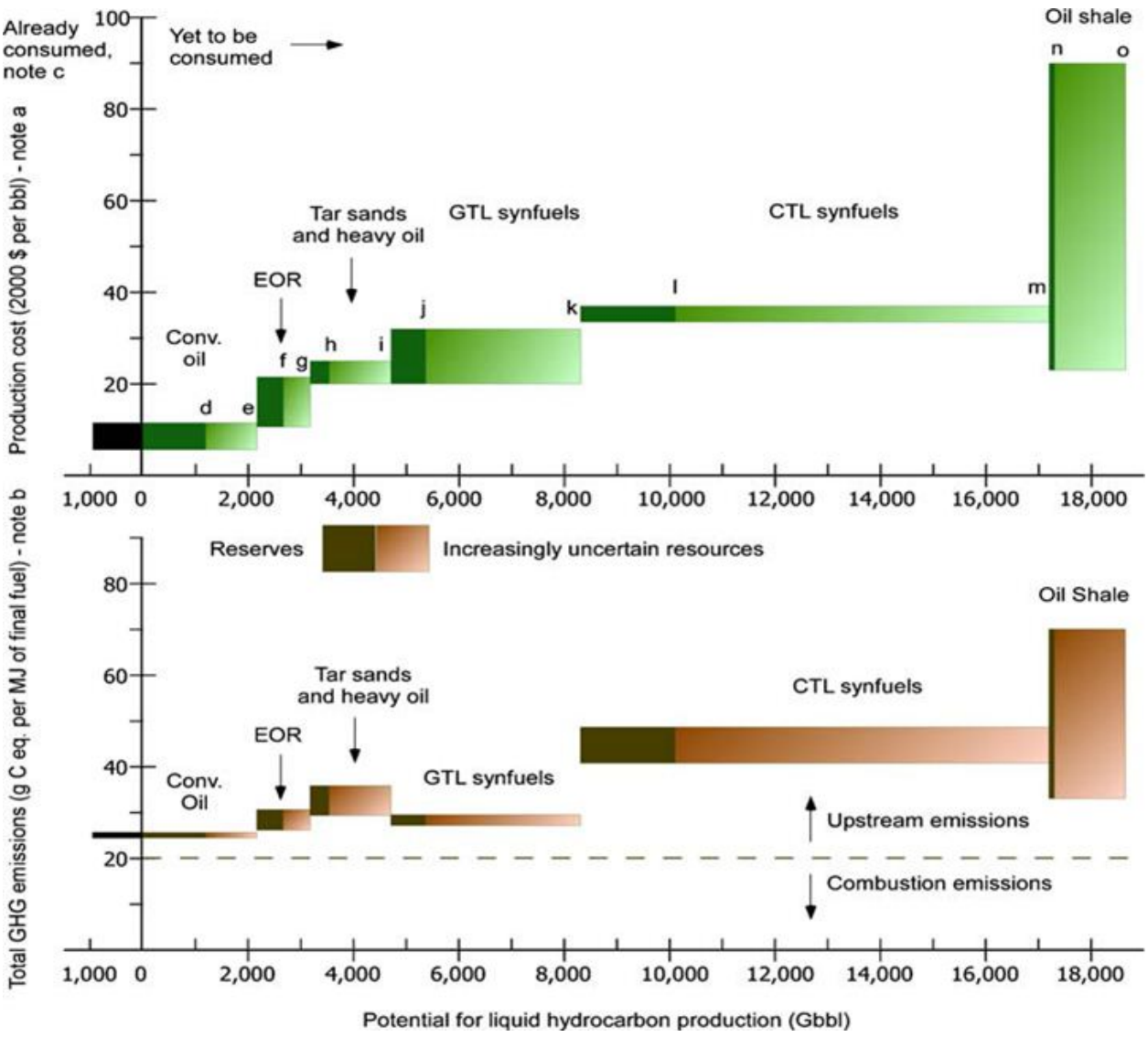


FIGURE 1.2. Consumed and potential oil reserves on Earth - used with permission from[5]

While there is no single technological solution for these omnipresent global challenges, a highly effective means of immediately addressing these concerns is to increase the thermodynamic efficiency of energy conversion devices that consume fossil fuels. Because of its

widespread use as a energy source, the internal combustion engine will continue to be a principal source of greenhouse gas emissions and the principal consumer of liquid fossil fuels.

As detailed in the 2007 IPCC report on climate change[6] the global transportation sector accounts for 13.1% of the total anthropogenic contribution to greenhouse gasses (GHG). In the United States, the EPA estimates that 27% of the over 6800 Tg of CO_2 Eq emitted in 2010 were from the transportation sector[7], and 62% of these emissions were from (LDV) light duty vehicles (i.e. passenger cars and light duty trucks, SUVs, and minivans). Furthermore, a recent report by National Energy and Technology Laboratory shows, overwhelmingly, that the majority of emissions comes from the end-use combustion of conventional transportation fuels (Figure 1.3). In fact, end-use combustion of fuels contributes more than four times the GHG emissions than raw material acquisition, transportation, and production combined! Therefore, increasing the efficiency of internal combustion engines, presents an immediate and major opportunity for greenhouse gas reduction and extension of fossil fuel reserves.

Many of the advanced internal combustion engine concepts under consideration, such as homogeneous charge compression ignition (HCCI)[10], reactivity controlled compression ignition (RCCI)[11], multi-zone stratified compression ignition (MSCI)[12] and other similar strategies, rely on a premixed or partially premixed autoignition event, which is typically governed by low temperature chemical kinetics. Many researchers have shown that combustion strategies such as HCCI or MSCI are more amenable to moderately reactive fuels (i.e. low to moderate Octane Number)[10, 12–14]. However, research has also shown that existing autoignition metrics such as Octane Number (ON), which is a measure of the tendency of a fuel to exhibit knock in a spark ignited engine, are not directly applicable toward characterizing autoignition under homogeneous premixed or partially premixed conditions.

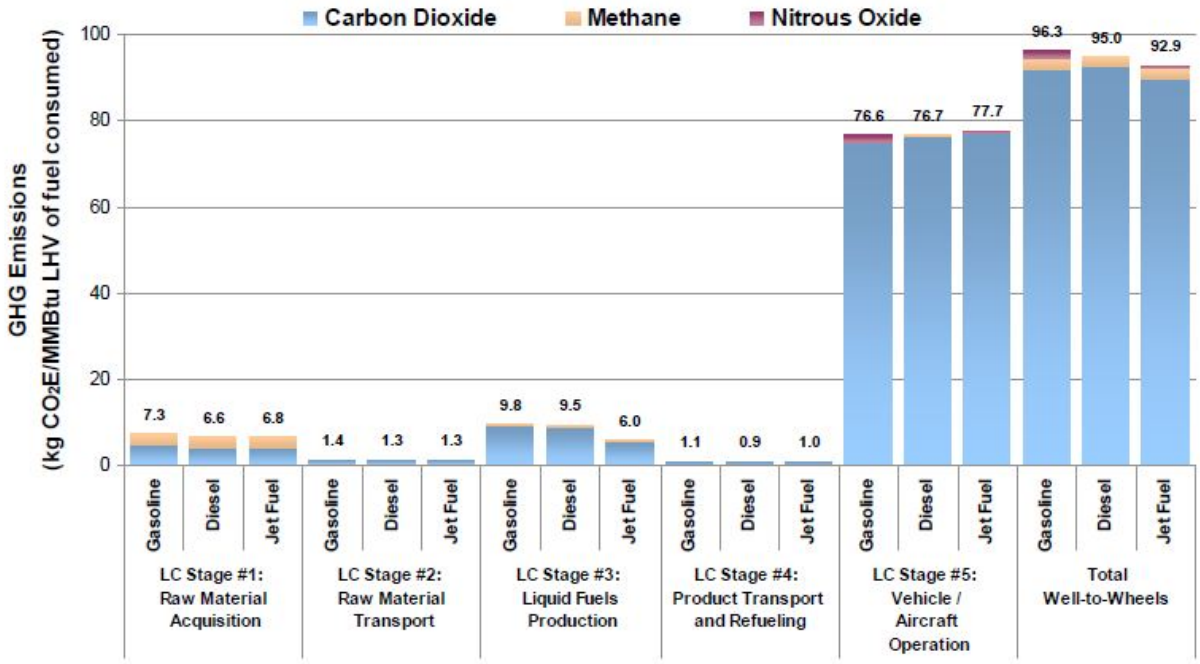


FIGURE 1.3. Life cycle emissions from conventional transportation fuels. Figure from[8], used under U.S. Government guidelines[9]

.

Therefore, described in this work is an analysis of fuel reactivity in traditional and advanced internal combustion engines. Firstly, conventional engine regimes are broken down to their basic components, providing a framework for investigating the context of fuel reactivity. This analysis allows a novel equation to be formulated which links the historic metrics of Octane Number (ON) and Cetane Number (CN). As part of this analysis a parameter, the knock length, is developed which explains the underlying principles of the Research and Motor Octane Number (RON and MON) scales and further shows why some fuels test differently in these two methods. The knock length is also used to investigate unusual behavior observed in Methane Number reference fuels data - behavior which traditional concepts such as ignition delay and flame speed are unable to explain on their own. Secondly, this work focuses on the application of fuels such as bio-derived alcohols (ethanol and butanol) and fatty acid methyl esters in traditional and advanced combustion applications. Reactivity

differences between alcohol and petroleum fuels are described and explained. Lastly, a new metric, the HCCI Number, is developed which allows the prediction of combustion timing in HCCI engines, and is highly amenable toward the development of bench-top laboratory apparatuses to facilitate practical adoption by fuel manufactures. Data from 23 different fuel blends tested in Cooperative Fuel Research (CFR) engines, a Fuel Ignition Tester, and a HCCI engine provide the experimental support for the theory presented herein. Additionally, a novel chemical-kinetic mechanism is developed and used to describe combustion of n-butanol/n-heptane fuel mixtures in both conventional and advanced combustion applications (HCCI). Computational modeling is also used to examine the experiments presented herein: single and multi-zone (CHEMKIN) as well as system-level (GT Power) and multi-dimensional (CONVERGE) modeling approaches are developed and discussed. For the HCCI experiments conducted herein, an engine test-bed that allows HCCI examination across a wide array of conditions was also designed and fabricated.

Major outcomes of this work can be summarized as follows:

(1) A novel way of characterizing fuel reactivity in SI engines called the knock length (b_k),

(2) Development of the fundamental relationship that connects the ON scale to the CN scale,

(3) A new chemical kinetic mechanism for n-heptane/n-butanol fuels,

(4) Design and fabrication of HCCI engine test bed,

(5) A novel way of using a Fuel Ignition Tester (FIT) to determine fuel performance in a HCCI engine,

(6) A more robust way of characterizing fuel reactivity in HCCI engines called the HCCI Number,

(7) Two possible test protocols to determine Derived HCCI Numbers (DHN).

1.2. Advanced Combustion Engines

Spark Ignition (SI) engines, despite having increasingly lower emissions due to the advancements of 3-way catalysts (i.e. catalytic converters) and homogeneous fuel/air combustion mixtures, are hindered by the narrow range of air/fuel ratios required for 3-way catalyst operation and low compression ratios limited by knocking combustion. The ultimate efficiency of an SI engine is thus restricted by this operationally low compression ratio range and to a lesser degree, pumping losses resulting from a throttled intake. Alternatively, direct injection compression ignition engines (DICI, i.e. diesel engines) operate at higher compression ratios with lower pumping losses due to fuel injection near top dead center (TDC) and no intake throttling, which results in higher efficiencies. However, the shortened fuel/air mixing time experienced in DICI engines causes a more heterogeneous fuel/air combustion mixture in the pre-mixed combustion phase, which can result in high concentrations of particulate matter (PM). High NOx emissions are also a result of high temperature zones due to gradients in equivalence ratio throughout the cylinder during the non-premixed diffusion flame burn-phase. As a result, despite being the most efficient internal combustion engine, DICI engines have historically been the heaviest polluters of NOx and PM, both of which are highly problematic in terms of atmospheric pollution and associated public health issues.

As mentioned above, the motivation to increase efficiency and reduce exhaust emissions from internal combustion engines has resulted in an increased interest in alternative combustion modes (HCCI, RCCI, MSCI, etc.). These high efficiency, clean combustion engines

are of particular focus because of their potential to deliver enhanced fuel efficiency and meet exhaust emissions mandates without the addition of costly after-treatment technologies[15]. These advanced combustion strategies thus seek to combine the advantages of SI and DICI engines while avoiding their disadvantages. The relative operational range of advanced combustion modes that have been proposed in recent years are shown in Figure 1.4 and 1.5. In Figure 1.5, the rich/lean limits refer to turbulent flame propagation limits for SI operation and that EGR reduces the the peak combustion temperatures. The middle Fuel/O_2 arrows refer to the area where combustion is controlled by large-scale mixing of fuel and oxidizer.

Despite the promise of these relatively new combustion modes, most have only been successfully observed in steady state, lab-scale demonstrations with traditional liquid fuels (gasoline, diesel or primary reference fuels). Those that have been developed beyond the lab scale (such as GM's HCCI development) still suffer from restricted range and require advanced control strategies to allow switching between advanced (HCCI) and traditional (e.g. SI) operation[16]. However, due to the many advantages of HCCI and other advanced combustion strategies the U.S. government and many other institutions have considered these research areas of paramount importance in achieving future emission standards and goals[17].

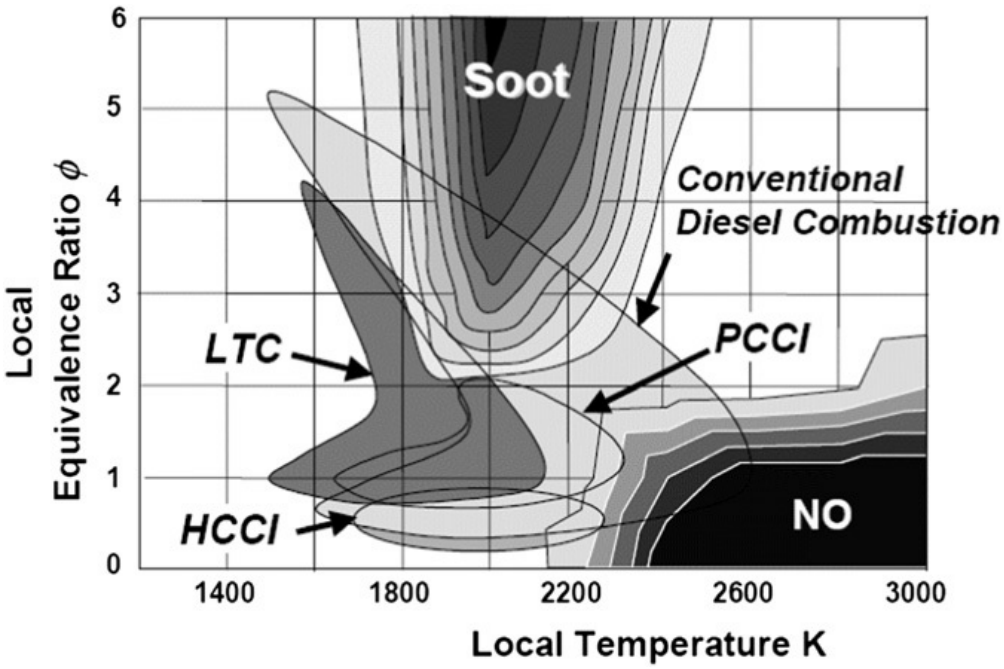


FIGURE 1.4. Emission isopleths of various combustion modes relative to phi and temperature operational ranges. Figure used with permission[18].

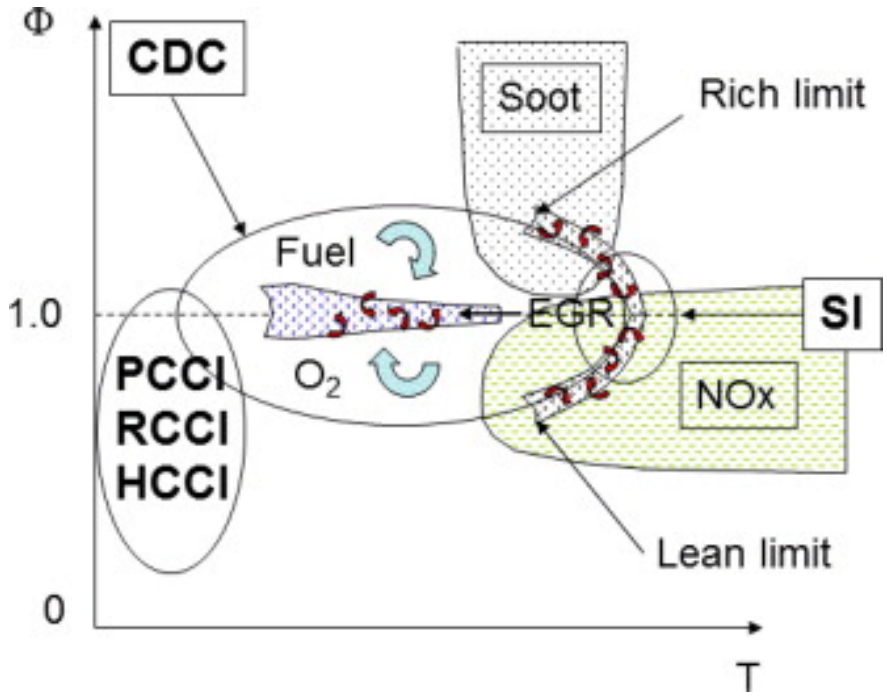


FIGURE 1.5. Individual emission isopleths of various combustion modes relative to phi and peak combustion temperature operational ranges Note that CDC refers to conventional diesel combustion. Figure used with permission[19]

1.3. Rationale for Studying Fuel Reactivity

The transportation sector has long relied upon fuel property targets in both the formulation of fuels and the design of the engines in which those fuels are used. The first modern test method was a single cylinder test engine developed in 1928 and was "a means of measuring and defining gasoline combustion characteristics"[20]. For the past 80 years, the transportation sector has been dependent on the Octane Number (ON) and the Cetane Number (CN) metrics. These scales essentially describe a fuel's particular propensity (or lack thereof) to ignite under a given set of standard conditions. These metrics provide fuel producers with the proper targets to meet industry needs for characterizing fuel performance in SI and DICI engines.

Recently, increasing levels of alternative fuels such as alcohols (ethanol, n-butanol, etc.) in liquid-SI, methyl esters in DICI, and hydrogen and carbon monoxide in gas-SI are being incorporated into fuel supplies and the ON, CN and MN metrics have become less suitable to fundamentally define the reactivity of these alternative fuels. Furthermore, as modern engines evolve away from traditional SI and DICI combustion modes to advanced combustion modes (low temperature combustion, partially premixed compression ignition, etc.) new reactivity metrics are needed that are not constrained by conditions present in existing metrics. Finally, the advent of Derived Cetane Number (DCN) instruments, which are bench top apparatuses that can readily measure ignition delay and DCN with low fuel requirements, presents an opportunity to use such instruments to qualitatively and quantitatively evaluate reactivity in SI, DICI, and advanced combustion modes. Although, quantitative assessments would require that accurate correlations can be made between DCN and the other metrics such as ON.

1.4. Reactivity in Traditional IC Engines

Essential to fuel reactivity is the idea of a kinetically-controlled induction period or ignition delay. The CN metric was developed to characterize the ignition delay of fuels under DICI conditions and uses heptamethlynonane and n-cetane (hexadecane)[21] as the reference fuels. Alternatively, in a SI engine the combustion event is triggered by electrical spark and the resulting flame propagation rate competes with the ignition delay. In SI engines, fuel is traditionally pre-mixed with the intake air and so is exposed to the oxidizer for a longer period of time thus requiring an induction period long enough to prevent uncontrollable autoignition, referred to as engine knock. The ON metric was developed as a means of characterizing the ability of a fuel to resist knock wherein n-heptane serves as the more reactive fuel and i-octane the less reactive[22]. A fuel blend with ON of 60 should have the same knock characteristics as a blend of 60%v i-octane/40%v n-heptane. The MN scale measures the reactivity of gaseous fuel blends such as in natural gas engines[23] and the method is directly analogous to the ON scale. Methane serves as the less reactive fuel while hydrogen the more reactive and MN blends are based on linear-by-molar blending scale. A fuel with MN of 80, ideally, has the same knock characteristics as a blend of 80%m methane/20%m hydrogen.

Douaud and Eyzat[24] (and later Heywood[25]) describe knock as being the result of the pre/unintended ignition of in-cylinder end-gas (gas furthest from the spark) due primarily to a rise in local temperature and pressure caused by an advancing flame front initiated by the spark. Therefore, knock is not solely a function of a fuel/air mixture's kinetically-controlled induction period, but rather is also dependent on the velocity of the turbulent flame front. The turbulent flame speed also impacts the rate at which energy is released and therefore the

combustion duration. Moreover, the turbulent flame speed combined with the fuel heating value will determine the pressure rise above the motored pressure and therefore the end-gas temperature and pressure. Accordingly, from a phenomenological standpoint, it may not be straightforward to compare SI engine knock directly to the auto-ignition that would occur in an HCCI-like engine. Indeed, many studies have shown (including those conducted in our laboratory) that fuels with the same Octane Number do not exhibit the same autoignition characteristics in HCCI mode. Based on the underlying physics, this result should come as no surprise. The limitations of existing methods are further confounded by the fact that both the RON (Research Octane Number) and MON (Motor Octane Number) ASTM tests are performed at conditions that are of limited relevance to loaded conditions for modern transportation engines (see Table 1.1). For example, the tested engine speeds in the RON and MON tests are 600 and 900 RPM, respectively. These engine speeds are drastically lower than the typical operational range in modern engines. This presents an issue since the engine speed is directly related the amount of time available for chemical reactions to occur. Additionally, increases in RPM (typically associated with increasing load) will often incite other changes such as increased in-cylinder temperature and pressure which can impact the observed relative reactivities between fuels.

TABLE 1.1. ASTM Octane Testing Conditions

test	intake T [$^{\circ}C$]	engine speed (RPM)
RON[22]	52	600
MON[26]	149	900

In his recent book, Kalghatgi explains that when RON test was first invented the test was found to not accurately capture the representative in-cylinder conditions at the time[27]. Specifically, the compressed temperature was too low compared to that found in engines at

the time. In response, the MON test was created, which due to the higher intake temperature, had a higher temperature at TDC (i.e. the top dead center position of the piston during its stroke). Engine technology eventually progressed toward lower in-cylinder temperatures and the RON test became more applicable. Now, however, engine technology is at a point where due to direct injection strategies and higher intake boost pressures engines are going 'beyond' the RON test to even lower temperatures for a given pressure. More regarding the differences between RON and MON and the resulting impact on present and future fuels will be explored further in later sections (namely Sections 1.5.2, 3.4, and 4.5).

Anderson et al.[28] showed that recalculating Octane Number on a molar basis (instead of a volumetric basis) did give better agreement between measured and predicted octane values when alcohols were used. Other petroleum reference fuel blends such as Toluene Reference Fuels have also showed promise categorizing petroleum fuels in HCCI operation[29, 30]. However, Karwat et al. found that oxygenated fuels such as butanol may have fundamentally different reaction routes when mixed with other hydrocarbons and so traditional chemical mechanisms and means of comparison such as knock might not be suitable[31].

1.4.1. Cetane versus Octane Number measurements. One way to approach the obfuscated effect of chemical induction time on knock is to examine fuels in the context of their Cetane Number or alternatively their DCN[21, 32], both of which are inherently representative of a chemical induction time, though it is also important to note fuel physical properties such as vaporization rate will also affect a fuel's DCN and CN. Current ASTM standards (D6890 and D7170) calculate DCN as being inversely proportional to a measured ignition delay, i.e. chemical induction time, and also incorporate the aforementioned vaporization/mixing time. Therefore, if a fundamental relationship between CN and ON were

developed, it might be possible to characterize reactivity of fuels in the context of DICI, SI, and advanced combustion modes such as HCCI based on the ignition delay period.

Relationships between CN and ON have been observed empirically since the 1960's[33]. One 1974 report examined "low" octane fuels for use in military diesel engines[33] and found that the relationship between CN and ON is approximately inversely proportional. This data and recent studies covering a wide range of fuels are presented in Figure 1.6. All five studies included in the figure (156 extremely different, but still traditional hydrocarbon-based fuel blends) show the same approximately inverse trend of ON vs. CN. The gray curve in Figure 1.6 is a regression of all the data shown and is represented by Eq. 1 ($R^2 = 0.94$).

$$CN = \text{-}0.0024 \cdot (ON)^2 - 0.1971 \cdot (ON) + 54.325 \tag{1}$$

All data in Figure 1.6 are RON values except the Stone data[34], which are Motor Octane Numbers (MON). The Stone data is included here to show the inherent variability of the traditional RON and MON tests (viewed in the context of associated CN values). If the Stone data is removed from Figure 1.6, then Eq. 1 changes only slightly (Eq. 2: $R^2 = 0.93$).

$$CN = \text{-}0.0024 \cdot (ON)^2 - 0.1903 \cdot (ON) + 54.182 \tag{2}$$

Within the five studies represented in Figure 1.6 there are two distinct data sets. The first was gathered prior to the year 2000 and the second gathered after 2000. Studies prior to 2000 used a Cooperative Fuels Research (CFR) engine to measure CN, while the 2002 and later works used bench-top, constant-volume combustion devices that actually measure DCN. These constant volume combustion devices are explained more in the next section.

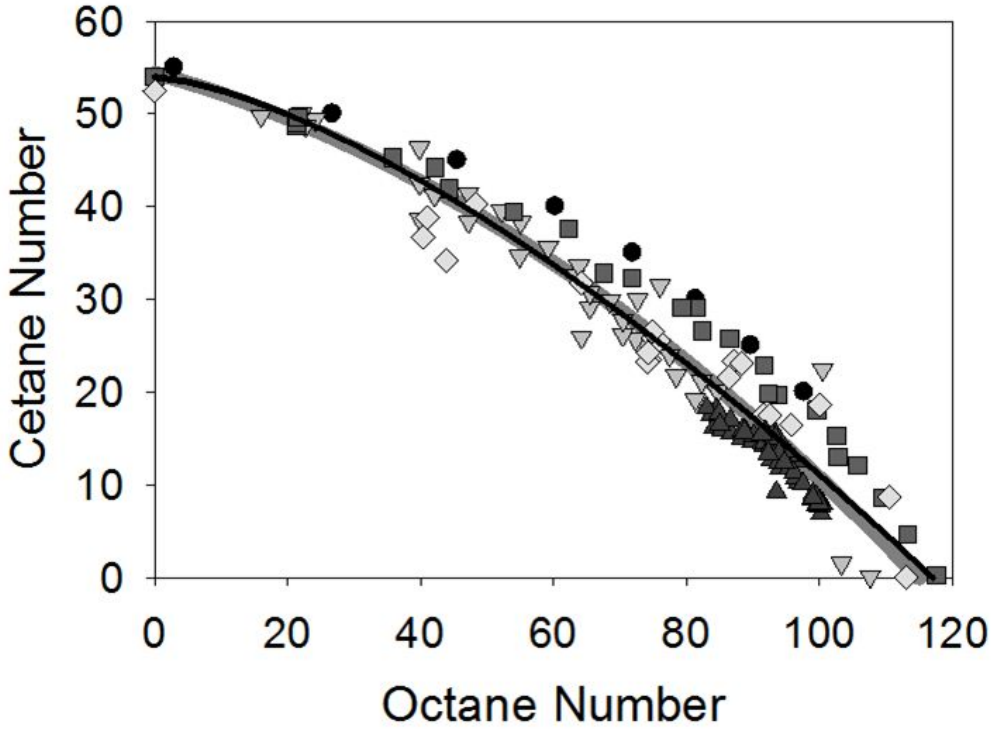


FIGURE 1.6. Cetane Number vs. Octane number data shown for five studies (156 fuels). Diamonds are a mix of surrogate gasoline fuels[35], squares a mix of gasoline and diesel fuels[36], circles an empirical correlation based on mixes of PRF, cetane reference fuels, Fischer-Tropsch naphtha, and gasoline-diesel blends[37], downward triangles a mix of "fuels distilled (not cracked) from crude oil"[34], and upward triangles are commercial gasoline blends ("leaded and unleaded")[33]. The thick gray line is a best-fit polynomial (Eq. 1) and the thin black line represents the best-fit of Eq. 13

1.5. Reactivity in Advanced IC Engines

The nature of HCCI and other advanced combustion engines demand accurate knowledge (i.e. the exact crank angle) of when a given fuel will ignite in order to maximize control, power, and efficiency and gain the most out of the technology. The fact that existing characterization methods/metrics fail to yield this knowledge is one of the motivating forces behind the present work. The next few sections will describe some of the most current methods of

defining reactivity in HCCI engines. Each method has its intrinsic advantages and disadvantages and the present work seeks to build upon these existing metrics and create a link between them and the current metrics of ON and CN.

1.5.1. EPAIT. One of the first major steps to identifying a common scale with which to examine potential HCCI fuels was that of Ryan et al.[37] at the Southwest Research Institute. This work, given the acronym EPAIT for Elevated Pressure Auto-Ignition Temperature, was based on data from an Ignition Quality Tester (IQT). The IQT is a constant volume combustion device and is similar to the Waukesha Fuel Ignition Tester (FIT) used in the research presented herein and has its own ASTM standard for calculating Cetane Numbers[21]. The IQT directly injects fuel into a horizontal, constant volume vessel that is initially at 21.37 $\pm$ 0.07 bar and within a temperature range of 788 to 848 K[38]; the corresponding ignition delay is then measured via an in-vessel pressure transducer. For each DCN test, the IQT performs a sequence of 32 such tests, all done at an approximate equivalence ratio of 0.7[21] and reports the average value as the ignition delay of the fuel. When the average ignition delay is between 3.3 and 6.4 ms the test is considered 'valid' and the average value is then used to calculate a DCN for that fuel via Eq. 3

$$DCN = 4.460 + \frac{186.6}{ID} \tag{3}$$

When the 32-test average ignition delay is greater than 6.4 ms, the DCN equation becomes highly non-linear (Eq. 4)[39].

$$DCN = 83.99 \cdot (ID - 1.512)^{(-0.658)} + 3.547 \tag{4}$$

In the EPAIT test method, several fuels of interest are chosen and run through a range of initial temperatures to obtain an ignition time vs. temperature data set. Next, an ignition delay time common to all fuels is chosen; the fuels are then "ranked" by their corresponding ignition temperatures at said common ignition delay period. Ryan et al. showed a 'fair' correlation between the ignition temperature for a given ignition delay period with the Start of Reaction (SOR) in an HCCI engine. Here SOR is analogous to (but not the same as) the crank angle of 50% heat release (CA50). The major limitation of this method is that it will only work when a narrow range of fuels is considered wherein all fuels can be forced to have the same ignition delay in an IQT (or presumably an FIT). This limitation has been pointed out by others[35] and judging from the results of this work would be difficult (or possibly even grossly inadequate) to implement for a wide range of fuels.

1.5.2. Octane Index. The Octane Index (OI) was developed by Kalghatgi in 2003[40] and borrowed heavily from his previous work studying knock in SI engines[41, 42]. The OI is a measure of a fuel's propensity for knock and is based on the Sensitivity (S) of the fuel defined as in Eq. 5.

$$S = RON - MON \tag{5}$$

where the S arises loosely from the chemical properties of a given fuel and is based on the differences between the RON and MON tests, which further relates to the temperature and pressure history of each test. Moreover, S is considered to be a measure of the "octane depreciation" that occurs as the engine test speed is increased[43]. In short, the antiknock properties of gasoline-type fuels (i.e. "real fuels" with aromatics, and alkenes, as well as alkanes) tend to diminish (relatively) as engine RPM increases. Note that the PRF fuels,

on which the RON and MON scales are based, have zero sensitivity (by definition). In theory, how a fuel behaves in the RON and MON scales should give some indication of the "alkane-likeness" of its combustion. Additionally, since the RON test has a lower in-cylinder temperature for a given cylinder pressure (due to the lower intake temperature and speed of the RON test vs. the MON) some degree of delineation should be obtained by comparing these two measures. However, both the RON and MON tests are done below 1000 RPM, a speed well below typical modern engine operation under load and the scales are inherently limited by being bracketed/based on two alkanes (i.e. i-octane and n-heptane). Kalghatgi tried to correct for the variability in engine operating conditions by introducing an empirical parameter, K, which is specific to temperature and pressure of the end-gas for a given operating condition. The OI, then, is fully defined in Eq. 6:

$$OI = (1 - K) \cdot RON + KS$$

or

$$OI = RON - KS \tag{6}$$

The specificity of K somewhat limits the applicability of this index with respect to real fuels across a wide array of engines, but Per Risberg (who worked with Kalghatgi developing the Octane Index) showed that K could be expressed as a function of the in-cylinder temperature at a pressure of 15 bar and that expressing K in such a way proved to be valid over a variety of engines and test conditions[44]. Experimental data for determining K values can be found in Figure 1.7.

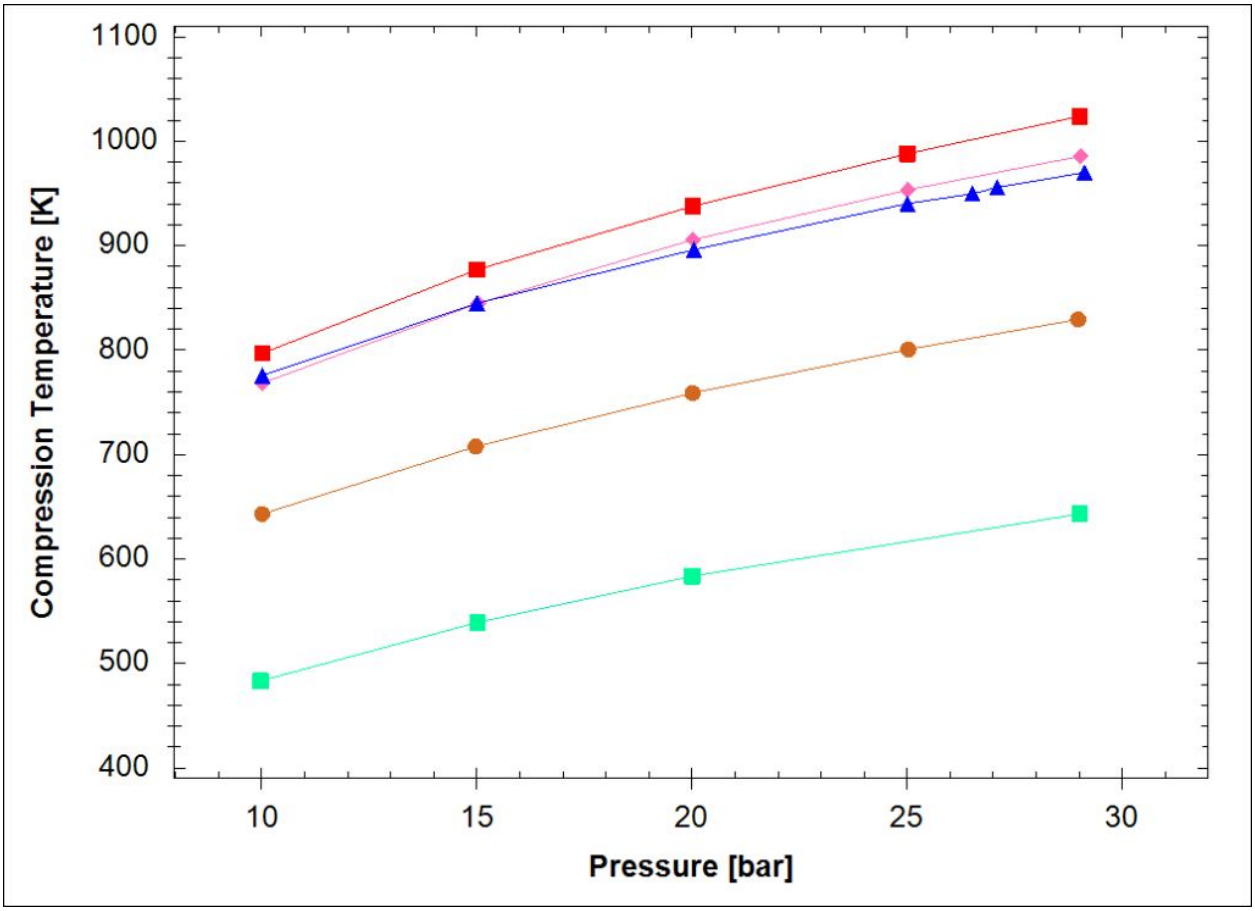


FIGURE 1.7. K values for different temperature vs. pressure curves; from[44]. Red squares are HCCI engine data where K = +2.2, pink diamonds the MON test (K = 0), blue triangles an HCCI engine test where K = +1.1, brown circles the RON test (K = 0), and green squares an HCCI test where K = -1.6

Building on these ideas, Figure 1.7 can alternatively be expressed in terms of the ignition delays of the RON and MON reference fuels. Figure 1.8 shows the RON and MON test temperatures at 15 bar (from Figure 1.7) overlaid on the reference fuels i-octane and n-heptane. Additionally shown is n-butanol which is considered a highly sensitive fuel, where S = 20. From Figure 1.8 it is clear that i-octane and n-heptane exhibit ignition behavior that is very different from n-butanol, which for the present can be considered a model "sensitive" fuel. The increasing/decreasing/increasing again behavior seen in the n-heptane and i-octane fuels is called a negative temperature coefficient (NTC) region and is common for alkane fuels.

The reasons for the exhibition of NTC behavior essentially result from the transition of one primary ignition pathway to another and are explained thoroughly elsewhere[45]. What is important to note in Figure 1.8 is that the ignition delay between the RON and MON tests remains in the same order of magnitude, whereas the ignition delay of n-butanol increases by a factor of 10 from the MON the RON tests. Therefore when Kalghatgi created the concept of fuel Sensitivity, what he was really describing is the magnitude of change in the ignition delay as a function of in-cylinder temperature. So, as future engines move to lower and lower relative in-cylinder temperature the fuel requirements will need to shift away from traditional alkane fuels and perhaps towards more sensitive fuels such as aromatics or alcohols, both of which are highly sensitive.

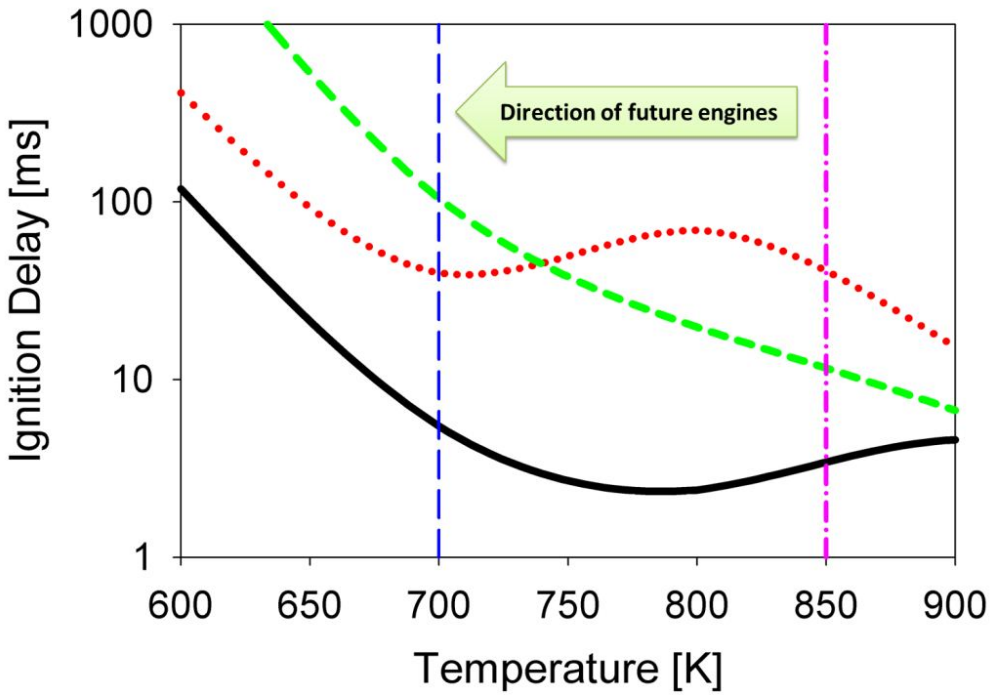


FIGURE 1.8. RON and MON test reference fuels shown on an Ignition Delay versus Temperature plot. The black line is n-heptane, the red dotted line i-octane, the green dashed line n-butanol, the thin blue dashed line the RON test at 15 bar, and the thin dash-dot pink line the MON test at 15 bar.

The idea that the temperature and pressure history greatly impact the combustion timing is one that will be further addressed below. However, although the OI was a great step forward in trying to understand and rank real fuels in HCCI operating conditions, several studies have found that this method ultimately does not correlate well with CA50 when a broader range of fuels is considered (specifically, when alcohols and other non-petroleum derived fuels are considered)[35, 46, 47]. One likely reason for this is that RON and MON values do not vary linearly with respect to volume when non-paraffins are considered[28]. Anderson et al. showed that RON and MON blending values varied nearly linear when expressed on a molar, rather than volumetric basis. Expressing the octane index on a molar basis is something that is explored later in this work and thus far shows promise as being able to predict the CA50 of fuels in situations where a volumetrically based OI is insufficient.

1.5.3. HCCI Index. Shibata and Urushihara[48] built upon the Kalghatgi work by further differentiating the contributions of low temperature heat release (LTHR) and high temperature heat release (HTHR) to RON and MON. They showed that the RON test, due to less severe conditions (i.e. lower in-cylinder temperature for a given pressure), was better at capturing the low temperature chemistry effects that exist in many blended component fuels. The MON test then better relates to the high temperature heat release of the various fuels. Specifically, the RON and MON tests show how the Octane Number of fuels, especially non-alkane fuels, can change as a function of engine conditions. Comparing the two tests allows one to encapsulate a transient response to in-cylinder temperature and pressure conditions in a single number. Shibata and Urushihara then rephrased the RON and MON tests within the context of the OI as follows:

$$RON = \Delta LTHR + HTHR$$

$$MON = HTHR$$

$$OI = (1 - K)\Delta LTHR + HTHR \tag{7}$$

Shibata and Urushihara thus were the first (to this Author's knowledge) to try and rank fuel performance in an HCCI engine by concentrating on the LTHR portion of the heat release. More specifically, Shibata and Urushihara examined 23 different "model" fuels made from 11 pure component hydrocarbons and tried to correlate the crank angle of 20% heat release (CA20) to what they refer to as a HCCI Index; where the HCCI Index was found by summing the individual component contributions to heat release given by Eq. 8:

$$HCCI\ Index(abs) = rRON + a'(n\text{-}P) + b'(i\text{-}P) + c'(O) + d'(A) + e'(OX) + Y' \tag{8}$$

where n-P, i-P, O, A, and OX refer to fractions of normal-paraffins, iso-paraffins, olefins, aromatics, and oxygenates, respectively. The empirical coefficients r, a', b', c', e', and Y' are given by Shibata and Urushihara (shown here in Table 1.2).

The temperature ranges at the top of Table 1.2 correspond to the in-cylinder temperature of a given fuel/air mixture during compression - as measured at an in-cylinder pressure of 15 bar. One shortcoming of this study was that these empirical coefficients were made without the acknowledgment of test-to-test error and so the accuracy of these numbers is likely overstated. The HCCI Index assigns these coefficients based on the assumption that all

TABLE 1.2. HCCI Index Coefficients from Shibata and Urushihara

temp at 15 bar		<670 K	670-700 K	700-730 K	730-790 K	790-820 K	>820 K
RON	r	0.848	0.858	0.831	0.523	0.207	0.161
n-P	a'	-0.203	-0.256	-0.320	-0.244	-0.103	-0.050
i-P	b'	-0.198	-0.267	-0.336	-0.187	-0.012	0.014
olefin	c'	-0.134	-0.193	-0.259	-0.176	-0.064	-0.043
arom	d'	0.006	-0.087	-0.186	-0.109	-0.009	0.008
ETBE	e'	-0.032	-0.072	-0.132	-0.088	-0.003	0.018
EtOH	e'	0.172	0.089	-0.036	-0.054	-0.026	-0.020
MTBE	e'	0.025	0.023	0.004	-0.004	0.018	0.031
y-intercept	Y'	-60.028	-56.041	-48.828	-32.109	-18.947	-19.276

functional groups have similar ignition delay behaviors, which works only for a narrow range of fuel-types even within a given category. As an example, the Authors assign all iso-parffins the same coefficients, but the ignition delay behavior for i-octane is quite different than, say iso-butane. With that said, for a narrow boiling point range (for example gasoline range fuels only) this method works reasonably well since the size-range of applicable functional groups will be relatively small.

Though not immediate apparent from looking at Table 1.2, the important conclusions from this study were:

(1) Paraffins show only LTHR characteristics, which suggests that they are the main contributors to the LTHR,

(2) Aromatics, since they show no LTHR, actually detract/inhibit LTHR,

(3) Olefins and naphthenes can show both LTHR promotion and inhibition effects.

An observation of those species considered "inhibiting" LTHR in Table 1.2, it shows that the inhibition coefficients are either positive or only slightly negative (greater than about -0.1). Also note that these coefficients can only be compared across fuels tested at the same K conditions (i.e. the same K factor from Kalghatgi's OI). Here again, since the HCCI Index method showed good correlation for the fuels originally tested, but has sense proven to provide poor resolution for fuels with similar octanes[35, 47]. Ultimately, the HCCI index suffers from the same disadvantages as the OI: namely that it is empirically based on the volumetrically blended RON and MON fuel values and does not consider many of the newly focused on alternative fuels (such as butanol or methyl esters).

1.5.4. Other IQT Studies. Numerous research studies using the IQT instrumenthave appeared in the literature over the past decade because of its ability to rapidly test the ignition delay of a variety of fuels at low to intermediate temperature[35, 38, 39, 49, 50]. Bogin et al. modeled the IQT with KIVA-3V which is a 3-D modeling software that incorporates full Navier-Stokes and small mechanism chemical-kinetics. Bogin et al. further used several different reduced mechanisms and concluded that the ignition behavior was dominated by chemical kinetics as compared to spray physics. Furthermore, they showed that the dominance of chemical effects over spray physics increased drastically for longer ignition delays[49] as the mixture became increasingly homogeneous, prior to ignition.

Perez et al. further showed that fuels (possibly) best suited for HCCI such as those with a RON of approximately 70 have IQT-ignition delays of $\geq$8 ms. In their study, $\geq$8 ms was deemed sufficiently long enough for the system to be modeled homogeneously[35], although Bogin et al. claimed that an ignition duration of 15-20 ms was needed before the system could be modeled as homogeneous.

Perez et al. further tested a wide range of gasoline-like fuels to see if HCCI autoignition behavior could be predicted or correlated to that in an IQT. They tested 21 different surrogate gasoline fuels in an IQT and a HCCI engine and found that the inverse of IQT-reported ignition delay correlated relatively well with the CA50 data from the HCCI engine (Figure 1.9). One important thing to note in the Perez et al. study is that fuels with ignition delays longer than about 15 ms did not correlate well with HCCI CA50 due to problems getting those fuels to combust at the tested equivalence ratios. They also found that while the inverse of IQT-reported ignition delays generally correlated with the RON and OI, there were significant differences between fuels of the same RON that could not be explained by either the RON or OI scales - though they did calculate RON values via polynomials and did not actually measure RON values for their tested fuel mixtures.

One goal of the work presented herein is to use the FIT results in a similar manner as Perez et al. Moreover, the present work more rigorously tests the hypothesis that a relatively low temperature combustion device like the FIT or IQT can be useful in predicting behavior in an HCCI by including full kinetic modeling and experiments across multiple platforms.

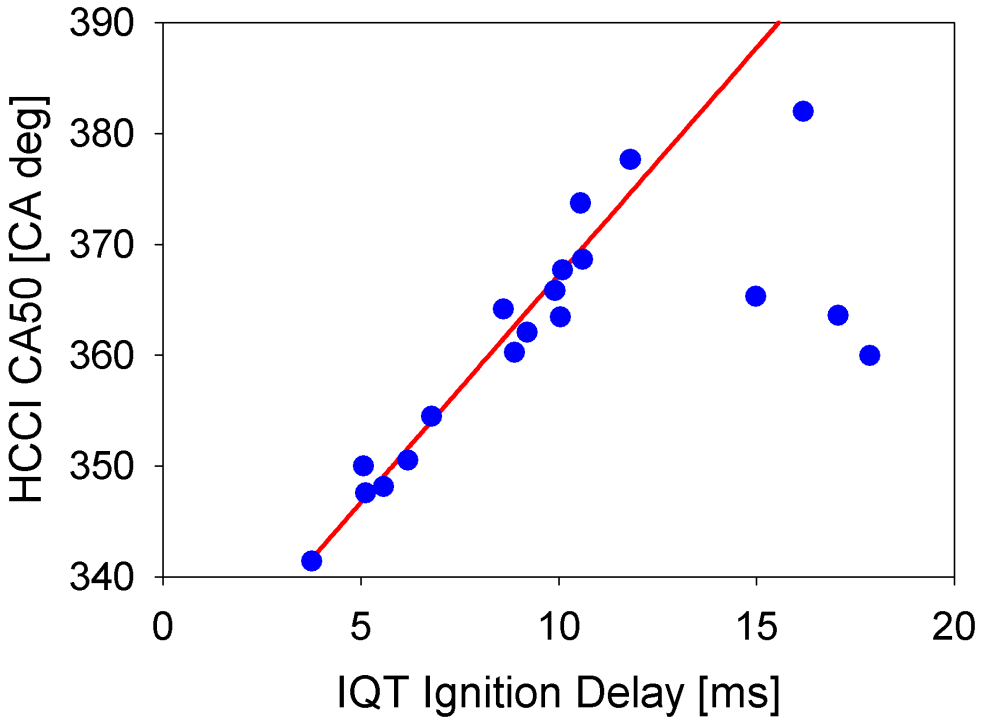


FIGURE 1.9. Combustion phasing (CA50) vs. IQT Ignition Delay for gasoline-like fuels (blue circles) from[35]. The red line is a best fit through data points with ignition delays below 15 ms.

1.5.5. BUTANOL BLENDS. Future fuels with desired properties for optimal performance in advanced combustion modes will most likely consist of mixtures of petroleum derived products (aromatics, straight and branched alkanes), alcohols, synthetic alkanes (straight and branched alkanes produced from natural gas, vegetable oil or animal fat) and fatty acid methyl esters. Fuel blends such as these with properties currently tailored for DICI or SI engines are already in widespread use throughout the world. For example, the U.S. currently mandates a 10%v minimum ethanol blending requirement and the U.S. Environmental Protection Agency (EPA) recently reported that mixtures up to 15%v will be considered for future blends[51].

Butanol has received much attention recently as a bio-alternative to ethanol due to its higher energy density and higher miscibility with other hydrocarbons. There have also been

a wide array of kinetic studies of butanol (and its isomers) and so well-validated experimental data and chemical mechanisms exist[31, 52–59]. Recent research[59] also suggests that butanol may possess an unique kinetic nature in that butanol (and blends with n-heptane) may have longer ignition delays than n-heptane at low temperature, but shorter ignition delays at high temperature (i.e.≥1000 K, in-cylinder conditions).

The work presented herein examines the combustion behavior of n-butanol mixtures and compares them to the behavior of PRF's and TRF's (toluene reference fuels[29, 30, 60, 61]). As explored in Chapters 3 and 4, contrasting ignition behavior is observed which facilitates the possibility of tailoring fuel blends to maximize HCCI performance. Furthermore, the observed contrasting reactivity is a major objective of the present research, which is to determine if simple devices such as FITs can be used to explain and possibly predict how such fuels will react in an HCCI engine; and ultimately if these devices can be used to rank fuels in terms of HCCI-reactivity.

1.6. Organization of the Dissertation

This Dissertation develops a theoretical understanding for the underlying basis of traditional fuel reactivity metrics as well as presents a method for describing fuel reactivity in HCCI engines. Chapter 2 is devoted to discussion and description of the main fuels, instruments, and methods used in varying level of detail corresponding to their contribution to the total work. Overall, three experimental platforms were used, one of which (the HCCI engine) was designed and fabricated during the initial phase of this work. Several computational approaches were also taken to describe the various experiments conducted. Chapter 2 concludes with a discussion of the primary chemical-kinetic modeling approach taken herein

and presents a new chemical mechanisms describing combustion of n-butanol/n-heptane fuel mixtures.

In Chapter 3, the theoretical understanding for the underlying basis of traditional fuel reactivity metrics is presented. The operational basis for the two most common combustion engines, DICI and SI, are broken down and used as a basis for understanding fuel reactivity. The long-known, but ill-described relationship between the CN and ON scales is examined and a novel functional (e.g. mathematical) foundation is presented linking the two scales. Out of this analysis a new parameter, the knock length, is derived which incorporates the essential aspects of SI combustion - namely flame speed and ignition delay. The knock length is then used to explain fuel sensitivity; i.e. the behavior of some fuels to increase/decrease relative to reference fuels as a function of temperature. Lastly, the knock length is used to examine the non-intuitive results of increased in-cylinder pressure/temperature observed in low MN fuels. Throughout this chapter, CFR and FIT experiments are examined and modeled to support the presented theory.

Chapter 4 builds on the analysis applied to conventional engines in Chapter 3. HCCI and FIT experiments are conducted using fuels with a range of reactivities and a novel method is developed to predict the relative combustion timing said fuels. This novel method examines the low temperature portion of the heat release observed for many of the fuels used in HCCI operation and correlates that low temperature release to the main combustion timing. The analysis in this chapter goes further to relate the low temperature release observed in the FIT to that in the HCCI engine. This chapter concludes with the presentation of a new metric (the HCCI Number) with which fuels can be ranked in an HCCI engine.

Chapter 5 discusses various ancillary efforts that contributed to the main goals of this work. Firstly, the operational range of the FIT is explored and efforts to extend the tested global air-fuel equivalence ratio is examined. Next, heat transfer modeling within the HCCI engine is discussed - the results of this section are incorporated in the HCCI modeling of Chapter 4. Other modeling efforts that support and extend those of Chapter 4, such as a GT Power model and a CONVERGE model are also investigated. Lastly, a 1-dimensional flame model is presented which is shown to have use in modeling non-premixed flames. This Section concludes with a short discussion on how this model could be applied to the non-premixed portion of DICI combustion.

CHAPTER 2

Experimental Methods

This chapter is devoted to discussion and description of the main fuels, instruments, and methods used in varying level of detail corresponding to their contribution to the total work. Overall, three experimental platforms were used, one of which (the HCCI engine) was designed and fabricated during the initial phase of this work. Additionally, several computational approaches were taken to describe the various experiments conducted. Single and multi-zone (CHEMKIN) as well as system-level (GT Power) and multi-dimensional (CONVERGE) modeling approaches are developed and discussed. Due to the heavy use of CHEMKIN modeling, that approach is discussed in this section; GT Power and CONVERGE modeling are discussed briefly in Chapter 5.

2.1. Liquid Fuels Examined

Table 2.1 shows the physical properties of the fuel mixtures investigated in the current work. Viscosity, density, bulk modulus measurements, and DCN values were performed by the Author. The viscosity and density were measured via an Anton Paar SVM 3000 Stabinger Viscometer instrument. The bulk modulus (BM) was calculated via density and speed of sound measurements carried out with an Anton Paar DSA 5000M. Bulk modulus was determined as it is a well-known physical property that can affect fuel injection and timing in cases, such as ours, where there is some significant distance between the fuel pump and the injector (such as for pump line diesel injectors or some rare configurations of unit injectors)[62–65]. However, as explored in Section 5.1, fuel viscosity was found to have the greatest influence on FIT fuel injection volume/mass.

TABLE 2.1. Properties of Tested Fuels

fuel	n-butanol [vol%]	n-heptane [vol%]	i-octane [vol%]	toluene [vol%]	viscosity[a] [mm^2/s]	density[a] [g/cm^3]	RON	DCN
nC7	0	100			0.442	0.684	0	54.1
PRF20		80	20		0.449	0.686	20	47.8
PRF40		60	40		0.462	0.687	40	42.4
PRF60		40	60		0.484	0.689	60	36.8
PRF80		20	80		0.507	0.690	80	28.4
PRF95		5	95		0.529	0.692	95	20.5
PRF100		0	100		0.542	0.692	100	11.1
nBuOH20	20	80			0.584	0.708	<40	40.5
nBuOH40	40	60			0.805	0.734	56	24.6
nBuOH60	60	40			1.144	0.760	72	16.5
nBuOH80	80	20			1.623	0.785	88	10.5
nBuOH95	95	5			2.090	0.804	96	5.4
nBuOH	100	0			2.248	0.810	96[b]	3.7
Tol20		80		20	0.470	0.720	28	45.4
Tol40		60		40	0.486	0.760	53	35.0
Tol60		40		60	0.502	0.789	78	23.6
Tol70		30		70	0.510	0.809	89	17.2
Toluene		0		100	0.533	0.867	120[c]	

[a] viscosity and density values were measured via an Anton Paar SVM 3000 Stabinger Viscometer.
[b] pure n-butanol RON value from[66, 67]
[c] toluene RON from[68]

2.2. FUEL IGNITION TESTER

In 2003 the ASTM approved a new method allowing the use of bench-top, constant-volume instruments for the measurement of DCN. The 2003 standard (D6890-03) and subsequent versions are based on the Ignition Quality Tester (IQT). In addition to measuring

DCN, the IQT has received much attention recently and is gaining popularity as a combustion research apparatus[35, 38, 39, 49, 50].

In 2006 the ASTM approved a similar standard based on the FIT (schematic diagram in Figure 2.1), which is also a bench-top, constant volume, combustion device. The first study using the FIT as a research instrument in detail was published by Baumgardner, et al. in 2013[69]. The IQT and FIT machines are similar in that they both operate by injecting a small quantity of fuel via a high-pressure fuel injector into a heated (∼540 °C), air-filled, pressure vessel held at a moderately high pressure (∼22 to 24 bar). Table 2.2 lists typical FIT test conditions.

TABLE 2.2. Nominal Operating Parameters for the Waukesha FIT apparatus

parameter	condition
volume	0.6 L
pressure	24 bar
wall temperature	580 $°C$ (853 K)[a]
global equivalence ratio	0.1-0.6

[a]Note that chamber gas temperature was measured as 32±10 $°C$ lower than the user-defined wall temperature.

Although DCN is typically reported, both the FIT and IQT devices actually measure the ignition delay period for the stated conditions and then convert that measured ignition delay period into a DCN. Due to various geometrical, injection-style, and other differences, the two devices have different equations describing the relationship between DCN and ignition delay[21, 32], as noted in Eq. 9 and 10, respectively. In both equations "ID" is the ignition delay period in milliseconds.

$$DCN = 4.460 + \frac{186.6}{ID} \tag{9}$$

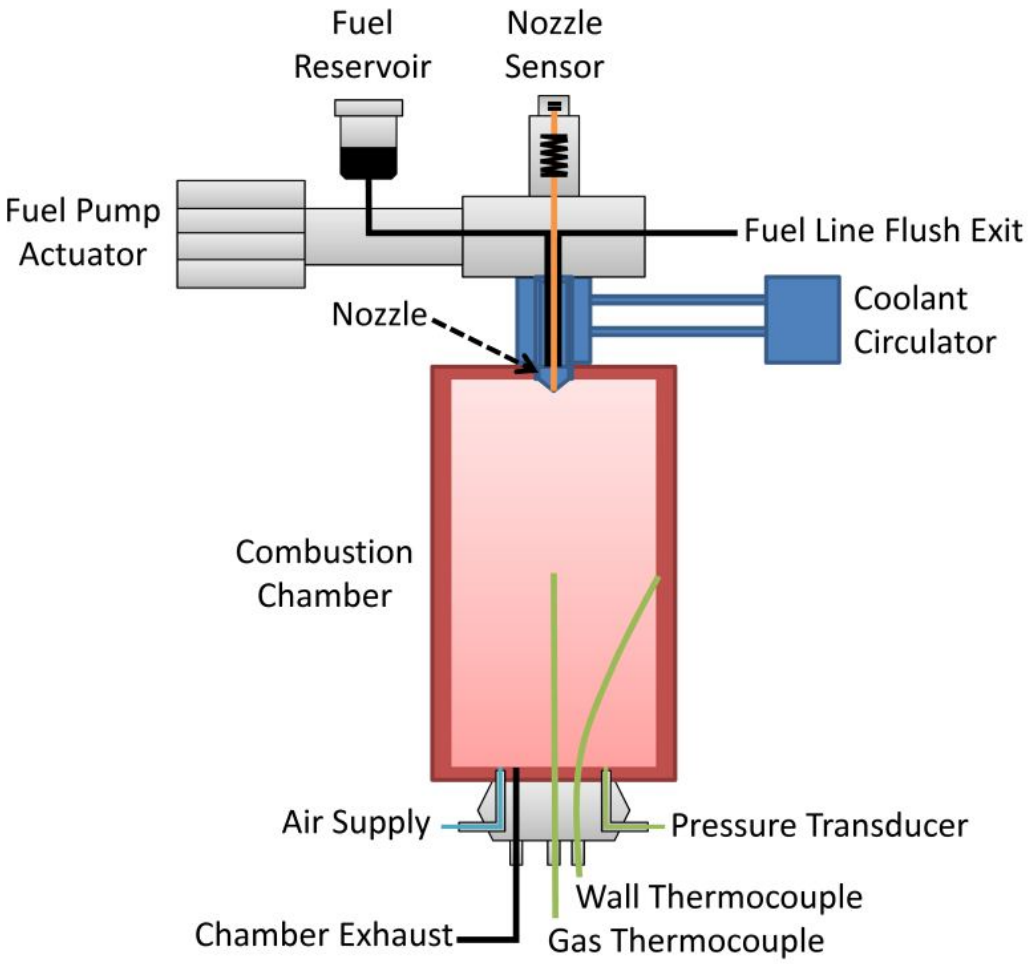


FIGURE 2.1. Schematic diagram of Fuel Ignition Tester.

$$FIT{:}DCN = \frac{171}{ID} \tag{10}$$

While both methods are less accurate when measuring ignition delay periods for low DCN fuels, the IQT method has a built-in biased "zero" at a CN of 4.460. As a result of these differences, below a DCN of approximately 10 ms, the two instruments will implicitly exhibit different DCN values for the same fuel. Note the separation point between the two methods in Figure 2.2.

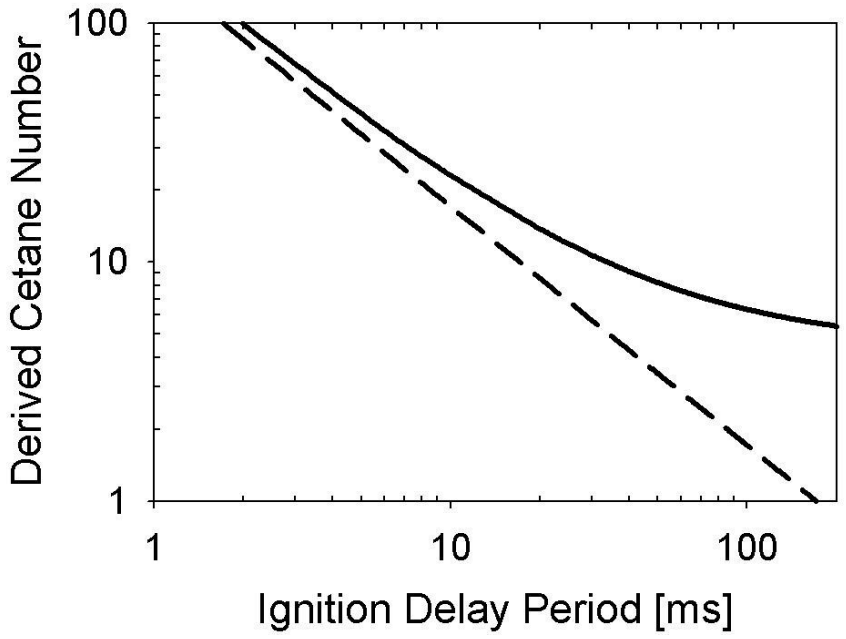


FIGURE 2.2. Log-log plot showing the deviation of DCN values calculated for a given ignition delay time for the IQT and FIT machines. The solid line is the IQT equation (Eq. 9) and the dashed line is the FIT equation (Eq. 10).

It should also be pointed out here that the ASTM standard for the FIT gives one equation (Eq. 10) for the whole DCN range, whereas the ASTM standard for the IQT lits a separate equation for when the 32-test average ignition delay is greater than 6.4 ms; when this is the case, the DCN equation becomes highly non-linear (Eq. 11)[39].

$$DCN = 83.99 \cdot (ID - 1.512)^{(-0.658)} + 3.547 \tag{11}$$

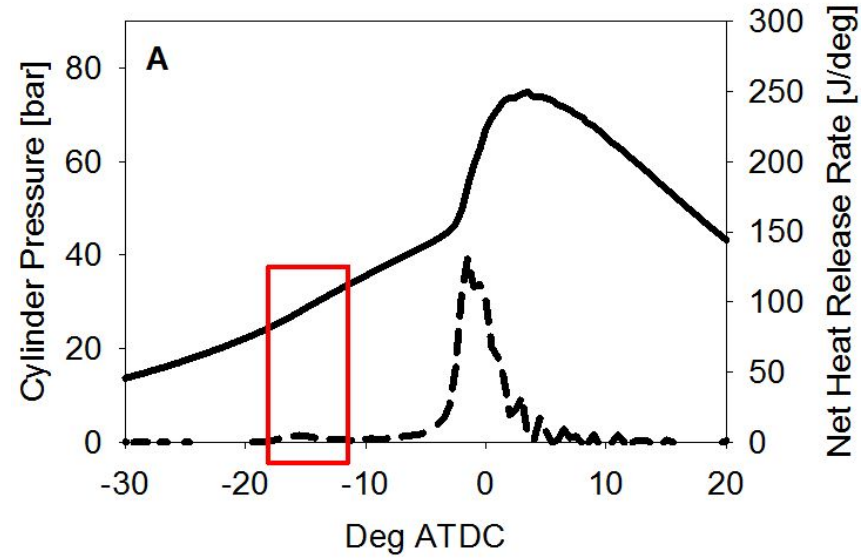
For the main component of this work, experiments were performed for three basic test fuel blends: n-heptane/i-octane, n-heptane/n-butanol, and n-heptane/toluene. In all, 18 different fuels were tested in duplicate (at minimum) with 27 injections for each test; in total there were >1000 injections for these fuels as some fuels were examined more than twice. Fuel physical properties are listed above, in Table 2.1. For all fuel mixtures n-heptane was chosen

as the high-reactivity fuel due to its prominent use as a reference fuel in both diesel and gasoline applications as well as having well-studied chemical kinetics[70–72]. In addition, mixtures of methyl decanoate/n-butanol and diesel/n-butanol were tested and preliminary indications are that methyl decanoate/n-butanol mixtures have advantageous properties as biofuel blends, although

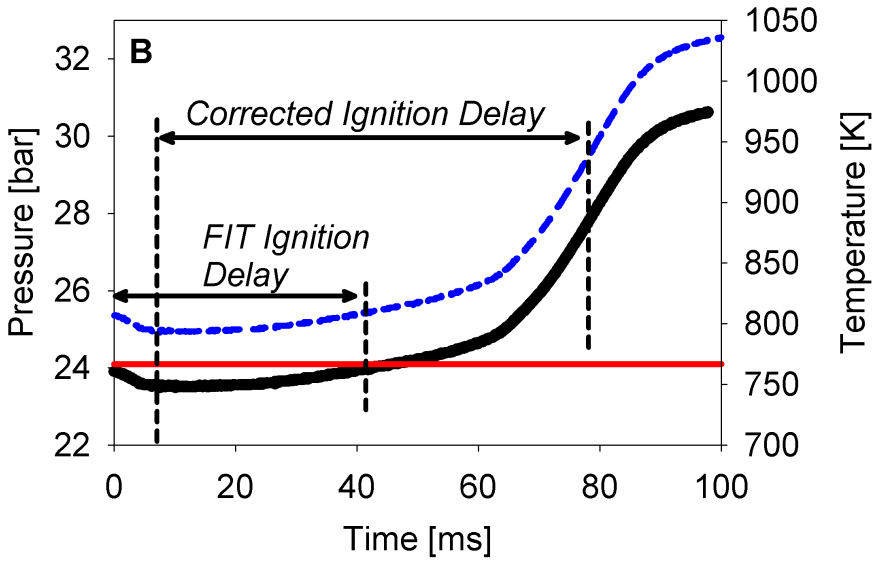
The FIT operating temperature and pressure range, shown in Table 2.2, is ideal for examining the prominent low temperature combustion region of a HCCI engine. The red box in Figure 2.3(a) highlights the region where the conditions in the FIT overlap with that in the Colorado State University (CSU) HCCI engine (described below in Section 2.3). Figure 2.3(b) is an example FIT pressure trace showing the average of 25 injections compromising one test for pure n-butanol. Here it is important to mention that the FIT (like the IQT) reports the ignition delay period based on an internal threshold response to the combustion pressure rising a set amount (+0.2 bar for the FIT) above the base pressure (see Figure 2.3(b)). This technique can produce erroneous ignition delay periods since low temperature chemistry can result in a small pressure rise prior to primary ignition. For the high reactivity diesel fuels that these devices were originally designed to accommodate, the low temperature pressure rise is not problematic for DCN measurements since it occurs at time periods very close to that of the primary ignition event. However, for fuels with longer ignition delay periods such as those tested in the present study, the low temperature pressure rise can be misinterpreted as the primary ignition event. Additionally, there is a decrease in system pressure and temperature due to fuel vaporization, which is also evident in Figure 2.3(b). Accordingly, reported herein are both the FIT-reported ignition delay period along with an ignition delay period calculated as the time from minimum pressure to the peak pressure

rise rate (PPR). For the CN-ON data presented in Chapter 3, the FIT-trigger ignition delay was used since it has been statistically correlated to the DCN values - additionally, the FIT-trigger is more indicative of LTHR and may correspond better to light knock conditions than the main ignition event.

Lastly, note that the FIT was purchased through Compass-Instruments and was essentially delivered ready to go and required minimal set-up. Although, after some of the more viscous fuels were examined, the fuel injection nozzle needed to be cleaned several times (cleaning procedure can be found in Appendix D).



(a) HCCI Engine Data



(b) FIT Pressure and Temperature trace

FIGURE 2.3. FIT and HCCI similarities: (a) HCCI engine data showing pressure and net heat release rate (from the present study). The red box shows that the region of low temperature chemistry seen in the experimental HCCI engine is in the same range as that tested in an FIT. The solid line is the pressure trace for nBuOH40 and the dotted line is the net heat release rate. The test conditions were 60%v n-butanol/40%v n-heptane at ϕ of 0.33, T_{in} of 70 $^{\circ}C$, P_{in} of 1.0 bar, 1500 RPM and 16:1 compression ratio. (b) Pressure trace average (black line) for a typical n-butanol ignition test in the FIT, calculated temperature (dashed blue line), and the FIT trigger point (red line).

2.3. HCCI Engine

To demonstrate the performance of the proposed fuel blends in HCCI mode, a diesel engine was converted for use as an HCCI test bed. Specifically, one cylinder of a John Deere PowerTech 2.4 L 4024 turbo-diesel engine was modified to operate in HCCI mode. The existing in-cylinder fuel injector was disconnected in favor of using port fuel injection (via a gasoline-type injector located approximately 50 cm upstream of the intake valve) to produce a homogeneous mixture of air and fuel that is typical of HCCI operation. The in-cylinder pressure was measured using a Kistler 6056A pressure transducer and data were recorded every $0.5°CA$, which was the resolution for the crank angle sensor used in this work.

The net heat release rate was calculated via a standard, 1st law analysis often used in literature[25] and based on Eq 12.

$$\frac{dQ}{dt} = \frac{\gamma}{\gamma - 1} P \frac{dV}{dt} + \frac{1}{\gamma - 1} V \frac{dP}{dt} \tag{12}$$

where γ is the ratio of specific heats, P the pressure, V the instantaneous cylinder volume. The heat release rate was computed assuming that the combustion gas was primarily air modeled as an ideal gas, but including the temperature dependence of γ (Eq. 13[73]). It should also be noted that the heat release rates shown herein are not filtered but rather slightly smoothed as a result of numerical integration and the fact that the results shown represent an average of 100 consecutive cycles.

$$\gamma = 1.375 - 6.99\text{x}10^{-5} \cdot T(K) \tag{13}$$

Additional modifications to the engine consisted of alterations to the intake and exhaust manifolds to allow isolation of the HCCI cylinder and the installation of an air preheater necessary to achieve the higher intake temperatures typically associated with HCCI operation[10, 74] . The intake heater was controlled within $\pm 2\ ^{\circ}C$ of the desired temperature ($70\ ^{\circ}C$) for all tests via a custom National Instruments interface. The piston head of the HCCI cylinder was also modified such that the compression ratio could be adjusted to allow HCCI tests at various compression ratios. Specifically, the bowl of the piston was milled down flat resulting in a compression ratio of 12:1. Various size disks were then bolted into the milled out pocket to increase the compression ratio up to a maximum of 18:1. For the results presented herein, the 16:1 compression ratio piston configuration was used. The specifications of the HCCI engine are detailed in Table 2.3.

TABLE 2.3. Parameters for CSU HCCI Engine

parameter	value
displacement volume	609 cm^3
compression ratio	16:1
speed	1500 RPM
intake temperature	$70\ ^{\circ}C$ (343 K)
intake pressure	1.0 bar
bore	86 mm
stroke	105 mm
global fuel-air equivalence ratio	0.33

2.3.1. HCCI CONVERSION OVERVIEW. Most of the conversion of the John Deere 4024T engine to HCCI mode was performed by the 2010-2011 Senior design team advised by Prof. Anthony Marchese and directly supervised by the Author (Marc Baumgardner). This section

includes a summary of the work necessary to isolate the HCCI cylinder and achieve consistent HCCI combustion.

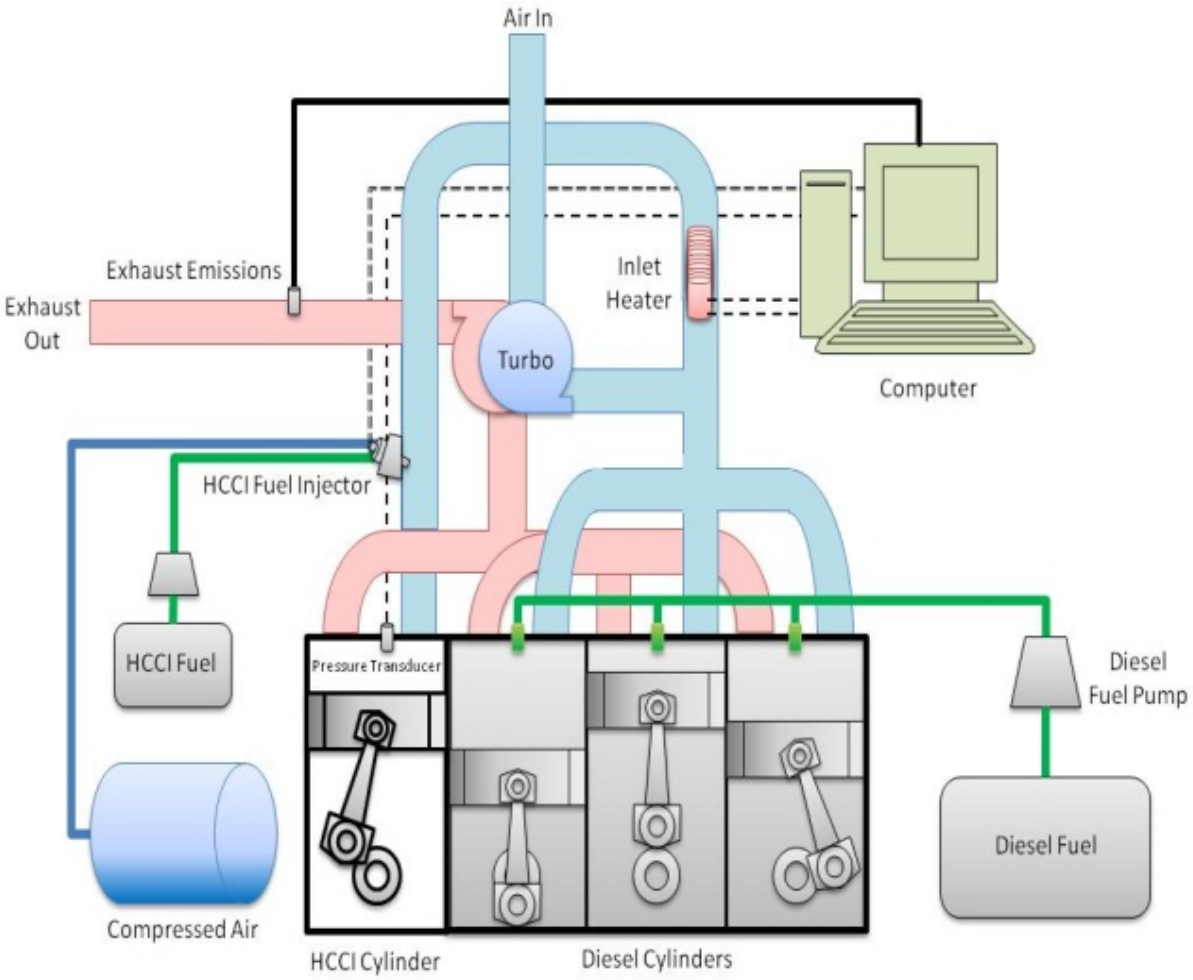


FIGURE 2.4. Schematic of HCCI Engine Layout

2.3.2. INTAKE AND FUEL SYSTEM. To convert cylinder #4 (the cylinder closest to the transmission) of the John Deere 2042T engine it was necessary to isolate it both with respect to intake and fuel from the other three cylinders. Isolating the intake was done so as to add both an intake air heater and port fuel injection. The intake was split downstream of the turbo with one path going to cylinder #4 and the other going to the first three cylinders. After the split, an in-line heater was placed in the HCCI intake pipe. The location of

peak pressure of HCCI is directly related to intake charge temperature and so the ability to modulate this variable is essential in studying HCCI combustion. The heater was designed to operate in relatively low pressure (7-10 psig max) and high mass flow rates (20-30 cfm) with a diameter restricted to the nominally 2" intake system. To achieve these specifications, a 1000 W AC heater from Omega was eventually selected (Figure 2.5).

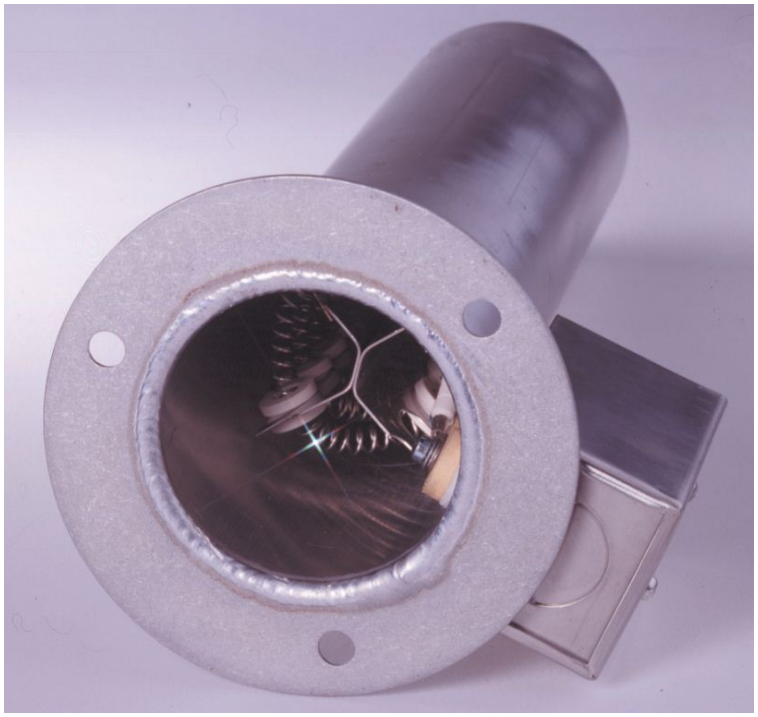


FIGURE 2.5. Photo of the Omegea Engineering 1000 W in-line heater used in the intake line of the CSU HCCI engine.

After the heater a Synerject air-assisted fuel injector (sold by Aprilia: P/N AP8276009 and AP3AGA000614, see Appendix A) was placed approximately 10 pipe diameters ($\sim$50 cm) upstream of the HCCI cylinder intake valve. The distance of 10 pipe diameters was chosen to ensure the injected fuel was fully mixed with the intake air stream. According to the manufacturer, this injector is capable of atomizing fuel into 8μm droplets, a factor of 3-4 times smaller than a typical automotive injector. It was initially hoped that this increase in atomization would aid in the fuel vaporization. To further aid in vaporization, the injector

was assisted by a 70-100 psi air flow. Note that the injector assembly has a built-in pressure regulator to ensure that the fuel is injected approximately 40 psi above the air pressure; therefore a high pressure ($\sim$ 200 psi) fuel pump (Aprilia: P/N 854933) was also required. To operate the injector system, a pulse modulator was used to send a signal to both the fuel and air injectors to fire at a speed of 40 Hz therefore allowing 2-4 pulses of fuel for every cycle (depending on engine speed). Figure 2.6 is a cutaway of the fuel/air injector from the patent application[75] showing how the fuel injector sits atop the air injector. Figure 2.7 is a photo of the intake system with heater and air-assisted fuel injector installed.

As stated, control of the fuel and air delivery to the Synerject air-assisted fuel injector was achieved via a pulse generator operating at 40 Hz (Figure 2.8). The open/offset time of the two pulses (fuel and air) was set to be such that the air injector was closed while the fuel injector was open. Initially it was thought that operating in such a manner would assist in fuel atomization. More importantly, however, this was the optimal operation as described by Envirofit International, who was consulted on this fuel injector since they had experience using this injector in other applications. The following equation was used to determine the open pulse width, in seconds,based on an assumed static open delivery rate of fuel:

$$PulseWidth = \frac{\frac{FoF}{Hz} - DF_f}{SoF} + DF_t \tag{14}$$

where FoF is the required flow of fuel [g/s], Hz the pulsing time in hertz, SoF the static open flow rate for the injector, DF_f the dynamic flow of fuel [g/pulse], and DF_t the dynamic flow time. Here the dynamic flow timing and amount are that which occur during opening and closing. The FoF was determined based on desired ϕ value, engine speed (RPM) and the

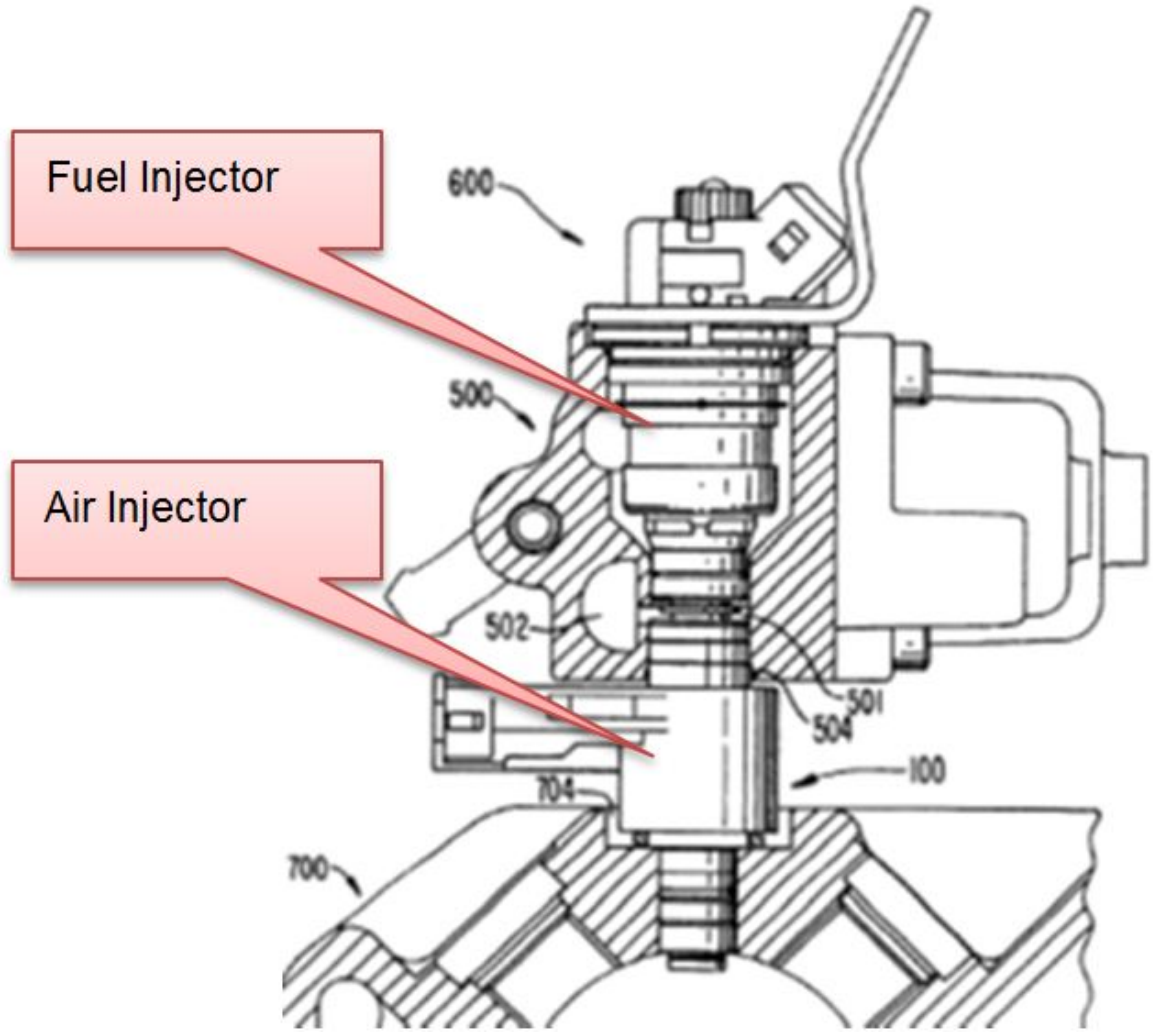


FIGURE 2.6. Cutaway of the air-assisted fuel injector. Photo from US Patent 7,104,477 B2[75]

displacement volume at a given compression ratio. The following equation gives the above parameters for the Synerject fuel injector used in this work.

$$PulseWidth[s] = \frac{\frac{FoF}{40} - 5\text{x}10^{-5}}{1.3} + 5\text{x}10^{-5} \tag{15}$$

Note that there were issues using both air and fuel injectors and eventually it was decided to switch to just the fuel injector - i.e. the air injector was removed from the injector

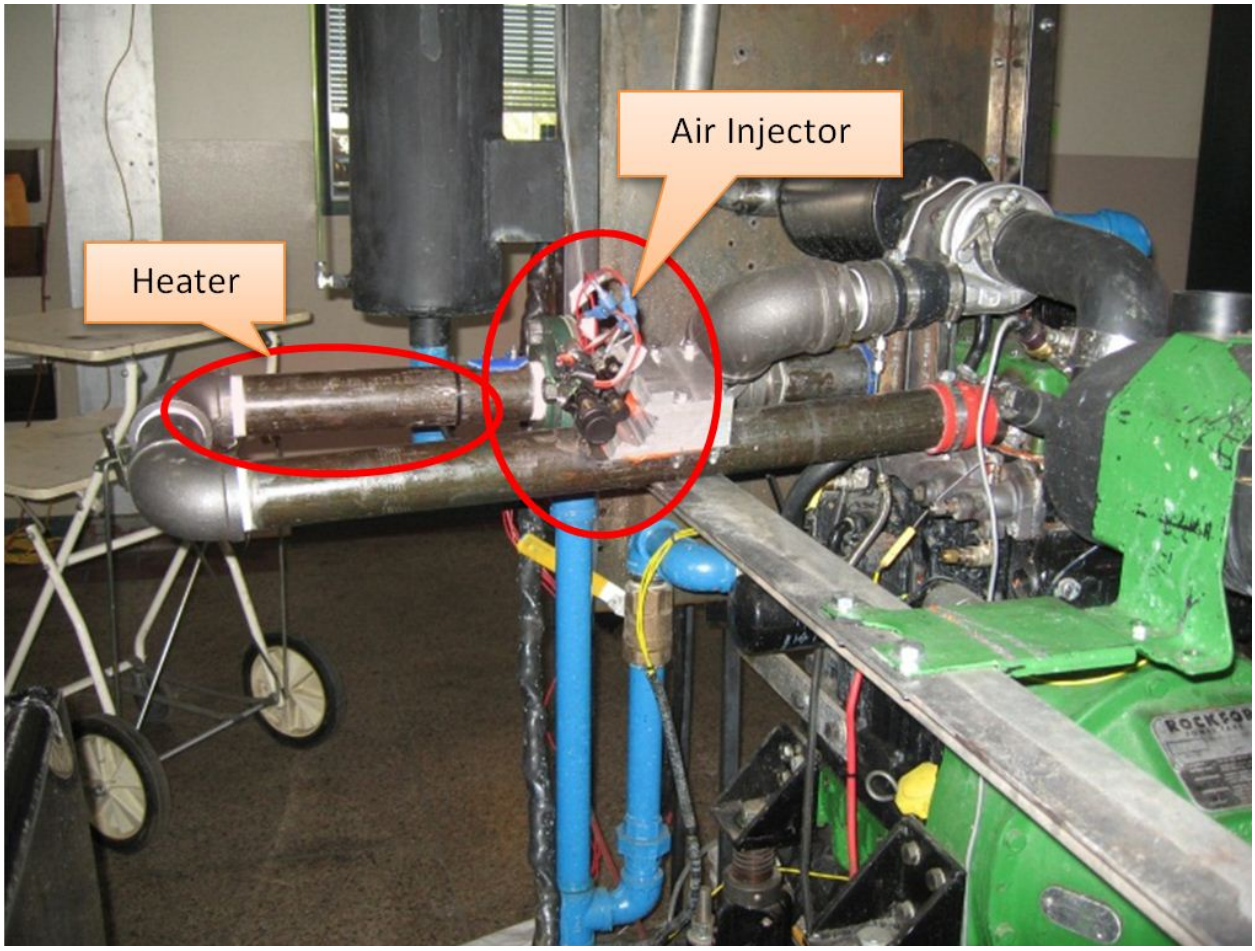


FIGURE 2.7. HCCI Intake System
Note that the intake piping has since been wrapped with exhaust wrap to reduce the load on the heater.

assembly. HCCI experiments for the same conditions (air-fuel ratio [ϕ], RPM, T_{in}, etc) showed no observable difference between operating with or without the air injector.

To calculate the fuel rate desired, the following two primary assumptions were made:

(1) Perfect mixing between the fuels (ex. n-heptane and i-octane). This assumption allowed the mixing of the fuels via volumes and then a density and mass were calculated based on the measured pure component densities.

(2) The volumetric efficiency of the HCCI engine was assumed to be 100%. This allowed the volume of air drawn into the cylinder each cycle to be set equal to the displacement volume.

Using the above assumptions and Eq. 15, data was taken at a minimum length of five minutes for each test point. The fuel reservoir was weighed before and after each test point to ensure that the desired amount of fuel was delivered over the test point. The fuel delivery rate was also assumed to be constant throughout the test point.

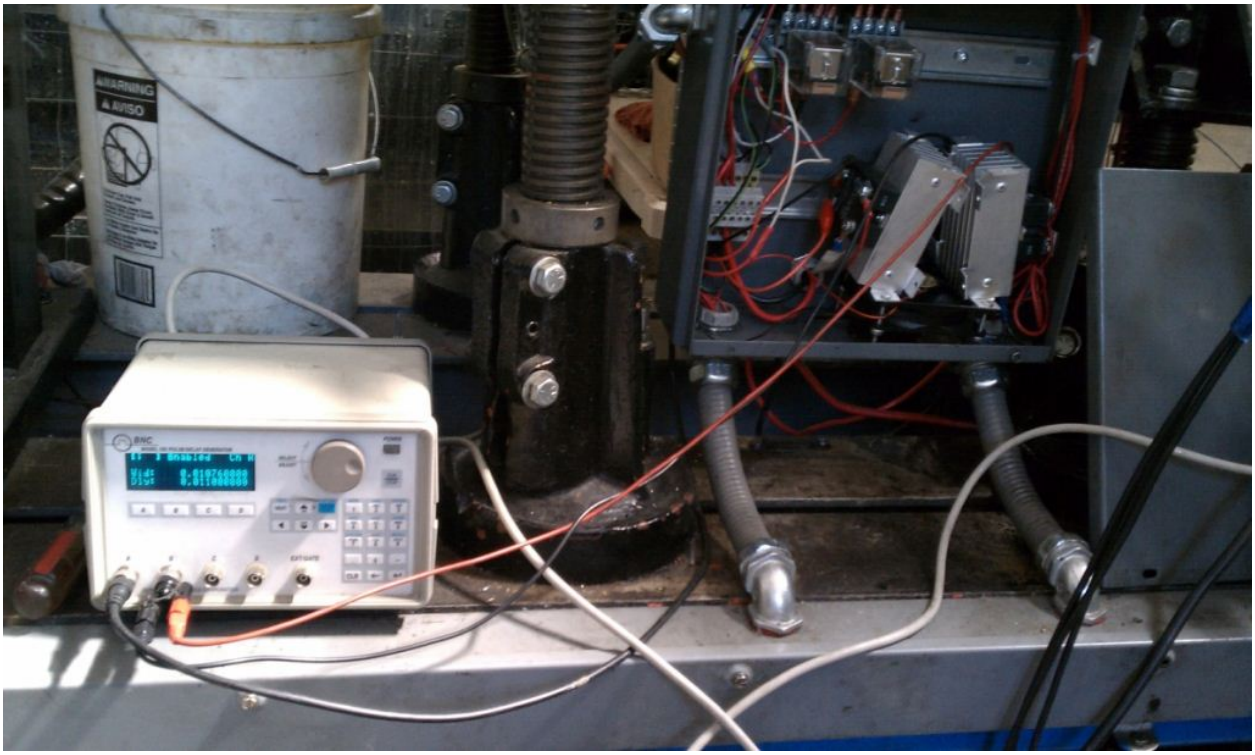


FIGURE 2.8. Control of fuel delivery to the HCCI engine was done via a pulse generator.

Lastly, the fuel rail of the 2042T engine is mechanical and in its stock configuration all four cylinders are connected via a common rail. Previously, the fourth cylinder had been isolated with respect to fuel by inserting a block into the fuel rail between cylinders 3 and 4 to prevent diesel fuel from reaching the last cylinder[76]. However, it was desired to have the ability to run the HCCI cylinder in diesel mode and so a block valve and associated piping

was plumbed between the stock diesel fuel delivery system and cylinder #4. For each test, the engine was warmed up in diesel mode and then the block valve connected to the HCCI cylinder was closed, stopping delivery of diesel fuel. At this point, the three cylinders still operating on diesel were "motoring" the HCCI cylinder and HCCI fuel could be initiated at any point, which was validated by observing the real-time pressure traces which are captured as a part of normal operation.

2.3.3. Variable Compression Ratio. It was further desired to have the ability to vary compression ratio between tests. A myriad of options were considered, but it was ultimately decided that the safest method for our operation was to mill out the head of the HCCI cylinder and insert blanks into the resulting pocket as shown in Figure 2.9 and 2.10. The width of the blank determined the final compression ratio.

To bolt in the various piston blanks, threaded inserts were installed into the milled-out cylinder. ACME Industrial 303 CRES stainless Keylocking Threaded Inserts (Figure 2.11) were purchased (ACME P/N 217-077534) and installed. Grade 8 bolts were then torqued to 20 ft-lb per the manufactures recommendation (Figure 2.12).



FIGURE 2.9. Picture of HCCI Piston. The four locking inserts have yet to be installed in this picture.

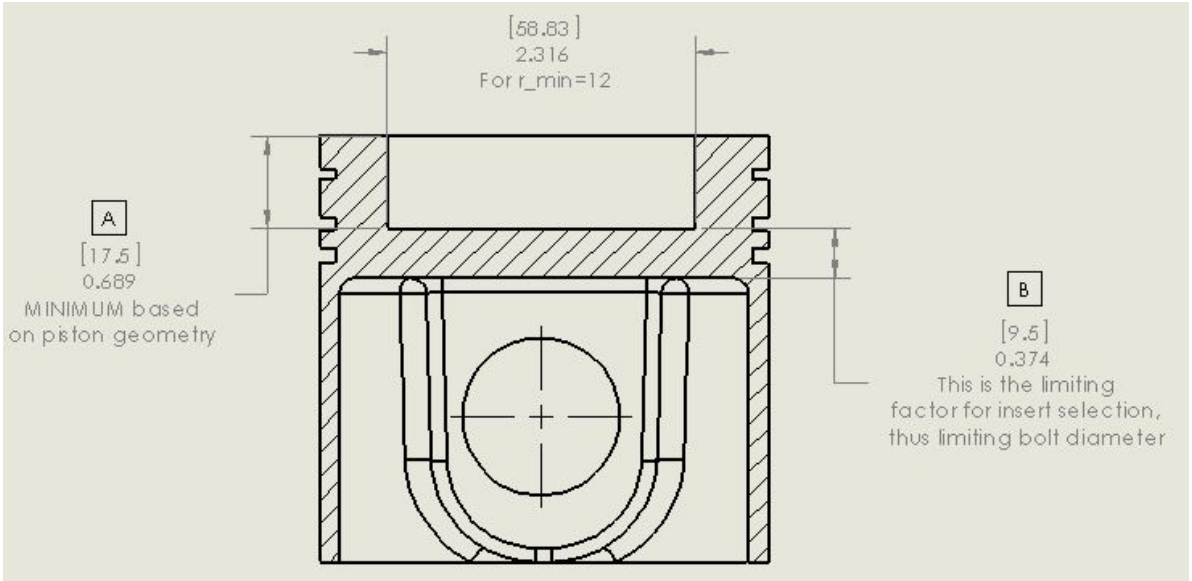
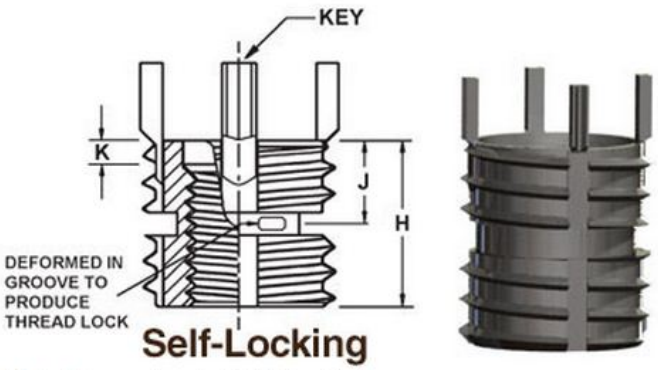


FIGURE 2.10. Cutaway View of the HCCI Piston



Material: Insert - 4140 Alloy Steel
Keys- 302 CRES
Finish: Cadmium Plate (QQ-P-416 Type II, Cl. 2)
Tolerances: ±.010 inch unless specified otherwise
Internal Threads: Per SAE AS8879
Dimensions: All dimensions below are in inches
Keys: Inserts with an internal thread size of 1/4 and larger are furnished with 4 locking keys. Smaller sizes have 2 locking keys.
Material Identification Mark: Two lines on top of insert
Lubrication: Dry Film Lube on Self-Locking Inserts only
Performance: MIL-I-45914A (MS51832)

FIGURE 2.11. HCCI Piston Inserts - ACME Industrial 303 CERS P/N 217-077534

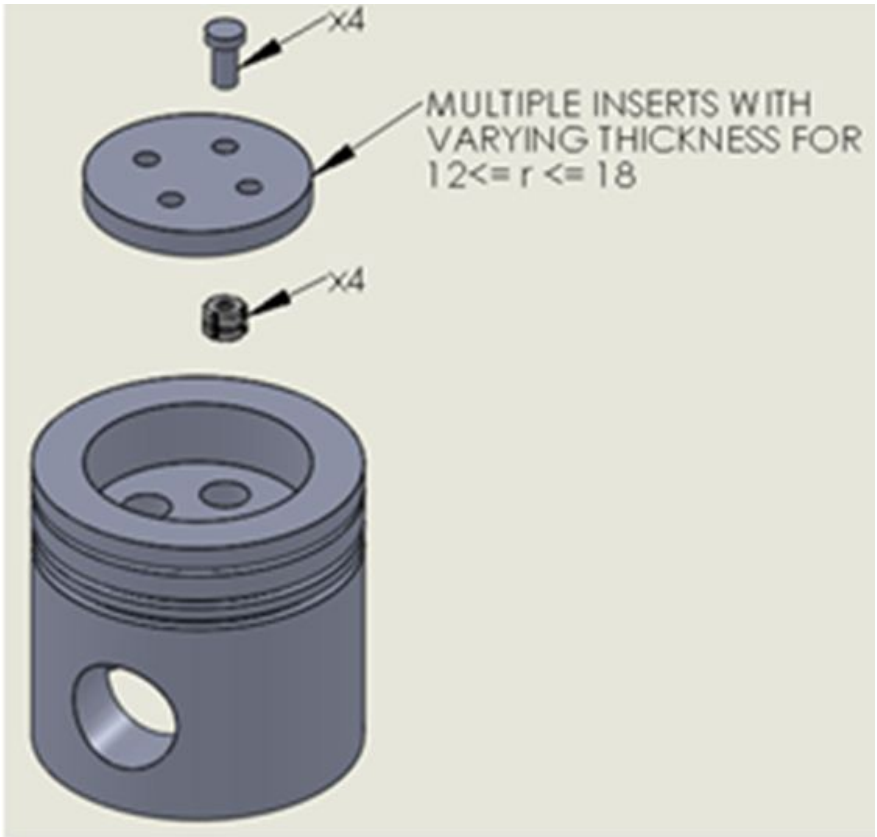


FIGURE 2.12. HCCI Piston Assembly Showing Install of the Inserts

2.3.3.1. *Procedure for Changing the Compression Ratio.* The following procedure was developed for modifying the compression ratio:

(1) The custom intake system is very heavy, carefully remove it and set it aside.

(2) Follow the user's manual for this engine to remove the alternator, exhaust manifold, valve cover, and cylinder head.

(3) Bring cylinder four to top dead center for easy access.

(4) Remove the four bolts holding the aluminum insert into the piston and then remove the aluminum insert.

(5) Each aluminum insert has the compression ratio stamped on the bottom. Choose the desired insert and ensure the stamped arrow is facing up and pointing toward the front of the engine.

(6) Install the four bolts and torque in an X-pattern to 20 ft-lbs.

(7) Follow the user's manual to reassemble all components.

2.4. CFR Engine

The methane and Octane Numbers for this work were all obtained via CFR engines. The Octane Numbers for the n-heptane/n-butanol mixtures followed ASTM D2699 procedures and were measured by Intertek[77], which is a third party fuel testing laboratory. The PRF data are by definition volumetric mixtures of n-heptane and i-octane, while the toluene reference fuel RON data were taken from Morgan et al.[68].

The methane number (MN) data were taken previously at the CSU Engines and Energy Conversion Laboratory (EECL) by Wise et al. and were originally reported in regards to studying producer gas blends[78]. Table 2.4 gives the test conditions for the CFR engine at the EECL that was used to test the MN values presented herein. Figure 2.13 shows a

photograph of the EECL CFR engine. This engine is primarily used for testing gaseous fuel blends and is currently set up to determine fuel methane number. More information on the CSU CFR engine can be found elsewhere[78].

TABLE 2.4. Parameters for CSU CFR Engine

parameter	value
engine speed	940 ± 5 RPM
ignition timing	15 °BTDC
global fuel-air equivalence Ratio	1.0
intake air temperature	40 $°C$
cooling water outlet temperature	95 ± 2 $°C$

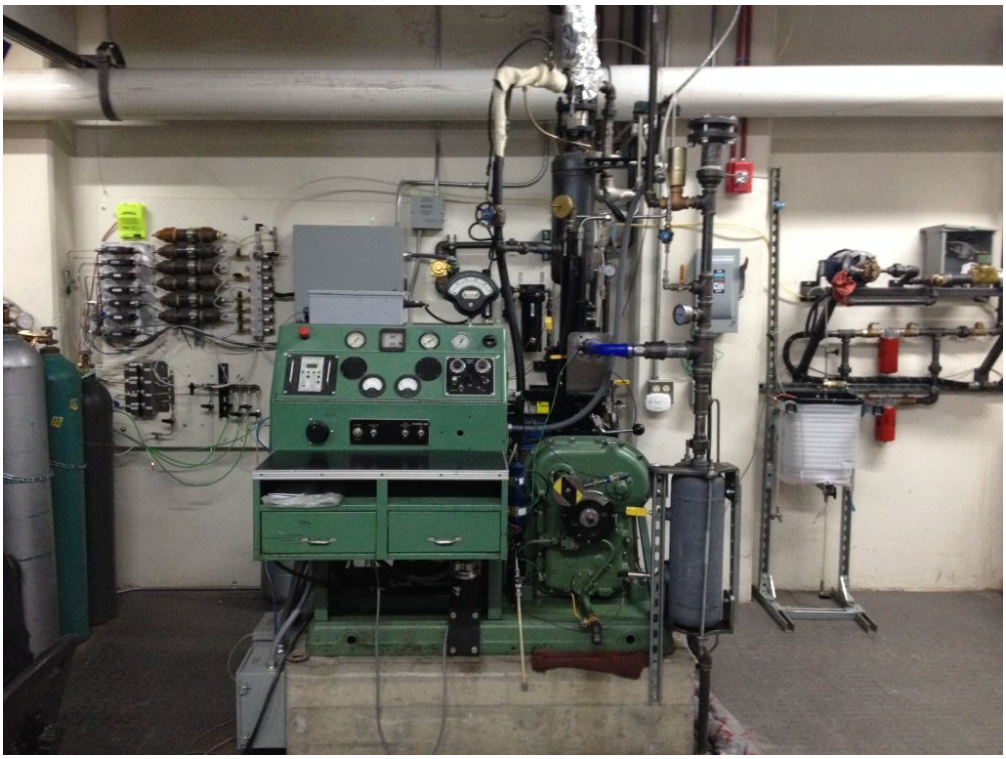


FIGURE 2.13. CSU CFR Engine

2.5. Single and Multi-zone Chemical Kinetic Modeling of HCCI and FIT Experiments

Accompanying the experimental data, zero-dimensional (single and multi-zone) models were performed using the CHEMKIN©[79] and CHEMKIN-PRO©[80] chemical kinetic modeling packages. For comparison, several chemical kinetic mechanisms were used to examine the experimental results. For the n-butanol fuel blends, mechanisms developed by Saisirirat et al.[54] and Sarathy et al.[58] were used. The Saisirirat et al. mechanism was chosen since it was one of the very few available mechanisms which included a well-tested n-heptane sub-mechanism. Several important distinctions exist between these two mechanisms, which are detailed in Table 2.5. Primarily it is important to note that while engine experiments were performed by Saisirirat et al.[54], no engine modeling was done to directly correlate against their data. Rather, the engine experiments were used to qualitatively interpret the mechanism. Therefore, the ignition behavior predicted by the Saisirirat et al. mechanism is based primarily on chemistry derived from Jet Stirred Reactor (JSR) data. Conversely, the Sarathy et al. mechanism has been validated against a very large data set, including some of the JSR data from Saisirirat et al.[54] as well as ignition experiments in both shock tubes and rapid compression machines.

However, as mentioned above, the Saisirirat et al. mechanism did include an n-heptane sub-mechanism, while the Sarathy et al. mechanism did not. Accordingly, in this work, the n-heptane sub-mechanism from Mehl et al.[72] was combined with the Sarathy et al.[58] n-butanol mechanism with the assistance of Prof. S.M. Sarathy of King Abdullah University of Science and Technology (KAUST). To merge the n-heptane model of Mehl. et al. mechanism to the existing Sarathy et al. mechanism, duplicate species and reactions were identified

and removed ensuring consistency in the base mechanisms while maintaining the predictive capabilities of the pure butanol and pure heptane models. No cross reactions were considered since interactions between the two fuels primarily occur via the smaller radicals generated from the parent fuels. It should also be noted that the Mehl et al. mechanism represents an update of the Curran et al. PRF model[81], which is the PRF sub-mechanism used in the Saisirirat et al. mechanism[54].

The simplest engine models use thermodynamic analysis of measured pressure data to calculate heat release and mass fraction burned in the engine cycle. Corresponding zero-dimensional models predict this same information by incorporating an appropriate chemical kinetic model. Specifically, single-zone models compute the average gas temperature, average cylinder pressure, equivalence ratio and residual gas fraction as a function of crank angle for prescribed initial conditions. These models are attractive as they require relatively short computational times while allowing for the use of detailed chemistry models[10]. Heat losses however are only attributed to convection based on the difference between the time-averaged wall temperature and the average gas temperature, which changes with crank angle. Radiation and heat losses due to blow-by are typically neglected.

Multi-zone models allow for the inclusion of crevices, boundary layers, and combustion chamber inhomogeneities while decoupling the fluid dynamics and the combustion chemistry. Engine flow turbulence is only indirectly accounted for as it affects the reaction through the heat transfer processes[82–84]. Like single-zone models, detailed chemical kinetics can also be accounted for while maintaining reasonable computational times. As such, multi-zone models have been successfully used to model the ignition and combustion processes in HCCI engines and, in some studies, have predicted the formation of emissions based on pressure,

temperature, and in-cylinder gas composition data[10]. Moreover, multi-zone models can also account for charge and thermal stratification where different zones are assigned various initial temperatures and compositions. In fact, it has been shown that the inclusion of thermal stratification can improve the accuracy of models based on comparison with experimentally measured pressure rise rates in HCCI engines[85]. With respect to the fidelity of multi-zone models there is no inherent limit on the number of zones. However improved accuracy can generally be achieved with more zones especially when boundary layers and crevices are accurately resolved since they may be cooler and result in higher hydrocarbon (HC) and CO concentrations.

To setup a multi-zone HCCI model, the engine geometry and operating conditions (displacement, bore, stroke, engine speed, compression ratio, etc.), the configuration of the zones and appropriate heat transfer correlations must be defined. For each zone an initial temperature, mixture composition, and residual gas fraction must also be specified[86]. Such models have received increasing attention and as mentioned are being explored to predict HC, CO, and NOx emissions and better understand the effects of crevices, boundaries, wall temperatures and operating parameters on the performance, combustion characteristics and emissions of HCCI engines[10, 85, 87–92].

Specifically, single-zone models were created for the FIT and HCCI experiments. Relevant geometrical and operational conditions were input into CHEMKIN and models were run with the mechanisms shown in Table 2.5. For the FIT experiments, a simple heat transfer model was developed to better match experimental results. CHEMKIN is unable to simulate sprays but the vaporization times for injected fuels in the FIT experiments were accounted for by starting the simulations at the minimum temperature and pressure seen in each test. Other

factors such as equivalence ratio were also taken from the experimental data and input to the CHEMKIN model. Since the measured ignition delays were primarily longer than ∼15 ms a single-zone model was deemed accurate. More information on the specifics of the FIT model can be found in Section 4.1.1. Single-zone models were also initially used to compare the various mechanisms used against the experimental HCCI data. Motored pressure curves were used to calculate heat transfer coefficients. To gain more precise modeling results however, a multi-zone model was created for comparison to the HCCI experiments. The process of developing the mulit-zone model consisted of using experimental and GT Power modeling to identify the in-cylinder temperature and pressure values at bottom dead center (BDC) just after intake valve closure (IVC). Getting these values correct is critical to correctly matching the resulting in-cylinder conditions at TDC. The in-cylinder region was split into five different zones, which were given different initial temperatures, volumes, and masses to better capture the inevitable in-cylinder stratification which exists experimentally. Other values such as equivalence ratio, engine speed, intake air temperature and intake pressure were taken from the experimental data and used in the CHEMKIN model. More information on the specifics of the HCCI multi-zone model can be found in Section 4.2.1.

TABLE 2.5. Chemical Kinetic Mechanisms for n-butanol/n-heptane considered herein.

mechanism	species	reactions	relevant fuel mixtures	experimental apparatus	temperature range	pressure range	equivalence ratios
Saisirirat et al.[a]	1046	4398	20/80m nBuOH/nC7	jet stirred reactor	530-1070 K	10 atm	0.3, 0.5, 1
			50/50m nBuOH/nC7				
			100%v nC7	HCCI Engine 1 of 4 cyl	80 $^{\circ}C$ intake	n/a	0.3
			18%v nBuOH in nC7	diesel engine motored	temperature		
			37%v nBuOH in nC7	at 1500 RPM			
			57%v nBuOH in nC7				
Sarathy et al. [b]	426	2335	100% nBuOH	laminar flame measurements	353 K	1 atm	0.6-1.6
			100% nBuOH	flat flame	n/a	40 mbar	1.7
			100% nBuOH	flat flame	n/a	15 torr	1.0
			100% nBuOH	shock tube	770-1250 K	10-80 atm	1.0
			100% nBuOH	rapid compression machine	725-855 K	15 atm	0.5, 1.0, 2.0
			100% nBuOH	jet stirred reactor	530-1070 K	10 atm	0.5, 1.0, 2.0

[a] data for Saisirirat et al. from [54, 93, 94]
[b] data for Sarathy et al. from [53, 56–58, 95–98]

CHAPTER 3

Traditional Metrics: Results and Discussion

This chapter focuses on developing a more fundamental understanding of the ON, MN, and CN scales, and how they relate to one another. Of primary importance will be the phenomenologicaly-based development of a new parameter called the 'knock length' (b_k), followed by further expansion of this concept as a fundamental basis for Kalghatgi's Octane Index. Moreover the highlighted concepts will be used to explain the ON-CN relationship on a fundamental level not previously done. Throughout, the effects of alcohols (namely ethanol and n-butanol) are considered and found to fundamentally change these concepts and relationships.

3.1. Knock Length

Knock in engines is generally accepted to occur when the pressure rise from a moving flame front across a cylinder reaches and raises the temperature in the end-gas to the point of autoignition before the flame front reaches the end-gas[25, 99]. It is this pre/unintended ignition that creates a competing pressure wave to that of the primary flame. If the ignition in the end-gas is large enough (generally thought to be on the order of 5-10% of the total fuel mass) the resulting oscillating pressure wave can be heard audibly - thus the term 'knock.' In fact, if this pressure wave is high enough, then it can physically damage the engine. The frequency of the knock is typically on the order of the speed of sound of the burn gas divided by size of the cylinder bore[100].

In equation form, therefore, knock occurs when:

$$\frac{bore_{atknock}}{s_T} \leq \tau_{ig} \tag{16}$$

where s_T is the turbulent flame speed, which is directly proportional to the laminar flame speed (s_L)[25, 101].

$$\frac{s_T}{s_L} = (1 + 0.018 \cdot \text{RPM}) \cdot \frac{\rho_u/\rho_b}{(\rho_u/\rho_b - 1) \cdot Y_{mb} + 1} \tag{17}$$

where Y_{mb} is the burned mass fraction of the mixture, and ρ the density of the burned (b) and unburned (u) mixture.

Note that both the flame speed and ignition delay (τ_{ig}) are necessarily dependent on end-gas temperatures and pressures and so will likely need to be examined across a range of temperature and pressure. It can further be shown that the laminar flame speed is related to the square root of the reaction rate[45]. One can go a step further and recognize that the reaction rate is proportional to the inverse of the homogeneous ignition delay period of the fuel/air mixture as follows:

$$s_L \approx \sqrt{(reaction\,rate) \cdot \alpha} \approx \sqrt{\frac{\alpha}{\tau_{ig}}} \tag{18}$$

where α is the thermal diffusivity and τ_{ig} the ignition delay. Combining Eq. 16 and 18 gives a relationship between what is defined herein as a "knock length" and a characteristic ignition delay τ_{ig}(T,P) where T and P are the end-gas temperature and pressure. The knock length is then the theoretical distance (bore) at which knock will occur. Knock length then can be defined as a laminar or turbulent knock length depending on which flame speed is

considered. Turbulent flame speed is dependent on the engine RPM and so may be more appropriate when discussing specific engine operating conditions or tests.

$$b_k \approx \tau_{ig} \cdot s_L \propto \tau_{ig} \cdot \sqrt{\frac{\alpha}{\tau_{ig}}} = \sqrt{\alpha \cdot \tau_{ig}} \propto \sqrt{\tau_{ig}} \tag{19}$$

Furthermore, a change in b_{knock} should be directly proportional to a change in ON since higher octane fuels would require that the physical size of the test cylinder bore be larger such that knock is achieved at or near the end-gas:

$$\Delta b_k \propto \Delta ON \propto \sqrt{\tau_{ig}} \tag{20}$$

It is tempting to use either the IQT (Eq. 9) or FIT (10) equations to relate CN to ignition delay period, however these equations (per their ASTM standards[21, 32]) are only strictly appropriate for fuels with CNs in the range of ∼30-60. However, the appendix of ASTM D6890 gives an equation (Eq. 11) for fuels outside this narrow range of DCN. According to ASTM D6890, equation 11 was determined by correlating IQT-DCN values with ignition delays for fuels including the reference fuels for the CN scale (heptamethlynonane and cetane[21]).

One can then arrive at the functional relationship in Eq. 11 (CN $\sim \tau_{ig}^{-0.66}$) by considering how the CN value of reference CN fuels change as a function of ignition delay. Westbrook et al. showed that CN values decrease "regularly" for given temperature vs. ignition delays plotted on an Arrhenius-type plot[102]. They showed that $\Delta CN \sim -ln\Delta(\tau_{ig})$; rearrangement yields Eq. 21:

$$exp(-\Delta CN) \sim \tau_{ig} \tag{21}$$

where τ is again a characteristic ignition delay and ΔCN is a characteristic or representative change in CN. The implication here is that the CN varies at a regular interval for a given temperature[102]. Taking the Taylor expansion of Eq. 21 and ignoring the smaller order terms gives:

$$\tau_{ig} = (\text{-}\Delta CN)^{O(2)} \tag{22}$$

Equation 22 can be mapped to fit the actual ON-CN scale by defining the scales in terms of the historical limits presented back in Figure 1.6 (i.e. DCN of 54 and a RON of ∼117) using the following equation:

$$CN = 54 - (\theta \cdot ON^{\alpha})^{\frac{1}{\beta}}$$

where $\theta = \frac{54^{\beta}}{117^{\alpha}}$ and α and β are parameter fits on the order of two. Equation 23 is one of the major developments of this Dissertation and represents the first equation (to the Author's knowledge) which gives a theory-based mathematical relationship between the CN and ON scales.

The best-fit of Eq. 23 for the historical data is found using $\alpha = 2.2$ and $\beta = 1.5$. Note that β of 1.5 closely approximates the functional relationship of Eq. 11. Equation 23 is plotted (black line) with the historical data from Fig. 1.6, shown here again as Figure 3.1 for convenience. The scatter of data in Figure 3.1 is quite large at high RON values, but a central hypothesis of this work is that this scatter is not necessarily inherent in the RON or DCN test methods but rather indicative of fuels with slightly different CN-ON relationships.

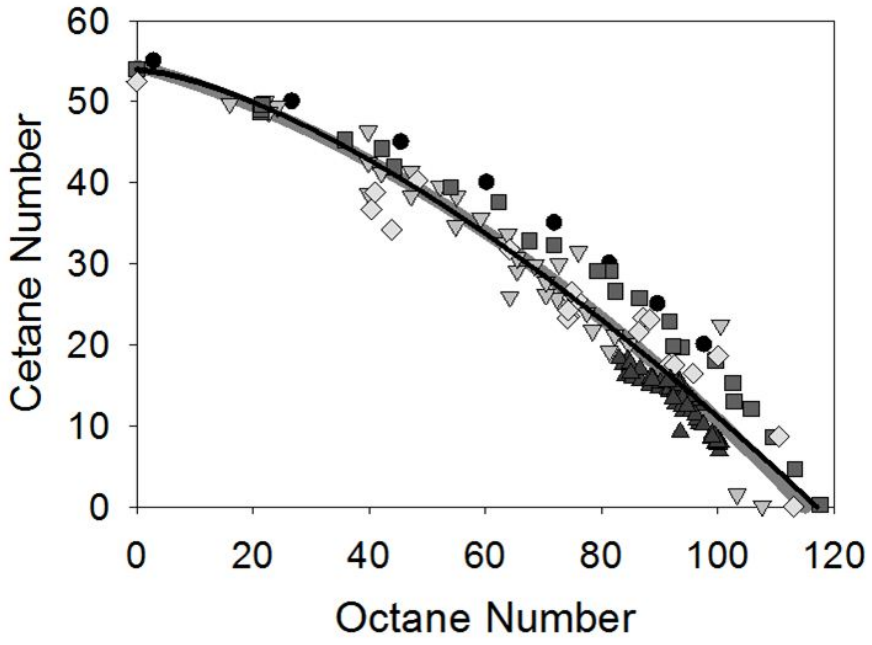


FIGURE 3.1. Cetane Number vs. Octane number data shown for five studies (156 fuels). Diamonds are a mix of surrogate gasoline fuels[35], squares a mix of gasoline and diesel fuels[36], circles an empirical correlation based on mixes of PRF, cetane reference fuels, Fischer-Tropsch naphtha, and gasoline-diesel blends[37], downward triangles a mix of "fuels distilled (not cracked) from crude oil"[34], and upward triangles are commercial gasoline blends ("leaded and unleaded")[33]. The thick gray line is a best-fit polynomial (Eq. 1) and the thin black line represents the best-fit of the CN-ON equation: $CN = 54 - (0.011 \cdot ON^2.2)^{\frac{1}{1.5}}$

3.2. Reference Fuels

Mixtures of reference fuels (PRFs and n-heptane/toluene blends) were tested in the FIT and plotted against historical trends to evaluate the ability of the FIT to yield a functional CN vs. ON relationship of the form of Eq. 23. The PRF fuels were chosen because they are the basis for the ON scale, while the n-heptane/toluene fuels were chosen since toluene reference fuels (TRFs) have recently been proposed as a better standard to model gasoline surrogates[29, 30, 60, 61]. The FIT reference fuel data is plotted (Fig. 3.2) against the polynomial-fit of the historical data from Figure 3.1; note excellent agreement not only of

the reference fuels with one another, but also in correlating DCN values with historical CN values.

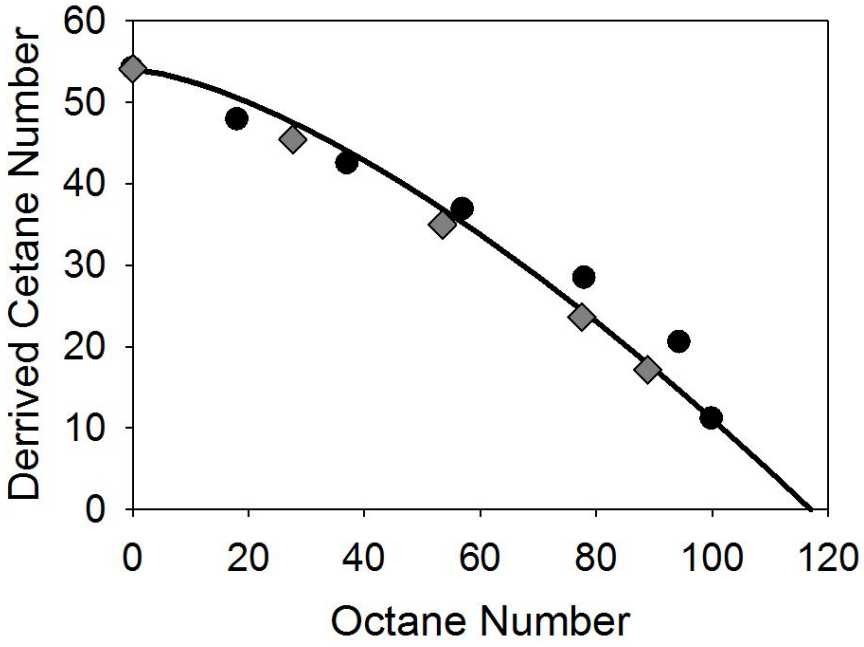


FIGURE 3.2. DCN vs. RON for various reference fuel mixtures: PRF (circles) and toluene/n-heptane (diamonds) from this study, solid black line is the polynomial fit of historical data (CN vs. RON) from Fig. 3.1

At this point it is also important to recall that the FIT defines the ignition delay as the point at which the combustion chamber pressure rises +0.2 bar above the injected pressure and therefore is not exactly determining the true ignition delay under the tested conditions. Thus, one can calculate a "corrected" ignition delay defined as the time from the minimum chamber pressure to the maximum rate of pressure rise shown in Figure 3.3.

As ignition delays become longer and longer, there exists a greater opportunity for the device-measured ignition delay to be different than the actual (i.e. "corrected") ignition delay. Moreover, despite the excellent agreement for the FIT data seen in Figure 3.2, it is important to highlight that the FIT is not strictly designed to give DCN values for fuels below about a CN of 30[32]. With all of this in mind, ignition delays were also obtained from

each FIT experiment and the results plotted in Figures 3.4 and 3.5. Also in these figures are constant volume CHEMKIN simulations using the FIT experimental parameters and the Mehl et al. gasoline surrogate chemical kinetic model, which includes n-heptane, i-octane, and toluene[72]. As part of modeling the FIT a simple heat transfer correlation was used to aid in convergence and better capture the observed pressure traces. More information regarding this heat transfer correlation and other FIT simulation parameters is included in Section 4.1.

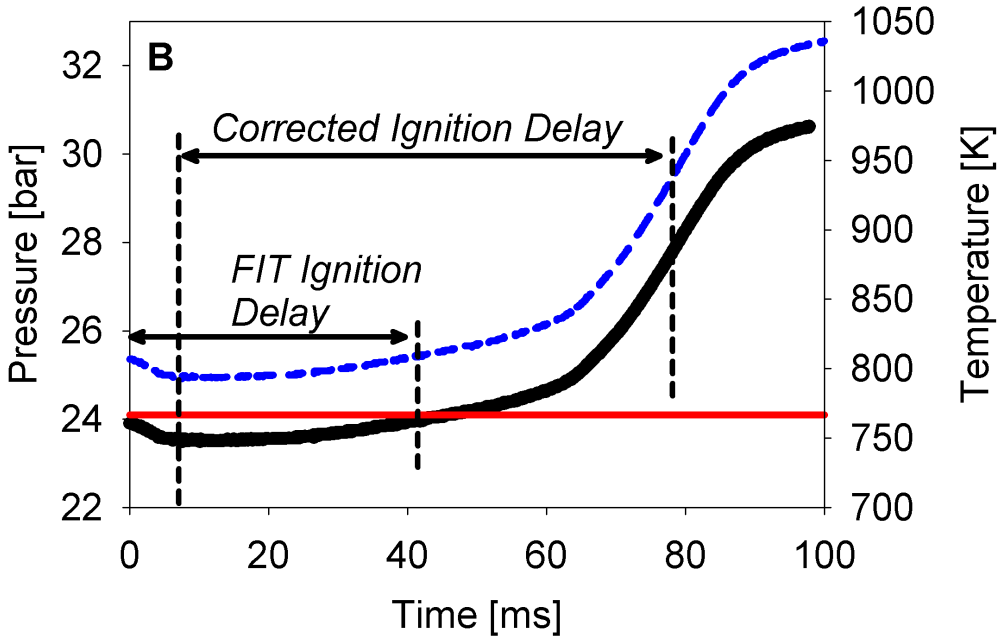


FIGURE 3.3. FIT device trace showing the pressure trace (thick black line) for a typical n-butanol ignition test in the FIT, calculated temperature (dashed blue line), and the FIT trigger point (thin red line) as well as the FIT device ignition delay and the ignition delay accounting for vaporization and corrected to coincide with the maximum rate of pressure rise.

Overall, there is excellent agreement between the model results and the ignition delay as measured from the minimum pressure to the maximum rate of pressure rise. Note however that the 70% toluene mixture (Tol70) is not shown as there was poor agreement with the model. It is assumed here that this error was due to excessive heat loss to the walls of the

vessel as a result of a long ignition delay. The pressure rise rate of Tol70 was also too slow to accurately determine a "corrected" ignition delay. Interestingly, the pressure rise rate of Tol70 (a RON of 89) was even slower than pure i-octane (a RON of 100). More testing with higher RON fuels is required to investigate this phenomena, but one possibility is that the lack of any LTC in toluene ignition may exacerbate reactivity differences in reactivity-controlled combustion conditions especially considering the much lower testing temperature of the FIT compared to the end-gas temperature for the RON and MON tests (which is closer to 900-1000 K)[103]. Further support of this hypothesis is that ethanol, another high RON fuel, was extremely difficult to ignite in the FIT. Only very low RON mixtures of n-heptane/ethanol fuels were able to be run in the FIT - above about 20 vol% ethanol, no ignition could be measured.

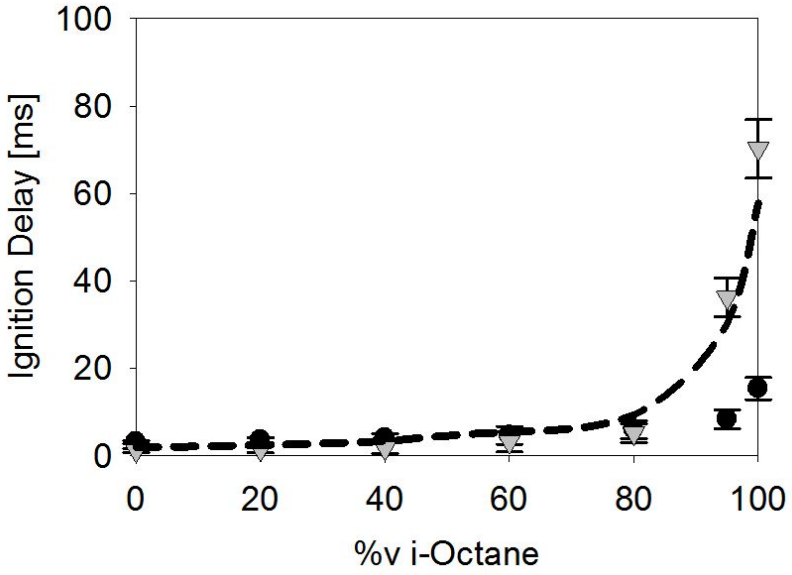


FIGURE 3.4. Ignition delays as a percent volume of i-octane in the PRF mixture. The black circles are FIT reported ignition delays, the gray triangles are the ignition delays measured as the time from minimum pressure to the maximum rate of pressure rise, and the black dashed line represents the CHEMKIN model results using the Mehl et al. mechanism[72].

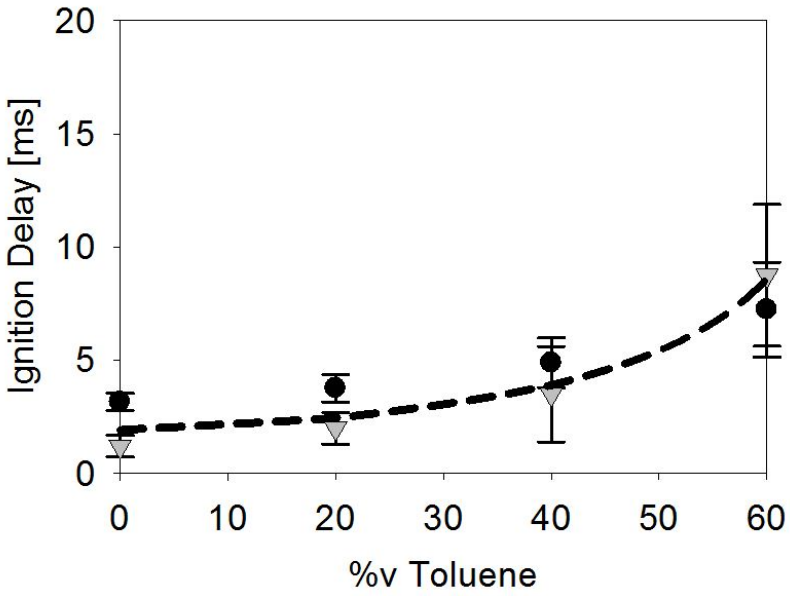


FIGURE 3.5. Ignition delays as a percent of toluene in the toluene/n-heptane mixture. The black circles are FIT reported ignition delays, the gray triangles are the ignition delays measured as the time from minimum pressure to the maximum rate of pressure rise, and the black dashed line represents the CHEMKIN model results using the Mehl et al. mechanism[72].

3.3. Effect of Alcohols

To further explore the impact that non-traditional fuels have on the ON-CN relationship observed above, n-heptane/n-butanol mixtures were also tested (Figure 3.6). The FIT injects a nearly constant fuel volume and therefore fuel properties like viscosity and density have a large effect on testing conditions in the FIT, namely the global fuel-air equivalence ratio (ϕ). By weighing the fuel before and after each set of FIT tests, ϕ was determined and found to correlate very well with fluid viscosity and density. The actual ϕ decreased approximately linearly from 0.5 for pure n-heptane to 0.2 for pure n-butanol. More information regarding the effect of fuel viscosity and density can be found in Chapters 4 and 5, but it is important here to highlight that, due to the physical effects of the fuels considered, constant ϕ comparison between PRFs and alcohol fuel mixtures could not be obtained. Modifying the FIT to operate under constant ϕ conditions is a topic of further research, but initial results

show that the variance in ϕ actually did not have a major impact on the measured DCN values. As proof of this, n-heptane/n-butanol values from this work were compared to similar mixtures tested by Haas et al.[38] in an IQT and a good correlation was found. Lastly, the tested ϕ was considered in the CHEMKIN models and so the ϕ-variance is captured in the figures/comparisons below.

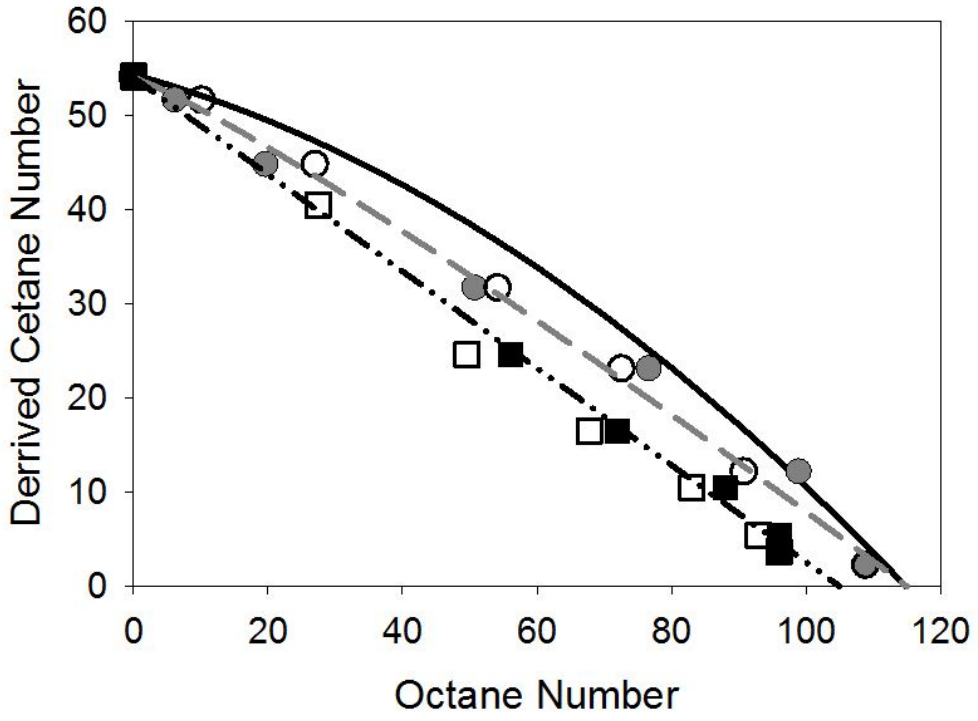


FIGURE 3.6. DCN vs. RON for reference fuels and butanol mixtures. The solid black line is the polynomial fit from Figure 3.1. The closed circles are ethanol/n-heptane mixtures combining data from two different studies[38, 104], the open circles are the ethanol data but using a linear-by-molar blending estimate, and the dashed gray line is the best-fit ethanol mixture line of the form of Eq. 23. The black squares are n-butanol/n-heptane mixtures using measured data from this study, the open squares are n-butanol/n-heptane data but using linear-by-molar blending estimates, and the black dash-dot-dot line is the best-fit butanol mixture line of the form of Eq. 23.

Figure 3.6 shows both measured and estimated RON values using a linear-by-molar blending approach. An important finding of this work is that it appears that the measured values for RON match well with the values determined on a linear-by-molar mixing basis.

Ethanol data from[38, 104] and historical data from Figure 3.2 are also included in Figure 3.6 and it is evident that the relationship between DCN and ON for alcohol blends differs from that of the reference fuels. Similar results have been observed using IQT data[38]. As noted by Foong et al.[104] and Andersen et al.[28], ethanol does not strictly blend linearly with molar percentages, but molar blending values do appear to be a good approximation across the whole range of ON/CN values. The data in Figure 3.6 support these studies and extends the argument to n-butanol. In Figure 3.6 are also best-fit lines for ethanol/n-heptane and n-butanol/n-heptane mixtures using Eq. 23. A summary of these parameters for the tested fuel blend types can be found in Table 3.1 and allow the prediction of ON/CN values for a range of fuels.

TABLE 3.1. CN-ON Equation Parameters for Tested Fuel Types

fuels	α	β	θ
hydrocarbons	2.2	1.5	0.011
ethanol/n-heptane	1.7	1.5	0.125
n-butanol/n-heptane	1.5	1.5	0.369

Haas et al. similarly observed that butanol isomer mixtures deviated from corresponding PRF mixtures with respect to the ON-CN relationship[38]. The explanation by Haas et al. was that n-butanol, as well as ethanol, 2-butanol, and i-butanol, all had roughly equivalent H atom abstraction coefficients by the OH radical as that of n-heptane. Thus, n-butanol and n-heptane competed roughly equally for the OH radical and approximately in proportion to their molar blending percentage. However, whereas the OH abstraction of H atom from the n-heptane molecule predominantly leads to more chain-branching reactions, the H atom abstraction from n-butanol leads to the creation of the relatively less reactive HO_2 molecule. Therefore, in going through n-butanol, the overall effect is to exchange a very reactive OH

radical with the comparatively much less reactive HO_2 radical. The tendency to go through the less reactive HO_2 radical effectively slows the overall combustion reaction.

Figure 3.7 depicts the four butanol isomers with the various bond strengths. It is evident here that the hydrogen on the α carbon is the most weakly bonded hydrogen for every case except t-butanol, which does not have an α carbon. Reactions 23 through 25 show the various H-abstraction paths possible through the parent n-butanol fuel molecule. Here it can be seen that both secondary H-abstractions (Eq. 24 and 25) preferentially result in an HO_2 molecule.

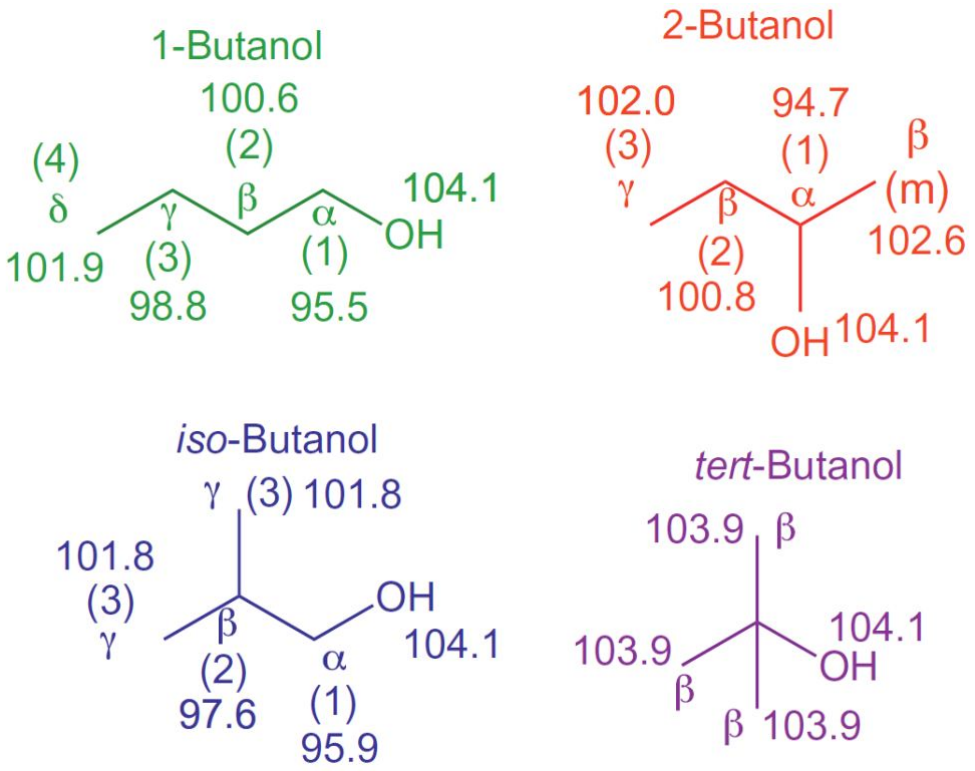


FIGURE 3.7. Butanol isomers showing relative bond strengths of the various hydrogen bonds.Used with permission from[58].

$$OH + C_4H_9OH \rightarrow \alpha\text{-}C_4H_8OH + H_2O \tag{23}$$

$$O_2 + \alpha\text{-}C_4H_8OH \rightarrow \alpha\text{-}C_4H_8O + HO_2 \tag{24}$$

$$O_2 + \alpha\text{-}C_4H_8OH \rightarrow \alpha\text{-}C_4H_7OH + HO_2 \tag{25}$$

A similar H atom abstraction-based argument can be made in the present case when considering reference fuels. Abstraction coefficients were taken from two of the mechanisms considered herein[58, 72] and plotted across the primary Negative Temperature Coefficient (NTC) range, i.e. approximately 500 K to 900 K. Shown in Figure 3.8, n-butanol has nearly the same rate of H abstraction by OH as n-heptane and so competes most strongly for the available OH radicals. However, the other fuels are 2-3 times less effective at consuming the OH radicals relative to n-heptane. For these fuels, the n-heptane is consumed relatively faster than in an equivalent n-butanol/n-heptane mixture. This faster rate of n-heptane consumption is most easily observed as the retardation of the drop in CN as mixtures move higher in RON value (i.e. higher in the percent of lower reactivity fuel refer to Figure 3.6).

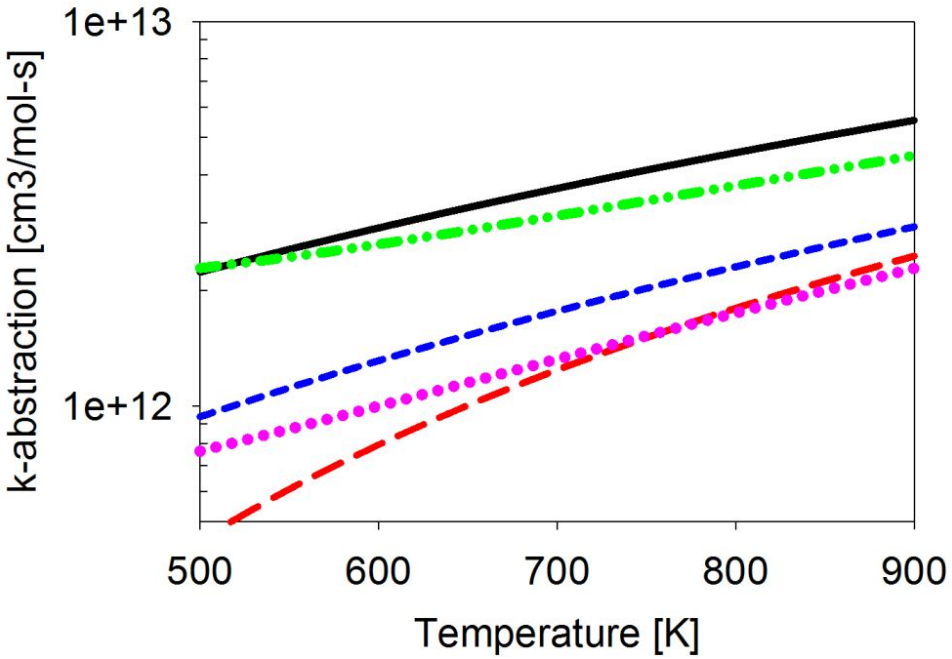


FIGURE 3.8. Abstraction rate coefficients for H atom abstractions by OH radicals for the most easily abstracted H atom from each parent fuel. Solid black line is n-heptane, green dash-dot-dot n-butanol, blue short-dashed line toluene, dotted pink line t-butanol, long-dashed red line i-octane.

3.4. KNOCK LENGTH APPROACH TO PRFS

Literature data[101, 103, 105] indicate that RON tests operate in the C.R. range of 4-9 and end-gas conditions of 700-900 K and 30-40 bar. Rapid compression machine data from Griffiths et al. further show ignition delays at ∼900 K have a basic correlation to RON values for PRF blends[105]. The Sarathy*, Mehl et al., and Ranzi et al. chemical mechanisms[69, 72, 106] were used to simulate homogeneous ignition delays and freely propagating laminar flame speeds for the gasoline-range fuels considered herein. As an example, laminar knock lengths for n-butanol and PRF fuels were calculated and plotted in Figure 3.9 along with approximated RON end-gas temperature for i-octane. From Fig 3.9 it is clear that for n-butanol to have the same b_k as i-octane under RON conditions, or rather for n-butanol to knock at the cylinder wall, the end-gas temperature must be lowered. This is accomplished

experimentally by reducing the compression ratio, thus resulting in a lower measured RON value for n-butanol. Also apparent from Figure 3.9 is the phenomenological basis for fuel sensitivity. "Sensitive" fuels such as n-butanol have a much steeper decrease in b_k throughout the RON/MON end-gas temperature range and therefore will manifest as having a lower RON than MON value whereas alkane fuels (i.e. PRF) are more consistent in b_k and thus less sensitive. Knock length is perhaps even more enlightening for methane number fuels since it helps to resolve unexpected behavior of low MN fuels.

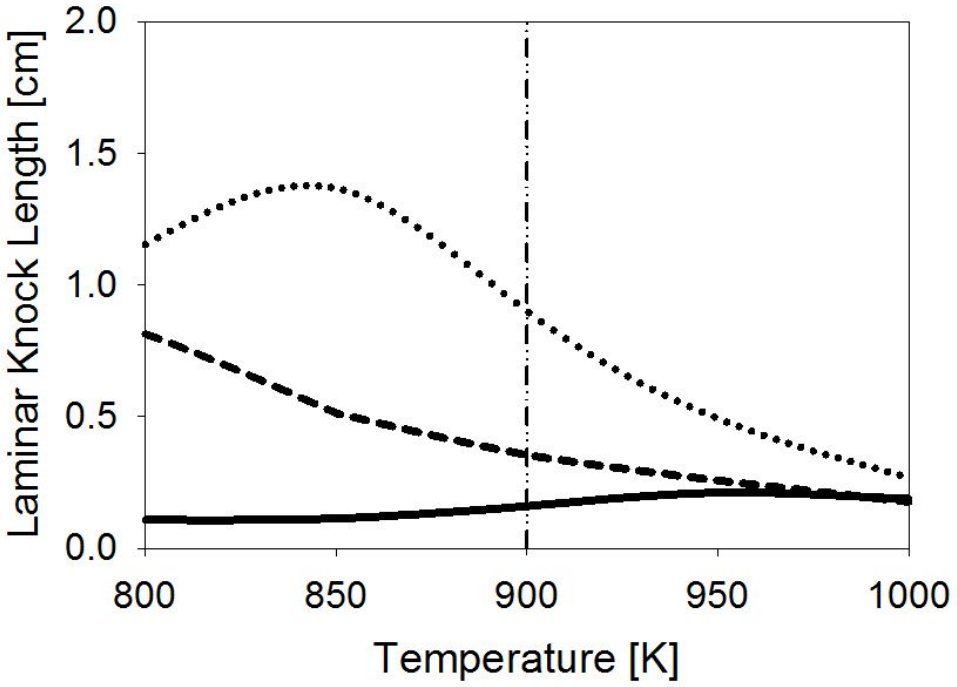


FIGURE 3.9. Calculated laminar knock lengths for n-heptane (black solid line), i-octane (dotted line), and n-butanol (dashed line). Also shown is the corresponding RON (dashed-dot-dot vertical line) test temperatures for i-octane. Simulations run at ϕ of 1.0 and 35 bar.

As suggested above and shown by Kalghatgi and others, the reactivity of fuels is also dependent on the engine conditions. Kalghatgi found that the in-cylinder temperature at 15 bar was an excellent prediction of the peak temperature conditions, which is the condition at which the end-gas may or may not knock. It is therefore also appropriate to consider the

knock length at these conditions. Similar to Figure 1.8, Figure 3.10 shows the calculated knock lengths based on the aforementioned Octane Index conditions and the approximate turbulent flame speed (from Eq. 17). As in Figures 1.8 and 3.9, the relative fuel sensitivities are obvious in Figure 3.10. Both n-heptane and i-octane change relatively little from the RON to the MON test, whereas n-butanol changes by a factor of three. Interestingly, the calculated knock lengths at various places between the RON and MON tests are all on the order of magnitude of the physical size of a CFR piston bore. As a reminder, these conditions are not meant to be reflective of the end-gas conditions of the actual knock length, but rather serve as a means for comparison and analysis.

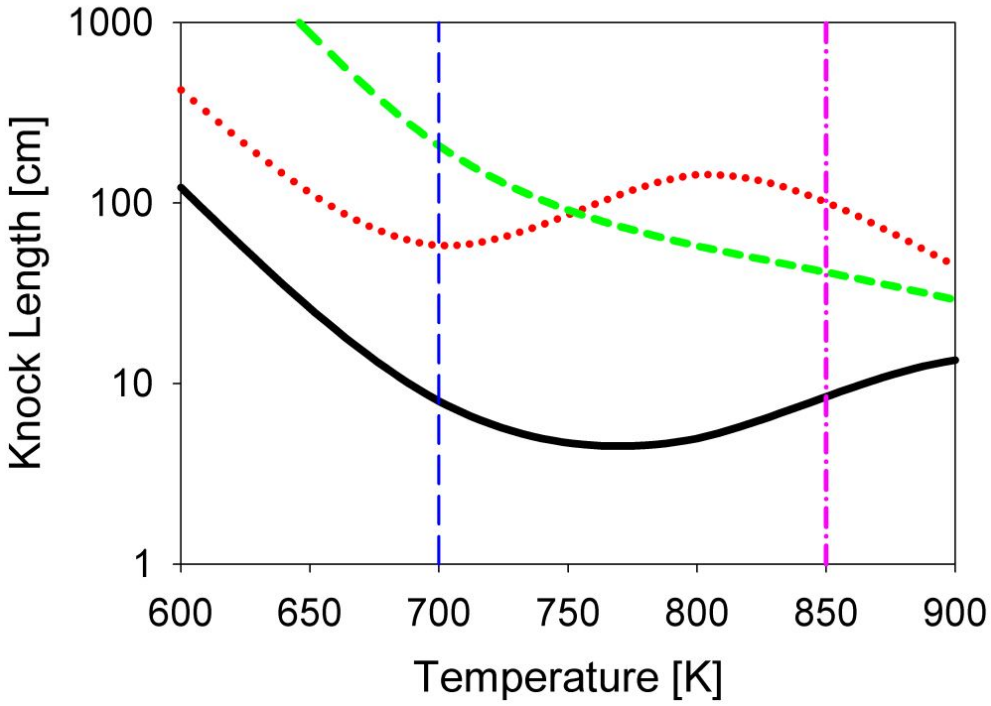


FIGURE 3.10. Calculated turbulent knock lengths for n-heptane (black solid line), i-octane (red dotted line), and n-butanol (green dashed line). Also shown are the corresponding RON (blue dashed vertical line) and MON (pink vertical dot-dash line) test temperatures at a pressure of 15 bar. Simulations run at ϕ of 1.0.

Another way of thinking about Figure 3.10 is that future engine designs are likely to transition to "beyond RON" conditions[27]. Referring back to Figure 1.7, this means that the T_{comp15} will decrease. There are two ways of interpreting the implications: (1) that for a given temperature the end-gas pressure will be higher, or (2) that for a given pressure the end-gas temperature will be lower. The result at TDC will be a higher pressure at the same or slightly lower temperature. Sensitive fuels have two advantages over non-sensitive (i.e. fuels that exhibit NTC behavior):

(1) Sensitive fuels such as n-butanol relatively increase in knock resistance (i.e. knock length) vs. non-sensitive fuels when moving lower in the likely end-gas temperature range for a given pressure.

(2) Sensitive fuels such as n-butanol relatively increase in knock resistance (i.e. knock length) vs. non-sensitive fuels when moving lower in the likely end-gas pressure range for a given temperature.

Figure 3.11 displays both of these characteristics. The top portion of Figure 3.11 shows that as pressure is increased from 15 to 35 bar, n-butanol only drops 20-30% in knock length, whereas i-octane drops 30-40%. The result is that n-butanol relatively increases in knock resistance as pressure is increased for a given temperature. This behavior suggests that the low temperature chemistry pathways of non-sensitive fuels are more sensitive to pressure than those of sensitive fuels. Similarly, the bottom portion of Figure 3.11 shows that for a given pressure (35 bar) the knock length of i-octane stays fairly constant as temperature is decreased while n-butanol increases steadily in knock resistance.

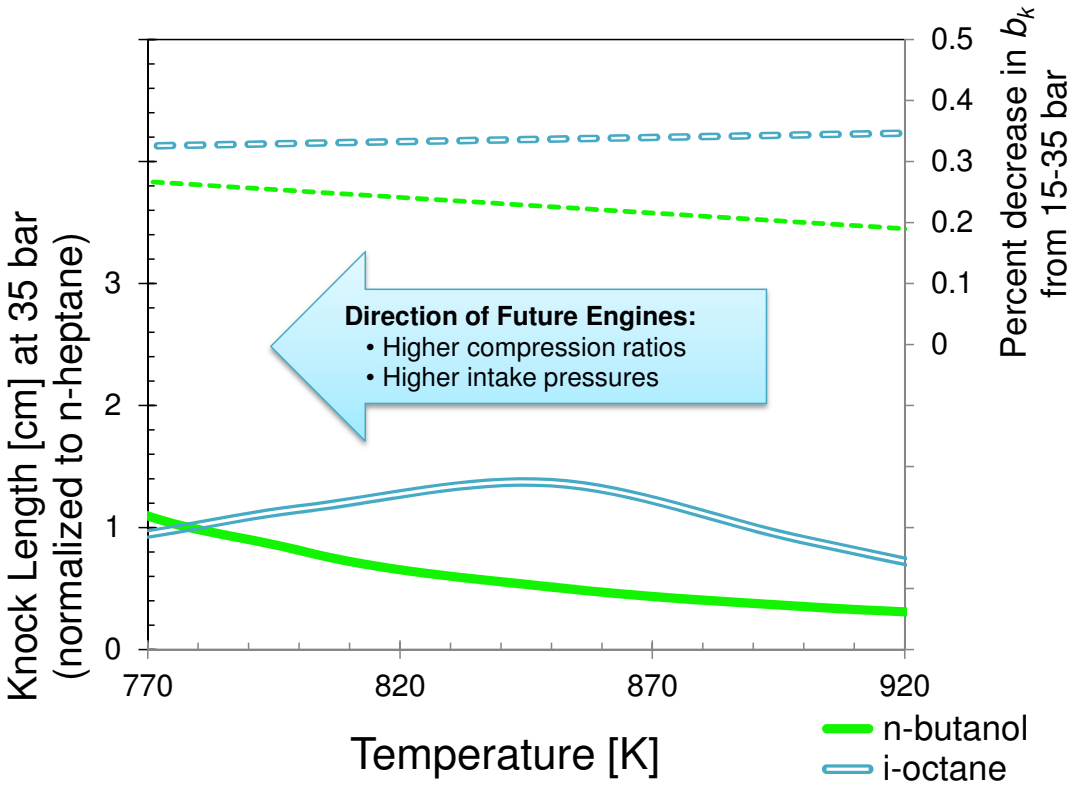


FIGURE 3.11. Laminar knock length for i-octane and n-butanol normalized to n-heptane at 35 bar (bottom). At top are the average percent decreases in knock length for these two fuels in going from 15 to 35 bar.

3.5. REFERENCE METHANE NUMBER EXAMINATION

In addition to the gasoline-range fuels tested, five reference blends of methane and hydrogen were also examined. The experimentally measured methane numbers for these fuels (see Table 3.2) were originally measured by Wise et al.[78] but they are examined in detail here to compliment the PRF/RON and CN data above. Additionally, the nature of the methane number scale makes it an ideal example of the importance of the knock length. Of primary interest is the effect of the extremely high flame speed of hydrogen and the non-linear impact this can have on the overall mixture reactivity in SI engines.

To provide input to Eq. 16, 18, and 19, homogeneous constant volume ignition delay periods and freely propagating laminar flame speeds were calculated for the methane number blends using CHEMKIN (Figures 3.12 and 3.13). Natural gas mechanisms from Healy, et al.[107] and Bourque, et al.[108] were used to perform the calculations. Laminar knock lengths were then calculated (Figure 3.14). All data were simulated at 60 bar and stoichiometric conditions to coincide with peak pressure conditions from the experiments. Choosing appropriate pressure and temperature conditions to represent the end-gas is critical to target an accurate knock length. Since the pressure wave travels much faster than the laminar flame speed, the end-gas should be at or near peak cylinder pressure when the flame front arrives, therefore b_k values were calculated at average peak cylinder pressure.

In the absence of actual pressure data, a Wiebe function could be used to approximate the burn profiles for most SI cases and end-gas temperatures could be approximated via polytropic equations. Alternatively, a lower reference temperature could be targeted such as in the Octane Index. In this case the knock length would not, necessarily, be equivalent to experimental data but would serve to provide qualitative analysis.

TABLE 3.2. Reference Methane Number Data

fuel name	methane number	compression ratio at knock detection	max combustion pressure [bar]
MN20	19.14	9.83	60.5
MN40	41.44	10.68	59.0
MN60	61.18	11.35	60.1
MN80	80.05	13.58	62.4
MN100	100	16.00	64.9

What is evident from the knock length data but obfuscated from both the ignition delay data and flame speed data is that as MN decreases the increased flame speed of hydrogen

starts to dominate and directionally lowers the propensity for knock. For example, for MN20 to have a lower b_k or methane number than MN40 (or equal for the same C.R.) the end-gas temperature needs to relatively increase. The increased flame speed and heating value of MN20 over MN40 results in a shorter combustion duration and greater overall energy release and therefore a higher end-gas temperature which results in a lower relative knock length for a given C.R., or rather a lower C.R. for a given knock length. Alternatively, via the arguments summarized by Eq. 19, and the fact that the estimated end-gas temperature for all the MN data is approximately 1000 K (as calculated from peak cylinder pressure), one can plot the square root of ignition delay as a proxy for b_k vs. MN (Figure 3.15.

Examining $(\tau_{ig})^{0.5}$ as proxy for b_k in this way allows for a plot analogous to Figure 3.1 but with respect to reference MN fuels: b_k vs. MN (Figure 3.15). Continuing along this line of thought would make way for a diesel or dual fuel application where the inverse of Figure 3.15 could allow investigation of high reactivity fuels for high pressure diesel-like engines using high hydrogen or otherwise low MN fuels.

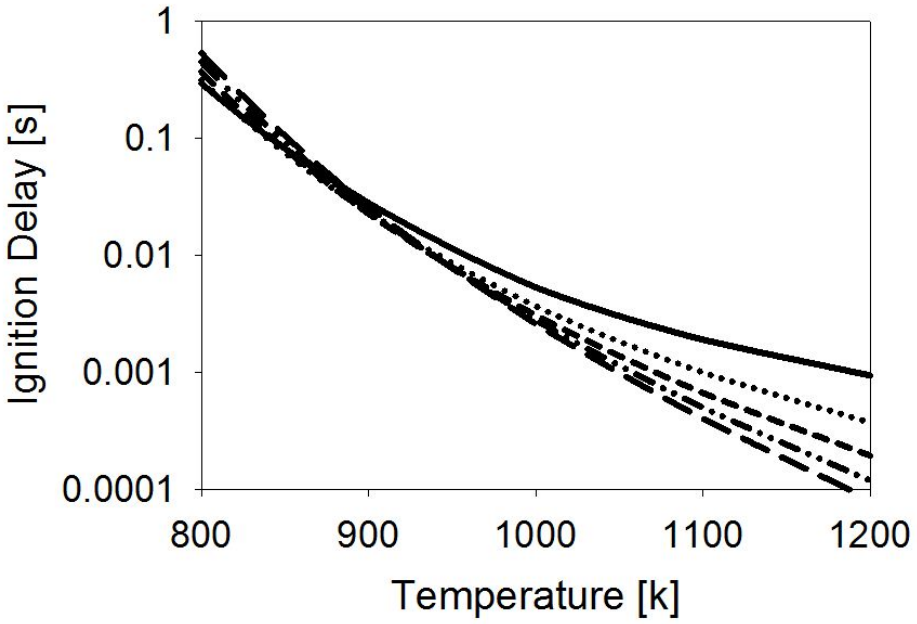


FIGURE 3.12. Calculated ignition delay times for MN fuels stoichiometrically combusted in air at 60bar: long dashed line is MN20, dash-dot-dot line is MN40, short dashed line is MN 60, dotted line is MN80, and the solid line is MN100.

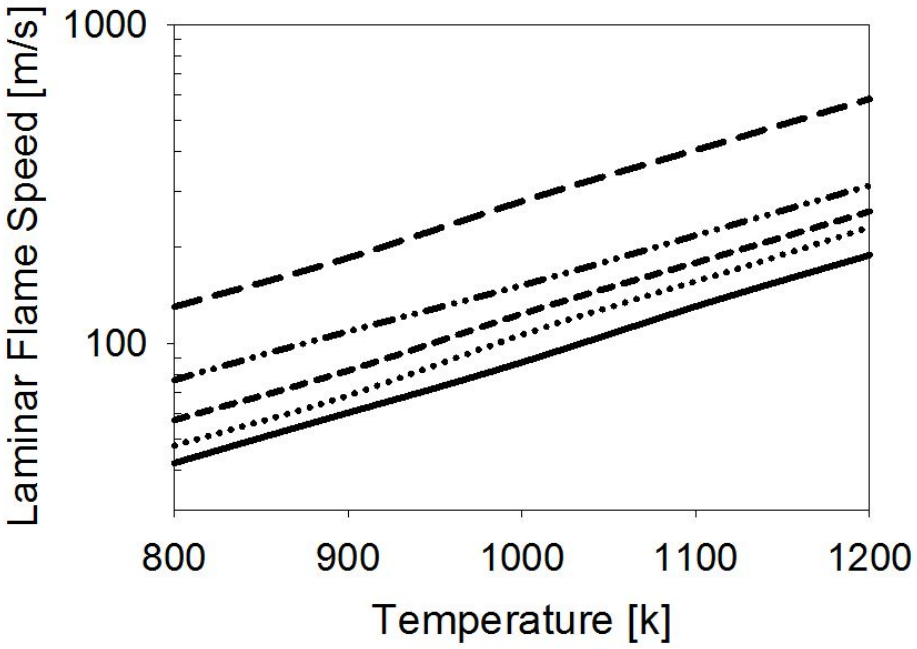


FIGURE 3.13. Calculated flame speed for MN fuels stoichiometrically combusted in air at 60bar: long dashed line is MN20, dash-dot-dot line is MN40, short dashed line is MN 60, dotted line is MN80, and the solid line is MN100.

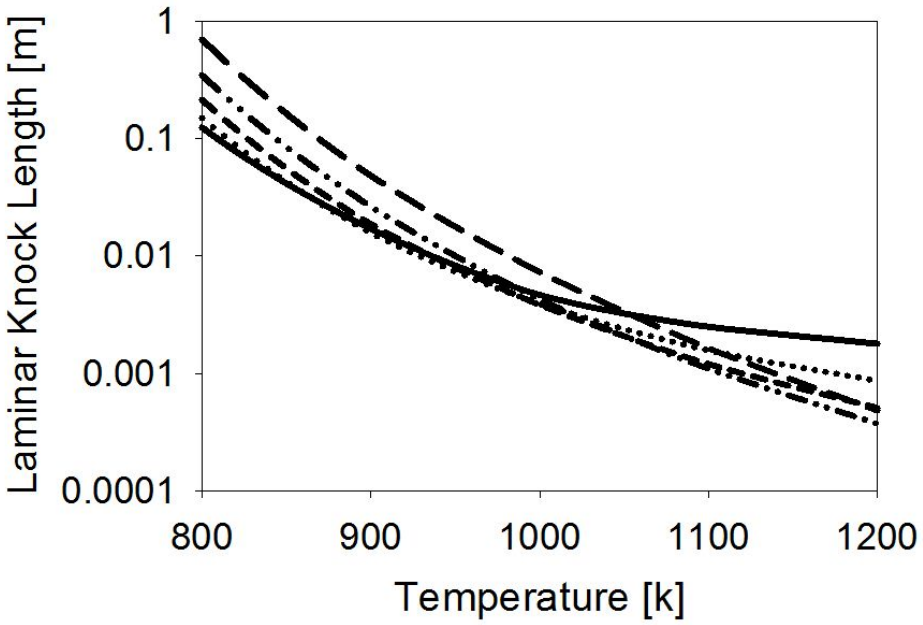


FIGURE 3.14. Calculated laminar knock length for MN fuels stoichiometrically combusted in air at 60bar: long dashed line is MN20, dash-dot-dot line is MN40, short dashed line is MN 60, dotted line is MN80, and the solid line is MN100.

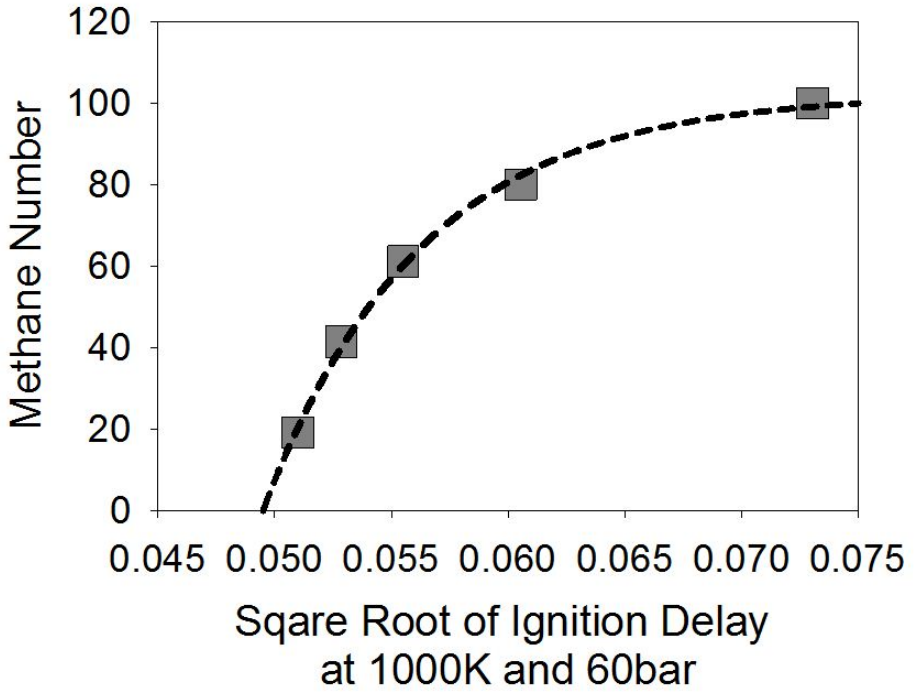


FIGURE 3.15. Square root of calculated ignition delay as proxy for bk vs. MN, squares are data points, dashed line is a curve fit.

CHAPTER 4

Future Metrics: Results and Discussion

This chapter builds on the results of Chapter 3 in that the use of the FIT is extended to examining an example of advanced engine technology, i.e. an HCCI engine. A chemical mechanism developed as part of this work was used to compare the FIT and HCCI engine results. Single and multi-zone models were developed for analysis of the FIT and HCCI engine, respectively. The results showed that the low temperature heat release proves critical in understanding ignition timing in HCCI. The concepts surrounding knock developed in Chapter 3 are extended to HCCI operation and a new metric called the HCCI number is developed and examined. Lastly, the applicability of the HCCI number is investigated and two methods are presented to predict this metric using apparatuses which are simpler and consume less fuel than an engine.

4.1. FIT Experimental Results

Fourteen different blends of i-octane, n-heptane, and n-butanol were tested in the FIT, consisting of 28 test runs with 25 ignition measurements for each test run, totaling 350 individual tests (not including duplicate runs). Figures 4.1 and 4.2 summarize these test results, wherein n-heptane is the "high reactivity fuel" and n-butanol or i-octane are the "low reactivity" fuels. As explained previously, the FIT records a Derived Cetane Number (DCN), which generally varies inversely with RON[37] insofar as fuels with high RON exhibit low DCN and vice versa.

The FIT (like the IQT) reports the ignition delay period based on an internal threshold response to the combustion pressure rising a set amount (+0.2 bar for the FIT) above

the base pressure (see Figure 2.3(b)). This technique can produce erroneous ignition delay periods since low temperature chemistry can result in a small pressure rise prior to primary ignition. For the high reactivity diesel fuels that these devices were originally designed to accommodate, the low temperature pressure rise is not problematic for DCN measurements since it occurs at time periods very close to that of the primary ignition event. However, for fuels with longer ignition delay periods such as those tested in the present study, the low temperature pressure rise can be misinterpreted as the primary ignition event. Additionally, there is a decrease in system pressure and temperature due to fuel vaporization, which is also evident in Figure 2.3(b). Accordingly, reported here are both the FIT-reported ignition delay period along with an ignition delay period calculated as the time from minimum pressure to the peak pressure rise rate (PPR). Both ignition delay periods along with the model results are presented in the next section. For the CN-ON data presented in Chapter 3, the FIT-trigger ignition delay was used since it has been statistically correlated to the DCN values - additionally, the FIT-trigger is more indicative of LTHR and may correspond better to light knock conditions than the main ignition event.

The results of this study further show that the injected fuel-air global equivalence ratio (ϕ) changes due to the near constant volume injection style of the FIT and the different physical properties of the fuels tested. In Figure 4.4 the measured fuel viscosity is plotted against the average value of the global equivalence ratio tested for each fuel mixture. Note that density and bulk modulus also showed strong correlations except for the toluene blends, which deviated from the rest of the fuels tested.

To determine a global equivalence ratio for a given test, the fuel was weighed before and after each test and the resulting mass difference was averaged over the 27 injections for that

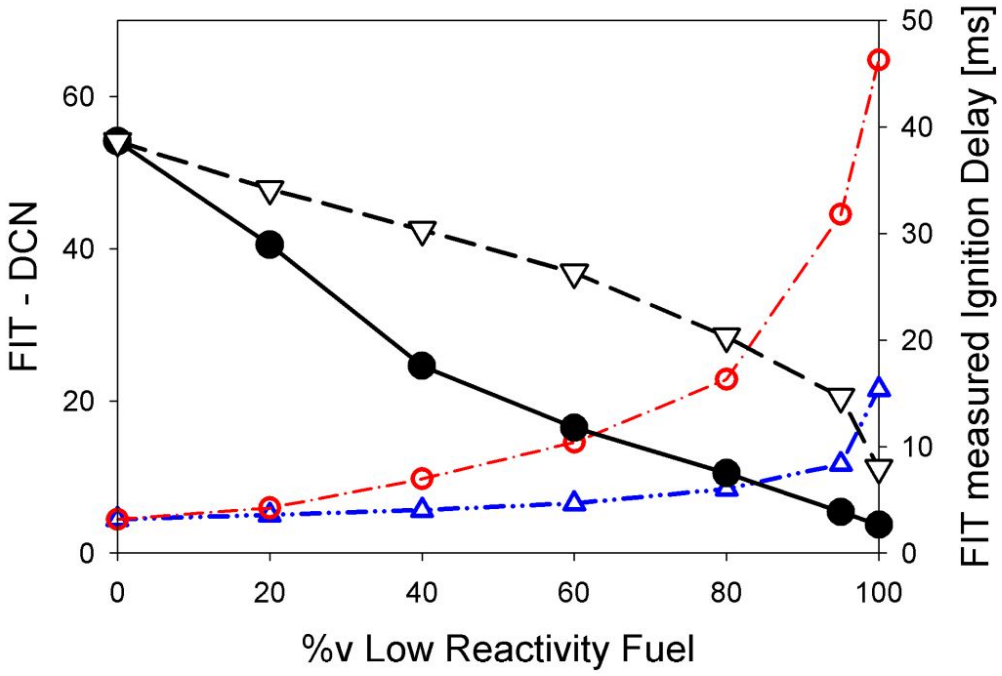


FIGURE 4.1. FIT Derived Cetane Numbers for blends of n-heptane/n-butanol (closed circle, solid line), n-heptane/i-octane (open triangle down, dashed line) per ASTM D7170 as a function of the percentage of low reactivity fuel component presented on a volume basis.

test. The FIT is equipped with a pressurized air system that is used to purge all the lines before and after a test. The fuel was gravimetrically weighed using a standard high precision scale (accurate to ± 0.001 g) before and after each set of 27 injections. The built-in air purge system ensured that the system was purged completely prior to weighing each sample. Next, the amount of air for each test was calculated based on ideal gas assumptions and the individual injection temperature and pressure readings. The assumption of ideal gas was compared versus both Peng-Robinson and Lee-Kesler real-gas methodologies and deviation from ideal gas assumption was less than 1% error. It is observed that for the PRF fuels, the tested ϕ is essentially constant at a value of approximately 0.5, whereas the tested ϕ varies for the nBuOH mixtures from approximately 0.2 to 0.5. Efforts to understand how the FIT can modulate ϕ are further explored in Chapter 5.

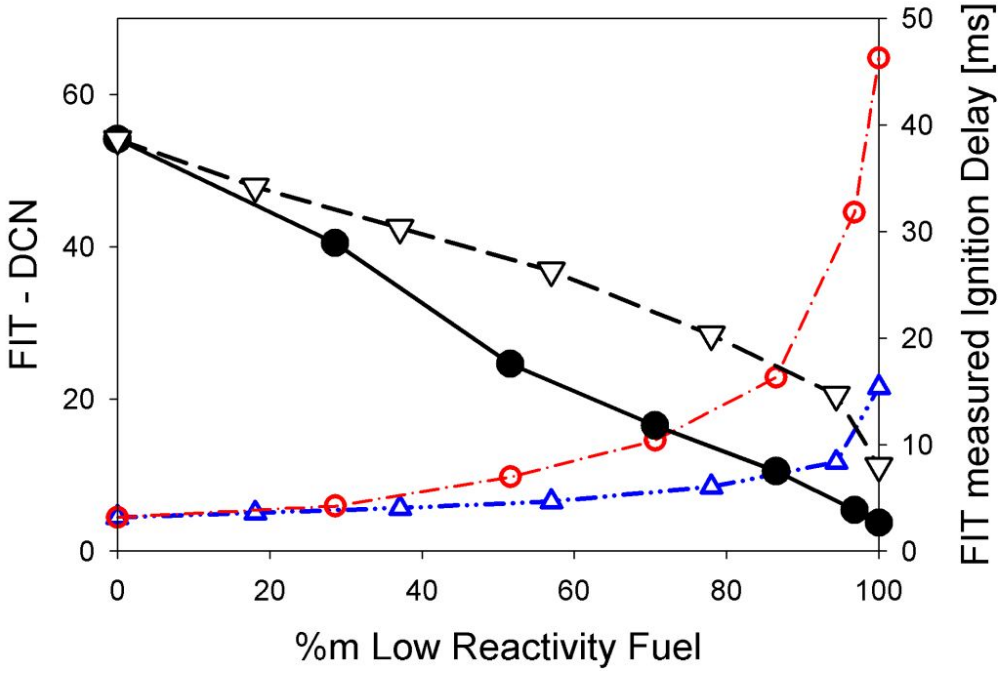


FIGURE 4.2. FIT Derived Cetane Numbers for blends of n-heptane/n-butanol (closed circle, solid line), n-heptane/i-octane (open triangle down, dashed line) per ASTM D7170 as a function of the percentage of low reactivity fuel component presented on a molar basis.

The experimental results in Figures 4.1 and 4.2 support previous findings that fuel blends with significant amounts of alcohols can exhibit very different ignition delay periods in an IQT or FIT[38] as compared to traditional petroleum fuels. The present experiments further show that n-butanol blends behaved unlike PRF blends when comparing the autoignition behavior (e.g. DCN values) as a function of the percentage of low reactivity component. Some of this behavior could be due to the tertiary carbon in i-octane where there are an increased number of primary carbon sites. H-atom abstraction by OH is highly prohibited at the primary carbon sites and so a higher percentage of primary carbons should directionally result in lower H abstraction - as explored in Chapter 3. As mentioned in Chapter 3, Haas et al.[38] attributed the concave down-like behavior of t-butanol/n-heptane blends to a lower OH hydrogen abstraction rate from t-butanol (compared to primary and secondary

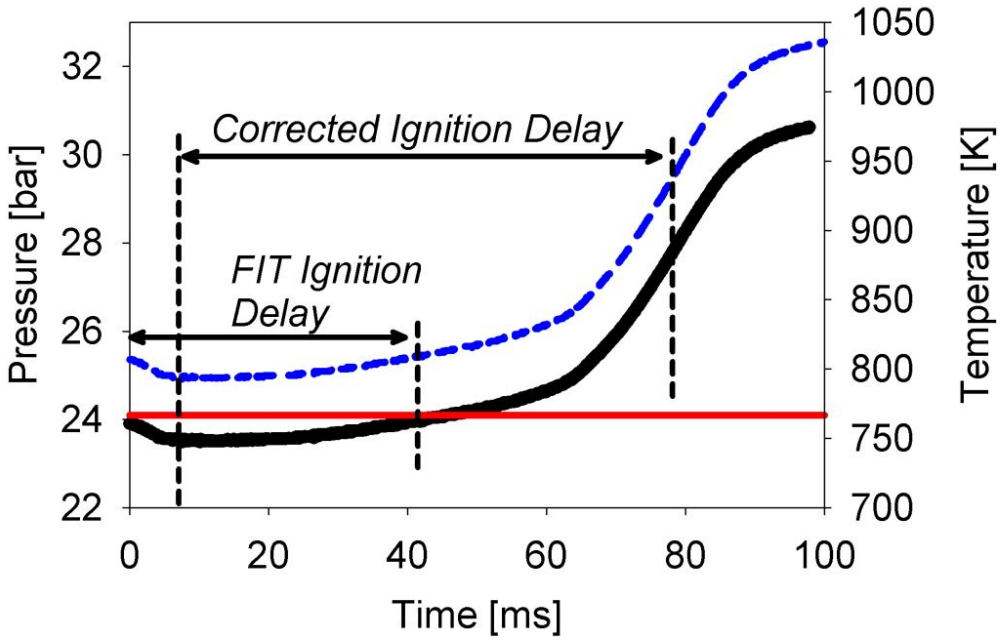


FIGURE 4.3. Pressure trace average (black line) for a typical n-butanol ignition test in the FIT, calculated temperature (dashed blue line), and the FIT trigger point (red line).

butanols), thus allowing more OH to be present to attack the base n-heptane fuel. This behavior led to generally shorter ignition delay periods for t-butanol blends in comparison to the other three butanol isomers considered by Haas, et al.[38]. Alternatively, the n-butanol competed relatively equally with n-heptane for the OH radicals, resulting in a more linear trend in observed DCN as a function of molar blending percentage. The latter result was also observed in the FIT results presented in Figures 4.1 and 4.2.

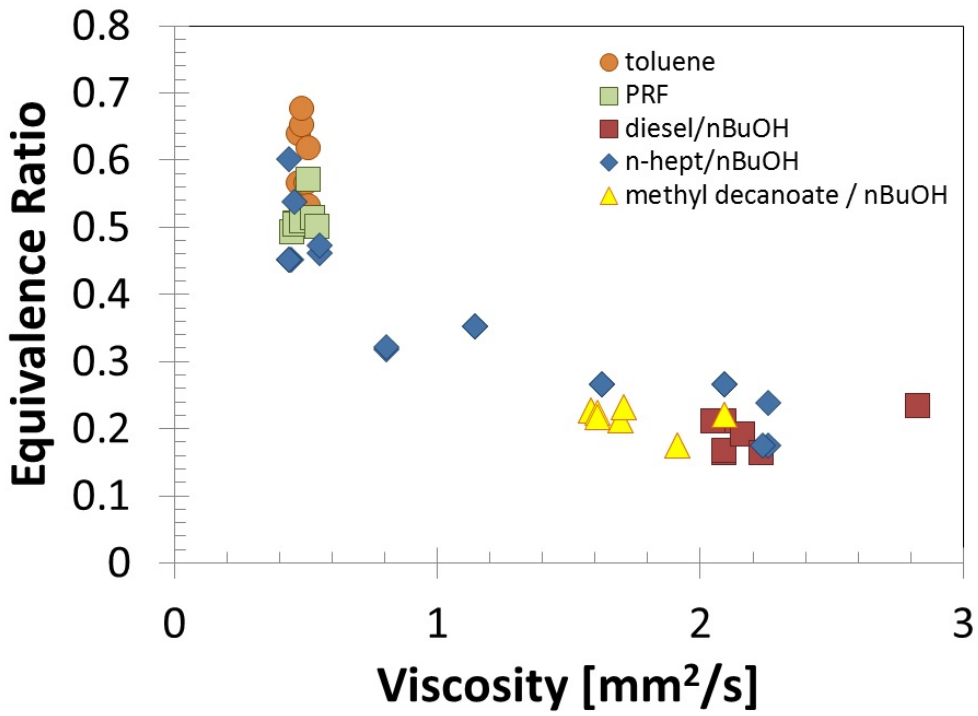


FIGURE 4.4. Injected global equivalence ratio as a function of viscosity for various fuels tested throughout ths work. Please see Chapter 5 for more detail on fuel physical effects on ϕ.

4.1.1. FIT MODELING RESULTS. For the n-butanol/n-heptane blend simulations, the Sarathy et al.[58] mechanism was updated with the n-heptane sub-mechanism from Mehl et al.[72], which is a well-validated mechanism that has been used for modeling gasoline surrogate fuels such as PRF's. The Mehl et al. mechanism was also used to simulate the PRF FIT experiments. Hereafter, the modified Sarathy et al. mechanism (which includes the n-heptane sub-mechanism from Mehl et al.) will be referred to as the Sarathy* mechanism. The resulting Sarathy* contains 855 species and 3835 reactions. Figures 4.5 and 4.6 are plots of measured and predicted FIT ignition delay period data for PRF fuels and n-butanol/n-heptane blends, respectively.

For the modeling results presented in Figures 4.5 and 4.6 a single-zone, constant volume model with heat transfer model was used. One important issue was developing an appropriate

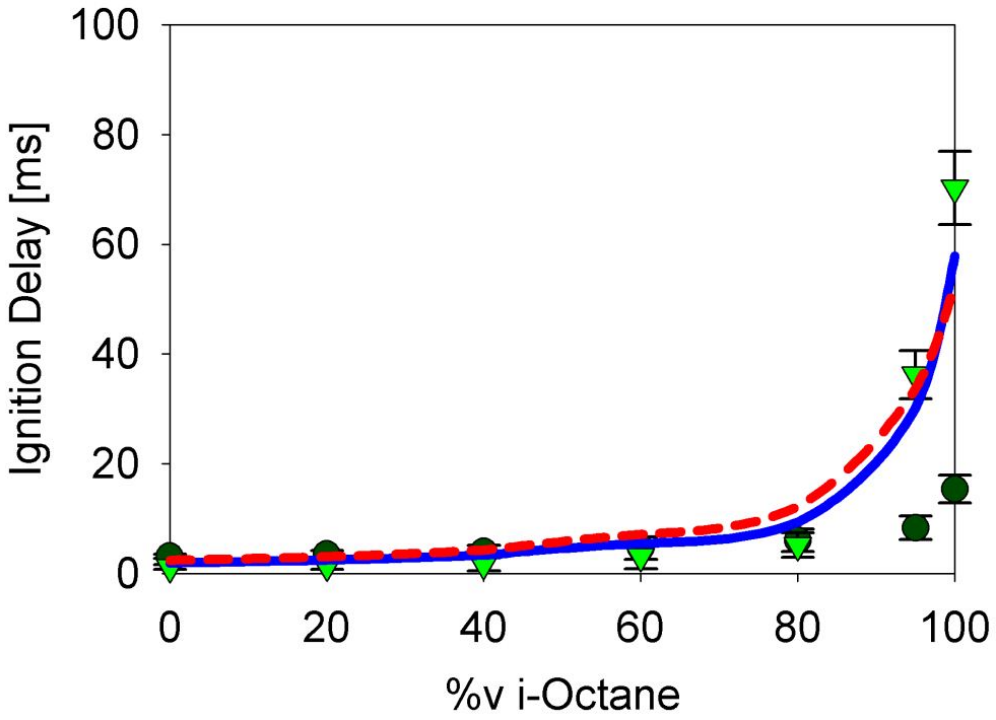


FIGURE 4.5. Ignition Delays for PRF blends. Shown are the ignition delays reported by the FIT (circles), ignition delay found as time from minimum pressure/temperature to max dP/dt (triangles), the Sarathy*/Mehl mechanism prediction (blue solid line), and Saisirirat et al. mechanism prediction (red dashed line)

heat transfer correlation for the FIT instrument. Due to the similar nature both in injection and pressure/temperature range to a diesel engine, the Taylor correlation[109] for the Nusselt number was used following the arguments set forth in Ferguson and Kirkpatrick[99]:

$$Nu = 10.4 \cdot Re^{0.75} \tag{26}$$

To use this correlation, a characteristic speed had to be determined to calculate the Reynolds number. It was decided to use the speed at which mixing occurs since this is somewhat representative of the turbulence within the vessel. From a review of FIT experimental vaporization times (i.e. the time from initial injection to minimum pressure) and reported

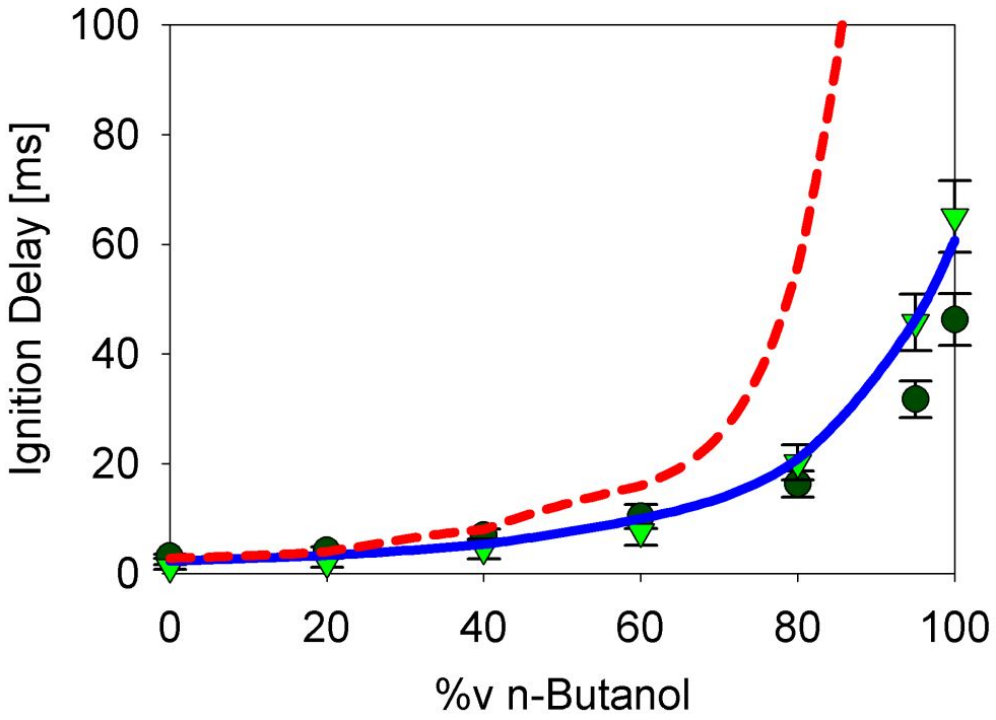


FIGURE 4.6. Ignition Delays for nBuOH blends. Shown are the ignition delays reported by the FIT (circles), ignition delay found as time from minimum pressure/temperature to max dP/dt (triangles), the Sarathy*/Mehl mechanism prediction (blue solid line), and Saisirirat et al. mechanism prediction (red dashed line)

mixing times for the IQT[49, 50] along with the diameter of the FIT combustion chamber, an average speed of 20 m/s was chosen to calculate the Reynolds number in Equation 26. Thus, with Eq. 26 and average properties of air at the initial FIT temperature and pressure a heat transfer coefficient of approximately 600 W/m^{2}K was used in the CHEMKIN FIT modeling. This value is about half to one fourth that found in HCCI engine heat transfer studies[110, 111]. To evaluate the sensitivity of these calculations to the heat transfer coefficient, adiabatic simulations as well as simulations with double the heat transfer coefficient (i.e. 1200 W/mK) were also performed. These calculations resulted in only a 3.8% variation in the calculated ignition delay period. Therefore, it was determined that the simulations were relatively insensitive to the value of the heat transfer coefficient. This heat transfer

coefficient is admittedly somewhat simplified and reflects some lumping of the heat transfer into a single parameter and accounting for the turbulence introduced by not only fuel injection but also the purging and filling of the vessel with air between injections.

The initial model conditions were chosen to coincide with an average value of minimum pressure and temperature in the FIT after fuel injection of 800 K and 23.5 bar, respectively. The general CHEMKIN model conditions for the FIT were then kept constant for both the PRF and nBuOH simulations (as well as the TRF presented in Chapter 3). The only changes made from the PRF to the nBuOH model calculations were the aforementioned ϕ value changes based on experimentally determined values. Note that the model predictions from both mechanisms compare favorably for PRF blends but diverge when applied to the nBuOH mixtures.

The Sarathy* mechanism agrees well with the experimental data for all injection timings. Previously, Bogin et al.[49] showed that the IQT could only be considered effectively homogeneous at ignition delays longer than $\sim$20 ms, the implication being that simulations assuming homogeneous conditions would deviate from experimental results at short ignition delay periods. This result is consistent with those obtained in the FIT in that the error between calculated and experimental results decreased monotonically with ignition delay for the more accurate models. However, simulation errors at low ignition delay periods can vary by a large percentage and still be within a few milliseconds of the actual value. Therefore, the observable error at low ignition delays is somewhat lessened by the nature of the experimental and simulation conditions. It is also worth mentioning that by taking the inverse of the ignition delay, errors at higher ignition delays are minimized in the DCN reporting.

4.1.2. Additional FIT Experiments: Methyl Decanoate and Diesel Blends. In addition to the butanol/reference blends, several other alternative fuel mixtures were investigated. Table 4.1 lists the fuel properties for mixtures of methyl decanoate/n-butanol and diesel/n-butanol. Methyl decanoate (MD) has been widely recognized as a satisfactory surrogate for real biodiesels in both fundamental combustion experiments as well as engine experiments[112–114]. Real biodiesels are primarily long chain fatty acid methyl esters (FAME), and MD is long enough (primary chain of 10 carbon-carbon bonds) that it is able to simulate some of the combustion properties of other FAMEs, namely ignition delay. Furthermore, real diesel is examined in this section to complement the n-heptane explored in more detail herein.

Table 4.1. Additional Fuels Tested in the FIT

fuel[a]	viscosity [mm2/s at 40 °C]	density at 20 °C	speed of sound [m/s]	phi	DCN
methyl decanoate (md)	1.6966	0.8721	1324.51	0.21	52.14
80md/20nBuOH	1.5825	0.8593	1309.29	0.23	37.27
60md/40nBuOH	1.6059	0.8462	1295.36	0.22	23.76
40md/60nBuOH	1.7106	0.8342	1283.45	0.23	17.38
20md/80nBuOH	1.9104	0.8219	1270.23	0.18	11.33
5md/95nBuOH	2.0895	0.8123	1250.07	0.22	5.28
diesel[b]	2.8241	0.8390	1375.11	0.29	49.68
80diesel/20nBuOH	2.0885	0.8299	1335.11	0.21	39.37
60diesel/40nBuOH	2.0492	0.8244	1313.12	0.21	27.62
40diesel/60nBuOH	2.0906	0.8192	1293.01	0.17	19.76
20diesel/80nBuOH	2.1599	0.8143	1274.64	0.19	12.52
5diesel/95nBuOH	2.2299	0.8106	1260.65	0.16	5.26

[a] all fuel mixtures are on a volume basis
[b] diesel fuel profile assumed to be $C_{14.4}H_{24.9}$[99]

Figures 4.7 and 4.8 show complementary results to previous n-butanol/n-heptane experiments (Figures 4.1 and 4.2). Methyl decanoate and diesel both show similar DCN values to n-heptane, as well as blending ratio trends with n-butanol. As expected methyl decanoate shows blending trends more closely related to diesel than n-heptane. This higher degree of similarity may be due to the longer carbon-carbon chain and the methly ester group in MD and the lack of these attributes in n-heptane. These results suggest that a fuel blend like MD/n-butanol might be a possible alternative to traditional fuels such as gasoline/diesel blends currently being investigated in advanced IC engines. Pure MD would likely be too expensive for practical use as a fuel, rather the ignition data suggests that a biodiesel/n-butanol blend could be a viable option as a fuel in a RCCI, dual-fuel, engine. Further testing on MD blends is an important topic of future work.

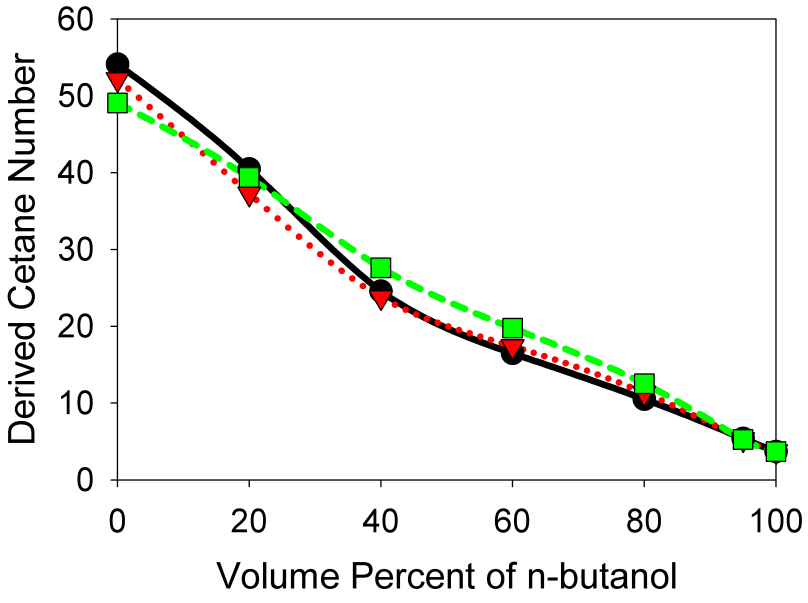


FIGURE 4.7. FIT results for mixtures of n-heptane/n-butanol (solid black line/circles), methyl decanoate/n-butanol (red dotted line/triangles), and diesel/n-butanol green dashed line/squares). Fuel mixtures shown on a basis of volume percent n-butanol in the blend.

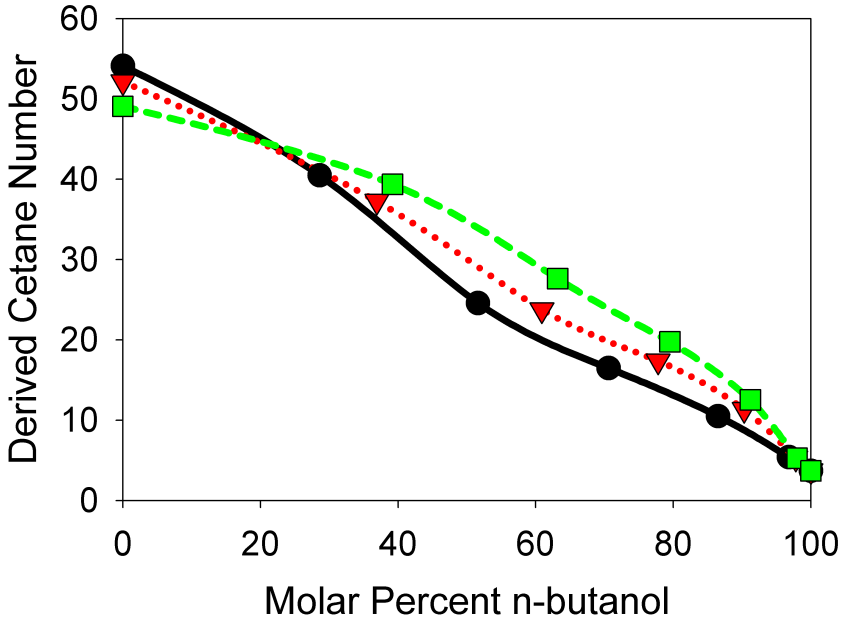


FIGURE 4.8. FIT results for mixtures of n-heptane/n-butanol (solid black line/circles), methyl decanoate/n-butanol (red dotted line/triangles), and diesel/n-butanol green dashed line/squares). Fuel mixtures shown on a basis of molar percent n-butanol in the blend.

4.2. HCCI Engine Experiments and Modeling

HCCI engine experiments were also performed and simulated using the aforementioned chemical kinetic mechanisms. For this work, six different fuels that span a wide range of reactivity but still ignite under the HCCI conditions of Table 4.2 were chosen for comparison. After base-lining the simulations against experimental data, simulations for the entire range of blended fuels in this study were performed and used to support the phenomenological argument proposed later in Section 4.3.

Figure 4.9 is a plot of the measured instantaneous cylinder pressure and apparent rate of heat release for nBuOH40 and PRF40 fuels operating in the HCCI engine under the conditions listed in Table 4.2. Comparing this data to that in Figures 4.1 and 4.2, it is apparent that under both engine and FIT conditions the nBuOH40 fuel is found to ignite

TABLE 4.2. Fuels Tested in HCCI Engine

Fuels	%M LRF[a]	fLTHR[b]	CA50
nC7	0	0.106	-9
PRF40	37.1	0.067	-3.5
PRF50	48.9	0.045	0.5
nBuOH40	51.6	0.044	-1
nBuOH50	61.5	0.040	1.5
nBuOH60	70.6	0.018	7.5

[a] molar percent of low reactivity fuel
[b] fractional low temperature heat release

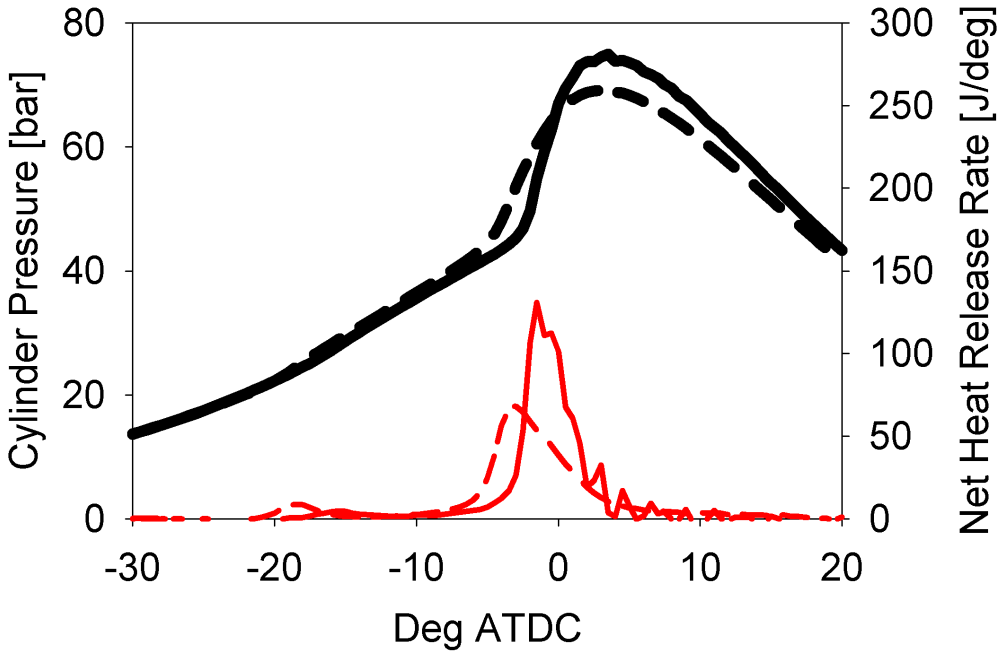


FIGURE 4.9. HCCI engine data for nBuOH40 (solid lines) and PRF40 (dashed lines). Shown are cylinder pressure (thick black lines) and net heat release rate (thin red lines) for HCCI test conditions listed in Table 4.2

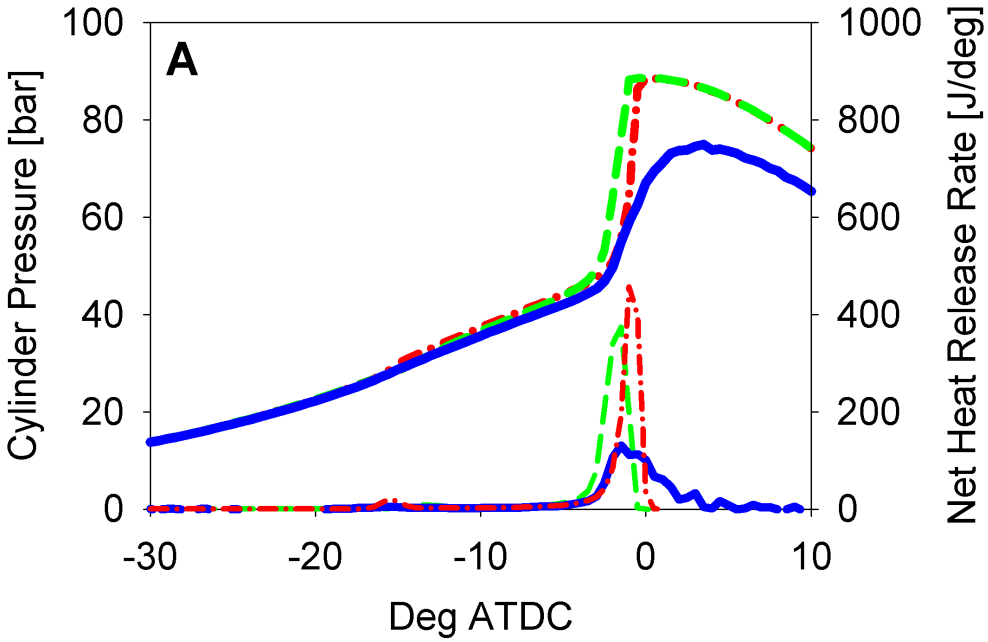
after the PRF40. This result is consistent with predictions based on the FIT data that suggest nBuOH40 is less reactive than PRF40. Though the trends are similar, the difference in ignition delay is not as great in the HCCI engine as that observed in the FIT. This result can be attributed to the fact that the temperature and pressure in an engine are constantly

rising from intake valve closure to near top dead center; and so ignition differences, which may be large at low temperature, manifest themselves more subtly as the accumulated effects of differences when the temperatures and pressures vary throughout the engine cycle. The effects of heat losses are also greater in the engine, so heat released as a result of chemical reactions do not lead to thermal runaway (i.e., ignition) at the same rate as in the FIT.

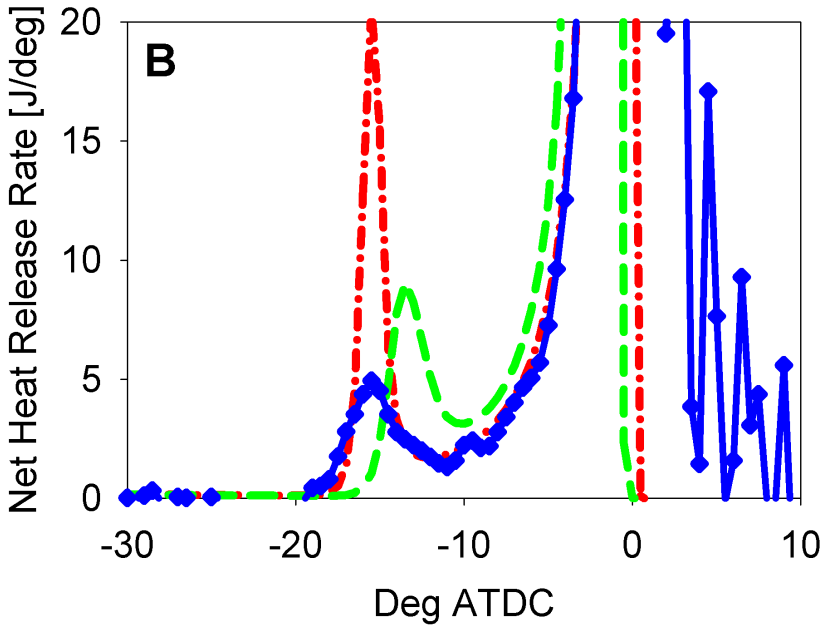
For all the single-zone CHEMKIN models, the in-cylinder temperature was slightly adjusted ($+7\ ^{\circ}C$ from measured intake conditions) to account for in-cylinder vs. intake conditions as well as to improve the agreement for both models. The initial conditions were then kept constant for all subsequent models to maintain consistency with the experimental tests. This section contains only the single-zone modeling results. Multi-zone modeling results are presented in the next section.

Figures 4.10 and 4.11 are comparisons between the HCCI engine data and single-zone modeling results. The figures include the instantaneous in-cylinder pressure data, along with the instantaneous net rate of heat release calculated from the in-cylinder pressure data. Figures 4.10(b), and 4.11(b) focus more closely on the low temperature component of the instantaneous net rate of heat release. Although single-zone models are known to not accurately capture the pressure rise rate within the system[10, 82], these simulations are an effective means of evaluating a mechanism's ability to capture ignition timing as well as the relative differences of ignition timing between different fuels. Moreover, the single-zone computations are also effective in isolating the chemical kinetic differences between different mechanisms under the same operating conditions (e.g. temperature, pressure and engine speed).

In all cases, the single-zone models over-predicted the magnitude of the heat release and the peak pressure, which is expected with a zero-dimensional, single-zone model since it does not take into consideration the inhomogeneity of actual equivalence ratio or temperature gradients within the cylinder. Use of multi-zone modeling has proven to be very accurate at matching pressure and heat release profiles[82, 115], and is explored further in the next section.

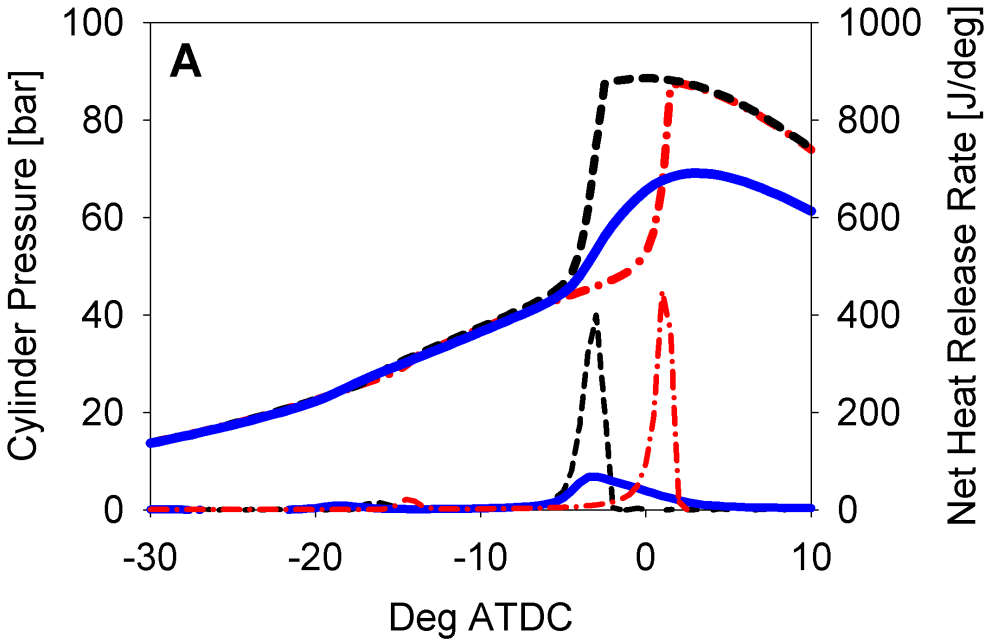


(a) HCCI nBuOH40 Pressure

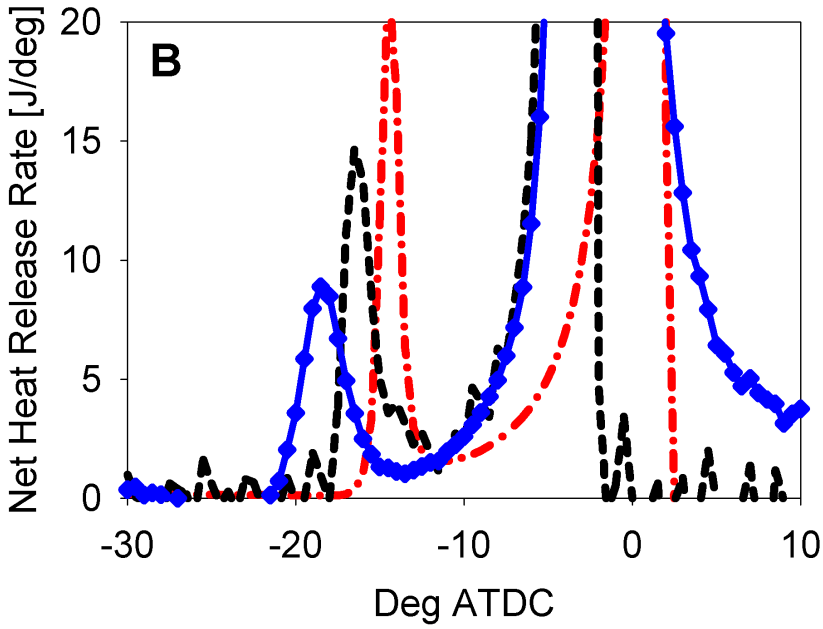


(b) HCCI nBuOH Heat Release

FIGURE 4.10. HCCI data for nBuOH40 (solid blue line) vs. single-zone model data from Sarathy* (green dashed line) and Saisirirat et al. (red dash-dot-dash line); (a) pressure (upper set of curves) and net heat release rate (lower set of curves), and (b) low temperature heat release



(a) HCCI PRF40 Pressure



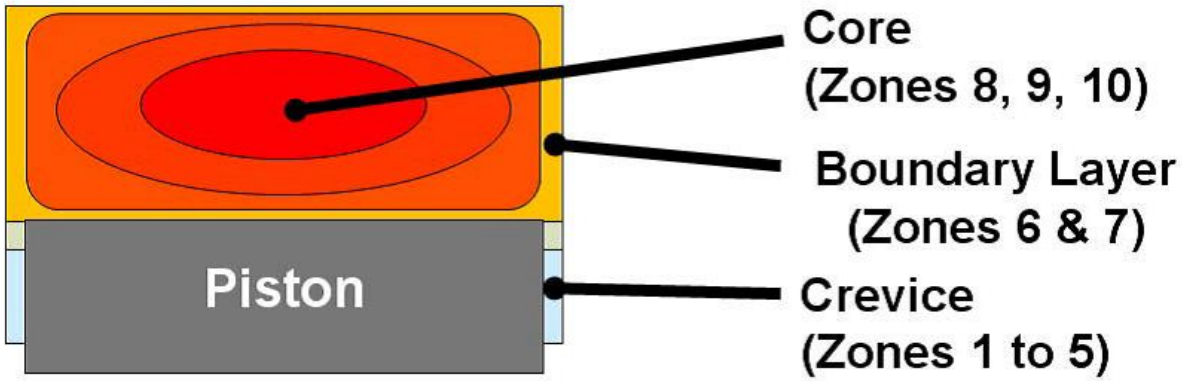
(b) HCCI PRF40 Heat Release

FIGURE 4.11. HCCI data for PRF40 (solid blue lines) vs. model data from Mehl et al. (dashed black line) and Saisirirat et al. (red dash-dot-dash line); (a) pressure (upper set of curves) and net heat release rate (lower set of curves), and (b) low temperature heat release

4.2.1. Multi-Zone Modeling. One of the major limitations of single-zone modeling is that it does not account for the inherent stratifications that exist within an actual cylinder. Even if the charge can truly be considered homogeneous in composition upon entering the cylinder, the thermal stratifications that develop within the cylinder as heat is transferred to/from the walls, piston, and head will affect how combustion occurs within the cylinder. By the time the piston reaches top dead center (TDC) there will have developed a thermal stratification that is not reflected in a single-zone model. To more accurately model this behavior many researchers have used a multi-zone modeling approach[82, 83, 89, 116–119].

In the multi-zone modeling approach, the in-cylinder gases are divided into multiple homogeneous zones (typically 2 to 10 zones) which interact via mass and/or heat transfer - Figure 4.12. In the present study, a relatively simple approach was taken using the multi-zone modeling module in CHEMKIN-PRO. The CHEMKIN-PRO multi-zone approach is based on the work by Aceves et al.[82] but more closely resembles the model by Visakhamoorthy et al.[120] wherein mass and heat is not transferred between zones. Rather, the governing equations are solved for each zone with the stipulation that all zones have the same pressure such that the only communication between zones is that of pressure-work. For the present study, a five-zone approach was used with mass distributed according to Table 4.3. The mass-distributions for the zones used in this study were determined based on average literature values for multi-zone models[82, 83, 89, 116–120] and distributed across five zones. More than five zones were tried, but no improvement was seen over the five zone model.

Heat transfer to the walls was also included in multi-zone modeling presented herein. By default, CHEMKIN-PRO has only functionality for a Woschni-type heat transfer correlation, but research[111] has shown that other correlations such as those presented by Chang et



(a) Illustration of CHEMKIN Zones

Zone #	1	2	3	4	5	6	7	8	9	10
Region	Crevice					Boundary Layer		Core		
Mass %	2	1	1	1	2	5	10	18	25	35
Wall Area %	7	2	2	2	3	6	9	16	22	31

(b) Example CHEMKIN Zone Distribution

FIGURE 4.12. Default examples of theorized "zones" simulated via the zone model in CHEMKIN (a) illustration of zones and (b) example of how zone masses and areas are distributed

TABLE 4.3. Muli-Zone Model Parameters

zone	core	core	core	boundary layer	boundary layer/ crevice
temperature	372 K	363 K	354 K	348 K	342 K
mass[a]	32	24	21	14	9
HTA[b]	5	10	15	34	36

[a] percent of total in-cylinder mass
[b] external heat transfer area as a percent of total

al.[121] and Hohenberg[122] may be better suited for HCCI operation. Since the model presented by Chang et al. is essentially a modified Woschni correlation, it was possible to use it within the current CHEMKIN-PRO interface.

To obtain the proper scaling coefficient for the Chang et al. heat transfer correlation as well as the proper initial temperatures/pressures, the CHEMKIN-PRO model was first matched to a motored-engine pressure curve (Figure 4.13). The heat transfer scaling coefficient from the motored curve was then applied to all of the fuel cases, resulting in good agreement with the experimental data. In addition to calibrating the heat transfer coefficient to the motored case, the initial in-cylinder temperature and heat transfer area stratification were adjusted proportionally to the zone masses. Specifically, the core zones had the highest temperature and lowest proportional heat transfer area while the boundary layer had the lowest temperature and largest percentage of heat transfer contribution. Overall initial temperature stratification was further adjusted to best fit all of the pressure traces. A zone-average initial in-cylinder temperature at intake valve closure (IVC) of 378 K was found to give the best agreement for all cases and no zone initial temperature was more than 20 $^{\circ}C$ from the average value. Figure 4.14 is a screen shot of the CHEMKIN setup profile for the five-zone model used herein.

Generally the multi-zone models (Figures 4.15 through 4.20) agree very well with the experimental data, although some small discrepancies are still observed. For the HCCI conditions considered in this study, both the Sarathy* and Mehl et al. mechanisms are reasonably accurate in predicting the location of peak heat release (which corresponds closely to the location of CA50) as well as the point of peak pressure rise for all fuels considered. Alternatively, the Saisirirat et al. mechanism accurately predicts for n-heptane, nBuOH40 and nBuOH50 cases, but accuracy retards as the fuels become less reactive. The deviations for Saisirirat et al. mechanism for the PRF fuels are likely a result of its n-heptane chemistry based on the older Curran et al. mechanism from 2002[81], while the Mehl et al. mechanism

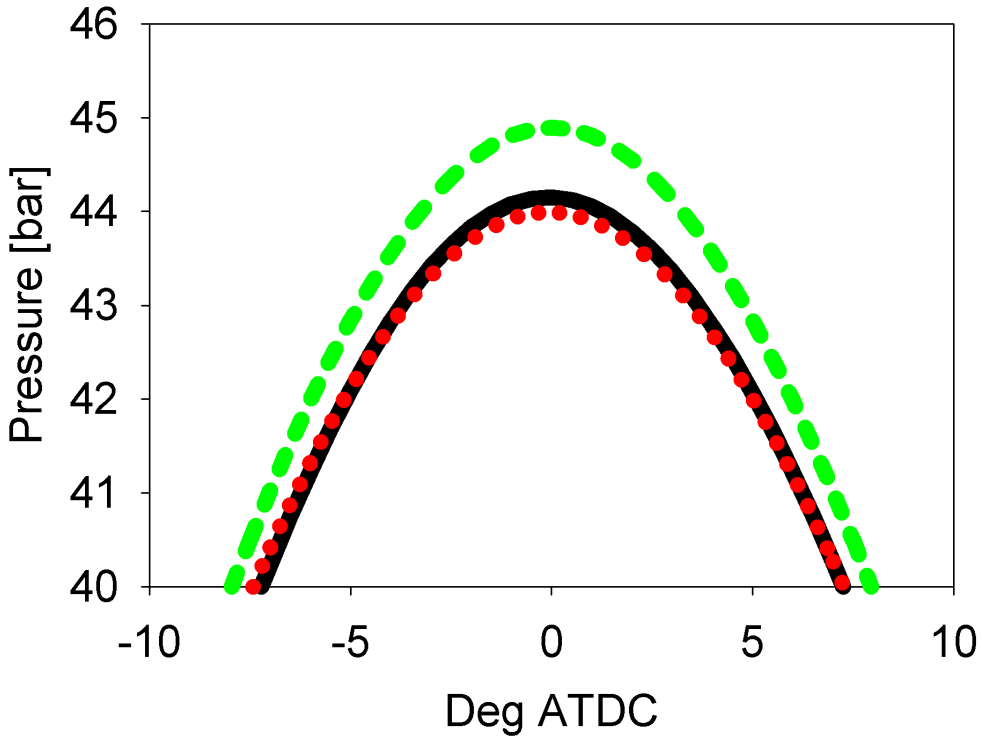


FIGURE 4.13. Motored (no fuel) pressure trace with actual data (black solid line), single-zone model without heat transfer (green dashed line), and multi-zone model with heat transfer (red dotted line).

is an updated version with more accurate kinetics. The predicted misfires in the Saisirirat et al. model for nBuOH60 may be due to the lack of validation of the mechanism against engine and ignition studies.

Additionally, the overall trends observed in the single-zone modeling apply again in the multi-zone results with the notable exception that the multi-zone results match the observed pressure rise rate extremely well. In all cases the LTHR data was slightly under predicted with multi-zone modeling. This mismatch in the ability of multi-zone modeling is not uncommon[82, 123] and is potentially due to the simplified modeling approach taken here where zones do not exchange heat or mass. Incorporating a more physics-based approach is currently a topic of further research.

Lastly, it is important to note that one area this study differs from others is that it was decided to not adjust the model parameters to exactly match the data for each case individually as is done in most studies[82, 83, 89, 116–120]. Rather, the goal was to compare the various mechanisms with constant parameters for all cases and to use the overall trends to observe the relationship between low temperature heat release and CA50 timing, which is explored in the next section.

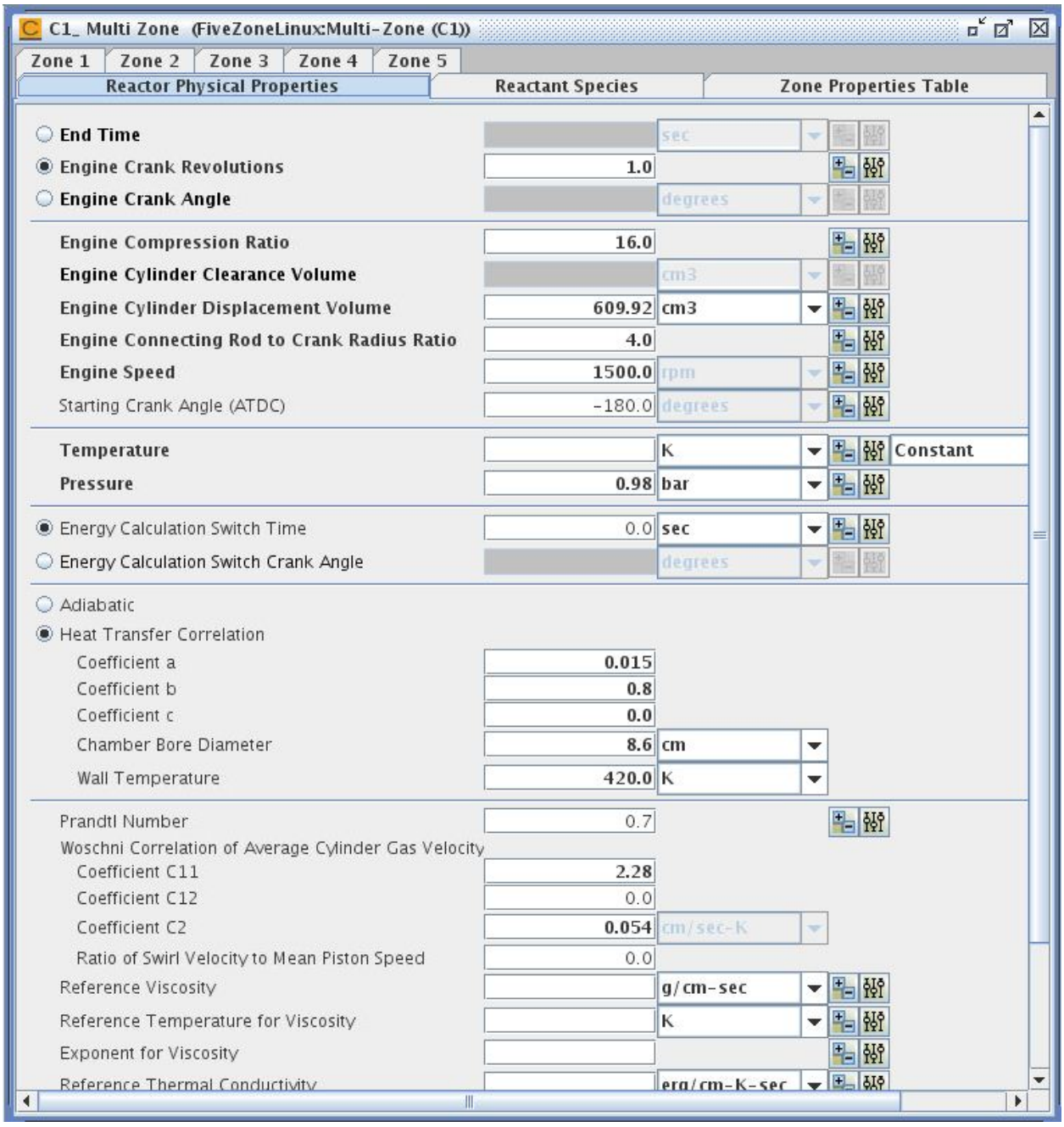


FIGURE 4.14. Screen shot for the five-zone model used herein

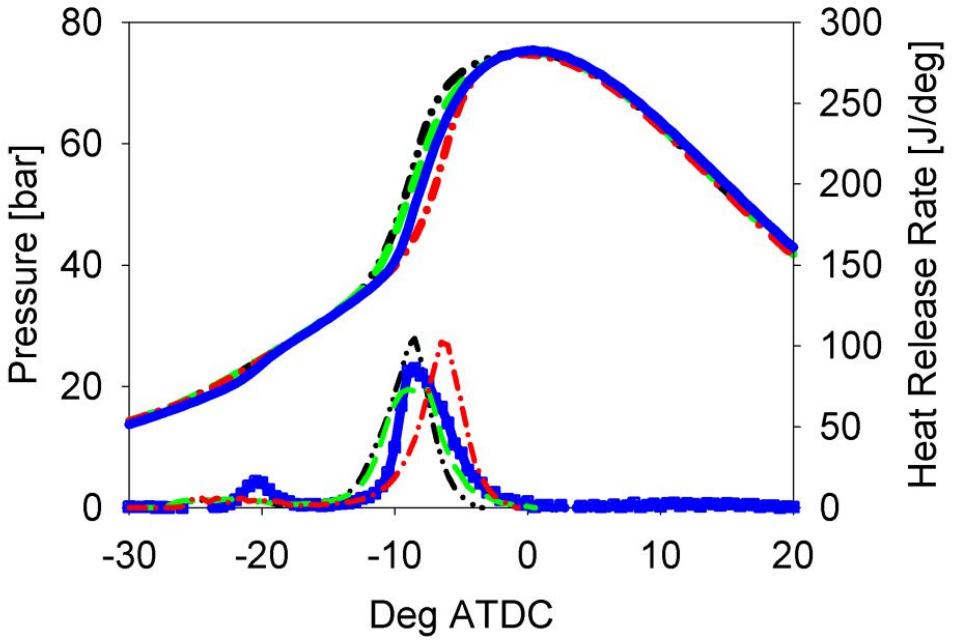


FIGURE 4.15. Multi-zone modeling results for n-heptane. The solid blue lines are the experimental data, the black dash-dot-dot line is the Mehl et al. model, the red dash-dot line is the Saisirirat et al. model, and the green dashed line is the Sarathy* model

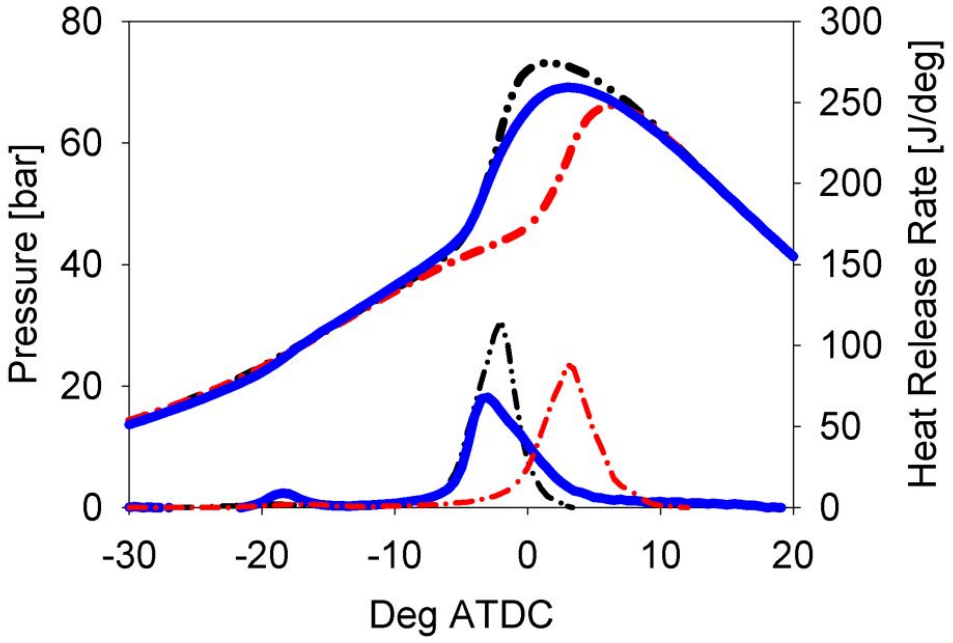


FIGURE 4.16. Multi-zone modeling results for PRF40. The solid blue lines are the experimental data, the black dash-dot-dot line is the Mehl et al. model, and the red dash-dot line is the Saisirirat et al. model.

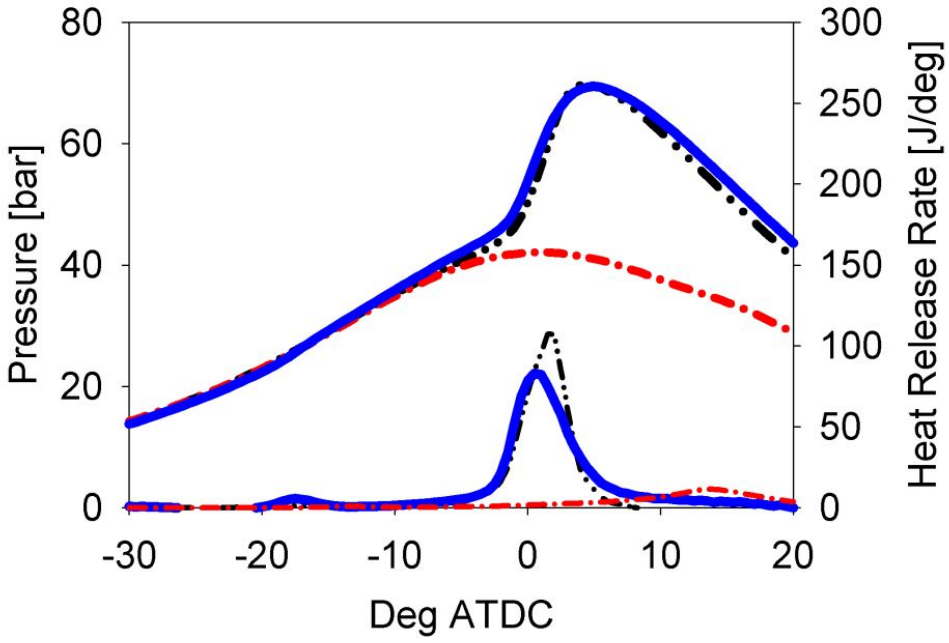


FIGURE 4.17. Multi-zone modeling results for PRF50. The solid blue lines are the experimental data, the black dash-dot-dot line is the Mehl et al. model, and the red dash-dot line is the Saisirirat et al. model.

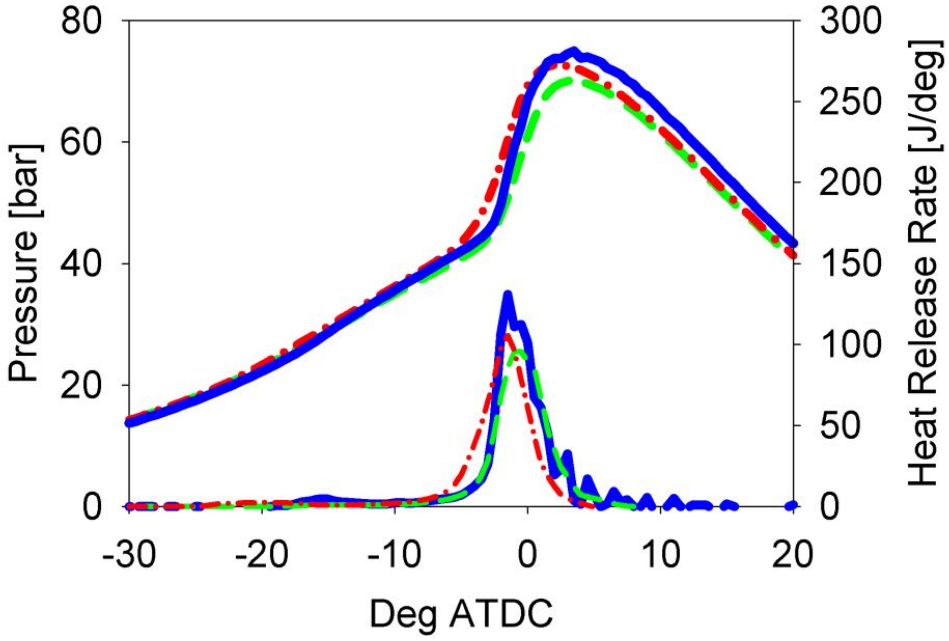


FIGURE 4.18. Multi-zone modeling results for nBuOH40. The solid blue lines are the experimental data, the red dash-dot line is the Saisirirat et al. model, and the green dashed line is the Sarathy* model

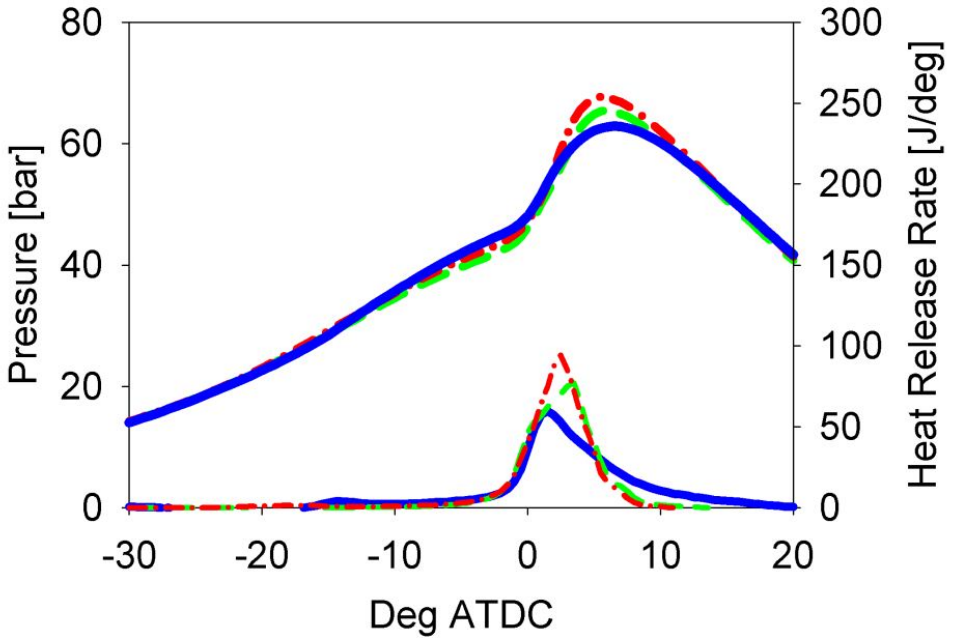


FIGURE 4.19. Multi-zone modeling results for nBuOH50. The solid blue lines are the experimental data, the red dash-dot line is the Saisirirat et al. model, and the green dashed line is the Sarathy* model

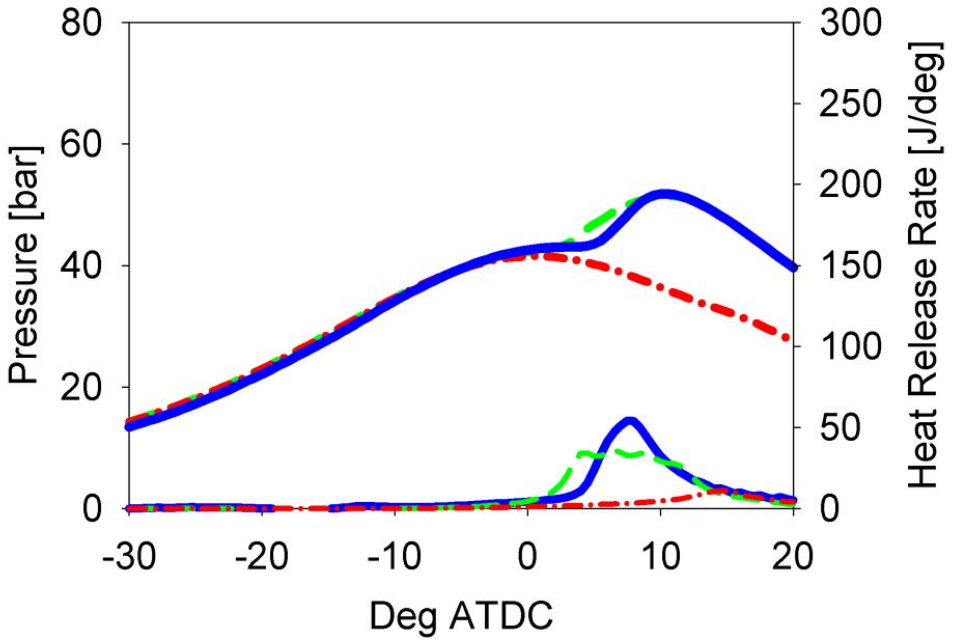


FIGURE 4.20. Multi-zone modeling results for nBuOH60. The solid blue lines are the experimental data, the red dash-dot line is the Saisirirat et al. model, and the green dashed line is the Sarathy* model

4.3. Impact of Low Temperature Heat Release on CA50

In a recent study[47] Rapp and coworkers show that the normalized LTHR release is a good indicator of the compression ratio at which the CA50 point is at 6 °ATDC (they showed a linear correlation). In that study, the LHTR was defined as the accumulated heat release occurring at temperatures <1000 K, the high temperature heat release is defined as the heat release that occurs at temperatures >1000 K and the normalized LTHR is defined as the ratio of the LTHR to the HTHR. Though the normalized LTHR of Rapp et al. showed reasonable correlation to CA50, it was felt that a more appropriate measure would be the fraction of low temperature heat release as a percent of the total heat release. Viewing the LTHR in this manner more fundamentally relates the ignition timing to temperature.

Therefore in the present work a fractional LTHR is defined as the fraction of the total heat release that occurs at "low" temperature (fLTHR). Specifically, the fLTHR is defined as the integral of the low temperature heat release spike seen in the net heat release data (as shown more clearly in Figures 4.10 and 4.11) divided by the integral of the entire heat release trace. For all fuels tested, the LTHR was completed by a temperature of 925 K and so this temperature was chosen as the cutoff for the fLTHR integral for all cases. There is some natural uncertainty in calculating a temperature for a given crank angle which translates into an additional error in calculating the fLTHR. This error is captured by incorporating the measured COV of the engine operating conditions and is included in the error bars for fLTHR shown in all plots below.

In the study by Rapp et al.[47] the normalized LTHR was found to correlate with the compression ratio. In the present work, the measured fLTHR correlates well with the measured CA50 point. This correlation was found in both the HCCI engine test results

and numerical modeling results using the Sarathy*/Mehl et al. mechanism (Figure 4.21). Contrary to other studies[40] the Sarathy* model predicts that the relationship between fLTHR and CA50 is not precisely linear. However, the predicted fLTHR shown spans nBuOH10 to nBuOH60, which represents a wide range of fuel reactivity. Therefore the correlation between fLTHR and CA50 could potentially be considered linear over a narrower range of fuel reactivity. Lastly, the nBuOH60 did not have a clearly defined LTHR. Indeed, it becomes much more difficult to determine the LTHR for fuels that react in this way although defining a cutoff temperature (such as the 925 K used in this work) does give a value for fLTHR. The model predictions for CA50 as a function of fLTHR from the Sarathy*/Mehl et al. mechanism in Figure 4.21 were shown to vary quadratically with an R^2 value of 0.996. The reasons for this quadratic variation are discussed below.

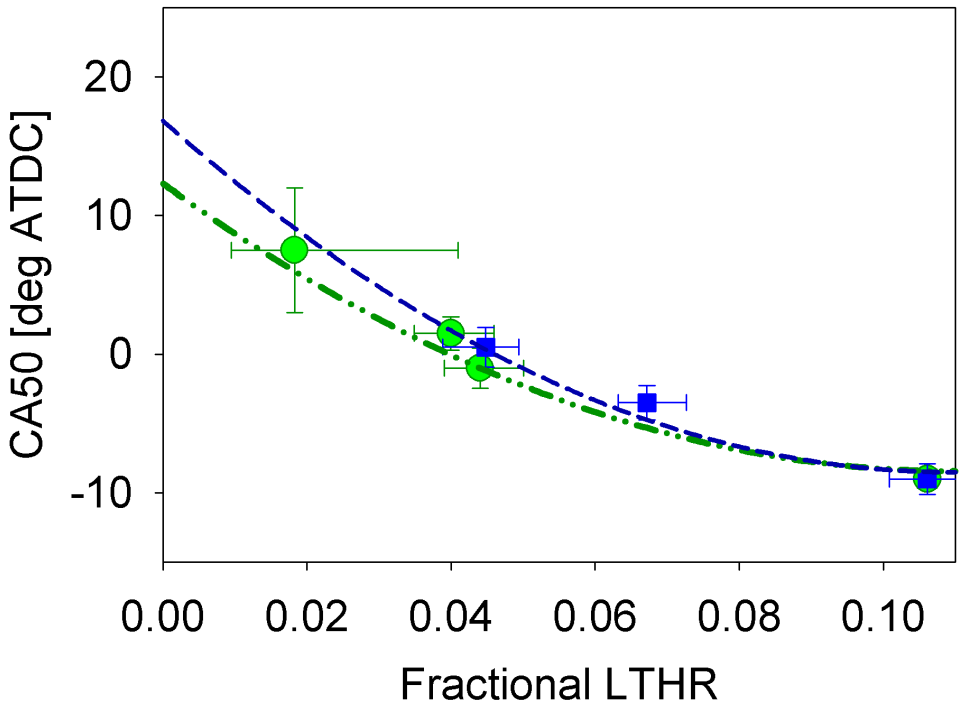


FIGURE 4.21. Predicted and measured variation in CA50 as a function of fractional low temperature heat release (fLTHR) for HCCI engine conditions tested herein. Experimental results are shown for two fuel blends: nBuOH (green circles) and PRF (blue squares). Model results using the Sarathy* and Mehl et al. models are shown for nBuOH (green dashed-dot-dot line) and PRF (blue dashed line).

4.4. Relation Between fLTHR and CA50

If a relationship exists between fLTHR and CA50, then it might be possible use the fLTHR observed in an FIT (or similar device) to further elucidate the observations seen in HCCI engines. To this end, a first attempt at a phenomenological understanding of the relationship between fLTHR and CA50 is presented in this section. Figure 4.22(a) is a plot of temperature history for the ignition of two fuel blends (nBuOH60 and pure nBuOH) at constant volume for 24 bar initial pressure and 820 K initial temperature (FIT conditions). It is apparent that the nBuOH60 exhibits LTHR, whereas the neat nBuOH exhibits no observable LTHR at these conditions. The net effect of the LTHR for the higher reactivity

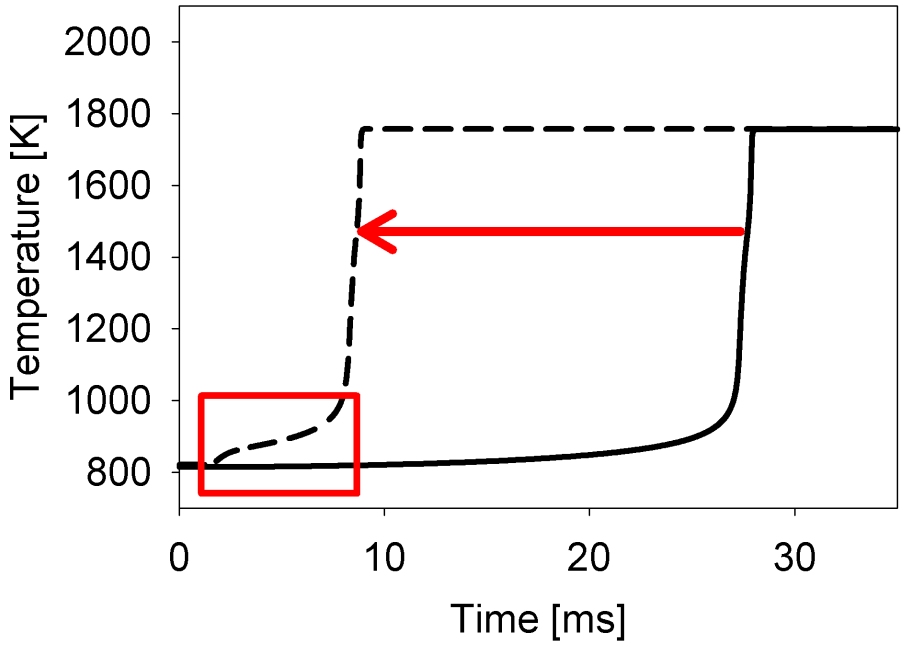
fuel blend is to raise the temperature of the homogeneous mixture, which results in a reduced ignition delay period before the primary ignition event.

To illustrate how increased fLTHR results in an advance in CA50 in an HCCI engine, one can begin by assuming that the overall ignition delay of a premixed homogenous fuel/air varies with temperature and pressure according to the Arrhenius form:

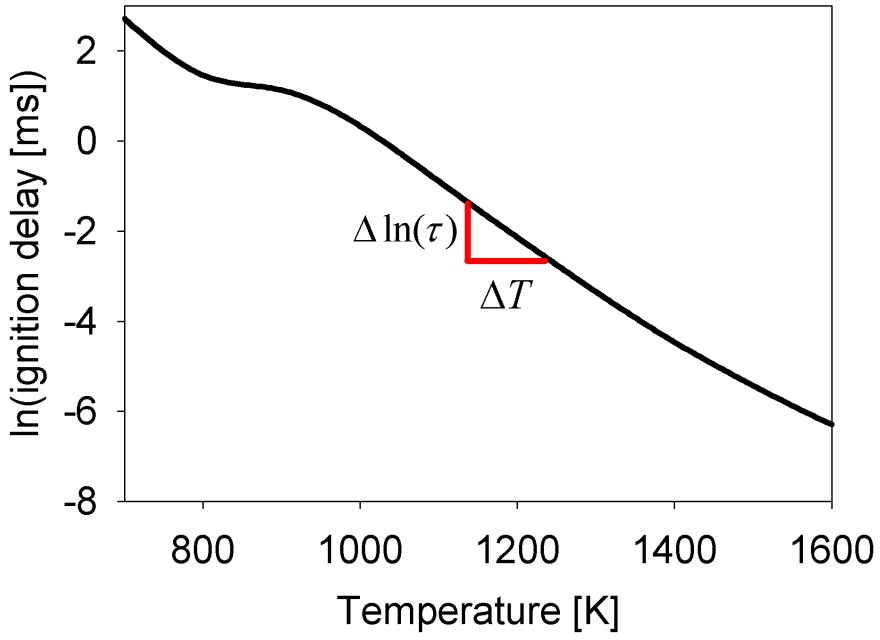
$$\tau = A \cdot P^{-n} \cdot exp\left(\frac{B}{T}\right) \tag{27}$$

where P is the pressure, T the temperature (which, in an HCCI engine varies with crank angle and therefore time), and A, B, and n are constants. Equation 27 is often presented in the form of an Arrhenius-type plot as shown in Figure 4.22(b) for nBuOH60 at 40 bar and $\phi = 0.33$. If one assumes that the ignition delay period is only weakly a function of pressure[124, 24] then Eq. 27 can be simplified as:

$$\tau \approx A' \cdot exp\left(\frac{B}{T}\right) \tag{28}$$



(a) Effect of LTHR on Ignition Delay



(b) Arrhenius Plot

FIGURE 4.22. Ignition plots for nBuOH60 showing (a) effect of LTHR on shortening ignition delay for nBuOH60 (dashed line) vs. pure nBuOH (solid line), and (b) the Arrhenius-type relation between ln(ignition delay) and temperature for nBuOH60 simulated with Sarathy* at 40bar and $\phi = 0.33$.

In an HCCI engine with ignition behavior that follows Eq. 27, an Arrhenius plot such as Figure 4.22(b) would be valid over some small pressure range such as for several crank angles near top dead center (TDC) in a motored engine cycle. Additionally, Figure 4.22(b) is nearly linear for temperatures greater than the negative temperature coefficient (NTC) region, i.e. greater than about 900 K for most hydrocarbons. Assuming a linear relation between temperature and ln(ignition delay) allows the derivative of Eq. 28 to be simplified as:

$$\Delta ln(\tau) = \text{-}C \cdot \Delta T \tag{29}$$

where C is a constant equal to the slope of the high temperature section of Figure 4.22(b). Equation 29 can be rearranged to yield the following relation:

$$ln(\tau_1) - ln(\tau_2) = -C \cdot (T_1 - T_2)$$

$$ln\left(\frac{\tau_1}{\tau_2}\right) = C \cdot \Delta T_{2-1}$$

$$\tau_1 = \tau_2 \cdot exp(C \cdot \Delta T_{2-1}) \tag{30}$$

Equation 30 can be put into the context of an HCCI engine by recognizing that the ignition delays, τ_1 and τ_2 are directly related to crank angles at which the fuel mixture within the cylinder will combust. From Figure 4.22(a) one can see that the time for the mixture to reach full heat release is essentially the same time as for the mixture to reach the 50% heat release, or in other words the τ can be thought of as the CA50 point for different fuels. The ΔT_{2-1} can be thought of as the fLTHR that shortens the ignition delay relative

to the pure component fuel with no LTHR. Furthermore, the fLTHR can be related to the overall heat release via the following:

$$f\text{LTHR} = \frac{\int_{CA_0}^{CA_L} dQ}{\text{Total Heat Release}} = \frac{\int_{T_0}^{T_1} m \cdot c_p \, dT}{\int_{T_0}^{T_f} m \cdot c_p \, dT} \approx \frac{T_1 - T_0}{T_f - T_0} = \frac{\Delta T_{low}}{\Delta T_{total}} \tag{31}$$

where CA_L is the crank angle at which low temperature heat release is completed, CA_0 is some initial reference crank angle, T_0 some initial reference temperature, T_1 the temperature at which the fLTHR is completed, and T_f the temperature upon complete heat release and is essentially the maximum temperature seen within the engine. Combining Eq. 30 and 31, the final general form relating fLTHR to CA50 is found to be:

$$CA50 = \tau_{LR} \cdot exp(C_Q \cdot f\text{LTHR}) \tag{32}$$

where τ_{LR} is the CA50 time of the base, low-reactivity, fuel and C_Q is a constant combining the total heat release of the fuel and the slope of the Arrhenius plot. Finally, since fLTHR is a small number, a simplified Taylor series expansion of Eq. 32 results in the following:

$$CA50 = \tau_{LR} \cdot \left(1 + \frac{C_Q \cdot f\text{LTHR}}{1!} + \frac{C_Q \cdot f\text{LTHR}^2}{2!} + O\left(\frac{C_Q \cdot f\text{LTHR}^3}{3!}\right)\right) \tag{33}$$

Equation 33 is consistent with the results in Figure 4.21, which showed that numerical predictions of CA50 varied quadratically with fLTHR. Note though that as the CA50 point retards further past TDC, increased error associated with dropping the higher order Taylor terms may necessitate the re-inclusion of some of these terms.

Since the low temperature heat release occurs at lower pressure it is reasonable to examine the fLTHR as measured at low pressure in the FIT ($f\text{LTHR}_{FIT}$) to see how well it relates

to that seen in the engine. To first examine the correlation between the low pressure ignition delay data and the HCCI engine data, the Sarathy* mechanism was again used since model results for FIT and engine conditions can be easily obtained for all fuels. Figures 4.23 through 4.25 are plots of the predicted CA50 for HCCI engine model using the Sarathy* mechanism against the fractional low temperature heat release predictions by the same mechanism under FIT conditions ($f\text{LTHR}_{24bar-model}$). A 2$^{\text{nd}}$ order polynomial in the form of Eq. 33 was fit to the data in Figure 4.25 with an R^2 of 0.99.

In its current configuration, measuring fLTHR directly from the FIT data is difficult because the sample rate at which the pressure data is recorded by the FIT is not sufficient to accurately resolve the LTHR. However, a proxy for this method is proposed. As shown in Figures 4.6 and 4.5, the FIT-reported ignition delay can be much earlier than the actual ignition delay (as defined by maximum pressure rise rate). As explained above, the FIT measures ignition delay as the time difference between injection and the chamber pressure rising above a set threshold pressure. If one makes the simplifying assumption that the FIT reported ignition delay is proportional to the LTHR then the ratio of the FIT reported ignition delay to the ignition delay found from maximum pressure rise rate (PRR_{max}) of FIT pressure trace should have a linear correlation against the fLTHR. This is indeed the case as is shown in Figure 4.24, which as an R^2 of 0.97. Additionally, the molar blending percentage of low reactivity fuel was found to correlate well with the measured FIT/PRR_{max} ignition delay ratio (Figure 4.23). Therefore a linear fit could be used to estimate the measured FIT/PRR_{max} ignition delay for the modeled results in Figure 4.24. Molar percentages were used since several studies have shown that the reactivity of fuel blends with large quantities of alcohol scaled much more linearly when the mixture was considered on a molar basis[28, 104]

as opposed to a volumetric basis. As discussed in Chapter 3, the tested RON values for the n-butanol fuels herein (Table 2.1) showed excellent agreement between the tested RON values and molar approximations.

Using the relationships in Figures 4.23 through 4.25, an estimated CA50 line can be drawn for the fuels tested based on the measured FIT/PRR_{max} ignition delays. This relationship shows good agreement with the experimental data as shown in Figure 4.26. One caveat to the proposed relationships in Figure 4.26 is that they are based on the ignition delay data for an n-heptane/n-butanol blend. A natural outcome of the derivation of Eq. 33 is that only fuels with similar ignition delay behaviors can be regressed using the same general equations. While there should be a fLTHR-CA50 relationship for every fuel (or fuel blend), the exact equation will depend on the blended fuels such that a given fuel blend may have a different relation, i.e. the curves in Figures 4.23 through 4.25 will shift based on the fuels in the blend. However, it is possible that these relations may be assumed to be rooted in the most and least reactive fuels in the blend. In other words, two different fuel blends may fall on the same blend line if the two fuel blends share the same least and most reactive fuels since these fuels will control the extreme bounds of reactivity.

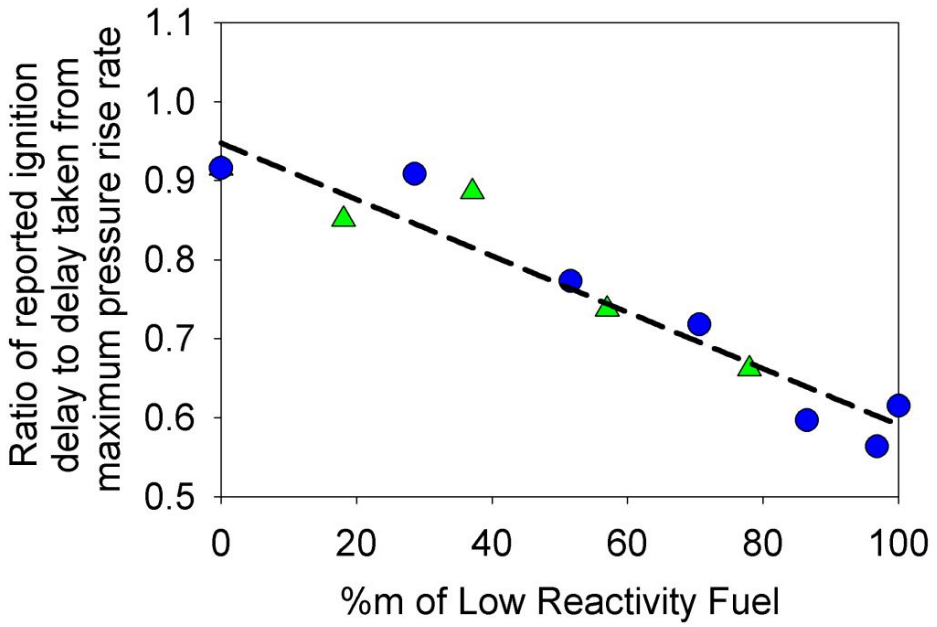


FIGURE 4.23. Simple model fit relating FIT to the observed HCCI engine data: molar percent of low reactivity fuel vs. measured ratio of FIT-reported to PRRmax ignition delay R^2 of 0.91 where green triangles are PRF data and blue circles are n-butanol/n-heptane data.

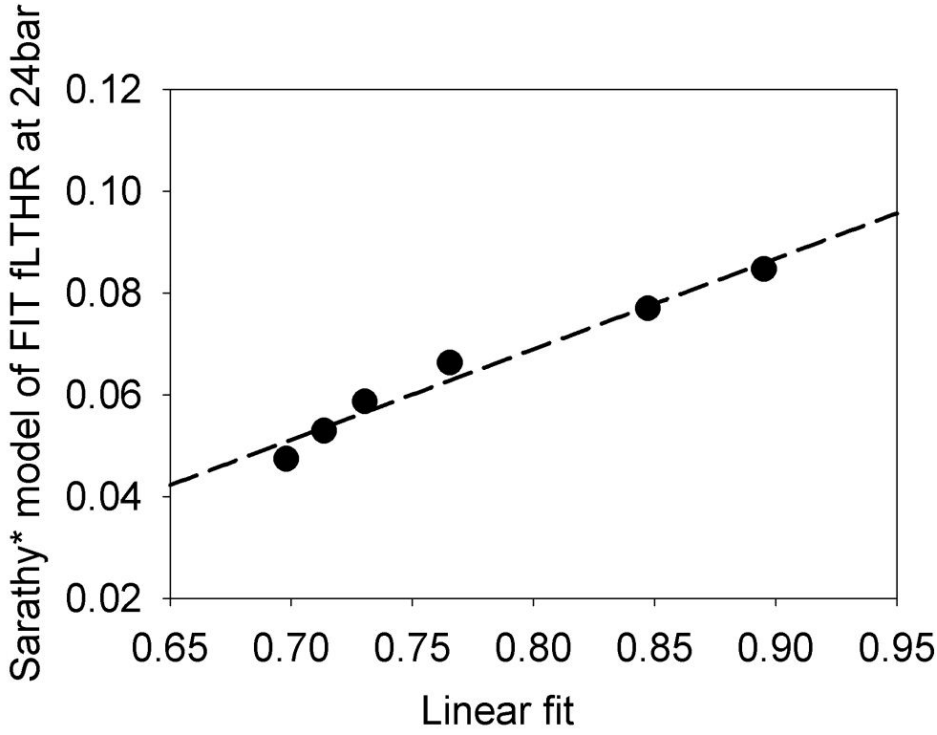


FIGURE 4.24. Simple model fit relating FIT to the observed HCCI engine data: 24bar FIT model vs. FIT/PRR_{max} ignition delay - R^2 of 0.97

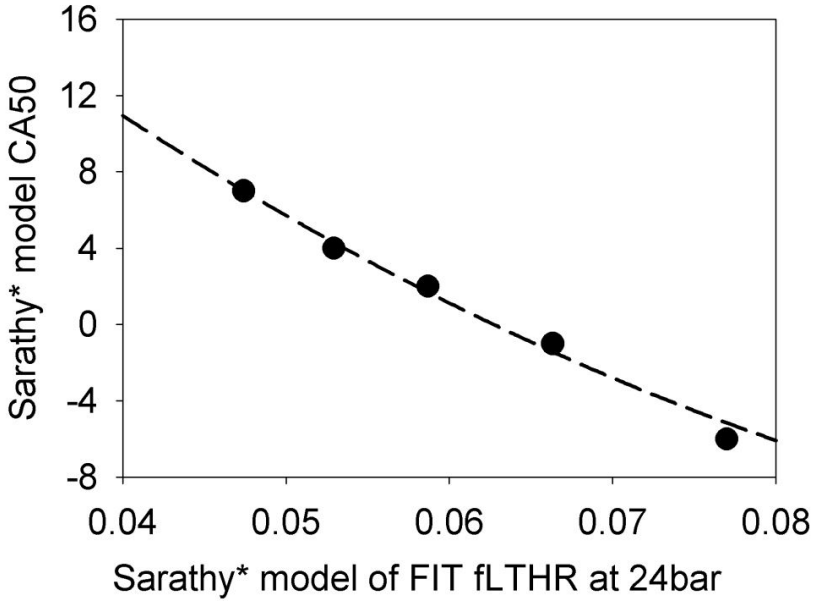


FIGURE 4.25. Simple model fits relating FIT to the observed HCCI engine data: Sarathy* model CA50 vs. 24bar FIT fLTHR - R^2 of 0.99

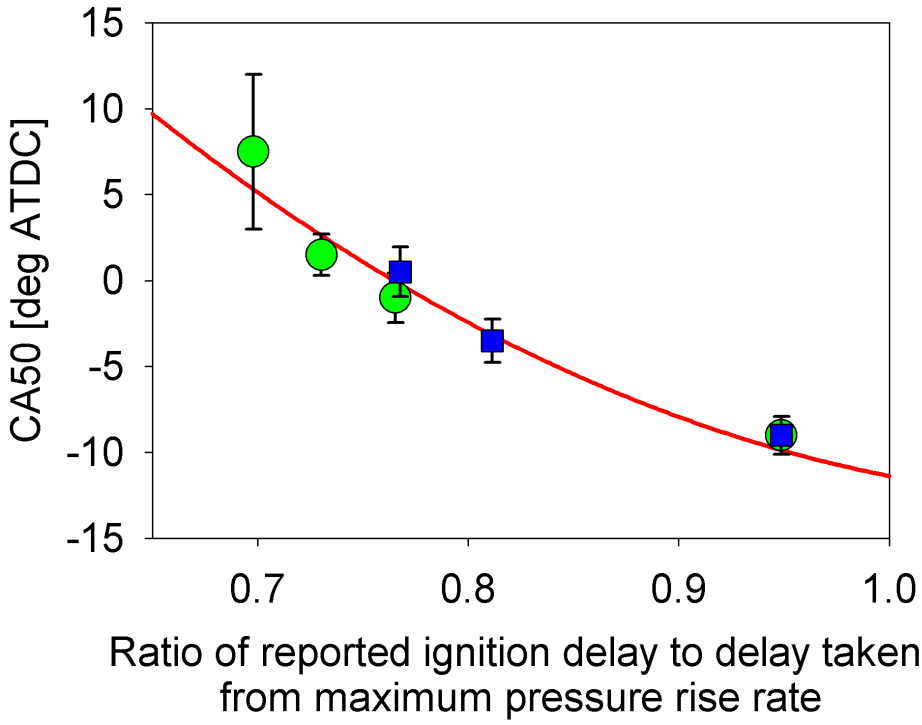


FIGURE 4.26. Simple model showing the relation between the ratio of FIT ignition delay to ignition delay found from max PRR curve vs. the CA50 found in an HCCI engine: PRF (green circles), nBuOH (blue squares), and simplified model (red line).

4.5. Development of a Molar Octane Index

The fact that the molar octane can be used to arrive at a CA50 (Section 4.4) suggests the question: can the idea of an Octane Number be derived based on fundamental principles such as the relationship developed for fLTHR above? What follows is an attempt at developing this very idea and, to the Author's knowledge, is the first time anyone has done such a derivation.

From the data presented in Section 4.4, one can simplify Eq. 33 and normalize the CA50 over the earliest value - in this case the CA50 of n-heptane is used to normalize. The simplified form of Eq. 33 can then be stated as such:

$$CA50_{normalized} \approx \tau_{ig,normalized} \approx O(f\text{LTHR}) \tag{34}$$

Equation 34 can be examined experimentally using the data already presented and normalizing against n-heptane - Figure 4.27.

It was discussed in Chapter 3 that in SI engines, knock is accepted to occur when the pressure rise from an approaching flame front reaches and raises the temperature and pressure in the end gas to the point of autoignition before the flame front actually reaches said end gas. The knock equation was examined:

$$\frac{bore_{atknock}}{s_T} \leq \tau_{ig} \tag{35}$$

where this equation can be further developed to show that the knock length is proportional to the square root of the characteristic ignition delay:

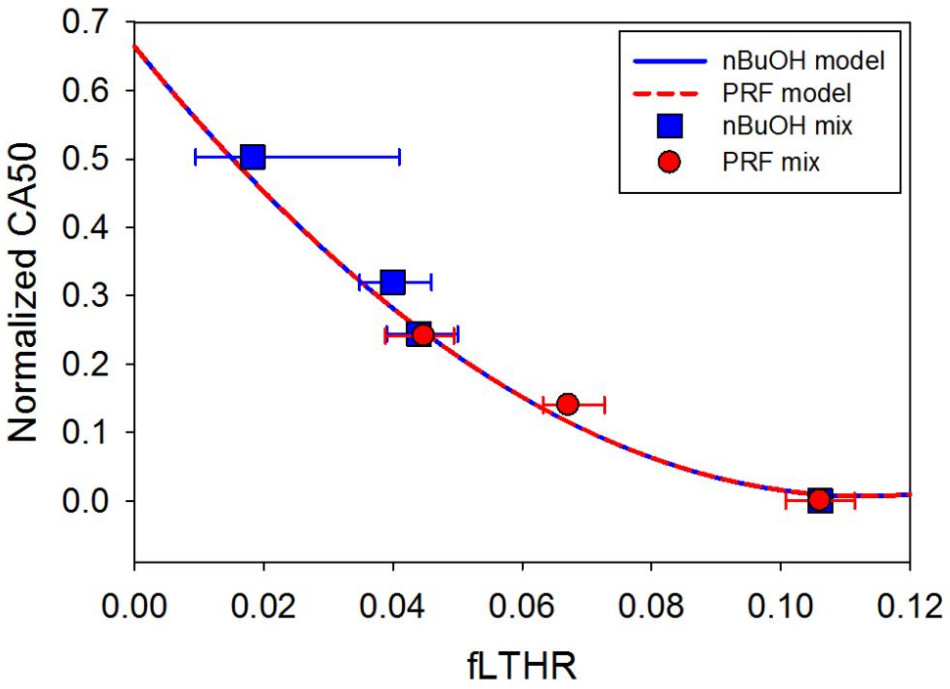


FIGURE 4.27. Normalized CA50 vs. fLTHR - showing a quadratic relationship in both model and experimental results

$$b_k \approx \tau_{ig} \cdot s_L \propto \tau_{ig} \cdot \sqrt{\frac{\alpha}{\tau_{ig}}} = \sqrt{\alpha \cdot \tau_{ig}} \propto \sqrt{\tau_{ig}} \tag{36}$$

Equation 36 then allows the following generalization:

$$\Delta b_k \propto \Delta ON \propto characteristic_{\sqrt{\tau_{ig,FOI}}}$$

$$ON = \frac{\sqrt{\tau_{ig,FOI}} - \sqrt{\tau_{ig,nC7}}}{\sqrt{\tau_{ig,iC8}} - \sqrt{\tau_{ig,nC7}}} \propto \text{characteristic}_{\sqrt{\tau_{ig,FOI}}} \tag{37}$$

where FOI stands for the fuel of interest. Lastly, the above equations can be combined/simplified, resulting in the general relationship relating the CA50 point with the ON. Eq 38.

$$CA50 \approx f_{quadratic}(mON) \tag{38}$$

As discussed previously, there has been much research showing that the RON value of fuels (especially oxygenated fuels) does not always blend in a linear-by-volume fashion[28, 104]. However, those same studies as well as data herein (see Figure 3.6) suggest that linear-by-mole fraction may be a better approach. Therefore upon simplifying Eq. 37, the notation is changed from ON to mON (molar Octane Number). Figure 4.28 then shows the change in CA50 vs. the mRON. Molar RON is shown here since the HCCI engine used in this work closely matches the RON testing pressure/temperature profiles.

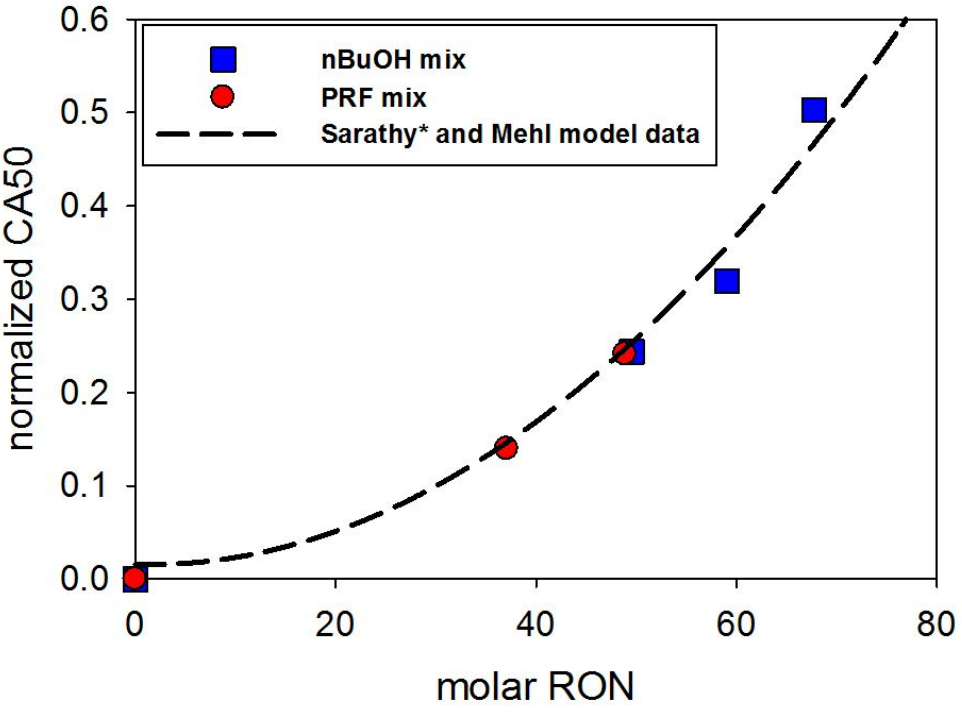


FIGURE 4.28. Molar RON vs. Normalized CA50 showing both actual and CHEMKIN predicted data

The desire then to translate Eq. 38 to a more useful version led to the examination and subsequent modification of the Octane Index. Figure 4.29 is a figure from one of the original Octane Index papers[40] and shows that Kalghatgi et al. were able to empirically demonstrate that the CA50 varied with the OI and that the relationship was likely quadratic

- though they assumed it to be linear. With that said, subsequent studies have shown that the volumetric OI does not always correlate well with experimental data[35, 47, 48].

Interestingly, a study by Liu et al.[46] which examined PRF, commercial gasoline, and ethanol mixes in an HCCI engine found that the OI did not correlate well for ethanol mixtures. However, the experimental set-up in that study was such that the charge-cooling effect of ethanol may have obfuscated the true ethanol vOI values. For the Liu et al. study, the intake temperature controller was located upstream of the fuel injection - Kasseris and Heywood[125] showed that in such cases the effective Octane Number boost from ethanol could be as much as 18 Octane Numbers. Taking into consideration the levels of ethanol used in the Liu study (20 and 25%vol), an octane correction of 6-8 Octane Numbers should have been applied to some of the fuels. Their "OP5 conditions" were chosen since that data set showed the poorest reported correlation with OI (R^2 of 0.431), however after ethanol charge-cooling octane correction, the R^2 for a quadratic fit is >0.94. Figure 4.30 shows the Liu et al. data with the applied Octane Index correction.

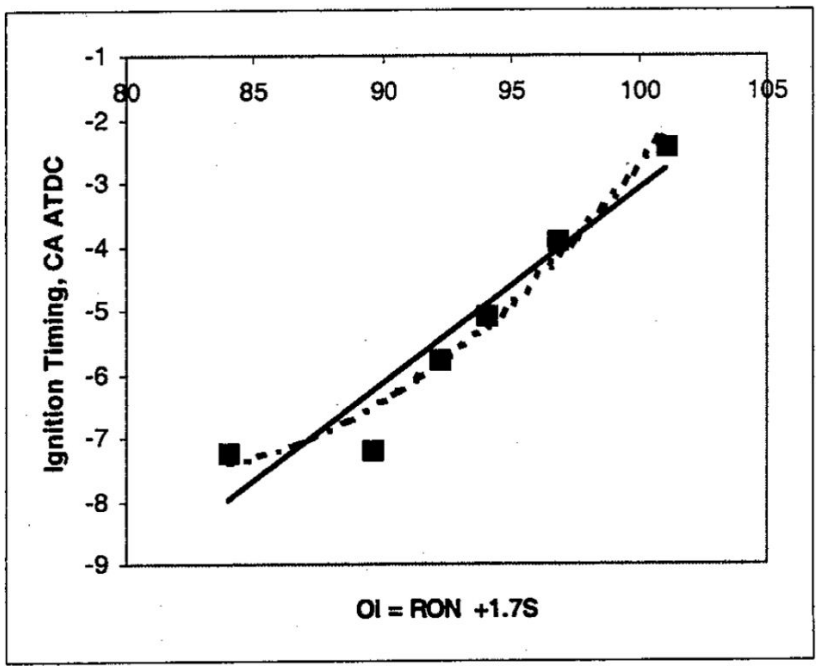


FIGURE 4.29. CA50 vs. OI from Kalghatgi et al. (2003) for one of their experimental conditions[40]

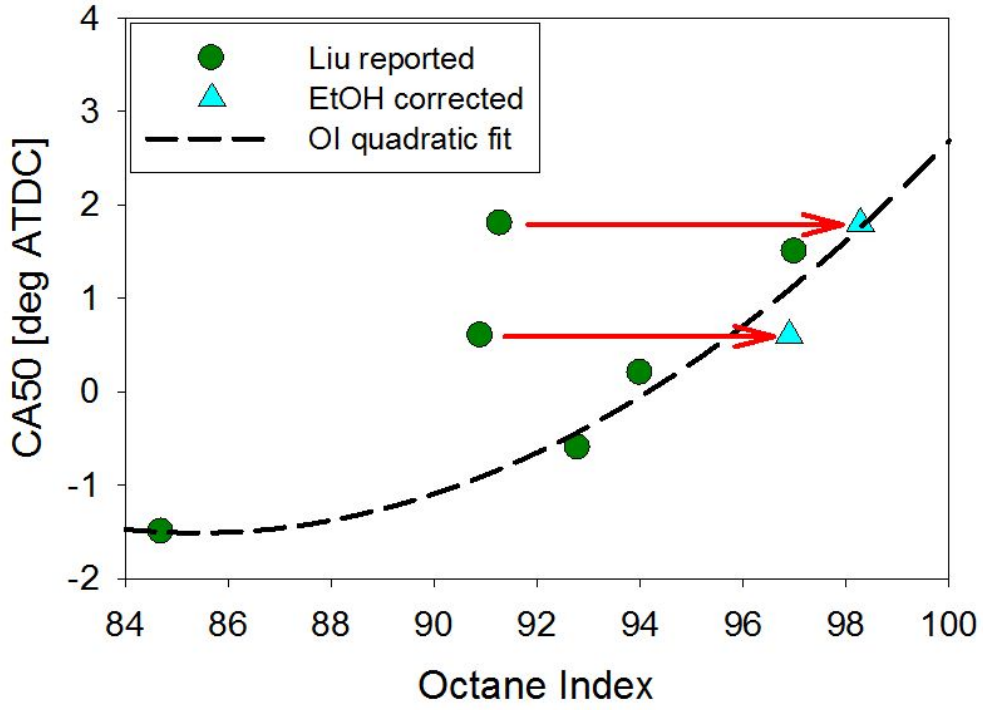


FIGURE 4.30. CA50 vs. OI for OP5 operating conditions in Liu et al. 2009 (data adapted from[46]) showing reported and corrected values

As noted, volumetric OI may not be the best metric when RON values for a given fuel blend may not be known. However molar OI does show promise. In order to determine the mOI values for the tested fuels in this work, the K value for the CSU HCCI engine needed to be determined. Based on Figure 1.7, the temperature-pressure history of the CSU-HCCI engine was plotted against the standard tests for MON and RON and found to be very similar to the RON test (Figure 4.31). Figures 4.32 and 4.33 show the difference between an Octane Index which assumes a linear by volume percent mixing rule and one that is linear by molar percent. The excellent agreement using the molar Octane Index instead of the volumetric Octane Index supports the findings by Andersen et al. and Foong et al. that Octane predictions using molar ratios instead of volumetric ones are much more accurate. Thus the basis for the more accurate mOI being proposed and used herein.

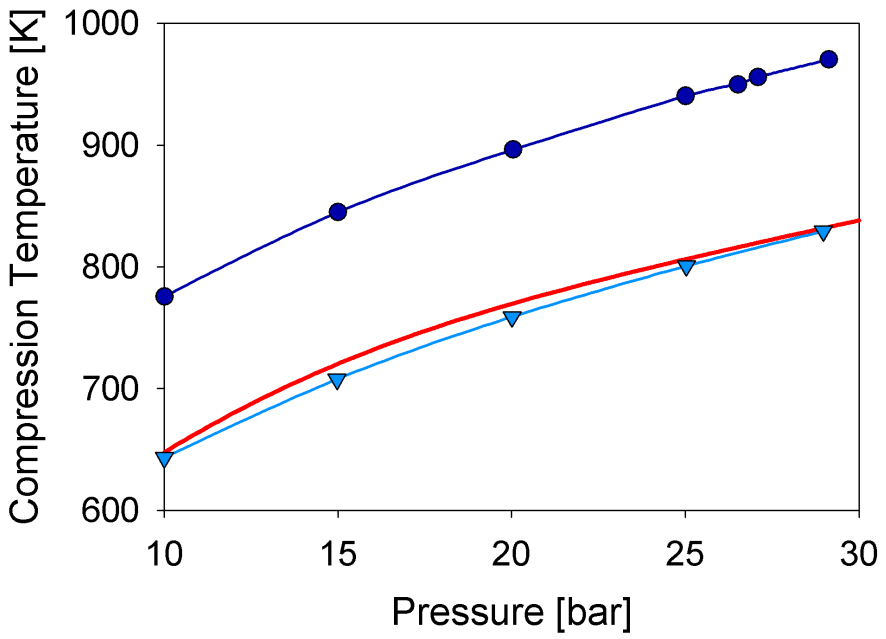


FIGURE 4.31. Compressed temperature for a given pressure for the CSU-HCCI engine (red line), the MON test (dark blue circles) and the RON test (light blue triangles).

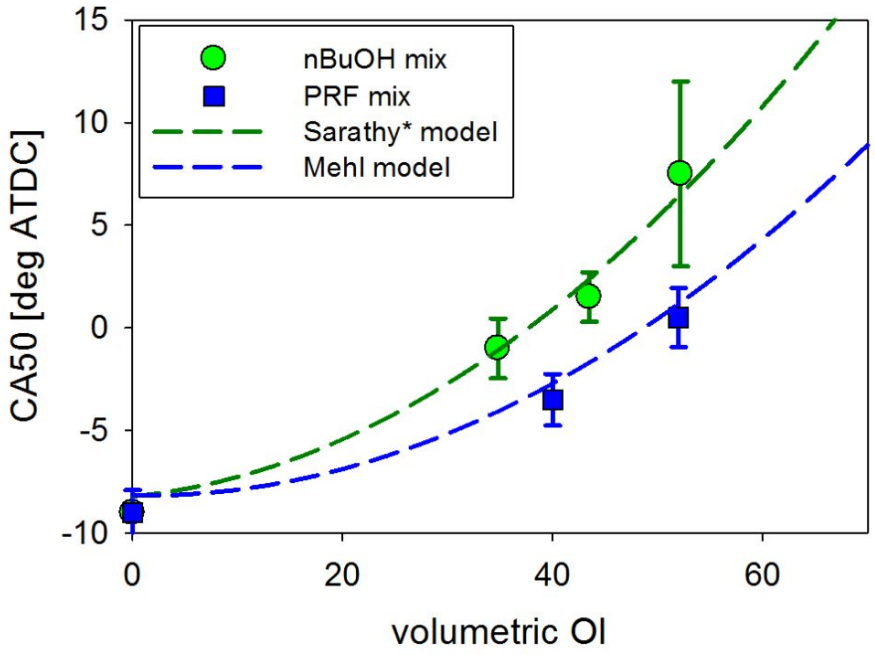


FIGURE 4.32. Octane Index assuming a linear by volume approach to n-butanol RON/MON values.

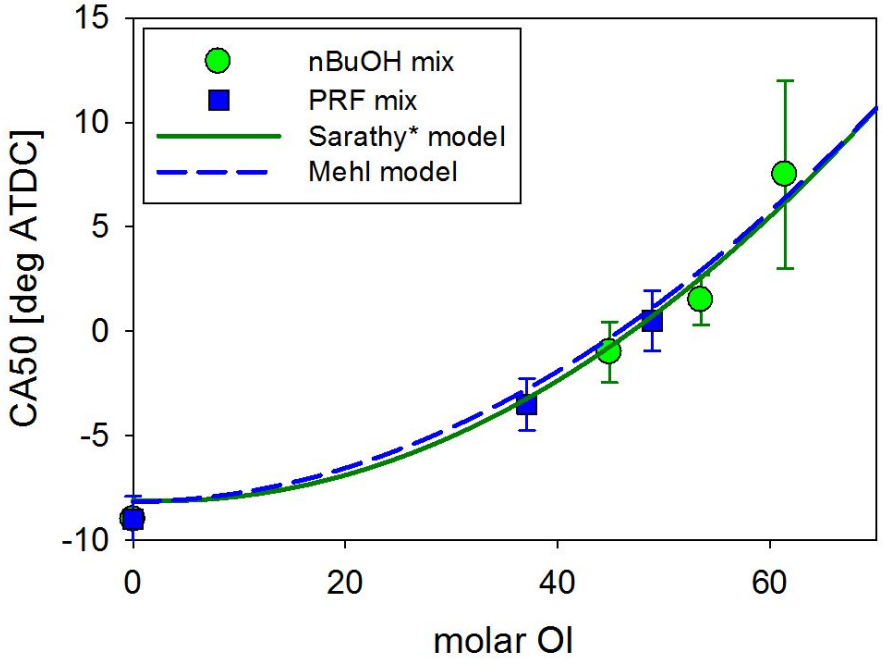


FIGURE 4.33. Octane Index assuming a linear by molar approach to n-butanol RON/MON values.

4.6. Development of the HCCI Number

As just explained, the base fuel as well as the engine conditions can have a large impact on the fit of Eq. 38. Therefore, it appears that there are two options moving forward regarding development of an advanced fuel metric. One option, as laid out by Kalghatgi in his recent book[27] is the continued development of the vOI including various parameters that have been shown to affect the OI such as Fuel-Air Equivalence ratio, engine speed, etc. The other option is to develop a more specific engine metric that can be tailored to the specific engine concept (eg. HCCI, PCCI, dual-fuel, etc.).

Proposed herein is the development of such a new metric for these advanced combustion modes that, similar to the Octane and Cetane Number scales, reproduces the appropriate engine environment but is amenable toward the development of a bench top laboratory apparatus. Unlike Octane Number, this new metric would isolate the chemical kinetic effects of a purely premixed homogeneous ignition event. This proposed scale can be thought of as assigning an HCCI Number to the fuel under consideration.

One such protocol to assign the HCCI Number would be as follows:

(1) Operate the premixed fuel/air mixture in an HCCI engine at typical engine loaded conditions such as 2000 RPM and a fixed intake temperature. Operating conditions will be chosen to target the 50% point of the heat release rate (HRR) at some crank angle just after top dead center (TDC). The target can be set to 5°ATDC to allow the fuel adequate time at near constant volume and temperature for the ignition delay to be measured but not so much time as to quench any reactivity. Zeroing in on the 5°ATDC mark would be achieved by adjusting the compression ratio.

(2) Once the engine conditions are set with the fuel of interest, reference fuels would then be run at these engine conditions. The reference fuel composition would be adjusted to match the HRR of the target fuel this ratio would then yield the HCCI Number. This test method is very similar to existing tests such as the Octane or Methane Numbers test methods, with the difference being that ignition is not initiated by a spark, but rather the compression ratio is high enough to produce HCCI.

Ideally, the above test protocol could be performed in a Cooperative Fuels Research (CFR) Engine, which in addition to being used for over 90 years[20] to test Octane and Methane Numbers, has been utilized by several research groups[47, 55, 126] to operate in HCCI mode. However, CFR engines have some drawbacks that make these devices less favorable for fuel analysis in analytical laboratory settings. For example, these engines are costly to operate and maintain, require technicians with engine related experience and are not amenable to typical laboratory settings. Moreover, as mentioned above, these engines operate at speeds that are not commensurate with typical on-road engines (600-900 RPM) and they require a substantial amount of fuel to run each test.

Accordingly, explored here is the evaluation of two further systems around which a new Derived HCCI Number (DHN) test method could be developed. Both systems are potentially amenable to the development of commercially available bench-top analytical instruments. The proposed methods proposed here are a Rapid Compression Machine based (RCM-based) method and an FIT-based method.

The compression time for an engine operating at 2000 RPM is approximately 15 ms, which is the same order of magnitude for a typical RCM apparatus. In fact, it is within a few

milliseconds of the RCM at the EECL. Additionally the RCM allows for better experimental control and requires much lower fuel amounts for testing in comparison to a CFR engine. Various effective compression ratios are easily obtained and very specific temperature and pressure targets can be achieved. Repeatability is also extremely high with most RCMs. Similarly, with regards to the development of an FIT-based method, the FIT standard test conditions (24 bar and 540 $^{\circ}C$ air temp) are ideal for examining the low temperature chemistry that dominates the early stages of auto-ignition for many advanced combustion modes that rely on low temperature combustion (LTC). The two proposed methods are described below.

4.6.1. FIT DHN. Previous modeling and experimental studies on the Ignition Quality Tester as well as the FIT experiments explored earlier in this chapter (Section 4.1) suggest that for low reactivity (i.e. higher Octane Number) fuels, the chemical induction period is much longer than vaporization and mixing times resulting in a total ignition delay period that approaches that which would be observed for a purely homogeneous premixed fuel/air mixture. Accordingly, outlined here is a FIT-based Derived HCCI Number (DHN) based on the following test protocol:

(1) Operate the FIT device with the test fuel of interest and adjust the temperature and pressure until the ignition delay period is long enough such that the chemical induction period is much longer than the vaporization and mixing times. Based on experience with the FIT, this approach would only be strictly valid for low DCN values (less than $\sim$20), but has some promise of examining higher values too.

(2) Using the same pressure and temperature settings, the reference fuels would then be blended accordingly until the ignition delay period was matched. The resulting reference fuel blend would thus yield the FIT-based DHN.

Figure 3.6 is a good representation of what data can be gleaned from a FIT DHN. The conclusion from that data is: subtle differences do exist primarily in the LTC portion of many fuels. With that said, the FIT/HCCI work herein show that such a FIT test could be accurate for given engine conditions (refer to Figure 4.34). In this case the fLTHR serves as a proxy for the HCCI number. For example, since PRF50 and nBuOH40 both have the same FIT-fLTHR and resulting CA50, nBuOH40 could be given a FIT-DHN of 50 since that is the PRF mix that matches the in-engine CA50.

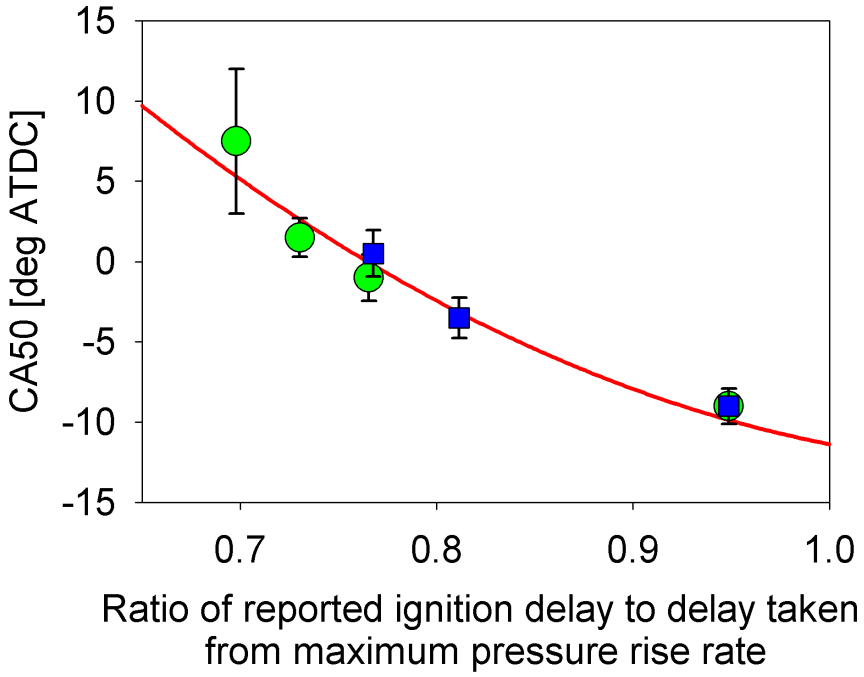


FIGURE 4.34. Simple model showing the relation between the ratio of FIT ignition delay to ignition delay found from max PRR curve vs. the CA50 found in an HCCI engine: PRF (green circles), nBuOH (blue squares), and simplified model (red line).

4.6.2. RCM DHN. A rapid compression machine (RCM) is an instrument designed to simulate the compression stroke of a single engine cycle thereby allowing autoignition phenomena to be studied in a much more controllable environment than would be possible in an actual engine. The RCM thus has an advantage over the FIT in that it can simulate an actual compression stroke and incorporate more of the subtle effects of compression heating such as occur in an engine. The RCM functions by rapidly compressing a homogeneous premixed volume of fuel and air. The rapid compression is accompanied by rapid heating of the mixture and the process results in an elevated final temperature and pressure with negligible heat loss. Since only the test gas is heated and not the vessel walls, wall reactions are avoided and the reactions that occur inside the cylinder are nearly homogeneous. Figure 4.35 shows the RCM at CSU.

The proposed RCM-based Derived HCCI Number (DHN) is based upon a similar protocol to that which would be performed using a CFR engine operating in HCCI mode. Specifically, the test protocol is as follows:

(1) The RCM would be operated such that the premixed, homogeneous ignition delay period is fixed for all fuels by modifying the operating conditions such that the ignition event occurs at a desired time after compression. This fixed ignition delay period could be achieved for a given reactivity fuel by changing the compression ratio, initial pressure, or initial temperature. The chosen ignition delay period would be commensurate with that observed in a typical on-road IC engine. For example, if we assume that the during the crank angle period from -5°ATDC to +5°ATDC the cylinder volume is approximately at constant volume, then a characteristic ignition delay period for an engine operating at 2000 RPM would be approximately 1 ms.



FIGURE 4.35. The Colorado State University RCM

(2) The RCM tests would then be repeated with reference fuels using the same test conditions as those which resulted in the measured characteristic ignition delay period for the test fuel (i.e. compression ratio, initial pressure, initial temperature). The reference fuel blend (e.g. primary reference fuels iso-octane/n-heptane) would then be varied until the ignition delay period for the reference fuel matched that of the test fuel. The final reference fuel composition would yield the DHN for the test fuel of interest.

In principal, this approach should result in a DHN that would be very close to an HCCI Number measured using a variable compression ratio HCCI engine. However, it is conceivable that such a method, once perfected, could be used to develop a commercially available instrument and associated standardized ASTM test method.

4.6.3. HCCI Number Computational Example. Since the actual HCCI Number and the RCM-based DHN are intended to measure autoignition propensity of purely homogeneous premixed fuel/air mixtures, it is possible to demonstrate the similarities between the two approaches using 0-dimensional models with detailed chemical kinetics. Indeed, the use of these computer simulations with detailed chemical kinetic mechanisms might not only dramatically reduce the time and cost involved in testing new fuels, but might allow the industry to forgo the development of a costly and potentially undesirable CFR-based HCCI test method against which new DHN methods are benchmarked. As a proof-of-concept, 0-dimensional modeling was performed using CHEMKIN to compare simulated CFR-based HCCI Number to a numerically predicted RCM-based DHN. The numerical computations presented herein were performed with a highly reduced chemical kinetic model[127] since validated mechanisms with the number of species in this example do not exist. However, since these calculations are 0-dimensional, a much more detailed mechanism could eventually be created and this numerical study repeated and further validated for the conditions of interest.

Table 4.4 shows the simulated fuel blend considered as well as reference blends for PRF and TRF fuels. The use of PRF and TRF blends for both of the proposed test methods is highly desirable because of their widely accepted/tested chemical kinetics and use within the industry to characterize various fuels. Additionally, this example shows how TRF fuels may

better serve as surrogates to real fuel blends across a range of temperatures. As shown in Table 4.4, a blend of 20.1% iso-octane, 45.9% n-heptane, 10% ethanol, 12% cyclohexane and 12% toluene, which has a RON of 55.1 would yield a HCCI Number of 71 for a PRF-based scale and 67 for a TRF-based scale under these simulated test conditions.

TABLE 4.4. HCCI Number Test Fuel Blends

	target blend	PRF	TRF
RON	55.1	70.2	85.5
mol wt [kg/kmol]	88.1	109.6	94
i-octane [vol%]	20.1	70.2	0
n-heptane [vol%]	45.9	29.8	33
ethanol [vol%]	10	0	0
cyclohexane [vol%]	12	0	0
toluene [vol%]	12	0	67
comp ratio at ignition	14:1	14:1	14:1

Figure 4.36 shows the results of simulated HCCI Number experiments summarized in Table 4.4. The conditions chosen for the simulated HCCI Number experiments were an engine speed of 2000 RPM, intake temperature of 100 $^{\circ}C$ and a compression ratio of 14:1. The compression ratio was chosen to target 5°ATDC for the point of maximum heat release. Also shown in Figure 4.36, almost directly overlapping the data for the target blend, is the data for the HCCI PRF and TRF blends targeted at the same 5°ATDC peak HRR. Note that though the blended RON of the example fuel is 55.1, the corresponding HCCI number is much different at 71 and 67 for the PRF and TRF scales, respectively. The HCCI number is defined as the volume percentage of the less reactive fuel (i.e. iso-octane or toluene) in the reference blend this approach is convenient as long as only two fuels are used in the reference blend. Note how the reference fuels adequately capture the LTC region.

Figure 4.37 shows the results of the corresponding simulated RCM-based DHN experiments using the same target and reference fuel blends. What should again be reinforced here is that the blended fuel, while having the same calculated RON, has very a different auto-ignition tendency. This difference in auto-ignition as seen in the HCCI test is adequately captured by the idea of the HCCI number.

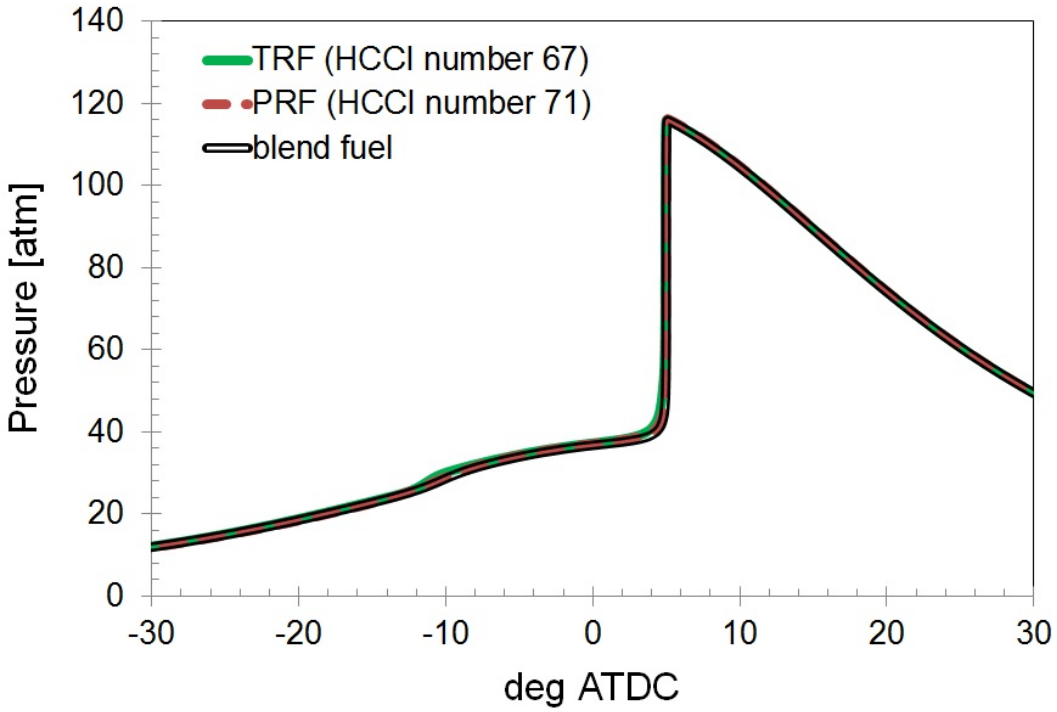


FIGURE 4.36. Simulated HCCI Number engine experiments.

Similar to the HCCI Number engine simulations, the RCM-based reference fuel composition suggests a much higher HCCI number than the calculated RON value. Moreover, as theorized above, the behavior of these fuels in the RCM simulation is very close to that seen in the HCCI simulation. Therefore, the RCM (or RCM-like device) is expected to produce a DHN that would be comparable to an Engine-based HCCI Number.

In addition to one HCCI or RCM point, the blended fuel will need to adequately match the ignition delay vs. time plot so as to have the same integrated reactivity. Figure 4.38

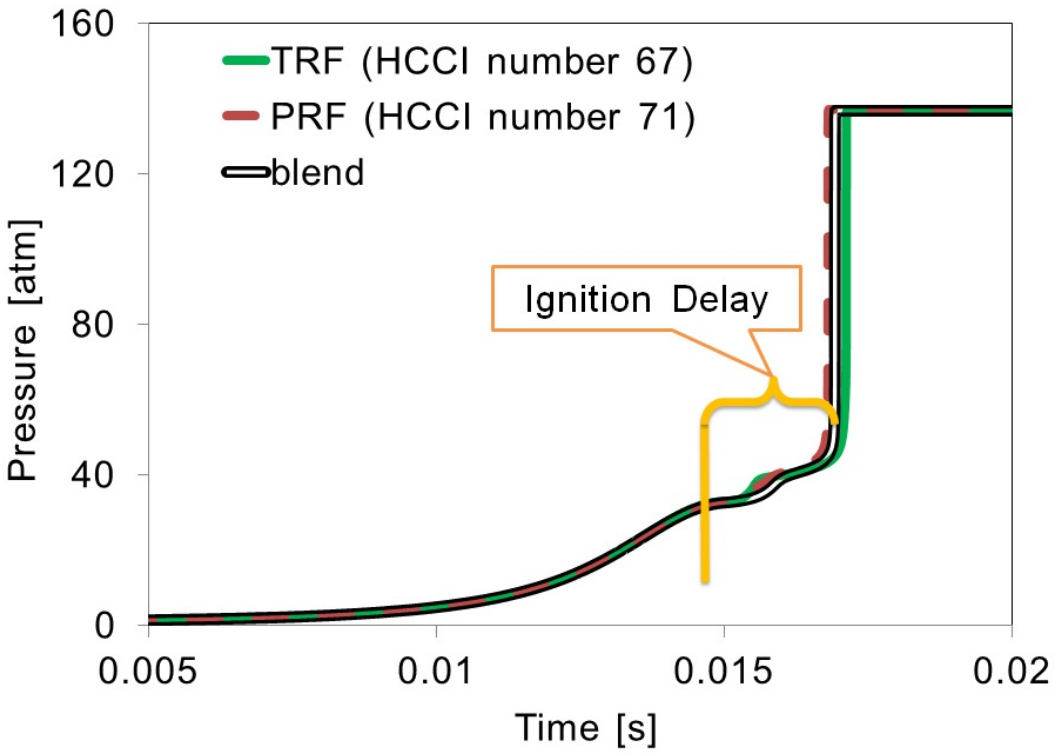


FIGURE 4.37. Simulated Derived HCCI Number (DHN) experiments using an RCM-based DHN test protocol.

shows that the reactivity is relatively consistent between the three fuels as they are within a few milliseconds of one another across the investigated temperature range. With that said, the TRF fuel blend much more closely matches the target fuel blend across a large range of temperatures; this better agreement lends credence to the hypothesis that TRFs are better surrogates than PRFs for "real fuels."

Again, it is important to point out that the above 0-D numerical simulations were performed with a highly reduced mechanism that does not fully capture all of the necessary chemical kinetics. Therefore, more work needs to be done in developing and testing chemical kinetic mechanisms that combine alkanes, aromatics, alcohols and esters that are reasonably accurate over a wide range of conditions.

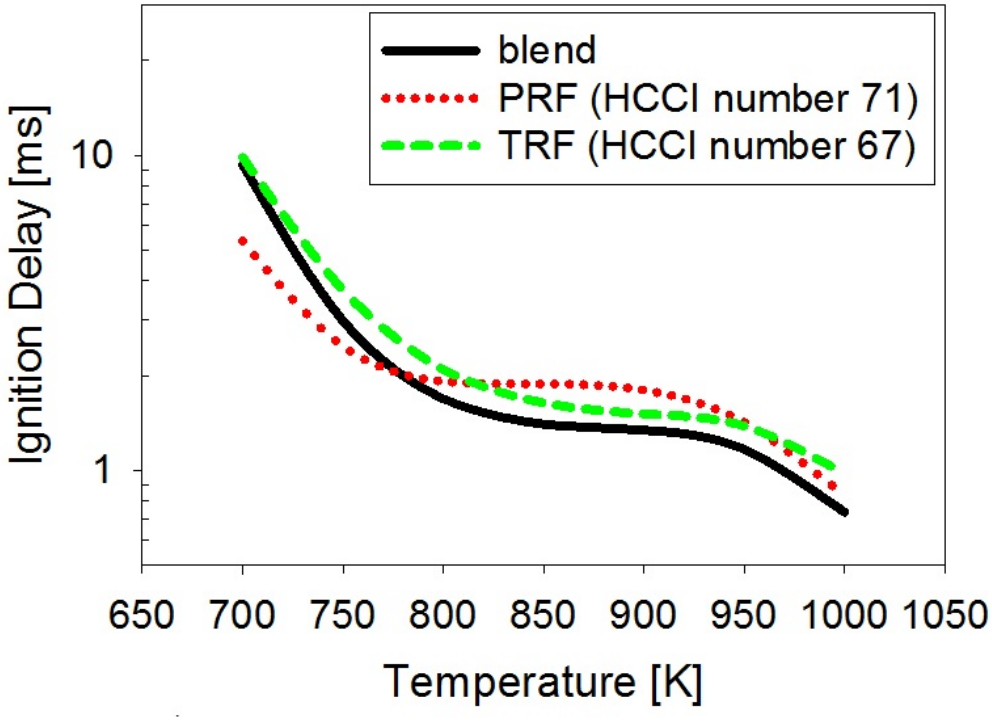


FIGURE 4.38. Calculated ignition delay period versus temperature for the fuel blends considered in the HCCI Number Computational Example.

CHAPTER 5

Other Modeling and Experimental Efforts

The majority of the work presented in this Dissertation centered around developing a more fundamental explanation of existing fuel reactivity metrics and the application and improvement of those metrics to advanced combustion applications. In addition to that work, however, there were a number of other experimental and modeling efforts that both supported and augmented the primary objectives already discussed. Among these were further exploration of the bounds of the FIT, more in-depth research regarding heat transfer in HCCI engines, more robust modeling techniques including modeling the engine from an overall process standpoint as well as 3-D spacial modeling that incorporates full Navier-Stokes and turbulent considerations.

Lastly, the kinetics knowledge gained as a result of studying engine fuels throughout this research was applied to a biomass cookstove to examine the impact of changing ϕ on combustion. The findings of the cookstoves work are relevant to DICI engine results in that they help to explain what occurs at the fuel-lean limit as well as the effect of turbulence on the non-premixed diffusion flame front within the cylinder. Additionally, a simple 1-D flame model was developed which might help to serve as a bridge to explore soot formation in both cookstoves as well as engines.

5.1. Control of Equivalence Ratio in the FIT

As explored in Chapter 4 (Figure 4.4 - shown here again for clarity as Figure 5.2), fuel viscosity was found to have the largest impact on the tested ϕ value. The most likely reason for this is due to the style of injector on the FIT (Figure 5.1). The physical injector unit is

a pintle-style injection. This style of injector appears to inject less volume as a function of a higher fuel viscosity. Initially bulk modulus and density (Figure 5.3) were thought to have an impact but both showed similar/inconclusive trends once the toluene data was considered.

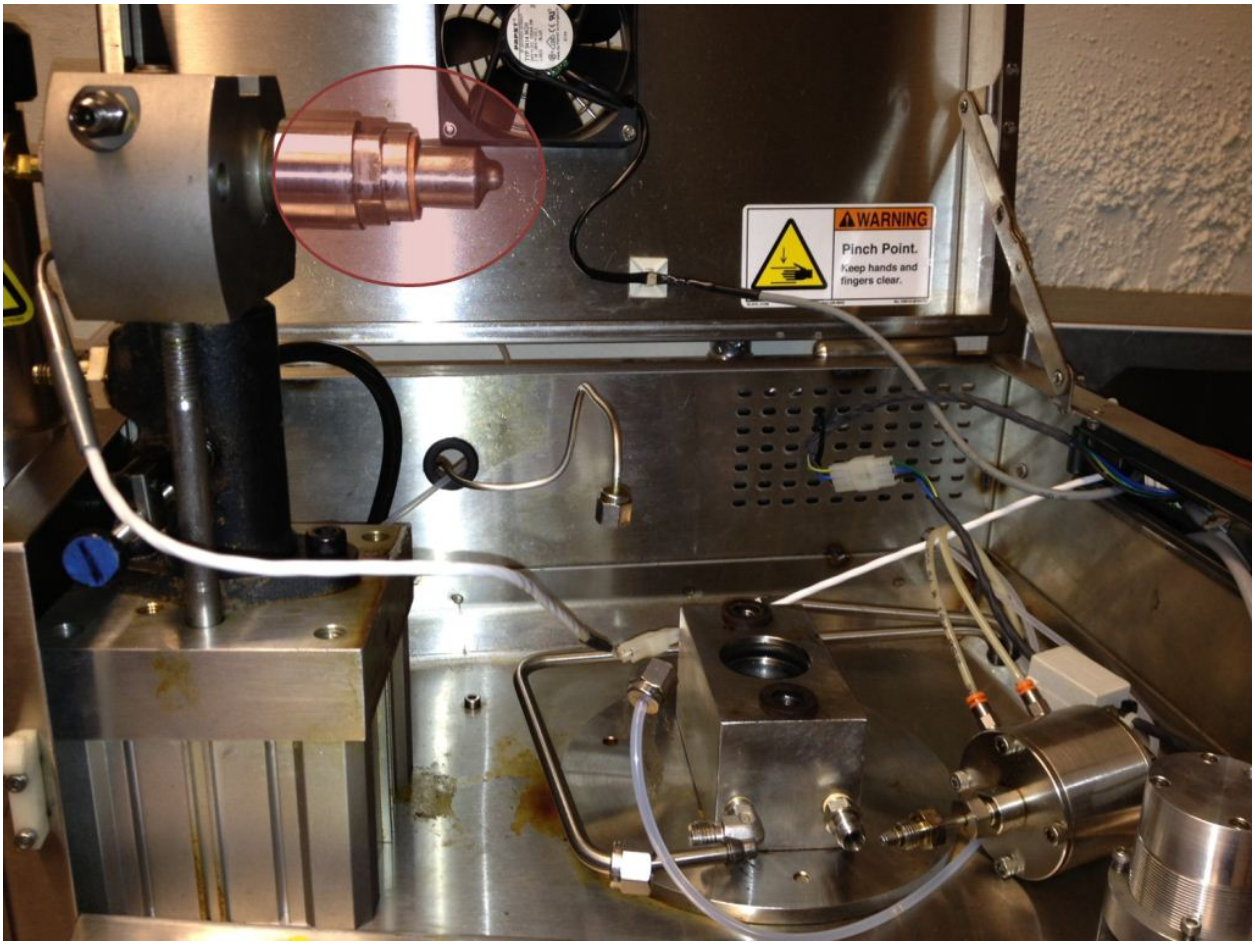


FIGURE 5.1. Picture of the FIT injector unit removed from the FIT for cleaning. The red circled portion is the injector unit.

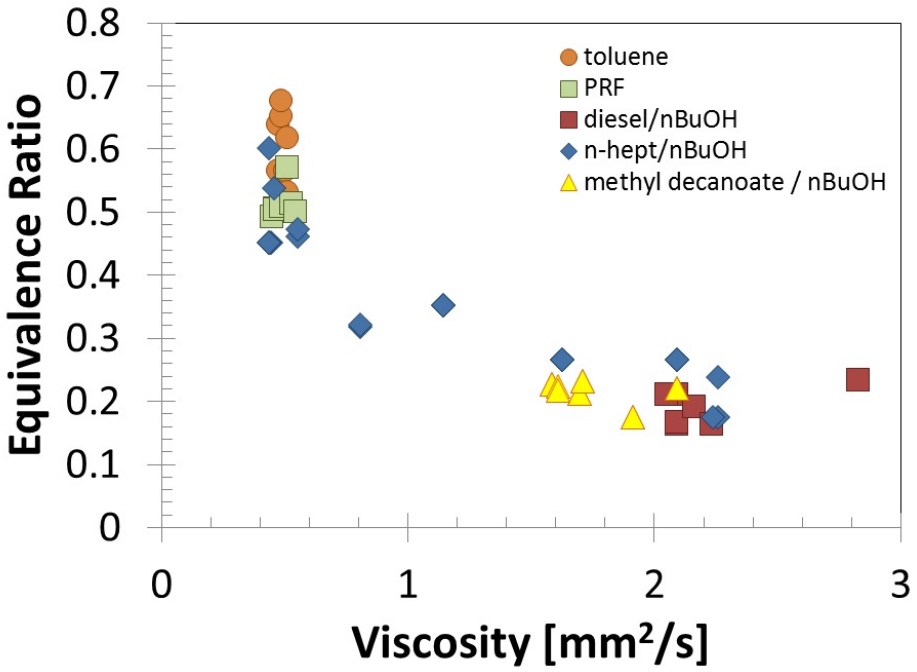


FIGURE 5.2. Measured ϕ values for a wide range of fuels tested in the FIT as function of measured viscosity. Viscosity values were measured via an Anton Paar SVM 3000 Stabinger Viscometer

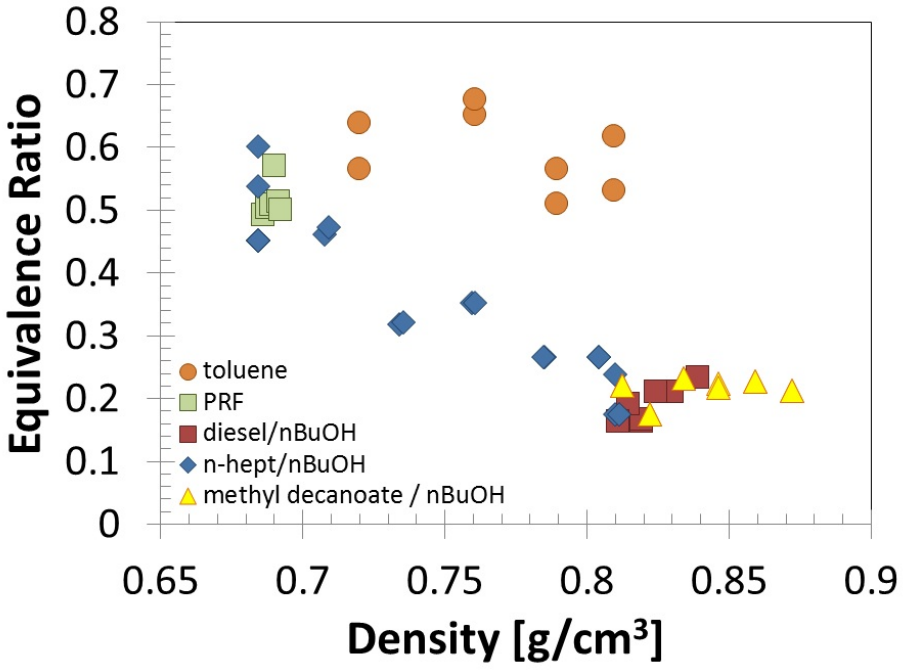


FIGURE 5.3. Measured ϕ values for a wide range of fuels tested in the FIT as a function of measured density. Density values were measured via an Anton Paar SVM 3000 Stabinger Viscometer

Once it was discovered that the FIT did not strictly measure all fuels at a constant equivalence ratio, efforts were undertaken to see if the FIT operation could be adjusted so as to readily adjust the injected ϕ.

As mentioned above, the FIT uses a pintle-style injector to insert fuel into the combustion chamber. The amount of fuel that is fed to this injector is fed via a fuel rack that slides back and forth to, essentially, open a valve. The fuel-adjustment rack is shown in Figure 5.4. Movement of the rack essentially opens and closes a hole through which the fuel flows. In fact, it was found that there is an intrinsic limit to the adjustment of the fuel rack.

According to the ASTM standard[32], the fuel adjustment rack is positioned such that the injection duration is set at 5±0.25 ms. The injection duration is, by default, measured and reported by the FIT. It was initially thought that one could change the injection duration such that it would alter the injected volume of fuel and thus change the ϕ. Experiments were undertaken with n-heptane and n-butanol as well as 40/60 and 60/40 volumetric mixtures of these two fuels to see if they could all be measured at the same ϕ.

For each fuel, the fuel adjustment rack was moved to target an injection duration beginning at ∼3 ms and going as high as ∼8 ms. The global equivalence ratio was then measured for each fuel and the experiment was repeated three times for each fuel-injection duration combination. The resulting 20 data points, representing more than 1500 individual injections, are plotted in Figure 5.5.

These results show that altering the injection duration, on average, allows alteration of the injected ϕ of about ±7.5 percent. These results thus show that some alteration is possible with reasonable repeatability, but that ultimately additional work will be required to alter the injected fuel volume if the FIT is to measure fuels with drastically different viscosities

on an equivalent ϕ-basis. With that said, as presented in Chapters 3 and 4, as long as the tested ϕ is known, then models can be run that correlate quite well with the results obtained from the FIT.

One option that could be considered in the future would be to replace the pintle-style injector with either a gasoline-direct injector or a common-rail diesel injector. This approach would allow greater control over the fuel amount injected. Additionally, if the new injector had high enough pressure, better mixing and heat transfer could be achieved. If this direction is chosen, then it is advised that the injector unit be more easily removable, which would allow better cleaning access as well as a more direct measure of the injected fuel mass.



FIGURE 5.4. Close-up photo of the FIT injection delay adjustment rack.

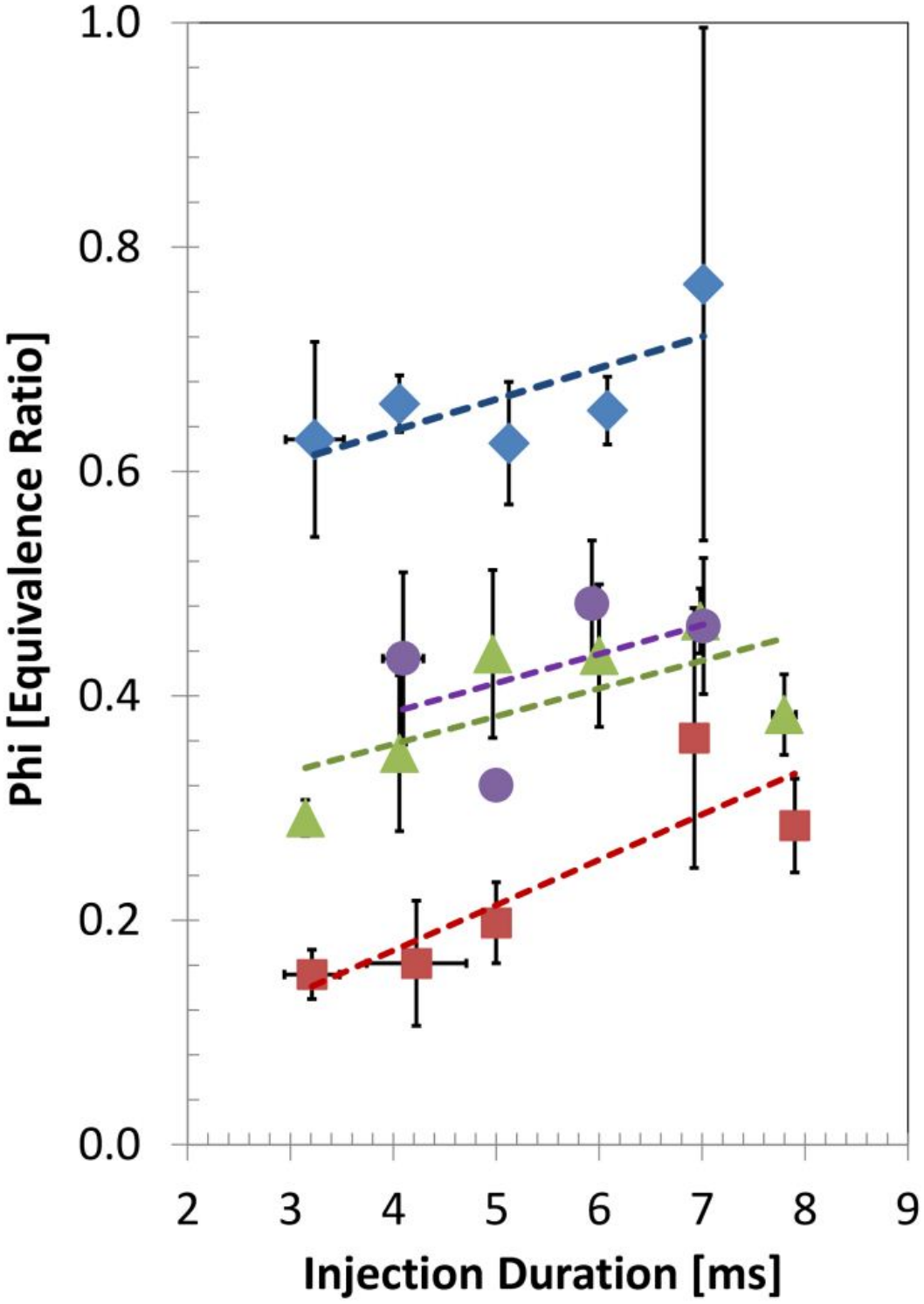


FIGURE 5.5. FIT injection duration effect on ϕ. Blue diamonds are n-heptane, purple circles 60/40v mix of n-heptane and n-butanol, green triangles 40/60v mix of n-heptane/n-butanol, and red squares pure n-butanol.

5.2. Heat Transfer Model Considerations in HCCI

Due to the nature of HCCI, combustion (i.e. ignition timing, ignition timing variance, combustion duration, etc.) is more heavily influenced by the in-cylinder conditions (e.g. instantaneous temperature and pressure) in comparison to SI and DICI engines. On a cycle-by-cycle basis, the in-cylinder temperature is greatly impacted by the heat transfer from the cylinder to the walls, head, and piston. For example, in real engines approximately ∼10-30% of the incoming fuel energy is lost due to such heat transfer[99]. Thus an accurate understanding of the heat transfer effects is essential to understanding and controlling HCCI combustion. This fact becomes more apparent when attempting thermo-kinetic computation analysis.

In this section, analysis of HCCI operation was done via 0-dimensional, sing-zone CHEMKIN HCCI engine simulations. At each solution time step, the energy equation includes a heat transfer term to account for heat lost to the cylinder walls. Most correlations for the heat transfer within engines are based on Newton's original equation for convective heat transfer:

$$\frac{q}{A} = h \cdot \Delta T \tag{39}$$

where q is the heat flux in W, A the area of heat transfer (m^2), and h the heat transfer coefficient in W/m^2K. Delta T in this case is taken as the temperature difference between the in-cylinder temperature and the cylinder wall temperature. The challenge then is to find a good measure of h, where h can be non-dimensionalized by determining the Nusselt number for the given situation. The Nusselt Number is defined in terms of the dimensionless numbers, Reynolds (Re) and Prandlt (Pr):

$$Nu_L = \frac{h \cdot L}{k} = a \cdot Re^b \cdot Pr^c \tag{40}$$

where k is the thermal conductivity, a/b/c are constants. The term, L, is the characteristic length and varies between the different correlations, but is commonly taken to be either the piston bore, or the instantaneous height of the combustion chamber. It should be pointed out here that many correlations take the Pr to be a constant for combustion gases[128]. This may not actually be a good assumption considering that the Pr is defined as:

$$Pr = \frac{c_p \cdot \mu}{k} \tag{41}$$

where the heat capacity (c_p), viscosity (μ), and thermal conductivity are all, individually, functions of temperature. With that said, their combined relationship is somewhat weakly dependent on temperature and the various correlations developed thus far have adjusted their parameter exponents to essentially account for this fact. Most engine heat transfer models are built upon the work of Annand[129], but several of the most widely accepted (and more modern) correlations are examined in this study to determine which one is best suited for modeling HCCI operation. The correlations considered in this work are the standard turbulence model, the Woschni[130] model, Assanis[121], and the Hohenberg[122, 111] model; these are summarized in Table 5.1. In all cases α_s is a scaling constant. Most authors give suggested ranges for this constant, but it ultimately may need to be calibrated for a given engine.

TABLE 5.1. Heat Transfer Coefficient Models

model name	characteristic length, L	model
standard turbulence model	will examine both piston bore and instantaneous combustion height	$h = \frac{k}{L} \cdot (0.0296) \cdot Re_L^{\frac{4}{5}} \cdot 0.7^{\frac{1}{3}}$
Woschni	piston bore	$h = \alpha_s \cdot L(t)^{-0.2} \cdot P(t)^{0.8} \cdot T(t)^{-0.73} \cdot \nu_{tuned}(t)^{0.8}$
Hohenberg	instantaneous combustion volume	$h = \alpha_s \cdot L(t)^{-0.06} \cdot P(t)^{0.8} \cdot T(t)^{-0.4} \cdot (\bar{s}_p + b)^{0.8}$
Assanis	instantaneous combustion height	$h = \alpha_s \cdot L(t)^{-0.2} \cdot P(t)^{0.8} \cdot T(t)^{-0.73} \cdot \nu'_{tuned}(t)^{0.8}$

In Table 5.1, $\bar{s}_p$ is the average piston speed and ν_{tuned} is some measure of gas speed, given by:

$$\nu_{tuned} = c_1 \cdot \bar{s}_p + c_2 \cdot T_o \cdot \frac{v_d \cdot \Delta P_c}{v_o \cdot P_o} \tag{42}$$

for Woschni where v_d is the displacement volume, $v_o/P_o/T_o$ are the values for volume, pressure, and temperature at intake valve closure, and ΔP_c is the pressure increase due to combustion relative to the motored case.

The ν'_{tuned} parameter in Assanis differs from ν_{tuned} in Woschni only by having c_2 being equal to one-sixth the value of that in Woschni. This lower c_2 value is supposed to account for the decreased dependency of HCCI combustion on gas velocity since the combustion process is not driven by a propagating flame, but rather occurs everywhere simultaneously[121]. For this reason, investigations thus far suggest that either the Hohenberg or Assanis correlations might be best suited for modeling HCCI[111, 131].

In an effort to better compare and contrast the various models, it is worthwhile to derive what is a basic form for these equations. By combining Eq. 39-41 with standard turbulent model in Table 5.1, derived using similarity arguments, one obtains:

$$h = \frac{k}{L} \cdot \alpha \cdot \left(\frac{\rho \cdot U \cdot L}{\mu} \right)^{\frac{4}{5}} \cdot \left(\frac{c_p \cdot \mu}{k} \right)^{\frac{1}{3}} \tag{43}$$

where ρ is the density and other variables are defined as above. Equation 43 can be further broken down by noting the following dependences for air, in SI units:

$$\mu \sim T^{0.81}$$

$$c_p \sim T^{0.16}$$

$$k \sim T^{0.8}$$

$$\rho \sim \frac{P}{T}$$

$$h(t) = \alpha_s \cdot L(t)^{-0.2} \cdot P(t)^{0.8} \cdot T(t)^{-0.6} \cdot U(t)^{0.8} \tag{44}$$

Here, α has become α_s and now has units of $(\frac{kg}{m \cdot s^3})^{0.2} \cdot K^{-1}$. At this point it is clear that the exponents of the Woschni and Assanis correlations are slight adjustments from Eq. 44 the differences are drawn from experimental data[121, 130]. The length scale for the Hohenberg correlation is the instantaneous combustion volume and thus its exponent is quite small so as to compare to the smaller length scales of the Woschni and Assanis correlations of piston bore and combustion height, respectively. Chang and Assanis, however, argue that when relying on a length scale to provide an accurate global heat transfer coefficient for a time dependent problem that the length scale should also vary so as to better reflect the overall flow and turbulent parameters. As such, for further development of Eq. 44, the length scale is taken to be the instantaneous combustion height, which is found by dividing the volume by the area at a given crank angle.

One further simplification that could be made to the traditional correlations is to combine the pressure and temperature terms so that the final correlation is expressed with respect to only values that can be readily experimentally measured. By using the ideal gas density relation between temperature and pressure one can obtain:

$$h(t) = \alpha_s \cdot L(t)^{\text{-}0.2} \cdot P(t)^{0.2} \cdot \rho(t)^{0.6} \cdot U(t)^{0.8} = \alpha_s \cdot (\rho(t) \cdot U(t))^{0.8} \cdot \left(\frac{P(t)}{\rho(t)L(t)}\right)^{0.2}. \quad (45)$$

Equation 45 can be further rearranged as:

$$h(t) = \alpha_s \cdot U(t) \cdot \rho(t)^{0.8} \cdot \left(\frac{P(t)}{\rho(t)U(t)} \cdot \frac{1}{L(t)}\right)^{0.2} \quad (46)$$

where the third term has the units of $\frac{\text{m}}{\text{s}}$ and can be thought of as a 'dynamic combustion velocity' and is given the symbol ν_c'. This leaves a density $\cdot$ velocity term in front that except for the exponent on density is much like a momentum term. By adjusting the scaling term appropriately, the density term can be effectively simplified to having a unity exponent, which leaves a momentum term (defined as ω_c) multiplied by the aforementioned "velocity" term; this all implies that the heat transfer coefficient can be defined as a function of something analogous to a dynamic combustion pressure:

$$h(t) = \alpha_s \cdot \omega_c(t) \cdot \nu_c'(t)^{0.2} \quad (47)$$

The scaling term, α_s now has units of $K^{\text{-}1} \cdot m^{1.4} \cdot s^{\text{-}1.8} \cdot kg^{0.2}$. The main advantage to Eq. 47 is that all the parameters can be empirically measured; henceforth Eq. 47 will be referred to as the Simplified Ht Model. Setting the heat transfer coefficient proportional to a 'dynamic combustion pressure' makes some intuitive sense in that the measured pressure is reflective of the in-cylinder temperature, which drives the heat transfer through the cylinder walls. The applicability of the Simplified Ht Model in combustion analysis is further explored below.

As mentioned in Chapter 2, the engine used in this study is a diesel engine that has been converted for use as an HCCI test bed. The HCCI data shown in this section (Figure 5.6) was acquired at compression ratio of 16:1, while the three diesel cylinders ran in the stock configuration of 18:1. Engine speed was kept constant at 1500 RPM, fuel/air equivalence ratio was 0.3, the inlet temperature was set at 70 $^{\circ}C$, and a 60/40%v mixture of n-heptane and n-butanol, respectively, was used as the HCCI fuel. To ensure accuracy, each data point consists of an average of 100 consecutive cycles.

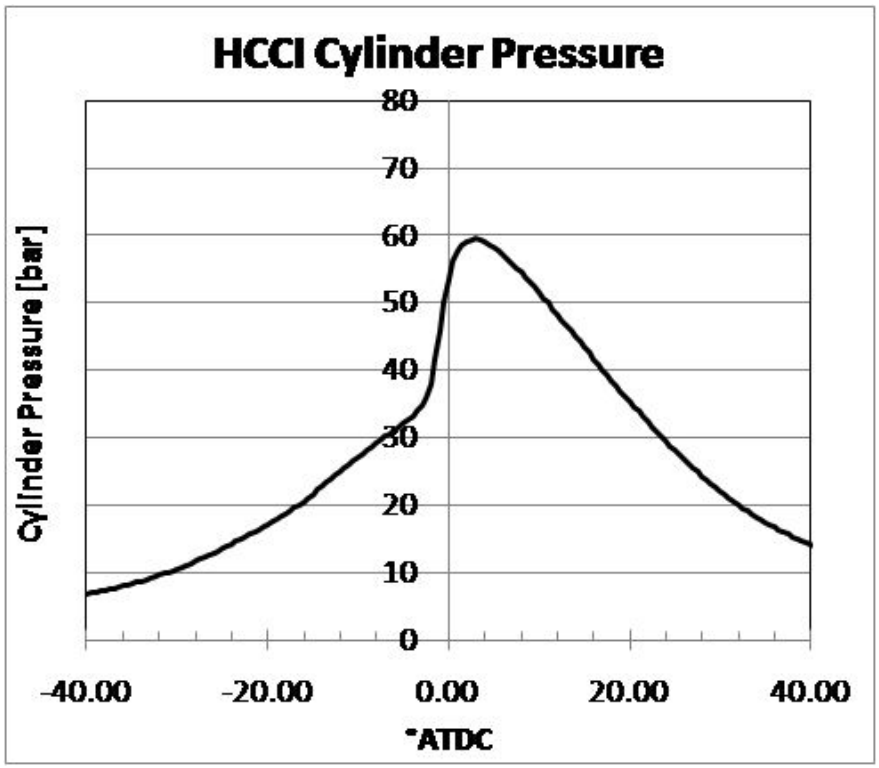


FIGURE 5.6. HCCI Example used in Heat Transfer Modeling. Trace taken at 1500 RPM, $\phi = 0.3$, $T_{in} = 70\ ^{\circ}C$, 60/40%v n-heptane/n-butanol.

To calibrate/scale each model to the specific engine used in this study, a motored pressure curve was first simulated via CHEMKIN using adiabatic conditions. Then each heat transfer model was included and the model scaling factor (α_s) was changed until the simulated curve

matched the experimental curve. Tables 5.2 and 5.3 show the differences in original and calibrated models.

TABLE 5.2. Default Heat Transfer Coefficient

correlations	Woschni	Hohenberg	Assanis
α_s	2	85	0.028
L coeff	-0.2	-0.06	-0.2
P coeff	0.8	0.8	0.8
T coeff	-0.55	-0.4	-0.73
U codff	0.8	0.8	0.8

TABLE 5.3. Tuned Heat Transfer Coefficient

correlations	Woschni	Hohenberg	Assanis
α_s	3.26	130	0.035
L coeff	-0.2	-0.06	-0.2
Length	bore	volume	comb height
P coeff	0.8	0.8	0.8
T coeff	-0.55	-0.4	-0.73
U coeff	0.8	0.8	0.8
speed	U'	U_{avg} + 1.4	U"

After being calibrated for the motored case, the simulations were run to predict the adiabatic HCCI case followed by cases with each heat transfer correlation using the scaling factors normalized to the motored case. Figure 5.7 shows the calculated heat transfer coefficient values as a function of crank angle. Notice that the Woschni correlation under-predicts the heat transfer prior to ignition and over predicts it after ignition compared to other correlations, which is typical according to the literature[111, 128, 131]. Even so Figures 5.8 and 5.9 show that overall, the tuned Woschni correlation under predicts accumulative heat transfer when compared to the experimental data.

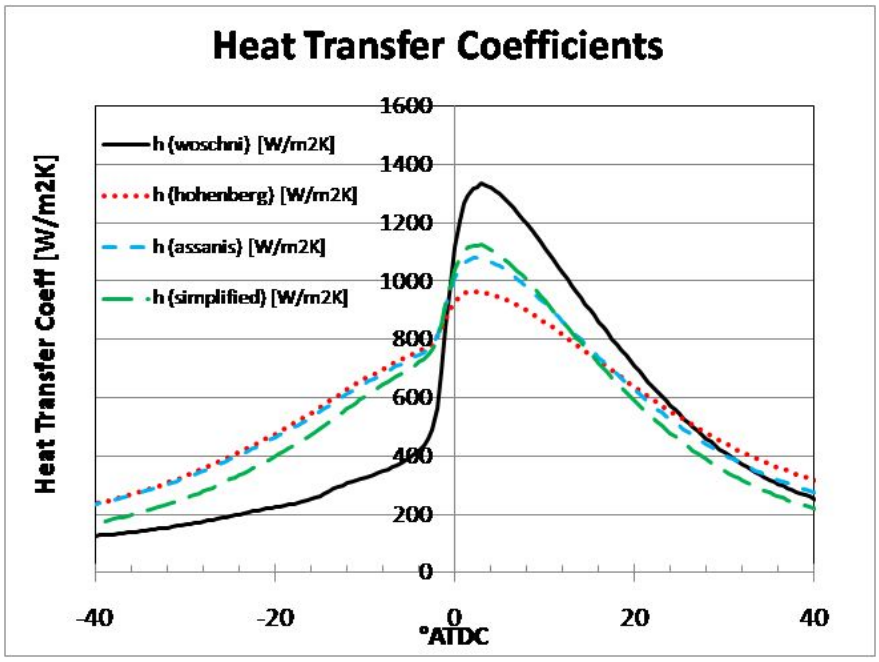


FIGURE 5.7. Single-zone CHEMKIN modeled heat transfer coefficients at experimental conditions: 1500 RPM, $\phi = 0.3$, $T_{in} = 70\ ^{\circ}C$, 60/40%v n-heptane/n-butanol.

Figures 5.8 and 5.9 show the resulting pressure traces for the different runs including heat transfer as well as the experimental and adiabatic cases. Overall the CHEMKIN models are fairly accurate at predicting what is observed experimentally. The Assanis and Hohenberg correlations are the best at matching the expected location of peak heat release as well as the value of peak pressure. Figure 5.9 shows that the pressure rise rate is much higher in the simulated cases than in reality. This is primarily a result of two main effects. The first is that the experimental mixture is likely not truly homogeneous and thus the combustion process will occur in a cascading effect first igniting in pockets of rich mixture and then transitioning to areas of leaner mixture. Secondly, the simulation results are modeled as only a single zone and so wall and crevice effects are not fully taken into consideration. Results shown in Chapter 4 as well as literature values have shown that increasing to multi-zone models better captures the exact pressure rise rate profile and does a better job of

predicting the peak combustion conditions and timing[10] as well as conditions throughout the cylinder which can be important when predicting emissions[132].

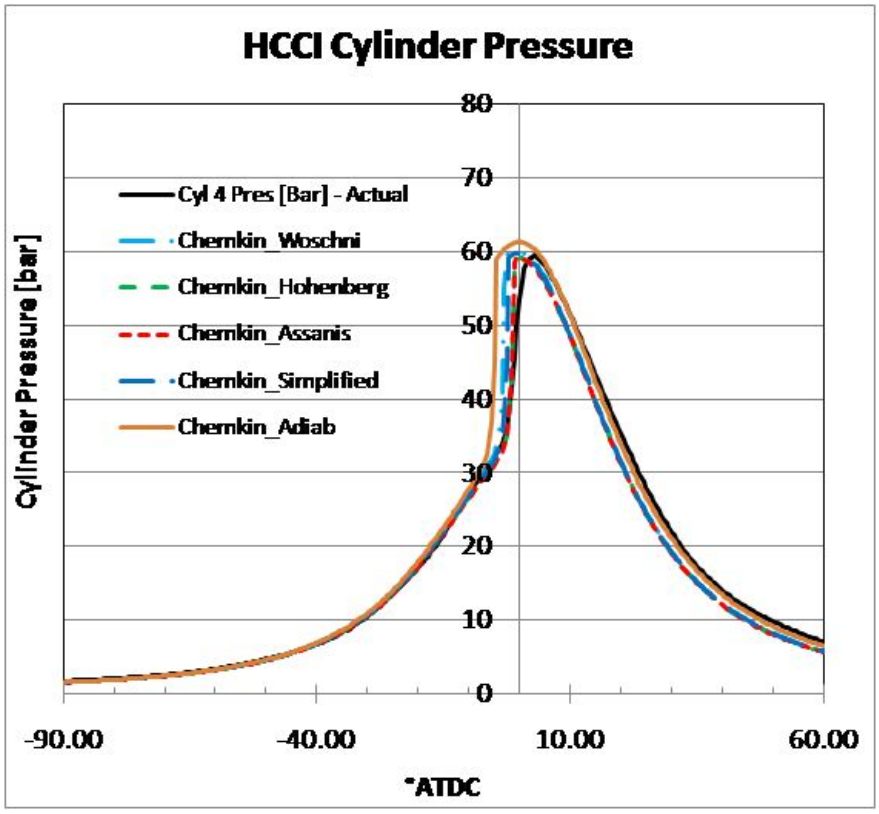


FIGURE 5.8. Pressure traces of actual, adiabatic, and single-zone model runs (including heat transfer) at experimental conditions: 1500 RPM, $\phi = 0.3$, T_{in} = 70 $°C$, 60/40%v n-heptane/n-butanol.

The fact that the Assanis and Hohenberg correlations best match the experimental data is supported by other studies[111, 131]. In fact both correlations exactly predict the location of peak heat release, which is critical in modeling proper HCCI operation. One of the biggest challenges in HCCI is predicting and controlling the ignition point[10]. The fact that these two correlations predict so similarly is not too surprising since, as shown in Figure 5.7, the calculated heat transfer coefficients are almost the same when tuned properly Soyhan showed similar results[111]. It is of note that the Simplified Ht Model is also very close to the Hohenberg and Assanis correlations, but predicts a premature ignition point due to

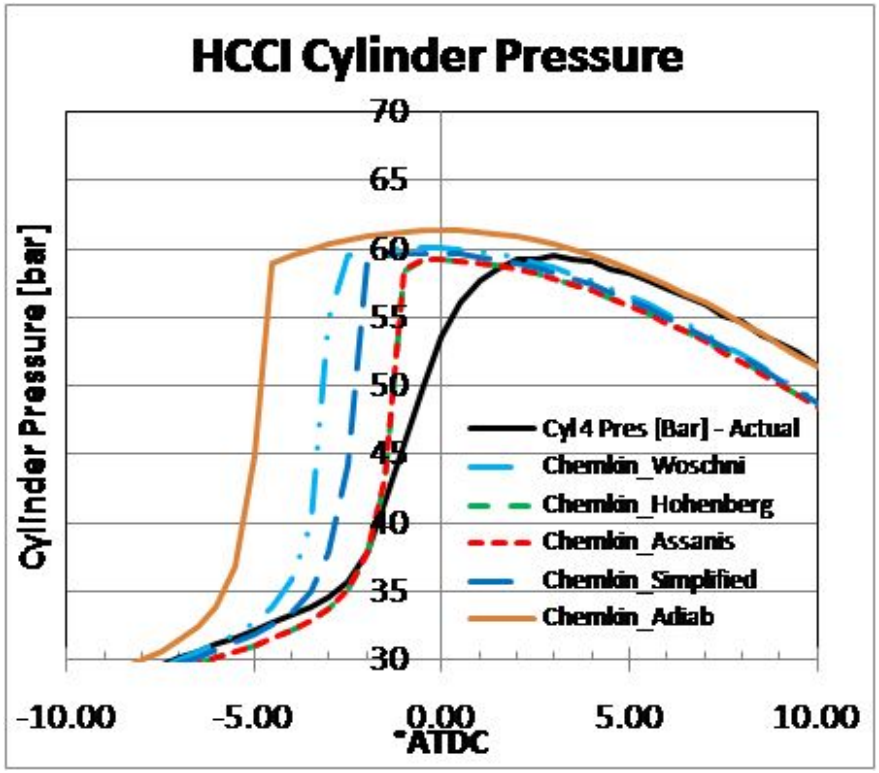


FIGURE 5.9. Close-up of pressure traces of actual, adiabatic, and single-zone model runs (including heat transfer) at experimental conditions: 1500 ron, ϕ = 0.3, T_{in} = 70 $°C$, 60/40%v n-heptane/n-butanol.

a lower heat transfer prediction in the pre-ignition regime. Table 5.4 shows the predicted location of peak heat release for all of the models considered. Again, note that though the simplified model makes more assumptions than any of the correlations it matches better than the tuned Woschni correlation and is only off by one degree crank angle.

TABLE 5.4. Location of Peak Heat Release Predicted by each Model

model	crank angle
actual	-1.5°ATDC
Woschni	-3°ATDC
Hohenberg	-1.5°ATDC
Assanis	-1.5°ATDC
Simplified	-2.5°ATDC
adiabatic	°ATDC

Next, the instantaneous heat release was found using:

$$\frac{dQ}{dt}_{gross} = \frac{\gamma}{\gamma - 1} \cdot P \cdot \frac{dV}{dt} + \frac{1}{\gamma - 1} \cdot V \cdot \frac{dP}{dt} + \frac{dQ}{dt}_{ht} \tag{48}$$

where γ is the ratio of specific heats and $\frac{dQ}{dt}_{ht}$ is used, when appropriate, to find the net heat loss. taking the integral of Eq. 48 yields the accumulative heat release for the cycle. Using the measured equivalence ratio and engine speed the total fuel use per cycle is noted and from this a total theoretical heat release of ∼475 J/cycle was calculated - assuming lower heating value (LHV) of 40.07 MJ/kg for the 1-butanol/n-heptane mixture.

Figure 5.10 shows the accumulative net heat released as work as well as the net heat loss calculated for each correlation. All four correlations are quite close and predict that the net heat loss is approximately 12% of the theoretical LHV. This is primarily due to calibrating all the models in the same fashion to the motored pressure case. Additionally, the measured HCCI engine efficiency is found to be ∼54%; where efficiency is found via:

$$\text{Efficiency} = \frac{\text{Accumulative Energy Released as work } [J]}{\dot{m}_{fuel,in} \cdot LHV_{fuel}} \tag{49}$$

This is much higher than traditional SI or DICI engines. The high efficiency is a result of the relatively short duration of heat release this fast ignition is also why the net heat loss to the cylinder walls is lower than typically seen in SI and DICI.

Though all models were able to closely match ignition timing, none of the models were able to show the low temperature chemistry that was seen experimentally. Figure 5.11 shows the period just prior to full ignition. It is commonly known that some fuels, especially alkanes with low branching and steric hindrances, such as n-heptane exhibit low temperature chemistry[70, 133]. This low temperature chemistry (LTC) is quite important in HCCI

combustion as it contributes to initiation of full ignition (Dec, 2009). The Assanis correlation comes closest to predicting the timing of the LTC but is premature by about 10 degrees and is also lower in magnitude by about a factor of four. This could be accounted for by adjusting the reaction kinetic constants, or possibly trying a different kinetic mechanism altogether.

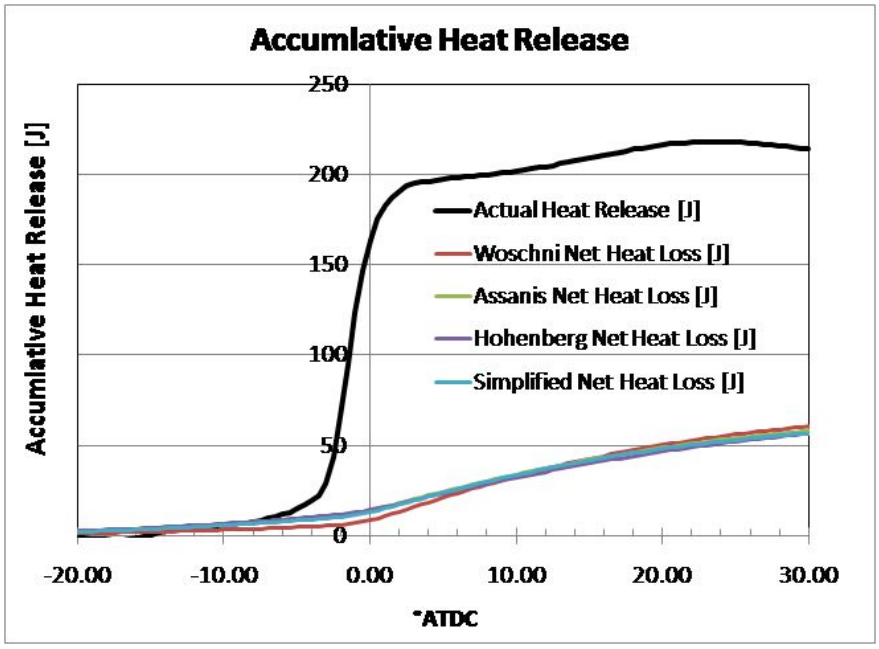


FIGURE 5.10. Accumulative net heat release for single-zone experimental and calculated heat release runs at experimental conditions: 1500 RPM, $\phi = 0.3$, $T_{in} = 70\ ^{\circ}C$, 60/40%v n-heptane/n-butanol.

In conclusion, three of the most widely used heat transfer models were examined and compared to actual HCCI engine data obtained by the Author. Additionally, a simplified model was developed and found to compare well with the traditional correlations. All models were scaled to match the experimental engine and found to give good agreement with experimental data. Out of the four correlations simulated, the Assanis and Hohenberg correlations most closely matched the experiment and were able to exactly predict the ignition timing and value of peak pressure. The single-zone CHEMKIN model was accurate for predicting these relevant control parameters but failed to accurately predict the rate of pressure rise

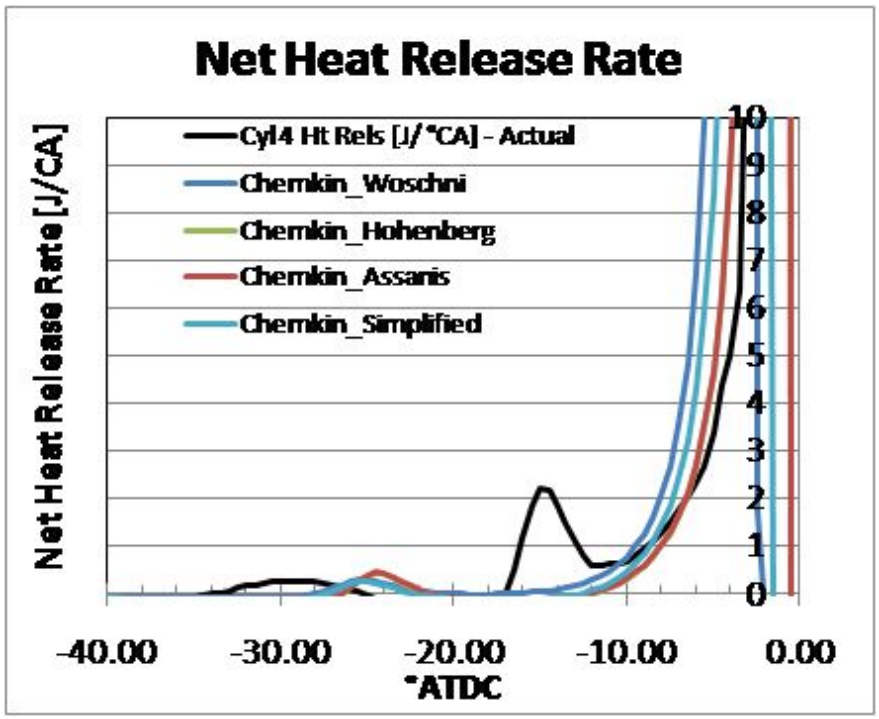


FIGURE 5.11. Low temperature heat release for single-zone experimental and calculated heat release runs at experimental conditions: 1500 RPM, $\phi = 0.3$, $T_{in} = 70\ ^{\circ}C$, 60/40%v n-heptane/n-butanol.

this was ultimately corrected by using a multi-zone simulation instead of a single-zone model (data shown in Chapter 4). However, the knowledge gained here was invaluable and carried over to the multi-zone modeling where the Chang and Assanis model was used.

5.3. GT POWER HCCI MODELING

The simulations in this section were carried out in GT-SUITE, developed by Gamma Technologies. GT-SUITE is a computer-aided engineering software package that allows modeling of most aspects of a vehicle, from complete suspension dynamics to engine and combustion models[134]. Thus, it is often used by both researchers and industry to perform various simulations in these areas[135]. As a reference, Version 7.1.0 was used in this study. Specifically, the engine simulation sub-model, GT-Power, was used. GT-Power simulations are one dimensional gas dynamic solutions of the nonlinear Navier-Stokes equations including

fully coupled mass, momentum, and energy equations. Additionally, GT-Power has the capability of using smaller (<2000 species by default) CHEMKIN-style chemical reaction mechanisms. Only zero-spacial dimension simulations can be run but GT-Power does have some capability to numerically simulate some fluid effects such as tumble and swirl.

The GT-Power work discussed here was presented at the Fall Technical Meeting of the Western States of the Combustion Institute[136]. The major focus of this GT-Power study was to examine the heat transfer capabilities of GT-Power. In the end, GT-Power proved to yield similar results to CHEMKIN. However GT-Power does have some advantages compared to CHEMKIN. As a result of solving the Navier-Stokes equations, GT-Power is able to run through several cycles of an engine and can get more accurate values for in-cylinder conditions such as the pressure and temperature at intake valve closure.

Figure 5.12 shows the block diagram used for the GT-Power model. The intake runner model begins just upstream of the intake heater, but downstream of the turbo, while the exhaust runner model ends just downstream of the exhaust valve but upstream of the turbo. The experimental valve profiles were input into GT-Power, but the measurements were somewhat coarse, therefore filters were added to the intake and exhaust valves to smooth the lift profiles. The lift profiles can be found in Appendix E.

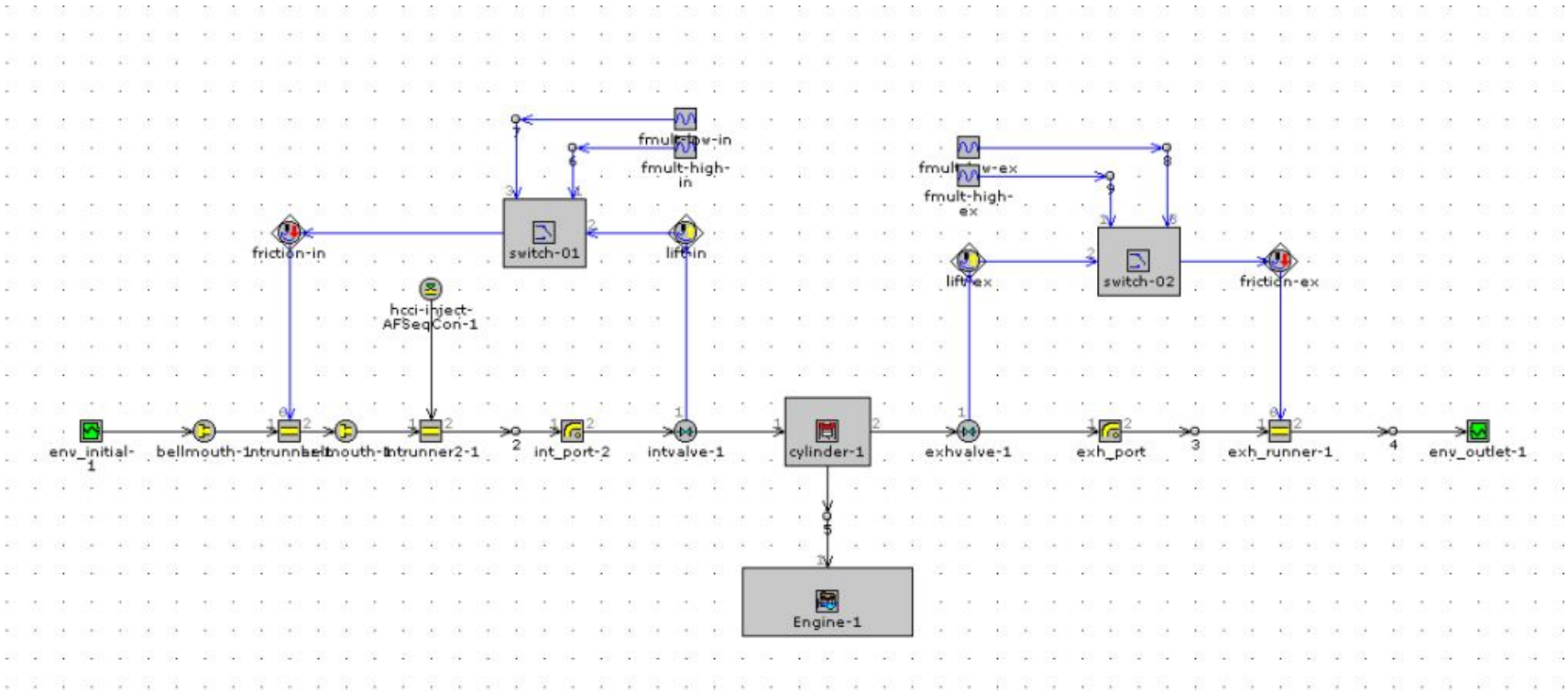


FIGURE 5.12. GT-Power Block Diagram of the CSU HCCI Engine

Figures 5.13 and 5.14 show the outputs of the GT-Power model run at an intake temperature of 70 $^{\circ}C$, intake pressure of 1.15 bar, speed of 1500 RPM, and ϕ of 0.33, and with a PRF40 as the fuel. These intake parameters were adjusted (primarily the intake pressure) slightly from the experimental values in order to get the best match possible between the simulation and the experimental data at TDC-combustion. The solved pressure and temperature at IVC were found to be extremely close to the experimental conditions and are within the error of the experiments. The similarity between the GT-Power and CHEMKIN simulations gives more confidence in the CHEMKIN values since those simulations do not take any sort of flow characteristics into account when solving.

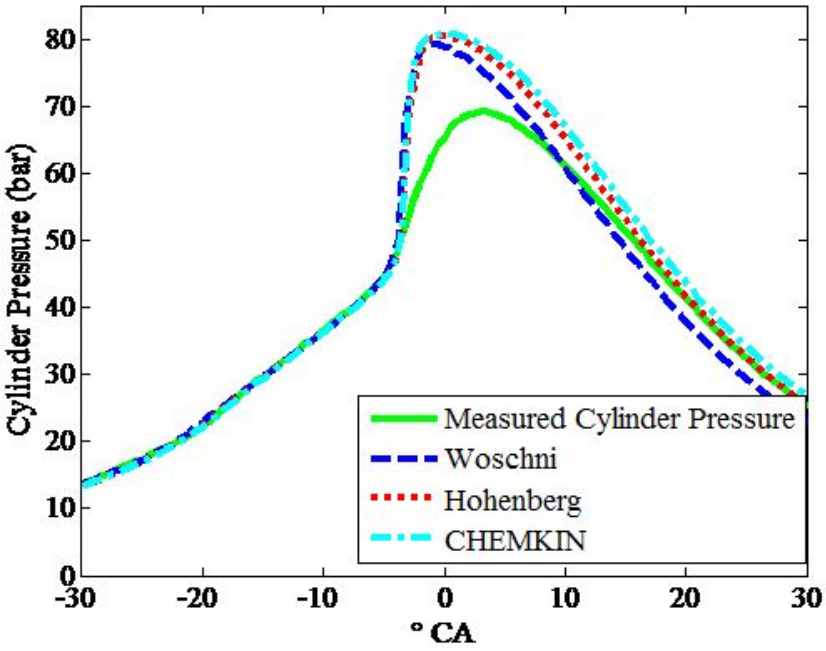


FIGURE 5.13. Measured, CHEMKIN, and GT-Power cylinder pressure traces. The GT-Power simulations cover both Hohenberg and Woschni heat transfer models.

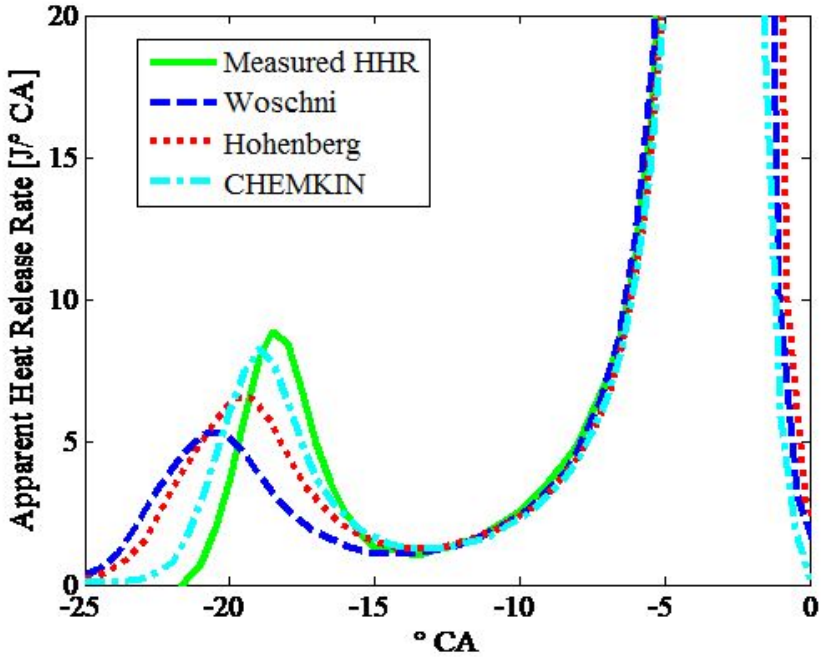


FIGURE 5.14. Measured, CHEMKIN, and GT-Power low temperature heat release traces. The GT-Power simulations cover both Hohenberg and Woschni heat transfer models.

One benefit of GT-Power is that operating conditions can be swept across ranges of interest. For example, Figure 5.15 shows a sweep in RPM for PRF40. In this case it is easy to see that in-cylinder temperature is predicted to increase with RPM, which should result in more advanced combustion timing for a given fuel. However, there is actually a retardation in combustion timing. These simulations suggest that the reduction in time near TDC (increased RPM) overwhelms the increase of in-cylinder temperature - all other things being constant.

This example further highlights the influence of the "K" term from the Octane Index equation, i.e. the engine operating parameter, on fuel octane requirements. The influence that held true for SI engines (see Figure 3.11), also holds true for HCCI engines. In this case, as in-cylinder temperature is increased, the octane requirement actually needs to decrease to allow peak combustion to remain close to TDC. Here again a more sensitive fuel will allow

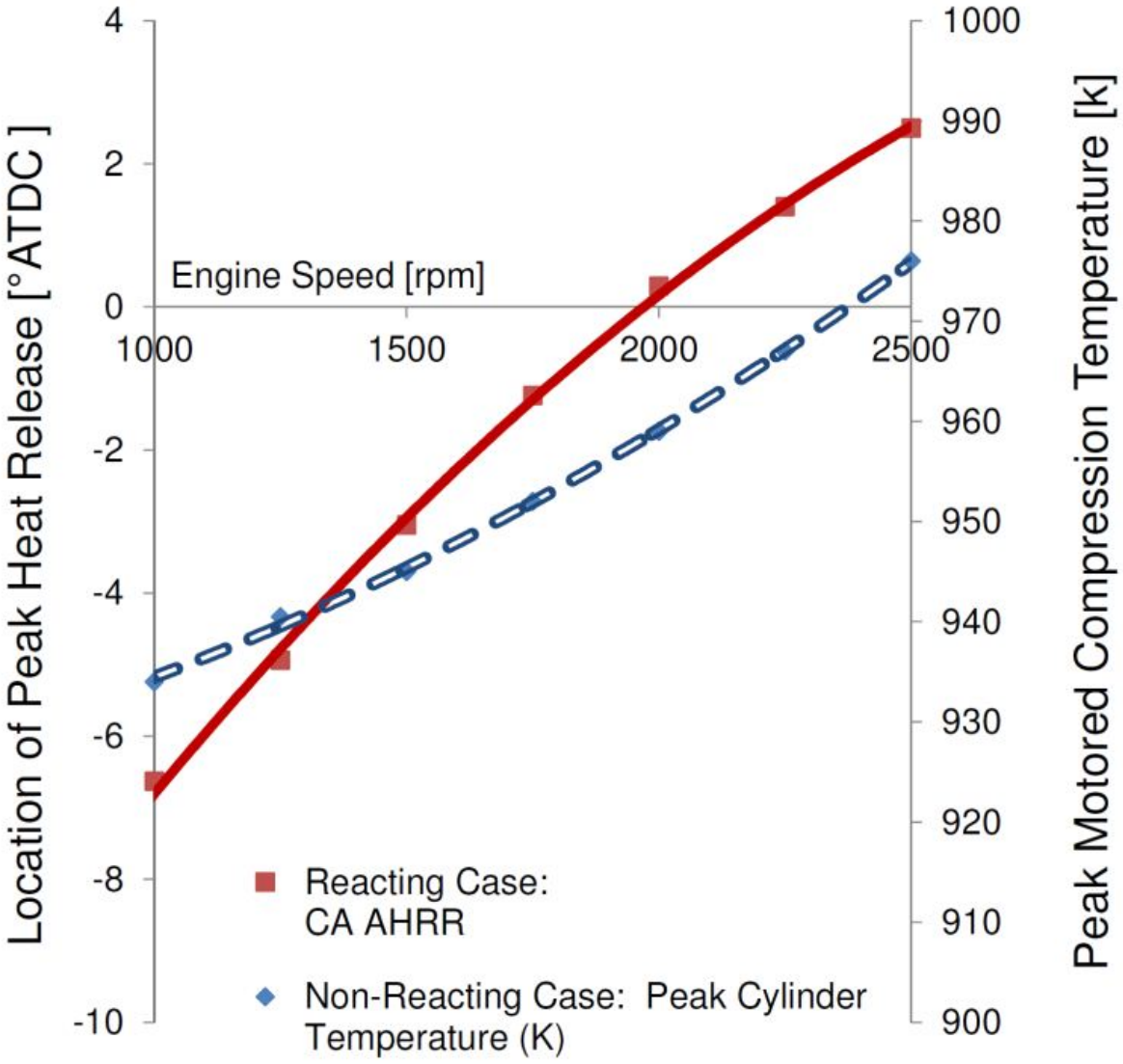


FIGURE 5.15. GT-Power simulated sweep in engine speed. Shown is data for the location of peak heat release for PRF40 and the peak compression temperature for a non-reacting case as functions of RPM.

further relative decrease in knock resistance (see how n-butanol moves closer to n-heptane in Figure 5.16), which results in peak combustion temperatures staying closer to TDC and actually extending the operational efficiency of HCCI engines.

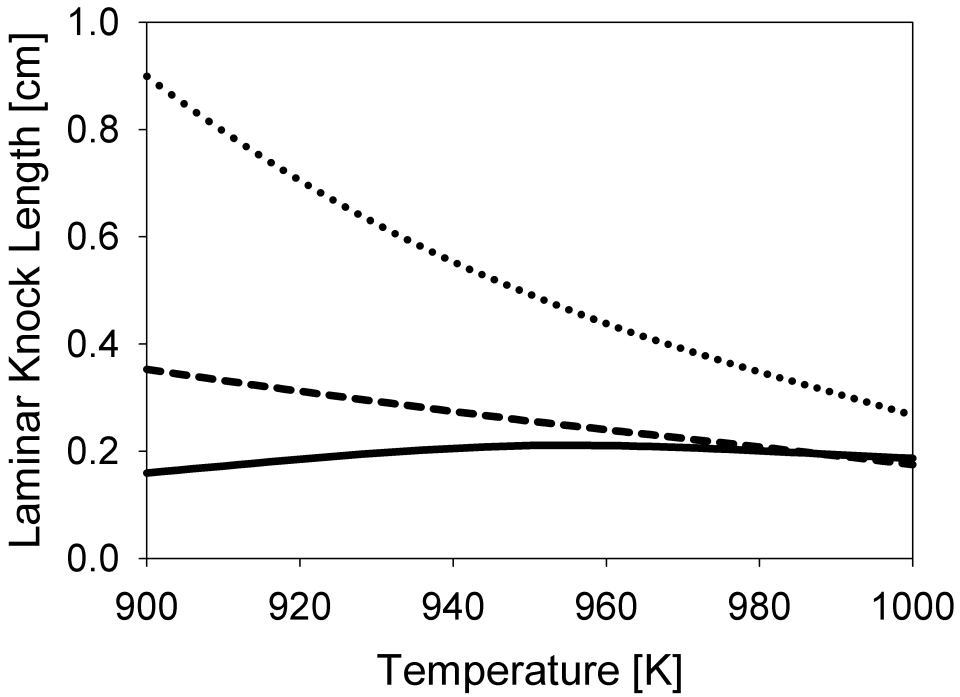


FIGURE 5.16. Calculated laminar knock lengths for n-heptane (black solid line), i-octane (dotted line), and n-butanol (dashed line) over the range covered in Figure 5.15.

The GT-Power model, thus provides a valuable way to better examine the likely in-cylinder conditions upon valve closure and opening. Although, it is important to consider the various advantages and drawbacks between the different simulations methods.

CHEMKIN is vital for considering full chemistry and kinetics. Single-zone CHEMKIN simulations are quick and easy to perform and give a great first estimate to a solution when comparing against experimental data. CHEMKIN-PRO increases the fidelity of the simulations allowing for multiple zones and better capability of capturing stratifications of in-cylinder temperature.

GT-Power simulations take longer to set-up but consider more fluid dynamics than do the CHEMKIN simulations. The main drawback of the default solver is the cap on species number ($\leq$2000 species) and only the capability of running 0-D simulations. However, the

benefit is that the fluid-dynamic capabilities allow the user to better model the in-cylinder conditions at valve closure. It is also important to mention that GT-Power can be integrated with CHEMKIN to combine the strengths of both. However, combining programs in such a way was beyond the scope of this work and is something to be considered for the future.

One further evolution in modeling is the CONVERGE commercial software, which is capable of combining full 3-D spacial modeling (using adaptive meshing techniques) with chemically reacting flow-kinetics. Unfortunately, computing power is the limiting factor for such software. Simultaneously solving for more than approximately 150 unique chemical species in the case of an engine simulation is prohibitively expensive in terms of time-cost. In short, the CONVERGE software is the "other-side of the coin" compared to CHEMKIN. Whereas CHEMKIN lacks fundamental physics, CONVERGE fully incorporates the relevant physics, but does so at a drastically reduced ability to model chemical-kinetics. The trade-offs are arguable, but the advantage for most CONVERGE applications is that often full chemical-kinetics are not required and an adequate solution can be developed with chemistry that is 'good enough.' CONVERGE is explored more in the next section.

5.4. CONVERGE HCCI Modeling

In this section, efforts to complete CONVERGE modeling of the CSU HCCI Engine are presented. Overall, much work still needs to be done to get a viable model of the engine, but the work done to date is presented herein. In general, most of the time-consuming construction of the model has been completed and what remains is to fine-tune the CONVERGE parameters and run cases against experimental data. The basic steps of creating a CONVERGE model are as follows:

(1) Build a 3-D model of the cylinder including intake/exhaust valves and runners (see Figure 5.17). Be sure that the valves and piston are 'mated' such that they are movable. Additionally, set the minimum clearance of the valve-head to the valve-seat to be 0.2 mm - this will ensure the fluid body is connected in CONVERGE.

(2) Extract the fluid volume contained by the 3-D model. This will consist of the in-cylinder volume as well as that in the intake and exhaust runners.

(3) Import the 3-D model into CONVERGE and define the surfaces. Identifying and naming the surfaces will entail an initial meshing of all the parts. It is critical at this point to define what is the 'cylinder,' 'piston,' valves', and 'runners.' See Figure 5.18.

(4) If the simulation is to solve for species fractions, then import the relevant chemical-kinetic mechanism.

(5) Chose 'Simulation Parameters' such as min/max time steps. For this portion, most of the defaults are acceptable for a first pass at a simulation.

(6) Set the initial/basic boundary conditions, which will include defining surfaces as stationary or moving boundaries, surface temperatures (and temperature boundary conditions), and roughnesses parameters. This portion will include things such as valve lift profiles.

(7) Set the inlet/outlet flow conditions including species names/fractions, pressures, temperatures, and if there is any sort of velocity gradient or turbulent energies. For example, typical turbulent kinetic energy boundary conditions are a intensity fraction of 0.02 and a length scale of 0.003.

(8) Input the 'Events' such as valve opening and closing times.

(9) Chose the proper 'Physical Models' such as combustion and turbulence models. This portion is primarily to set the solver bounds for these models - again defaults are typically fine for first passes.

(10) Finally, set the 'Grid Controls' including the max and min grid sizes.

Once all the parameters are set, then CONVERGE can be run from the appropriate Linux Cluster or other computing network. At the time of this writing the Marchese Research group has a Linux Cluster (56 core processors) capable of running a CONVERGE simulation. Generally, a properly executed CONVERGE simulation including a full 720 degrees can be completed within 10-20 hours using ∼100 species chemical mechanism.

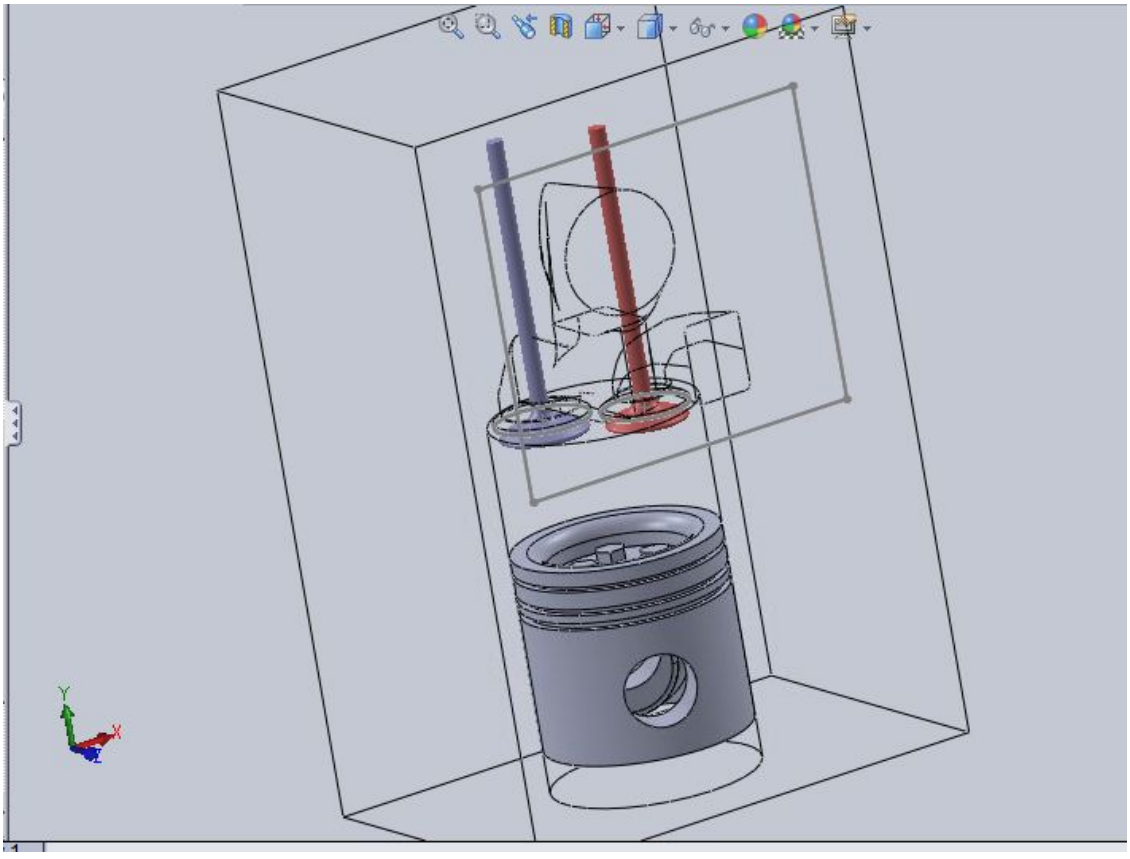


FIGURE 5.17. Solidworks 3-D Model of the CSU HCCI Engine

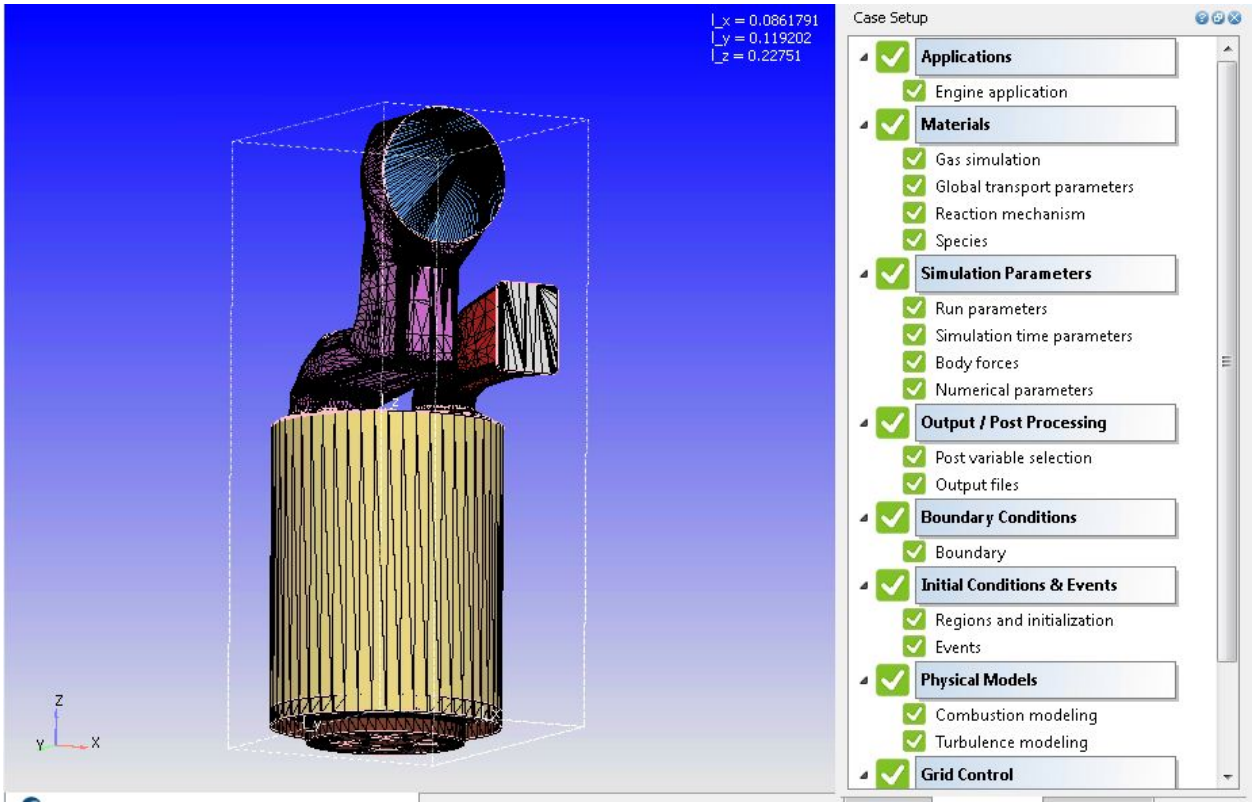


FIGURE 5.18. Picture of the HCCI 3-D cylinder model imported into CONVERGE

5.5. CHEMKIN 1-D FLAME MODEL

This section describes the chemical kinetic modeling approach that was undertaken to accompany a collaborative study with Dr. Jason Prapas of CSU in which we analyzed chimney-based biomass cookstoves. The findings presented here are potentially relevant to DICI engines as both DICI engines and open flame cookstove combustion center around the non-premixed diffusion flame front. Note that much of this work was submitted as a journal article to Biomass and Bioenergy, and is currently under review.

Attempts were made to, as accurately as possibly, represent the combustion approach that is thought to occur in the combustion of non-premixed diffusion wood flame. It was decided to focus on the detailed chemistry in this process and use a simplified-physics approach as

it was too computationally intensive to try and capture both effects. Note that a similar approach could possibly be taken in examination of DICI engines.

5.5.1. Chimney CHEMKIN-PRO Model. Often, the combustion of wood has been described by a generalized, one-step overall reaction process:

$$wood\,gas + a(O_2 + 3.76 \cdot N_2) \rightarrow n_1 \cdot CO_2 + n_2 \cdot H_2O + n_3 \cdot N_2 + n_4 \cdot O_2 + n_5 \cdot CO + n_6 \cdot H_2 \quad (50)$$

where the wood gas is described by some overall elemental composition similar to any hydrocarbon-based fuel: $CH_yO_zN_f$. The overall carbon content of wood can vary based on wood type and harvest environment, i.e. hardwood, softwood, local climate where the wood is harvested, nutrient availability, etc. The carbon content ultimately affects the quantity of air that will be required for combustion. A more accurate estimation of wood combustion can be obtained by considering the actual chemical structure of wood and the subsequent evolution of pyrolysis gas; to this end, a good estimate of the stoichiometric amount of air to burn 1kg of wood is approximately 6.4kg of air[137].

In order to determine the constituents of pyrolysis gas, first the structure of wood must be considered. Wood is primarily comprised of chains of cellulose ($C_6H_10O_5$), hemi-cellulose, and lignin connected together in a complex molecular structure[138]. The combustion of wood occurs in several steps. First the wood must be heated to the point where trapped water vapor is expelled and the molecular chains between wood molecules, such as cellulose and lignin, break down and the molecules are subsequently vaporized. Next, the trapped oxygen within the evolved wood molecules begins to pyrolyze. The pyrolysis gases quickly transition into a semi-stable, thin, flame region where the gas mixes with the surrounding

air (i.e. a non-premixed diffusion flame). Due to the radiation losses to the wood below the flame and the surrounding air, as well as convection losses to the air, flame temperatures have been calculated to be between 1100 K and 1700 K[139, 140]. Additionally, wood-gas flame temperatures have been measured in our own laboratory to be between approximately 1300-1500 K[141] for natural convection cookstoves. After the flame front, excess air is mixed with the combustion products and allows for some additional oxidation of CO and other products However, the gas quickly cools to the point where significant oxidation is quenched. The steps just described are summarized in Figure 5.19.

Recent interest in the applications of pyrolysis stoves as well as improvements in experimental techniques and analysis have increased the depth of knowledge of the components of wood gas[139, 140, 142]. Several studies have analyzed pyrolysis gases for different solid fuels using thermogravametric (TG) mass spectrometry and Fourier transform infrared (FTIR) analysis of the evolved and reacted gases[143–145]. Ranzi et al. summarized this research and developed a chemical reaction mechanism with 327 species and 10934 reactions detailing not only the oxidation of evolved wood gases but also the interactions between these species in the pyrolysis zone prior to the flame[142].

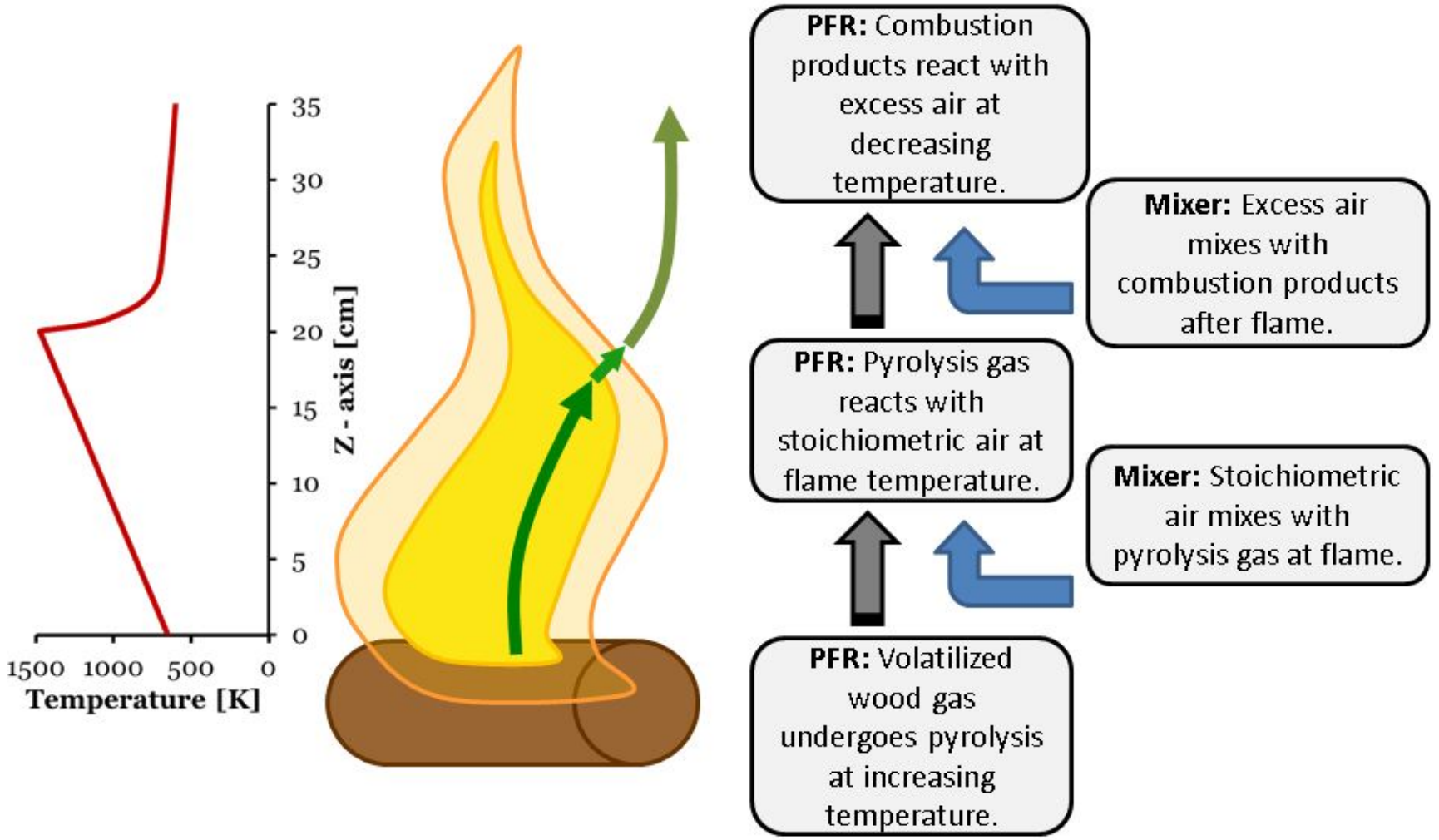


FIGURE 5.19. Simplified 1-D Model of a Wood Flame. Shown at left is the assumed temperature profile within the flame, while at right are the corresponding steps.

TABLE 5.5. Evolved Wood-Gas Composition

species	mass fraction
$C_{11}H_{12}O_4$	0.238
$C_5H_8O_4$	0.029
$C_6H_{10}O_5$	0.338
C_3H_5OH	0.044
$C_2H_4O_2$	0.010
C_2H_5OH	0.008
C_2H_4	0.007
CH_3OH	0.065
CH_2O	0.030
CH_4	0.003
CO_2	0.098
CO	0.058
H_2O	0.062
H_2	0.009
total	1.000

The Ranzi et al. mechanism was used to model the gas phase chemical kinetics of the chimney stoves tested. Only the major vaporized wood species from the softwood Ranzi et al. model were taken to represent the evolved wood gas; the fuel mass fractions can be found in Table 5.5. Using the species distribution in Table 5.5, the stoichiometric amount of air was found to be 6.1kg for 1kg of fuel, which is consistent with previous studies[137]. Charcoal was excluded from the chemical modeling for simplification. This was believed to be reasonable given that charcoal accumulation is relatively small in both stoves that were tested.

CHEMKIN-PRO was utilized to explore the interaction between various parameters such as air-to-fuel ratio, reaction zone temperatures, wood combustion rate, and combustion

efficiency. Specifically, the chimney stove combustion processes studied herein were modeled as a series of plug flow reactors as follows:

(1) The fuel species from Table 5.5 are reacted through a short pyrolysis section approximated by a plug flow reactor (PFR) beginning at 650 K and ending at the flame. Several models were run, ranging from 1300-1700 K in order to reflect the inherent temperature ranges encountered during the wood burn rates tested experimentally.
(2) A stoichiometric amount of air is mixed (non-reactively) with the pyrolysis products.
(3) The stoichiometric mixture of fuel and air is reacted through a very short (1-2 mm) reaction zone, which is held at the flame temperature (1300-1700 K)
(4) Excess air (also at the flame temperature) is then mixed (non-reactively) with the combustion products
(5) The fuel-lean mixture is allowed to react whilst being subjected to a decreasing temperature profile for the remainder of the stove gas path (note the temperature profile is taken from experimental measurements).

The entire connected model was solved via CHEMKIN-PRO. The non-reactive mixing sections were simulated using the embedded mixer model, while the reacting sections were all simulated using PFRs with the experimental stove dimensions, velocity measurements, and temperature profiles applied where necessary. It was found experimentally that the firepower during a given test fluctuates slightly and thus affects the overall bulk flame temperature. Therefore, the model results are shown as a band ranging in a peak flame temperature from 1300 to 1700 K.

The temperature profiles in Figure 5.20 were obtained from experimental results and represent the linear path (z-dimension) along the gas path through the stove. Described

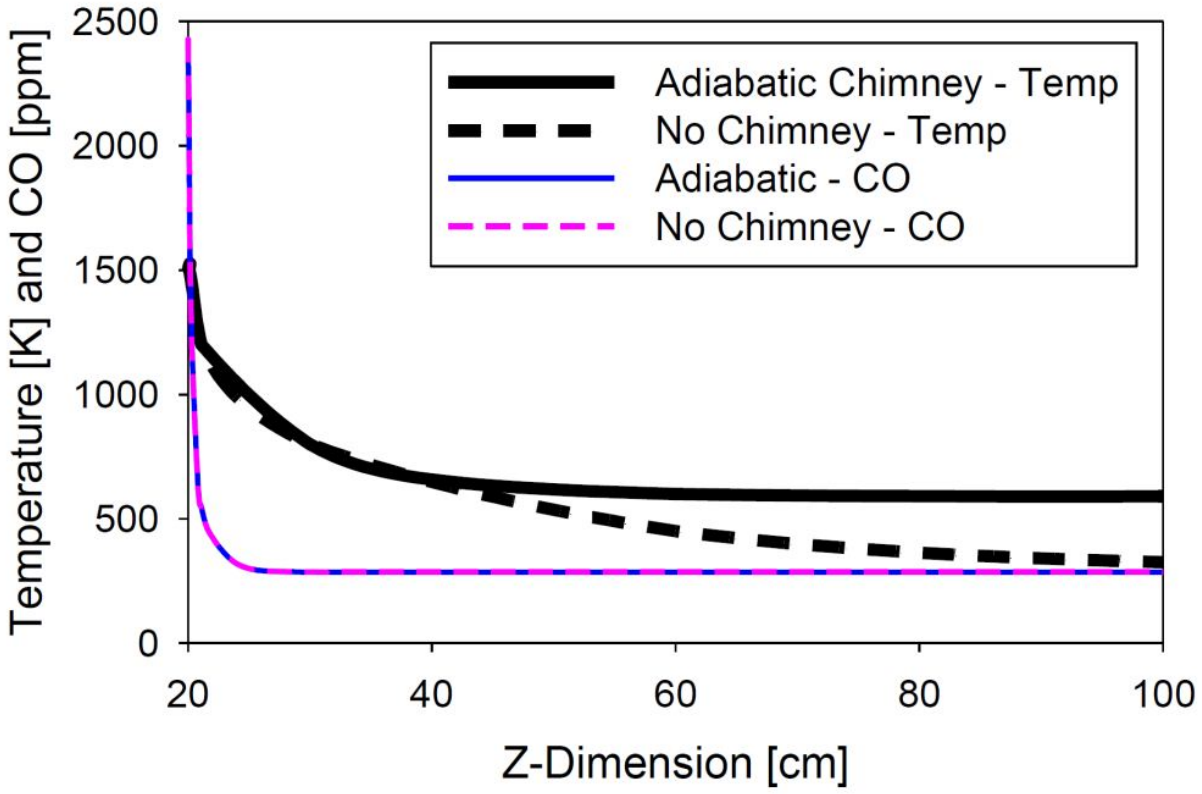


FIGURE 5.20. CHEMKIN-PRO results for hypothetical oxidation of CO in both an adiabatic chimney and a case with no-chimney (note the chimney inlet begins at 100 cm). These temperature profiles (thick black solid and dashed lines) are based on experimental data which inform the modeling results, i.e. the CO trends (thin blue solid and pink dashed lines).

earlier in Figure 5.19, the pyrolysis flame is considered the start of the chemistry model; therefore the flame exists from 0-20 cm, the stove path from 20-80 cm and the chimney path from 80-300 cm. The adiabatic case represents a very hot chimney inlet temperature of 600 K with no heat lost through the chimney portion while the no-chimney case exits to ambient air and is considered cooled within 40 cm from the stove exit. Due to the sharp drop in temperature downstream of the flame the CO concentrations for these two extreme cases are essentially identical. Therefore, even very high temperature chimneys are not predicted to provide any advantage when compared to colder or ambient scenarios. The results shown in Figure 5.20 should not come as too much of a surprise since it is known that appreciable

oxidation of CO effectively terminates below temperatures of approximately 1100-1300 K (depending on pressure and turbulence), which is well above reasonable or safe chimney temperatures for residential stoves.

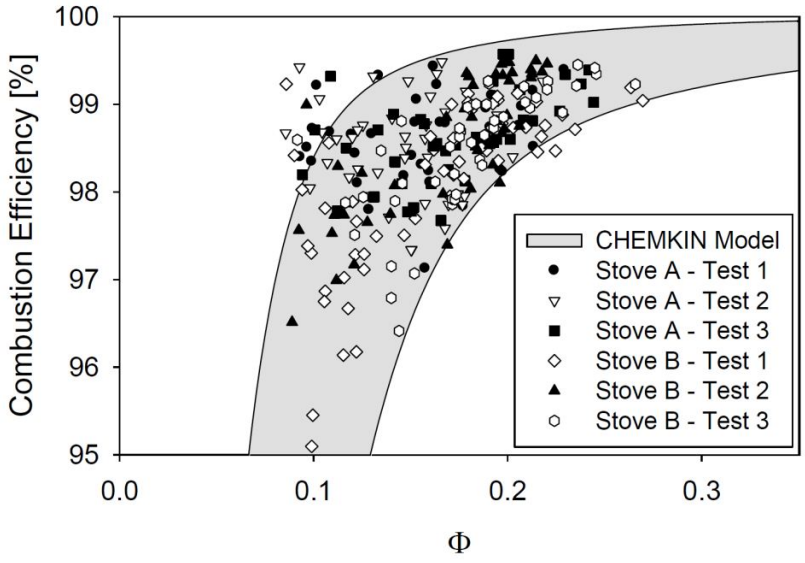


FIGURE 5.21. Modified combustion efficiency vs. phi for steady state data shown overlaid on chemical kinetic modeling results for a range of temperatures from 1300-1700 K.

The model results bracketing the data in Figure 5.21 are a result of running the chemical kinetic model described in Figure 5.19 over a range of flame temperatures (1300-1700 K) and ϕ values (0.01-0.6). The model data is shown as a band to reflect the inherent fluctuations in temperature that can occur even for fairly consistent wood burn rates. The combustion efficiency is predicted to drop off around upon decreasing phi below a value of approximately 0.1. This decrease is primarily due to nature of phi as it approaches zero specifically, the amount of excess air increases exponentially as phi decreases. This large increase in excess air serves to drastically decrease the CO concentration at the flame exit, which lowers the conversion driving force. Additionally, at a constant fire power, the flame can only deliver so much heat to the incoming air and so above a certain point, the excess air actually cools

the local temperature such that the temperature downstream of the flame zone decreases so fast that CO conversion to CO_2 is effectively frozen.

5.5.2. 1-D Flame Model Applications to DICI Engines. The results of Figure 5.21 are overlaid against DICI engine data presented originally by Reitz[19] in Figure 5.22. The CHEMKIN calculated stove emissions agree well with those shown by Retiz. The overlap between stoves and DICI engines should come as no surprise as both are, at their foundation, based on non-premixed flames. The application of the CHEMKIN model presented in section 5.5.1 is basically a single spacial dimension model which is not unlike that used in droplet combustion (one of the primary means of simulating the non-premixed portion of diesel flames). The application of this 1-D model to DICI and other non-premixed flames is a topic of future research.

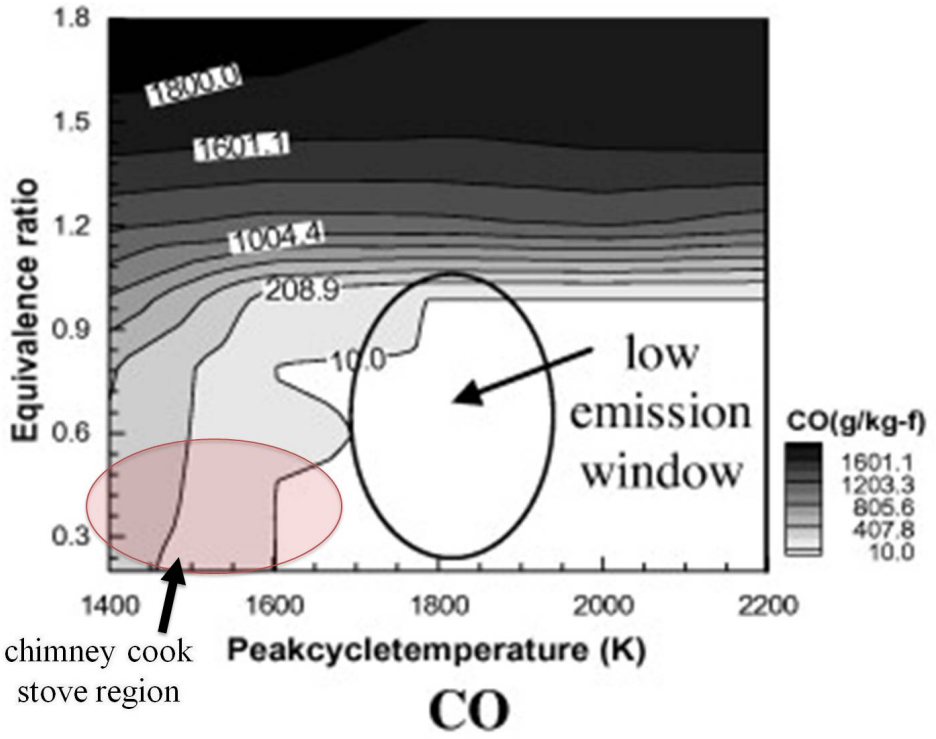


Figure 5.22. CO emissions for a range of in-cylinder temperatures and equivalence ratios from[19] (used with permission). Also overlaid on this plot is the range of chimney stove conditions considered in Section 5.5.1.

CHAPTER 6

Conclusions and Future Work

The goal of this work was to achieve a fundamental understanding of how the various traditional fuel scales (ON, CN, and MN) relate to one another on a physical and chemical level. That knowledge was then leveraged to better compare fuels to one another in an HCCI engine. Additionally, the derivations laid out as a result of this work should serve to allow better understanding of how fuel chemical-kinetics relate to current and future fuel metrics.

Major outcomes of this work are as follows:

(1) A novel way of thinking about fuels in SI engines called the knock length (b_k),

(2) Development of the fundamental relationship that connects the Octane Number scale to the Cetane Number scale,

(3) A new chemical kinetic mechanism for n-heptane/n-butanol fuels,

(4) A novel way of using a Fuel Ignition Tester (FIT) to determine fuel performance in a HCCI engine,

(5) Design and fabrication of a HCCI engine test bed,

(6) A more robust way of characterizing fuel reactivity in HCCI engines called the HCCI Number,

(7) Test protocols to determine Derived HCCI Numbers (DHN),

(8) One peer-reviewed journal article published and two currently under review, three conference papers, and multiple technical and poster presentations.

In more detail the first portion of this work examined the three main fuel metrics used today (ON, CN, and MN) via their respective phenomenological bases. The results of FIT and CFR experiments were compared against historical data from which a general correlation

between a new parameter call the knock length (b_k) and MN and ON as well as a relationship between CN and ON were developed.

The data suggest that ethanol and butanol fuel mixtures have somewhat different ignition behavior than traditional hydrocarbon fuels and that these differences can be attributed to chemical-kinetics. Specifically the higher H abstraction coefficients by OH from parent alcohol fuels vs. traditional hydrocarbons result in a more linear transition between CN and ON. These findings have great implications when mixing alcohols with traditional fuels, especially in the middle CN and ON ranges which are important for advanced combustion applications.

The CN-ON derivation also allowed for the development of the knock length parameter, which was shown to be more informative in characterizing fuel reactivity and highlighting fuel effects than current metrics. Since b_k is based on fundamental fuel parameters, it could also be used to compare real fuels across various engine platforms without the use of reference fuels. Furthermore, b_k could be calculated or measured at varying conditions (including ϕ) and applied to different combustion modes whereas traditional metrics are fixed.

For the second phase a FIT and an HCCI engine were used to compare n-butanol/n-heptane and PRF fuel blends. Three chemical models were examined and tested against the experimental data. The Sarathy et al. mechanism was updated to include a current n-heptane sub-mechanism by Mehl et al. - the combined mechanism being dubbed Sarathy*. This novel mechanism showed the best ability to model the results obtained from both sets of experiments for both single-zone and multi-zone models. The FIT accurately reproduced relative fuel ignition rankings, though the magnitude of the differences was greater than that seen in an HCCI engine. However, the FIT experimental data proved quite useful, serving

as further support of the accuracy of the examined models at low temperatures. As part of this work, single and mulit-zone CHEMKIN simulations of the FIT and HCCI engine were created in addition to a GT-Power and CONVERGE HCCI model.

In the third and final phase, several methods of better characterizing fuels in HCCI engines were investigated. For the HCCI conditions examined, the fLTHR displayed promise of being an indicator for the location of combustion timing (i.e. lcoation of CA50). The FIT-fLTHR was further able to similarly predict combustion timing when plotted against experimental CA50 timing. Existing ways of characterizing HCCI fuels were reviewed; the most used metric, Kalghatgi's Octane Index, was found to be improved when fuel RON/MON values were calculated on a molar instead of volumetric basis - thus the Molar Octane Index was proposed. This idea was combined with the fLTHR model to create the HCCI number which is an analogous test to existing RON and MON tests, except for HCCI conditions. Data showed that PRF fuels could be used as a preliminary basis for HCCI Numbers, but that perhaps more sensitive fuels may be necessary to better capture fuel behavior across the whole temperature range experienced in HCCI engines.

Lastly, the central fuel of this work, n-butanol, proved to be an excellent fuel for use in both traditional and advanced (HCCI) engines and it is the sincere hope of this author that it, along with other bio-fuels, will be used to further reduce our dependence on other less-renewable fuel resources.

6.1. Future Work to be Considered

Although this work stands on its own, there were many topics that were only touched upon and should receive further attention. The following list is a collection of such questions/topics raised during the course of this work.

(1) Knock Length: the knock length concept was shown herein to be a tool with which to analyze differences between fuels in both SI and HCCI combustion. Further work is required to determine whether or not a true Turbulent Knock Length could physically match the bore of a given engine. Additionally, more work is needed to apply the knock length to a broader range of fuels and combustion applications.

(2) FIT RON Prediction: Further exploration of the FIT's ability to investigate high RON fuels is needed. Investigations thus far show that the FIT has some ability to predict the RON value of low DCN fuels, but further work is needed with a larger variety of fuels to determine the true accuracy of the FIT at high RON conditions.

(3) fLTHR: The fLTHR proved to accurately be able to predict combustion timing for the fuels tested, but more testing is needed to see how this metric might change as a function of fuel type and engine conditions.

(4) Mehtyl decanoate: Engine and RON testing of methyl decanoate/n-butanol blends is needed to investigate the possibility of this fuel mixture or one of biodiesel/n-butanol for use in advanced combustion applications. Preliminary investigations show DCN trends that suggest it may be a promising mixture, but challenges such as high viscosity and fuel stability may still hinder its use and may need to be overcome to increase its usefulness.

(5) mOI: Testing of ethanol and butanol suggest that calculating fuel octane values based on their molar percentages is an acceptable way of determining their actual octane values - more investigation is needed to definitively prove this one way or the other.

(6) FIT injection strategies: work has already been done with the IQT in expanding its operational ranges[49, 50]. Similar work needs to be done with the FIT. Some options are replacing the injector with one that more easily allows constant mass fuel injections. Temperature and pressure range for experiments is also an area that could be improved. As a comparison, the Combustion Research Unit (CRU - http://www.fueltechsolutions.com/) could be used as a basis for further improvements/possibilities for the FIT.

(7) RCM verification of FIT and HCCI experiments: The FIT and modeling results presented go a long way to examining and interpreting the HCCI data. However, running RCM experiments would be a nice bridge between the FIT and HCCI. Furthermore, better model validation would be gained from the simpler, more easily modeled RCM experiments. Future work will consist of finishing set-up of the RCM facilities and preparing to investigate some of the fuels used in this work.

(8) Connection of GT-Power and CHEMKIN modules: Although the GT-Power model developed as a result of this work proved adequate in examining the PRF fuels. More work is needed to validate the model not only for use with butanol fuel mixtures, but also for more engine operating conditions.

(9) Improvements to the CONVERGE model: the base CONVERGE has been created, but full 3-D runs have not been done. Further work is needed to reduce the PRF and Sarathy* mechanism for use in CONVERGE. Additionally, the heat transfer, flow characteristics, and other CONVERGE parameters will need to be tuned for better modeling.

(10) Exploration of the 1-D flame model: the 1-D flame model developed for chimney stoves has great potential in regards to analyzing diesel flames. As a first step, the model could be compared with non-premixed flat flame or droplet experiments.

Bibliography

[1] R. Hirsch, R. Bezdek, and R. Wendling, "Peaking of world oil production: Impacts, mitigation and risk management," *U.S. DOE, National Energy Technology Laboratory*, 2005.

[2] B. McKibben, "A deeper shade of green," *National Geographic*, vol. August, 2006.

[3] J. Wright and J. Conca, *The GeoPolitics of Energy:: Acheiving a Just and Sustainable Energy Distribution by 2040*. BookSurge Publishing, 2007.

[4] A. Pasternak, "Global Energy Futures and Human Development: A Framework for Analysis," *DOE/LLNL URCRL-ID-140773*, October 2000.

[5] A. Brandt and A. Farrell, "Scraping the bottom of the barrel: green house gas emission consequences of a transition to low-quality and synthetic petroleum resources," *Climatic Change*, vol. 84, pp. 241–263, 2007. DOI 10.1007/s10584-007-9275-y.

[6] R. Pachauri and A. Resinger, "Climate change 2007: Synthesis report," *IPCC*, 2007.

[7] EPA, "Inventory of u.s. greenhouse gas emissions and sinks: 1990-2010," *EPA*, 2012.

[8] T. Skone and K. Gerdes, "Development of Baseline Data and Analysis of Life Cycle Greenhouse Gas Emissions of Petroleum-Based Fuels," *DOE/NETL-2009/1346*, 2008.

[9] "http://www.usa.gov/copyright.shtml," 2014.

[10] J. E. Dec, "Advanced compression-igniton engines understanding the in-cylinder processes," *Proc. Combust. Inst*, vol. 32, no. 2, pp. 2727–2742, 2009.

[11] S. L. Kokjohn, R. M. Hanson, D. A. Splitter, and R. D. Reitz, "Fuel reactivity controlled compression ignition (RCCI): a pathway to controlled high-efficiency clean combustion," *Int. J. Engine Res*, no. 12, pp. 209–226, 2010.

[12] S. Ciatti, "The Gasoline Diesel: Research at a national lab aims to break barriers in fuel economy and emissions performance," *Mechanical Engineering Magazine*, 2012.

[13] P. W. Bessonette, C. H. Schleyer, K. P. Duffy, W. L. Hardy, and M. P. Liechty, "Effects of fuel property changes on heavy-duty HCCI combustion," *SAE 2007-01-0191*, 2007.

[14] N. Kaneko, H. Ando, H. Ogawa, and N. Miyamoto, "Expansion of the operating range with in-cylinder water injection in a premixed charge compression ignition engine," *SAE 2002-01-1743*, 2002.

[15] X. Lu, D. Han, and Z. Huang, "Fuel design and management for the control of advanced compression-ignition combustion modes," *Progress in Energy and Combustion Science*, vol. 37, no. 6, pp. 741–783, 2011.

[16] H. Yun, N. Wermuth, and P. Najt, "High load hcci operation using different valving strategies in a naturally-aspirated gasoline hcci engine," *SAE 2011-01-0899*, 2011.

[17] "Homogeneous charge compression ignition (hcci) technology: A report to the u.s. congress," *U.S. Department of Energy Energy Efficiency and Renewable Energy Office of Transportation Technologies*, 2001.

[18] G. Neely, S. Sasaki, Y. Huang, J. Leet, and D. Stewart, "New diesel emission control strategy to meet us tier 2 emissions regulations," *SAE 2005-01-1091*, 2005.

[19] R. Reitz, "Directions in internal combustion engine research," *Combustion and Flame*, vol. 160, pp. 1–8, 2013.

[20] "CFR engine brocure," *ASME*, 2012.

[21] "Standard test method for determination of ignition delay and derived cetane number (DCN) of diesel fuel oils by combustion in a constant volume chamber," *ASTM International*, 2012.

[22] D2699-12, "Standard test method for research octane number of spark-ignition engine fuel," *ASTM International*, 2012.

[23] M. Leiker, K. Christoph, M. Rankl, E. Cartellieri, and U. Pfeifer, "Evaluation of Antiknocking Property of Gaseous Fuels by Means of Methane Number and its Practical Application to Gas Engines," *ASME Technical Report 72-DGP-4*, 1972.

[24] A. M. Douaud and P. Eyzat, "Four-octane-number method for predicting the anti-knock behavior of fuels and engines," *SAE 780080*, 1979.

[25] J. Heywood, *Internal Combustion Engine Fundamentals*. New York: McGraw-Hill, Inc., 1 ed., 1988.

[26] D2700-12, "Standard Test Method for Motor Octane Number of Spark-Ignition Engine Fuel," *ASTM International*, 2012.

[27] G. Kalghatgi, *Fuel/Engine Interactions*. SAE International, 2013.

[28] J. E. Anderson, U. Kramer, S. A. Mueller, and T. J. Wallington, "Octane numbers of ethanol- and methanol- gasoline blends estimated from molar concentrations," *Energy&Fuels*, vol. 24, pp. 6576–6585, 2010.

[29] J. Andrae, P. Bjornbom, R. Cracknell, and G. Kalghatgi, "Autoignition of toluene reference fuels at high pressures modeled with detailed chemical kinetics," *Combustion and Flame*, vol. 149, pp. 2–24, 2007.

[30] J. Andrae, T. Brinck, and G. Kalghatgi, "Hcci eperiments with toluene reference fuels modeled by a semidetailed chemical kinetic model," *Combustion and Flame*, vol. 155, pp. 696–712, 2008.

[31] D. M. A. Karwat, S. W. Wagnon, M. S. Wooldridge, and C. K. Westbrook, "On the combustion chemistry of n-heptane and n-butanol blends," *The Journal of Physical Chemistry*, vol. 116, no. 51, pp. 12406–12421, 2012.

[32] "Standard test method for determination of derived cetane number (DCN) of diesel fuel oilsfixed range injection period, constant volume combustion chamber method," *ASTM International*, 2012.

[33] J. Bowden, A. Johnston, and J. Russell, "Octane-Cetane Relationship," *Southwest Research Institute AD-799 512*, 1974.

[34] R. Stone, *Introduction to Internal Combustion Engines*. Oxford, England: University of Oxford, 3 ed., 1999.

[35] P. L. Perez and A. L. Boehman, "Experimental Investigation of the Autoignition Behavior of Surrogate Gasoline fuels in a Constant-Volume combustion bomb Apparatus and Its Relevance to HCCI Combustion," *Energy&Fuels*, vol. 26, no. 10, pp. 6106–6117, 2012.

[36] M. Haas, J. Shim, A. Ramcharan, and F. Dryer, "Ignition quality evaluation of valerate alkyl esters," *34th International Symposium on Combustion*, 2012.

[37] T. Ryan, "Fuel requirements for hcci engine operation," *Diesel Engine Emissions Reduction (DEER) Conference*, 2002.

[38] F. M. Haas, A. Ramcharan, and F. L. Dryer, "Relative reactivities of the isomeric butanols and ethanol in an ignition quality tester," *Energy&Fuels*, vol. 25, no. 9, pp. 3909–3919, 2011.

[39] N. Bezaire, K. Wadumesthrige, K. Y. S. Ng, and S. O. Salley, "Limitations of the use of cetane index for alternative compression ignition engine fuels," *Fuel*, vol. 89, pp. 3807–3813, 2010.

[40] G. K. P. Risberg and H. Angstrom, "A method of defining ignition quality of fuels in hcci engines," *SAE 2003-01-1816*, 2003.

[41] G. Kalghatgi, "Fuel anti-knock - Part I, Engine Studies," *SAE 2001-01-3584*, 2001.

[42] G. Kalghatgi, "Fuel anti-knock - Part II. Vehicle studies - how relevant is Motor Octane Number (MON) for modern engines?," *SAE 2001-01-3585*, 2001.

[43] M. Mehl, T. Faravelli, F. Giavazzi, E. Ranzi, P. Scorletti, A. Tardani, and D. Terna, "Detailed chemistry promotes understanding of octane numbers and gasoline sensitivity," *Energy&Fuels*, vol. 20, pp. 2391–2398, 2006.

[44] P. Risberg, "Describing the Auto-Ignition Quality of Fuels in HCCI Engines," *Royal Institute of Technology: School of Industrial Engineering and Management (Doctoral Thesis)*, 2006.

[45] S. Turns, *An Introduction to Combustion: Concepts and Applications*. McGraw-Hill International, 2 ed., 2006.

[46] H. Liu, M. Yao, B. Zhang, and Z. Zunqing, "Influence of fuel and operating conditions on combustion characteristics of a homogeneous charge compression ignition engine," *Energy&Fuels*, vol. 23, no. 3, pp. 1422–1430, 2009.

[47] V. Rapp, W. Cannella, J. Y. Chen, and R. Dibble, "Predicting fuel performance for future HCCI engines," *Combustion Science and Technology*, vol. 185, no. 5, pp. 735–748, 2013.

[48] G. Shibata and T. Urushihara, "Auto-Ignition Characteristics of Hydrocarbons and Development of HCCI Fuel Index," *SAE 2007-01-0220*, 2007.

[49] G. E. Bogin Jr., A. DeFilippo, J. Y. Chen, G. Chin, J. Luecke, M. A. Ratclif, B. T. Zigler, and A. M. Dean, "Numerical and experimental investigation of n-heptane autoignition in the ignition quality tester (IQT)," *Energy&Fuels*, vol. 25, no. 12, pp. 5562–5572, 2011.

[50] G. E. Bogin Jr., E. Osecky, M. A. Ratcliff, J. Luecke, X. He, B. T. Zigler, and A. M. Dean, "Ignition quality tester (IQT) investigation of the negative temperature coefficient region of alkane autoignition," *Energy&Fuels*, vol. 27, no. 3, pp. 1632–1642, 2013.

[51] "EPA Announces E15 Partial Waiver Decision: EPA-420-F-11-003," *U.S. EPA*, 2011.

[52] P. Dagaut and C. Togbe, "Oxidation kinetics of butanol-gasoline surrogate mixtures in a jet-stirred reactor: Experimental and modeling study," *Fuel*, vol. 87, no. 15-16, pp. 3313–3321, 2008.

[53] P. Dagaut, S. M. Sarathy, and M. J. Thomson, "A chemical kinetic study of n-butanol oxidation at elevated pressure in a jet stirred reactor," *Proceedings of the Combustion Institute*, vol. 32, no. 1, pp. 229–237, 2009.

[54] P. Saisirirat, C. Togbe, S. Chanchaona, F. Foucher, C. Mounaim-Rousselle, and P. Dagaut, "Auto-ignition and combustion characteristics in hcci and jsr using 1-butanol/n-heptane and ethanol/n-heptane blends," *Proceedings of the Combustion Institute*, vol. 33, no. 2, pp. 3007–3014, 2011.

[55] Y. Zhang and A. L. Boehman, "Oxidation of 1-butanol and a mixture of n-heptane/1-butanol in a motored engine," *Combustion and Flame*, vol. 157, no. 10, pp. 1816–1824, 2010.

[56] K. A. Heufer, R. X. Fernandes, H. Olivier, J. Beeckmann, O. Rohl, and N. Peters, "Shock tube investigations of ignition delays of n-butanol at elevated presures between 770 and 1250 k," *Proceedings of the Combustion Institute*, vol. 33, no. 1, pp. 359–366, 2011.

[57] B. W. Weber, K. Kumar, Y. Zhang, and C. J. Sung, "Autoignition of n-butanol at elevated pressure and low-to-intermediate temperature," *Combustion and Flame*, vol. 158, no. 5, pp. 809–819, 2011.

[58] S. M. Sarathy, S. Vranckx, K. Yasunaga, M. Mehl, P. OBwald, W. K. Metcalf, C. K. Westbrook, W. J. Pitz, K. Kohse-Hoinghaus, R. X. Fernandes, and H. J. Curran, "A comprehensive chemical kinetic combustion model for the four butanol isomers," *Combsution and Flame*, vol. 159, no. 6, pp. 2028–2055, 2012.

[59] J. Zhang, S. Niu, Y. Zhang, C. Tang, X. Jiang, E. Hu, and Z. Huang, "Experimental and modeling study of the auto-igntion of n-heptane/n-butanol mixtures," *Combustion and Flame*, vol. 160, no. 1, pp. 31–39, 2013.

[60] J. Andrae, D. Johansson, P. Bjornbom, P. Risberg, and G. Kalghatgi, "Co-oxidation in the auto-ignition of primary reference fuels and n-heptane/toluene blends," *Combustion and Flame*, vol. 140, pp. 267–286, 2005.

[61] J. Andrae, "Comprehensive chemical kinetic modeling of toluene reference fuels oxidation," *Fuel*, vol. 107, pp. 740–748, 2013.

[62] Y. Zhang and A. L. Boehman, "Impact of biodiesel on nox emissions in a common rail direct injection diesel engine," *Energy&Fuels*, vol. 21, no. 4, pp. 2003–2012, 2007.

[63] M. Lapuerta, J. R. Agudelo, M. Prorok, and A. Boehman, "Bulk modulus of compressibility of diesel/biodiesel/hvo blends," *Energy&Fuels*, vol. 26, no. 2, pp. 1336–1343, 2012.

[64] K. Varatharajan and M. Cheralathan, "Influence of fuel properties and composition on nox emissions from biodiesel powered diesel engines: A review," *Renewable and Sustainable Energy Reviews*, vol. 16, no. 6, pp. 3702–3710, 2012.

[65] S. Pinzi, P. Rounce, J. M. Herreros, A. Tsolakis, and M. P. Dorado, "The effect of biodiesel fatty acid composition on combustion and diesel engine exhaust emissions," *Fuel*, vol. 104, pp. 170–182, 2013.

[66] C. Jin, M. Yao, H. Liu, C. F. Lee, and J. Ji, "Progress in the production and application of n-butanol as a biofuel," *Renewable and Sustainable Energy Reviews*, vol. 15, no. 8, pp. 4080–4106, 2011.

[67] P. G. Aleiferis and Z. R. van Romunde, "An analysis of spray development with iso-octane, n-pentane, gasoline, ethanol and n-butanol from a multi-hole injector under hot fuel conditions," *Fuel*, vol. 105, pp. 143–168, 2013.

[68] N. Morgan, A. Smallbone, A. Bhave, M. Kraft, R. Cracknell, and G. Kalghatgi, "Mapping surrogate gasoline compositions into RON/MON space," *Combustion and Flame*, vol. 157, pp. 1122–1131, 2010.

[69] M. Baumgardner, S. Sarathy, and A. Marchese, "Autoignition Characterization of Primary Reference Fuels and n-Heptane/n-Butanol Mixtures in a Constant Volume

Combustion Device and Homogeneous Charge Compression Ignition Engine," *Energy&Fuels*, vol. 27, pp. 7778–7789, 2013.

[70] H. Curran, W. Gafuri, P.and Pitz, and C. Westbrook, "A comprehensive Modeling Study of n-Heptane Oxidation," *Combustion and Flame*, vol. 114, pp. 149–177, 1998.

[71] M. Mehl, Pitz.W.J., M. Sojberg, and J. Dec, "Detailed kinetic modeling of low-temperature heat release for PRF fuels in an HCCI engine," *SAE Powertrains, Fuels and Lubricants Meeting - SAE 2009-01-1806*, 2009.

[72] M. Mehl, W. J. Pitz, C. K. Westbrook, and H. J. Curran, "Kinetic modeling of gasoline surrogate components and mixtures under engine conditions," *Proceedings of the Combustion Institute*, vol. 33, no. 1, pp. 193–200, 2011.

[73] J. Gatowski, E. Balles, k.M. Chun, F. Nelson, J. Ekchian, and J. Heywood, "Heat Release Analysis of Engine Pressure Data," *SAE 841359*, 1984.

[74] S. Saxena and I. D. Bedoya, "Fundamental phenomena affecting low temperature combustion and HCCI engines, high load limits and strategies for extending these limits," *Progress in Energy and Combustion Science*, vol. 39, pp. 457–488, 2013.

[75] D. Kilgore, W. Rogers, S. Dillon, G. Maschke, and J. Kimmel, "Air Assist Fuel Injector," *U.S. Patent 7104477 B2*, 09 2006.

[76] B. Fisher, "Characterization of Gaseous and Particulate Emissions from Combustion of Algae Based Methyl Ester Biodiesel," *Colorado State University*, 2009. M.S. Thesis.

[77] Intertek *http://www.intertek.com*.

[78] D. M. Wise, D. B. Olsen, and M. Kim, "Characterization of Methane Number for Producer Gas Blends," *ASME ICEF2013-19221*, 2013.

[79] "Chemkin 10101(x64)," *Reaction Design*, 2011.

[80] "Chemkin-pro 15101 (x64)," *Reaction Design*, 2011.

[81] H. J. Curran, P. Gaffuri, W. J. Pitz, and C. K. Westbrook, "A comprehensive modeling study of iso-octane oxidation," *Combustion and Flame*, vol. 129, no. 3, pp. 253–280, 2002.

[82] S. M. Aceves, D. L. Flowers, C. K. Westbrook, J. R. Smith, and W. J. Pitz, "A multi-zone model for prediction of hcci combustion and emissions," *SAE 2000-01-0327*, 2000.

[83] S. Fiveland and D. Assanis, "Development of a Two-Zone HCCI Combustion Model Accounting for Boundary Layer Effects," *SAE 2001-01-1028*, 2001.

[84] S. Fiveland and D. Assanis, "Development and validation of a quasi-dimensional model for hcci engine performance and emissions studies under turbocharged conditions," *SAE 2002-01-1757*, 2002.

[85] J. Dec, W. Hwang, and M. Sjoberg, "An investigation of Thermal Stratification in HCCI Engines Using Chemiluminescence Imaging," *SAE 2006-01-1518*, 2006.

[86] K. Seshandri, T. Lu, O. Herbinet, S. Humer, U. Niemann, W. Pitz, R. Seiser, and C. Law, "Experimental and kinetic modeling study of extinction and ignition of methyl decanoate in laminar non-premixed flows," *Proceedings of the Combustion Institute*, vol. 32, pp. 1067–1074, 2009.

[87] M. Sjoberg and J. Dec, "Comparing late-cycle autoignition stability for singel and two-stage ignition fuels in HCCI engines," *Proc. Combust. Inst.*, vol. 31, pp. 2895–2902, 2007.

[88] J. Minj and X. Mao-Zhao, "Simulation of HCCI engine with a multi-zone model," *Journal of Combustion Science and Technology*, vol. 11, pp. 261–276, 2005.

[89] N. P. Komninos, D. T. Hountalas, and C. D. Rakopoulos, "A parametric investigation of hydrogen hcci combustion using a multi-zone model approach," *Energy Conversion and Managment*, vol. 48, no. 11, pp. 2934–2941, 2007.

[90] H. Barths, C. Felsch, and N. Peters, "Mixing models for the two-way-coupling of CFD codes and zero-dimensional multi-zone codes to model HCCI combustion," *Combustion and Flame*, vol. 155, pp. 440–449, 2008.

[91] N. Komninos and D. Hountalas, "Improvement and validation of a multi-zone model for HCCI engine combustion concerning performance and emissions," *Energy Converstion and Management*, vol. 49, pp. 2530–2537, 2008.

[92] P. Kongsereeparp, B. Kashani, and M. David Checkel, "A stand-alone multi-zone model for combustion in HCCI engiens," *Proceedings of the 2005 Fall Tech. Conf. of the ASME ICE Division*, pp. 265–274, 2005.

[93] P. Dagaut and C. Togbe, "Experimental and modeling study of the kinetics of oxidation of ethanol-n-heptane mixtures in a jet-stirred reactor," *Fuel*, vol. 89, no. 2, pp. 280–286, 2010.

[94] P. Dagaut and C. Togbe, "Experimental and modeling study of the kinetics of oxidation of butanol-n-heptane mixtures in a jet-stirred reactor," *Energy&Fuels*, vol. 23, no. 7, pp. 3527–3535, 2009.

[95] W. Liu, A. P. Kelley, and C. K. Law, "Non-premixed ignition, laminar flame propagation and mechansim reduction of n-butanol, iso-butanol, and methyl butanoate," *Proceedings of the Combustion Institute*, vol. 33, no. 1, pp. 995–1002, 2011.

[96] P. OBwald, H. Guldenberg, K. Kohse-Hoinghaus, B. Yang, T. Yuan, and F. Qi, "Combustion of butanol isomers - a detailed molecular beam mass spectrometry investigation of their flame chemistry," *Combustion and Flame*, vol. 158, no. 1, pp. 2–15, 2011.

[97] N. Hansen, M. R. Harper, and W. H. Green, "High-temperature oxidation chemistry of n-butanol - experiments in low-pressure premixed flames and detailed kinetic modeling," *Phys. Chem.*, vol. 13, no. 45, pp. 20262–74, 2011.

[98] I. Stranic, D. P. Chase, J. T. Harmon, S. Yang, D. F. Davidson, and R. K. Hanson, "Shock tube measurments of ignition delay times for the butanol isomers," *Combustion and Flame*, vol. 159, no. 2, pp. 516–527, 2012.

[99] C. R. Ferguson and A. T. Kirkpatrick, *Internal Combustion Engines*. John Wiley & Sons, Inc., 2 ed., 2001.

[100] D. Wise, "Investigation into Producer Gas Utilization in High Performance Natural Gas Engines," *Colorado State University*, 2013. Ph.D. Dissertation.

[101] A. DeFilippo, G. Chin, and J. Chen, "Development and Validation of Reaction Mechanisms for Alcohol-Blended Fuels for IC Engine Applications," *Combustion Science and Technology*, vol. 185, pp. 1202–1226, 2013.

[102] C. Westbrook, W. Pitz, M. Mehl, and H. Curran, "Detailed chemical kinetic reaction mechanisms for primary reference fuels for diesel cetane number and spark-ignition octane number," *Proc. Combust. Inst.*, vol. 33, pp. 185–192, 2011.

[103] W. Leppard, "The Chemical Origin of Fuel Octane Sensitivity," *SAE 902137*, 1990.

[104] T. M. Foong, K. J. Morganti, M. J. Brear, G. da Silva, Y. Yang, and F. L. Dryer, "The octane numbers of ethanol blended with gasoline and its surrogates," *Fuel*, vol. 115, pp. 727–739, 2014.

[105] J. Griffiths, P. Halford-Maw, and C. Mohamed, "Spontaneous ignition delays as a diagnostic of the propensity of alkanes to cause engine knock," *Combustion and Flame*, vol. 111, pp. 327–337, 1997.

[106] E. Ranzi, A. Frassoldati, R. Grana, A. Cuoci, T. Faravelli, A. Kelley, and C. Law, "Hierarchical and comparative kinetic modeling of laminar flame speeds of hydrocarbon and oxygenated fuels," *Progress in Energy and Combustion Science*, vol. 38, pp. 468–501, 2012.

[107] D. Healy, D. Kalitan, C. Aul, E. Petersen, G. Bourque, and H. Curran, "Oxidation of C1-C5 Alkane Quinternary Natural Gas Mixtures at High Pressures," *Energy&Fuels*, vol. 24, pp. 1521–1528, 2010.

[108] G. Bourque, D. Healy, H. Curran, C. Zinner, D. Kalitan, J. de Vries, C. Aul, and E. Petersen, "Ignition and Flame Speed Kinetics of Two Natural Gas Blends with High Levels of Heavier Hydrocarbons," *Proc. ASME Turbo Expo*, vol. 3, pp. 1051–1066, 2008.

[109] C. F. Taylor, *The internal-combustion engine in theory and practice, Vol. 1.* Cambridge, Massachusetts: MIT Press, 2 ed., 1985.

[110] A. J. Torregrosa, P. C. Olmeda, and C. A. Romero, "Revising engine heat transfer," *J. Eng. Annals of Faculty of Engineering Hunedoara*, vol. 6, no. 3, pp. 245–265, 2008.

[111] H. S. Soyhan, H. Yasar, H. Walmsley, B. Head, G. T. Kalghatgi, and C. Sorusbay, "Evaluation of heat transfer correlations for hcci engine modelling," *Applied Thermal Engineering*, vol. 29, no. 2-3, pp. 541–549, 2009.

[112] S. Sarathy, M. Thomson, W. Pitz, and T. Lu, "An experimental and kinetic modeling study of methyl decanoate combustion," *Proc. Combust. Inst.*, vol. 33, pp. 399–405, 2011.

[113] Z. Luo, M. Plomer, T. Lu, S. Som, D. Longman, S. Sarathy, and W. Pitz, "A reduced mechanism for biodiesel surrogates for compression ignition engine applications," *Fuel*, vol. 99, pp. 143–153, 2012.

[114] S. Hoffman and J. Abraham, "A comparative study of n-heptane, methyl decanoate, and dimethyl ether combustion characteristics under homogeneous-charge compressionignition engine conditions," *Fuel*, vol. 88, pp. 1099–1108, 2009.

[115] "Using multi-zone engine modeling with detailed chemistry for accurate ignition and emissions predictions in hcci engines," *Reaction Design Pro-APP-MZ (v2.0)*, 2010.

[116] W. Easley, A. Agarwal, and G. Lavoie, "Modeling of hcci combustion and emissions using detailed chemistry," *SAE 2001-01-1029*, 2001.

[117] T. Noda and D. Foster, "A numerical study to control combustion duration of hydrogen-fueled hcci by using multi-zone chemical kinetic simulation," *SAE 2001-01-0250*, 2001.

[118] H. Xu, M. Liu, S. Gharahbaghi, S. Richardson, M. Wyszynski, and T. Megaritis, "Modelling of hcci engines: Compariosn of single-zone, mulit-zone and test data," *SAE 2005-01-2123*, 2005.

[119] A. Y. Nobakht, R. K. Saray, and A. Rahimi, "A parametric study on natural gas fueled hcci combustion engine using a multi-zone combustion model," *Fuel*, vol. 90, no. 4, pp. 1508–1514, 2011.

[120] S. Visakhamoorthy, T. Tzanetakis, D. Haggith, A. Sobiesiak, and J. Z. Wen, "Numerical study of a homogeneous charge compression ignition (hcci) engine fueled with biogas," *Applied Energy*, vol. 92, pp. 437–446, 2012.

[121] J. Chang, O. Guralp, Z. Filipi, D. Assanis, T. Kuo, P. Najt, and R. Rask, "New heat transfer correlation for an hcci engine derived from measurments of instantaneous surface heat flux," *SAE 2004-01-2996*, 2004.

[122] G. F. Hohenberg, "Advanced approaches for heat transfer calculations," *SAE 790825*, 1979.

[123] N. P. Komninos, "Modeling hcci combustion: Modification of a multi-zone model and comparison to experimental results at varying boost pressure," *Applied Energy*, vol. 86, no. 10, pp. 2141–2151, 2009.

[124] J. C. Livengood and P. C. Wu, "Correlation of autoignition phenomena in internal combustion engines and rapid compression machines," *Fifth Symposium (Int'l) on Combustion, Reinhold Publ Corp.*, 1955.

[125] E. Kasseris and J. Heywood, "Charge Cooling Effects on Knock Limits in SI DI Engines Using Gasoline/Ethanol Blends: Part 2-Effective Octane Numbers," *SAE 2012-01-1284*, 2012.

[126] D. L. Flowers, S. M. Aceves, J. R. Smith, J. Torres, J. Girard, and R. W. Dibble, "HCCI in a CFR Engine: Experiments and Detailed Kinetic Modeling," *SAE 2000-01-0328*, 2000.

[127] Y. Ra and R. Reitz, "A combustion model for IC engine combustion simulations with multi-component fuels," *Combustion and Flame*, vol. 158, pp. 69–90, 2011.

[128] A. Sanli, A. Ozsezen, I. Kilicaslan, and M. Canakci, "The influence of engine speed and load on the heat trasnfer between gasses and in-cylinder walls at fired and motored conditions of an IDI diesel engine," *Applied Thermal Engineering*, vol. 28, pp. 1395–1404, 2008.

[129] W. Annand, "Heat transfer in the cylinders of reciprocating internal combustion engines," *Proc. Inst. Mech. Eng.*, vol. 177, pp. 973–990, 1963.

[130] G. Woschni, "A Universally Applicable Equation for the Instantaneous Heat Transfer Coefficient in the Internal Combustion Engine," *SAE 1967-670931*, 1967.

[131] M. Lounici, K. Loubar, M. Balistrou, and M. Tazerout, "Investigation on heat transfer evaluation for a more efficient two-zone combustion model in the case of natural gas SI engines," *Applied Thermal Engineering*, vol. 31, pp. 319–328, 2011.

[132] C. Rakopoulos, K. Antonopoulos, D. Rakopoulous, and D. Hountalas, "Multi-zone modeling of combustion and emissions formation in DI diesel engine operating on ethanol-diesel fuel blends," *Energy Conservation and Management*, vol. 49, pp. 625–643, 2008.

[133] F. Battin-Leclerc, "Detailed chemical kinetic models for the low-temperature combustion of hydrocarbons with application to gasoline and diesel fuel surrogates," *Progress in Energy and Combustion Science*, vol. 34, pp. 440–498, 2008.

[134] "Tutorials and Supporting Documentation for GT Suite v.7.1.0," *Gamma Technologies, Inc.*, 2010.

[135] L. Wang and S. Yang, "Turbo-cool turbocharging system for spark ignition engines," *Proc. IMechE - Part D: J. Automobile Eng*, vol. 229, pp. 1163–1175, 2006.

[136] A. Thompson, M. Baumgardner, and A. J. Marchese, "Modeling In-Cylinder Heat Transfer for a Single Cylinder HCCI Engine," *Fall Technical Meeting of the Western States Section of the Combustion Institute*, 2013.

[137] R. Curkeet, "Wood Combustion Basics," *Intertek, EPA (Burnwise) workshop*, 2011.

[138] F. Browne, "Theories of the combustion of wood and its control: A survey of the literature," *Forest Products Laboratory, Forest Survice (FDA) Report 2136*, 1958.

[139] S. Kausley and A. Pandit, "Modelling of solid fuel stoves," *Fuel*, vol. 89, pp. 782–791, 2010.

[140] K. Ragland and D. Aerts, "Properties of Wood for Combustion Analysis," *Bioresourse Technology*, vol. 37, p. 161168, 1991.

[141] J. Agenbroad, "A Simplified Model for Understanding Natural Convection Driven Biomass Cooking Stoves," *Colorado State University: M.S. Thesis*, 2010.

[142] E. Ranzi, A. Cuoci, T. Faravelli, A. Frassoldati, G. Migliavacca, S. Pierucci, and S. Sommariva, "Chemical Kinetics of Biomass Pyrolysis," *Energy&Fuels*, vol. 22, p. 42924300, 2008.

[143] J. Manya, E. Velo, and L. Puigjaner, "Kinetics of Biomass Pyrolysis: a Reformulated Three-Parallel-Reaction Model," *Ind. Eng. Chem. Res.*, vol. 42, p. 434441, 2003.

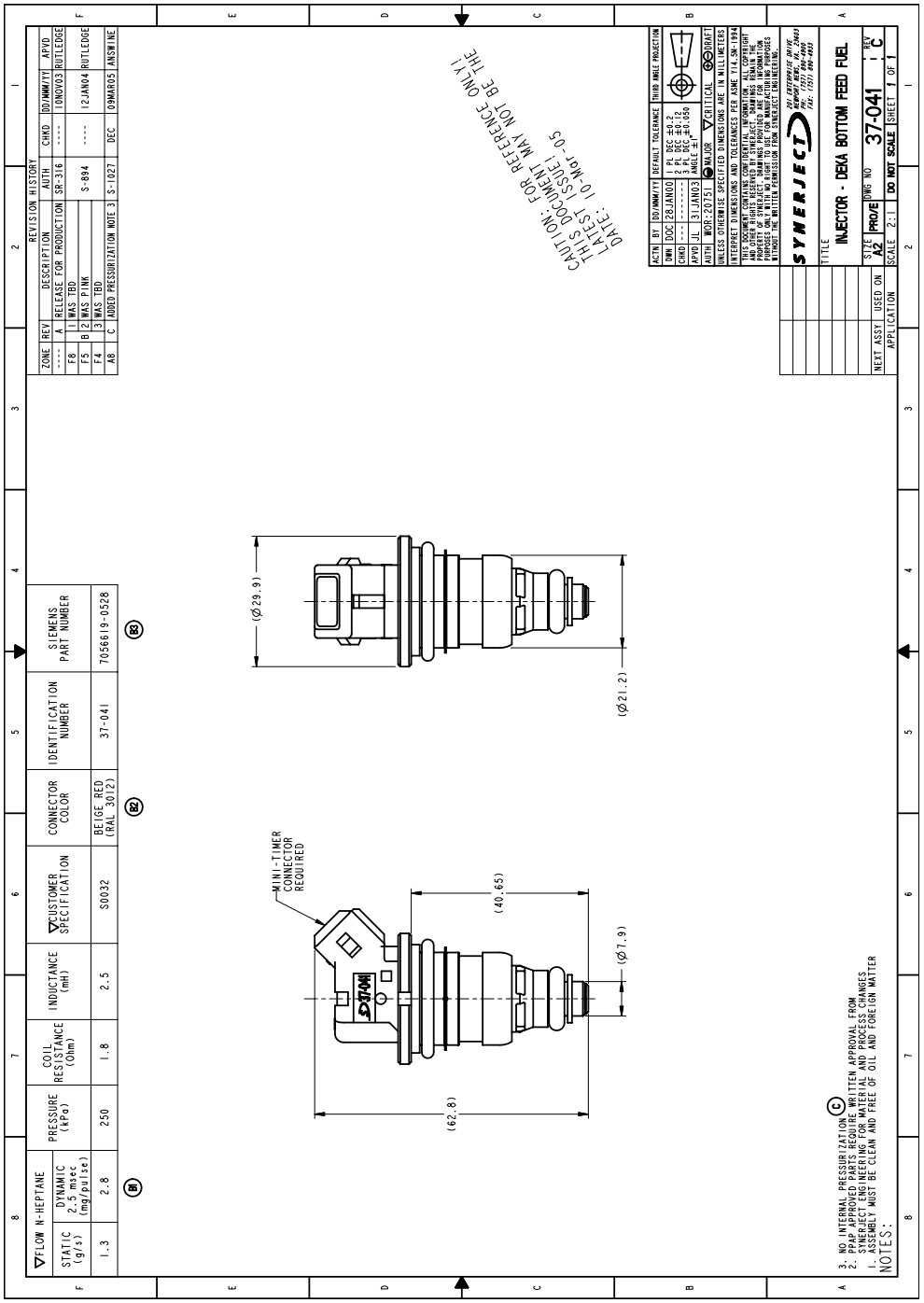
[144] T. Hosoya, H. Kawamoto, and S. Saka, "Cellulose-hemicellulose and cellulose-lignin interactions in wood pyrolysis at gasification temperature," *Journal of Analytical and Applied Pyrolysis*, vol. 80, p. 118125, 2007.

[145] R. Radmanesh, Y. Courbariauz, J. Chaouki, and C. Guy, "A unified lumped approach in kinetic modeling of biomass pyrolysis," *Fuel*, vol. 85, p. 121120, 2006.

[146] N.Pekoc, "Fit cleaning procedures," *personal communications*, 2 2011.

APPENDIX A

Synerject Fuel Injector



APPENDIX B

Single-Zone Ignition Delay Derivation

Detailed modeling of both the FIT and RCM experiments proposed in Section 4.6.3 makes use of certain basic combustion assumptions that will be described here.

The concept of an ignition delay is essential to nearly all of the subject matter presented in this proposal. From chemistry we know that, given a closed and adiabatic system the following is a certainty:

$$Fuel + Oxidizer \xrightarrow{K} Products \tag{51}$$

where K is the rate constant for the reaction. How long Eq. 51 will take to proceed depends on kinetics, or the time rate of change from Fuel and Oxidizer to Products. The ignition delay, then, is the overall time it takes for Eq. 51 to occur. The ignition delay time is different for every fuel, but the concept and equations describing ignition delay are the same.

Figure B.1 is a plot comparing predicted ignition delays for stoichiometric ethanol in air for a simulated RCM experiment using eight of the most current/accepted mechanisms for ethanol. The ignition delay is then determined as the time from peak compression temperature (around 5 ms) to the maximum dT/dt. The experiment modeled in Figure B.1 can be done for a variety of compression temperatures and a plot similar to Figure B.2 can be created.

Figure B.2 is known as an Arrhenius Plot (specifically for predicted stoichiometric ethanol and n-butanol in air at 40bar initial pressure); this sort of plot shows that as the temperature goes up the ignition delay decreases exponentially. This exponential decrease in ignition delay with increasing temperature is in line with the idea that the kinetic rate constants for

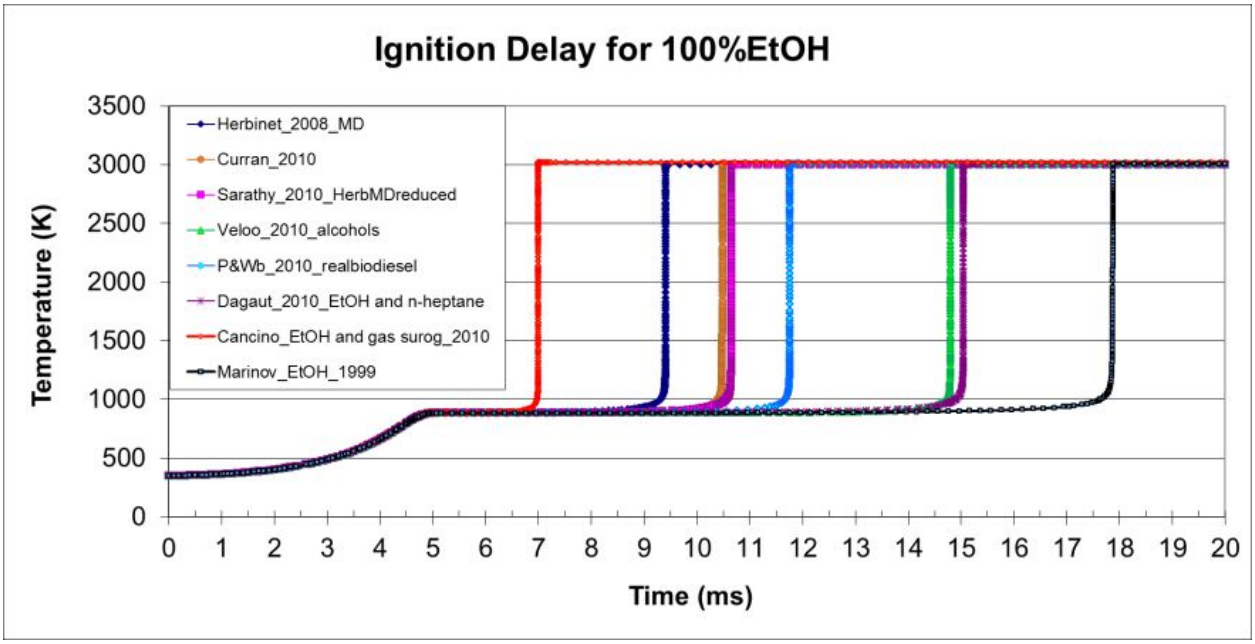


FIGURE B.1. Model RCM ignition delay times for 100% ethanol (stoichiometric) in air using the most current chemical mechanisms

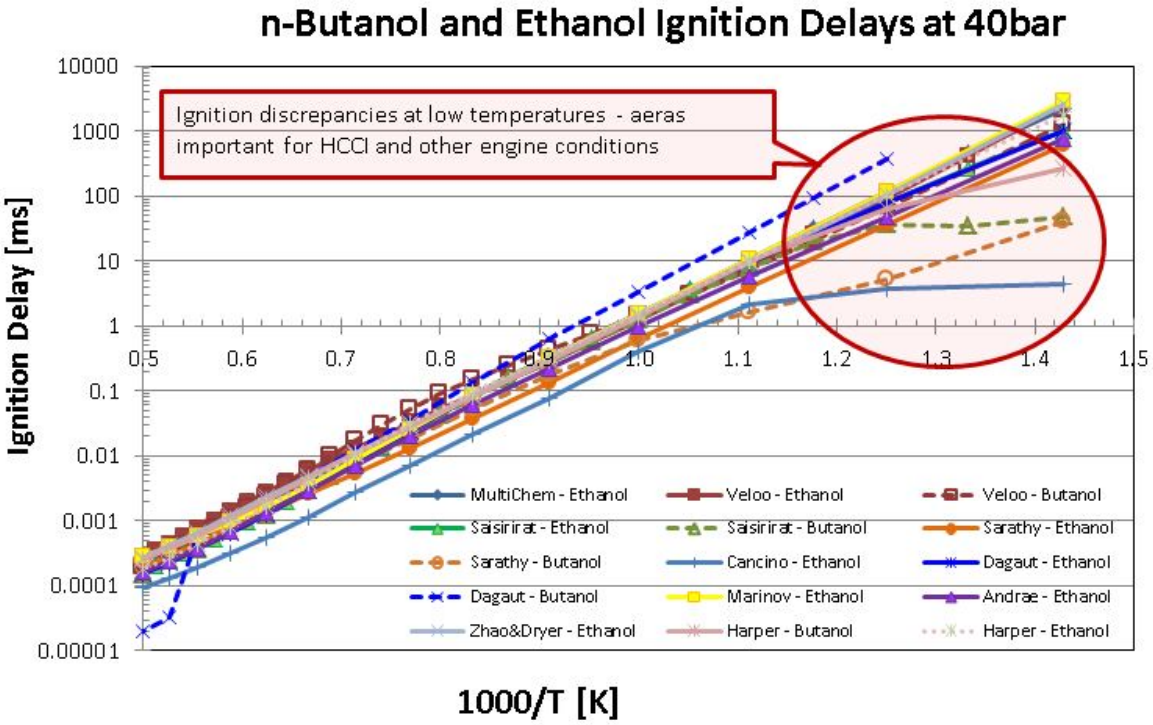


FIGURE B.2. Arrhenius plot for stoichiometric ethanol and n-butanol in air at 40 bar

combustion reactions will correlate exponentially with temperature. From a review of both kinetic theory (i.e. physical kinetics of the molecules) as well as experimental results, it is know that the reaction rate 'constant', K is dependent upon temperature via the following form:

$$K = A \cdot T^b \cdot exp\left(\frac{\text{-}\epsilon_A}{R_u \cdot T}\right) \tag{52}$$

where: A is the pre-exponential constant, b the temperature exponent, -ϵ_A the activation energy, and R_u the universal gas constant. If we rearrange Eq. 52 we get:

$$ln(K) = \frac{\text{-}\epsilon_A}{R_u} \cdot \frac{1}{T} + ln(A \cdot T^b) \tag{53}$$

Furthermore, the temperature exponent is often very small, such that there is a weak dependence upon K with respect to b. Taking advantage of this fact the $ln(A \cdot T^b)$ term often approximates a constant. If one next considers that the time rate of change of a given reaction is inversely proportional to the rate constant; i.e. a faster rate constant means the reaction occurs in a shorter period of time then the ignition delay (t_{ign}) is representative of the time it takes for a combustion reaction to occur. From this we can see that the ignition delay should be inversely proportional to the rate constant:

$$K \propto \frac{1}{t_{ign}} \tag{54}$$

plugging Eq. 54 into Eq. 53 above:

$$ln\left(\frac{1}{t_{ign}}\right) \propto \frac{\text{-}\epsilon_A}{R_u} \cdot \frac{1}{T} + ln(A \cdot T^b)$$

or alternatively

$$ln(t_{ign}) \propto \frac{\epsilon_A}{R_u} \cdot \frac{1}{T} + ln(A \cdot T^b) \tag{55}$$

Often $ln(A \cdot T^b)$ is approximated as a constant. Equation 55 is the relation seen in the $\log(t_{ign})$ vs. 1/T plot above.

Interestingly, all of mechanisms in Figure B.2 agree well at higher temperatures ($\sim$1000 K and above), but do differ quite a bit as the temperature decreases. This is likely due to experimental differences as the constants, A, b, and ϵ_A are determined experimentally. These differences continue to be a source of much research as better and better chemical kinetic mechanisms are being developed.

APPENDIX C

FIT Operating Conditions and Testing Procedure

Summary

(1) Power on both the FIT and Julabo cooling system.

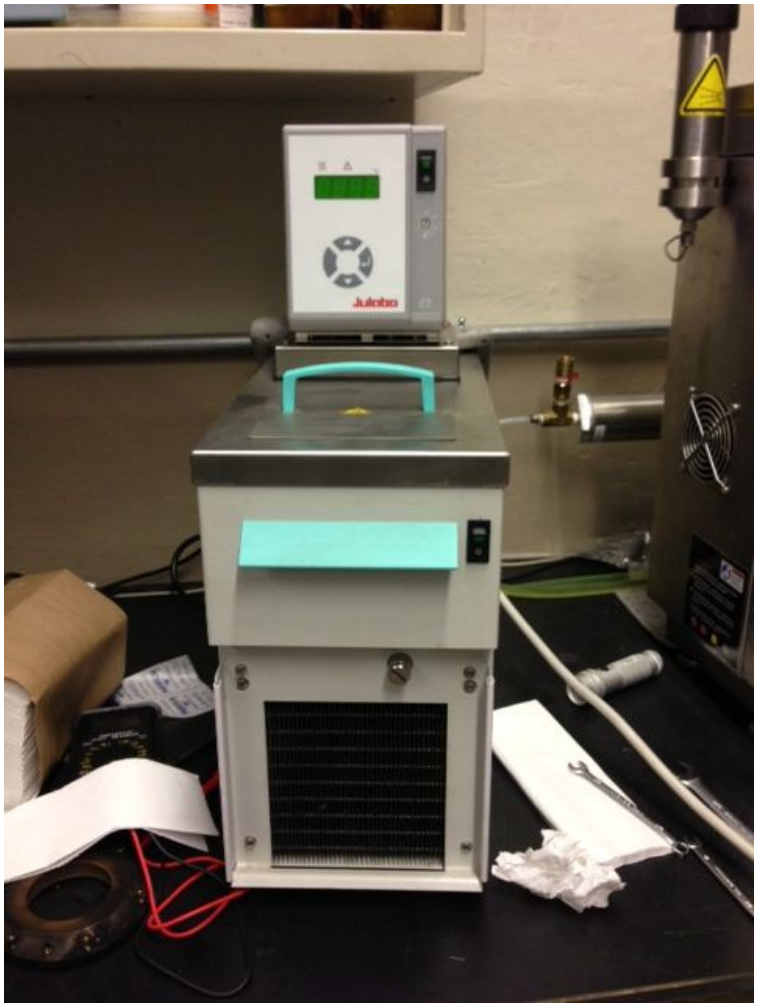


FIGURE C.1. Image of the Julabo cooling system running to the FIT to maintain temperature

(2) Set Julabo cooling system on and set system to $\sim$30 $^{\circ}C$

(3) Set the Process Air to 105 psi and the combustion air to 420 psi.

(4) Start FIT program. FIT takes approximately 1 hour to warm-up.



FIGURE C.2. Image of the process air system running to the FIT.



FIGURE C.3. Image of the process air system running to the FIT.

(5) Prep fuels during warm-up. You will need one 120 mL sample of off-road diesel and one 150 mL sample of whatever fuel will be tested. The diesel sample will be run at the beginning of every test day. The FIT takes approximately 100 mL to fill the fuel reservoir but only consumes about 5-10 mL per set of 27 injections. Note that you will need to know/measure/record the density for each fuel tested.

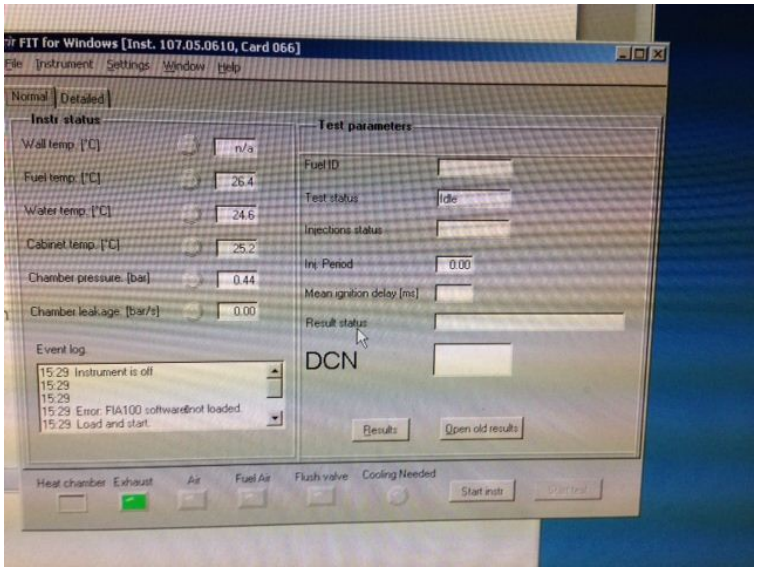


FIGURE C.4. Image of the process screen for the FIT.

(6) Once warm-up is completed, run one complete diesel test to flush the system. This will allow for optimal performance of FIT since the diesel will serve to lubricate the internals. Additionally, the diesel will give a daily check as to the performance of the FIT.

(7) After completion of the diesel run, wash FIT fuel collector thoroughly to ensure no cross contamination of fuels

(8) Begin fuel testing. Weigh sample before and after each run. Complete three runs and average the data. Repeat for as many fuel samples as needed.

(9) Compile all the data (i.e. max and min pressure, average temperature, and the time of maximum pressure rise rate). Finally, calculate ϕ value for each test.

(10) After testing is complete, initiate machine cool-down. Close process air and combustion air flows. Let coolant run through the system for approximately 20 minutes before completing shutdown by turning off the Julabo and FIT.

APPENDIX D

FIT Cleaning Procedure

The following procedure is a modified version of that sent from Compass-Instruments[146]. The procedure was modified to include additional photos and instructions that were omitted from the original from Compass-Instruments. This procedures should be completed when the FIT begins to exhibit erratic or atypical injection periods for standard fuels such as n-heptane or diesel. Prior to cleaning be sure the instrument is completely shutdown and cool to the touch (this will take at least 1 hr after shutting down the FIT).

Tools required:

(1) 5/16" allen wrench

(2) 7/16" open end wrench

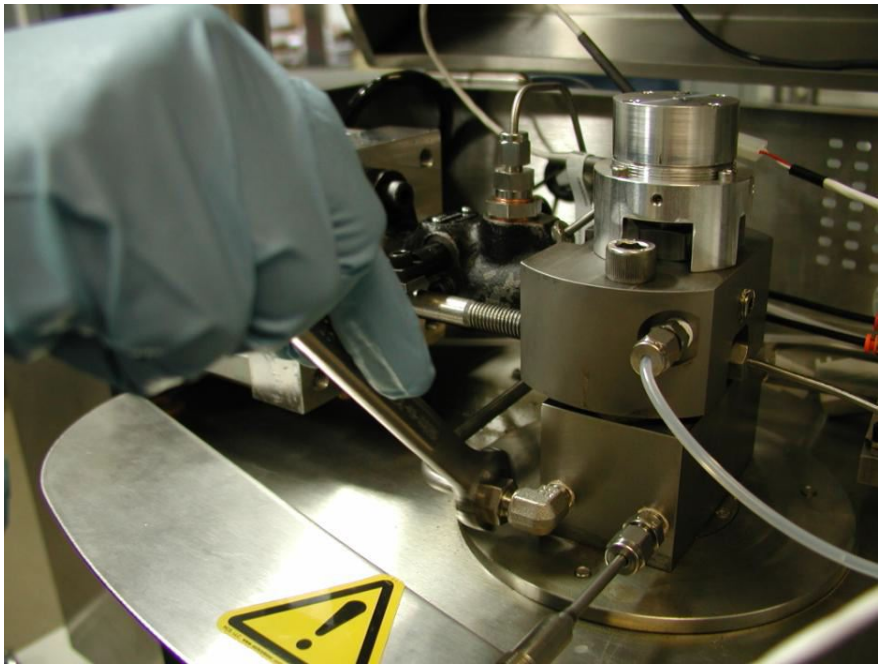
(3) 1/2" open end wrench

(4) 9/16" open end wrench

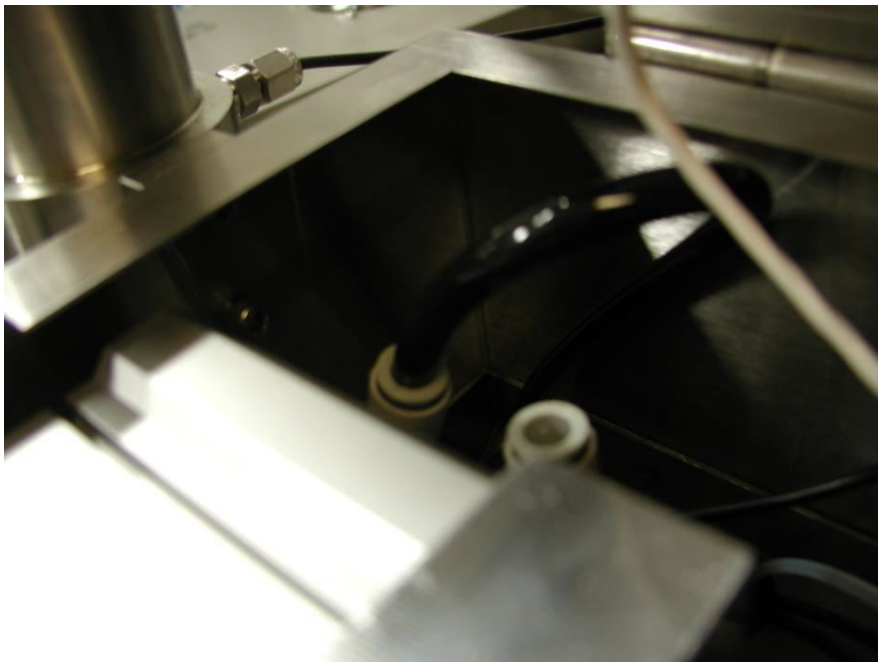
(5) 27mm open end wrench

Removal and Cleaning Procedure:

(1) Remove coolant lines from the coolant block surrounding the injector. Fitting is standard Swagelok. Removal of these fittings will prevent coolant from entering the combustion chamber when the injector is removed. Be careful in removing these lines since coolant will likely spill out. Ensure that the Julabo cooling tower is not above the height of the injector unit; if it is, then coolant will continue to drain from the Julabo.



(2) Disconnect the air line at the fuel pump actuator - the actuator is the square block at the left end of the injector assembly.

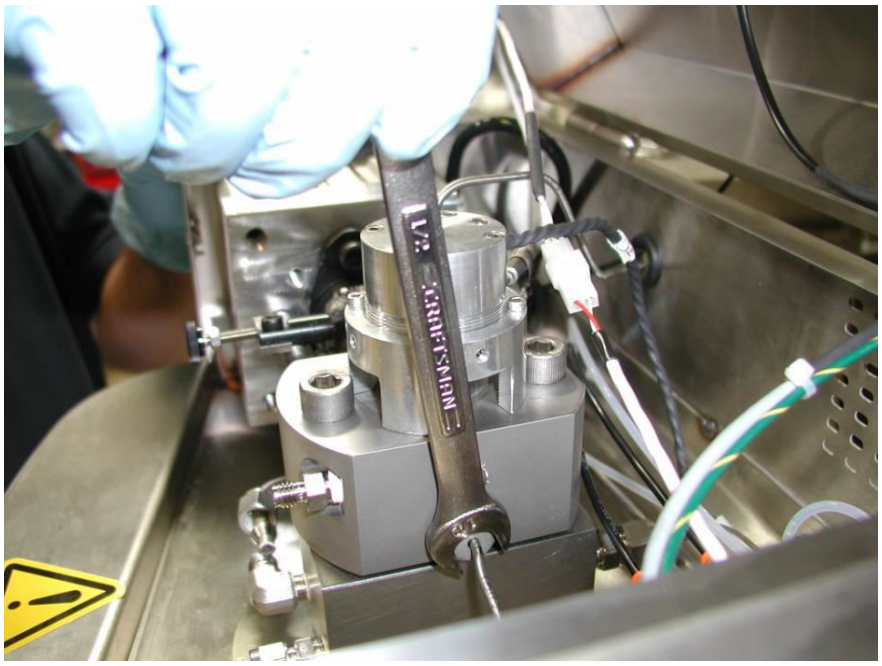


(3) Remove the fuel line from the top of the injection pump. This is just above the adjustment rack.

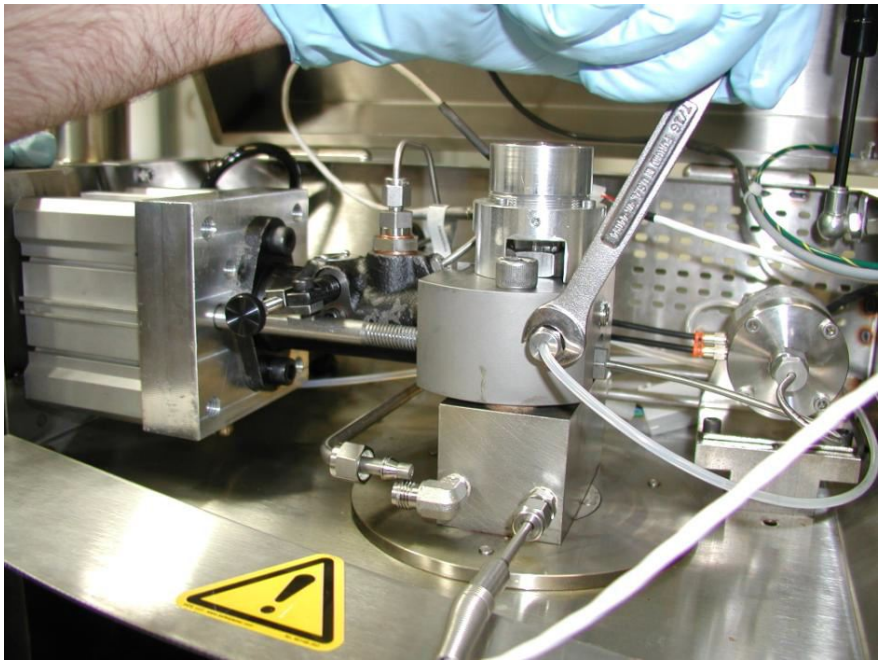


(4) Remove the nozzle sensor via the four long allen head bolts. The nozzle sensor does not need to be electrically disconnected, but will need to be installed in the same position as it was prior to removal to maintain the sensor alignment. DO NOT DO NOT DO NOT remove the large nut at the base of the sensor!! If you do you will have to send the injection unit in to get the sensor recalibrated.

(5) Remove the waste lines right side (small stainless steel tube) and the bypass line (tygon tube)at the front of the injection block and set aside.

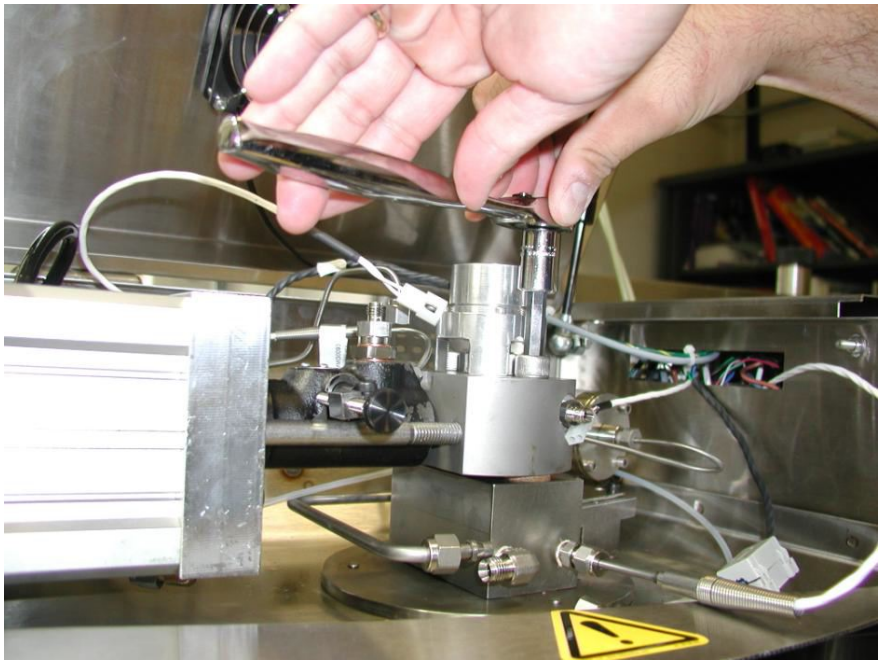






(6) (Optional) Disconnect terminals 15 and 16 on the top terminal strip of the circuit board. These are the fuel RTD leads.

(7) Remove the two large allen bolts holding the injection block to the top of the combustion chamber.

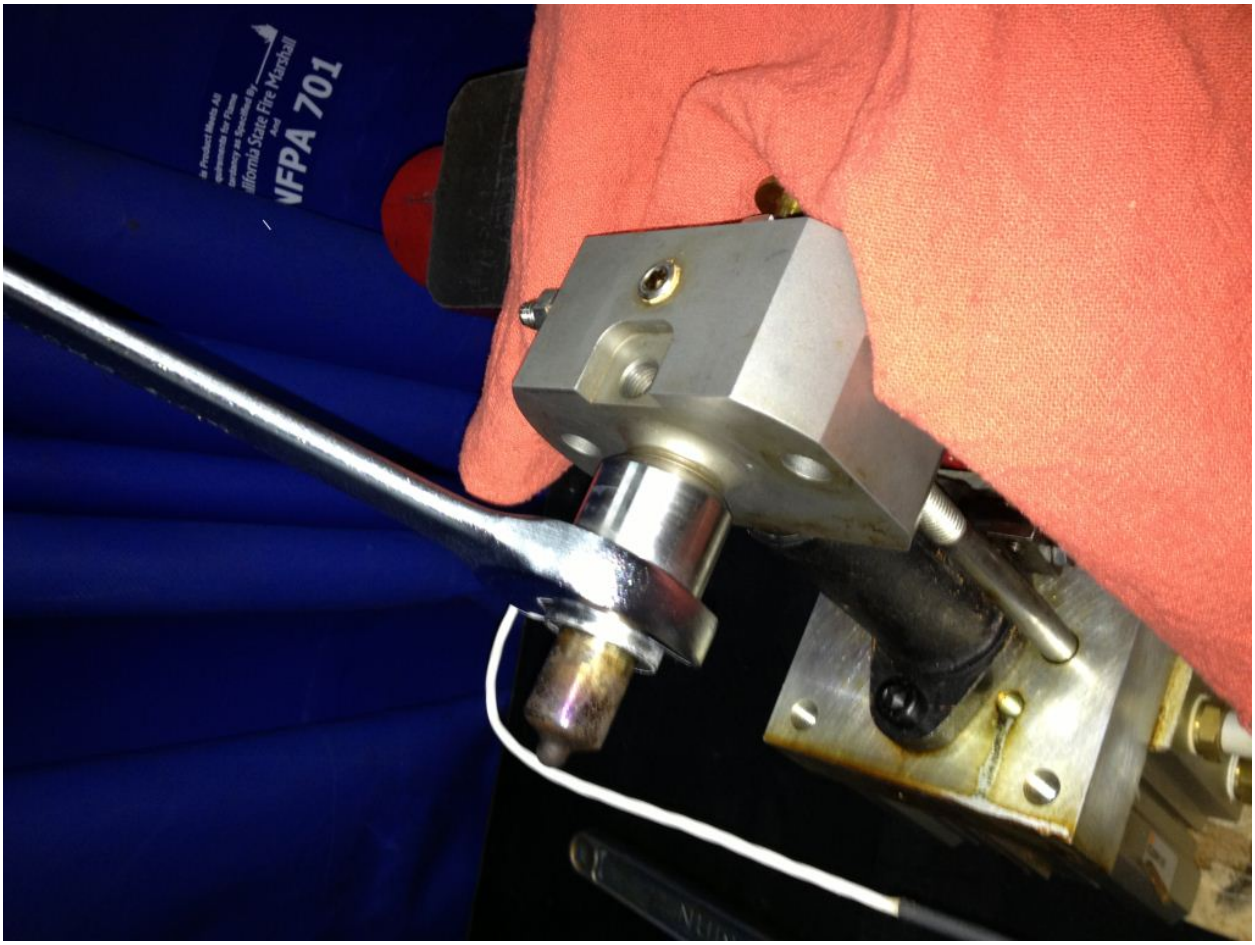


(8) Remove the WHOLE injection assembly by lifting and turning counter clock wise. The nozzle may stick a little so you can slightly rock the unit back and forth to dislodge the injector. Take care not to damage either the o-ring in the cooling block OR the copper washer at the top of the combustion chamber.



(9) With the injection assembly set aside, inspect the inside of the combustion chamber for signs of coolant or fuel pooled at the bottom. If any liquid is present, clean it out.

(10) With the injection unit actuator (large cube) in a vice, turn the nut at the base of the injector counter clockwise. Take care in removal as there are two locater pins and the inner pintle that may fall out of the injector.



(11) Inspect the nozzle for signs of wear. Note that as of the writing of this there is a small amount of pitting on the nozzle itself. Cleaning is best accomplished via soaking the nozzle and pintle in a de-greasing agent and $\geq$30 min in an ultrasonic bath. Be sure that the injector tip is clean and clear (you should just be able to see light when looking through the pin hole).







(12) Reassembly is the opposite of disassembly. Put a small amount of diesel on the pintle for lubrication. Tighten the nozzle nut to 42 lb-ft. Take care as over-tightening can damage the nozzle.

APPENDIX E

CSU HCCI Engine Valve Profiles

Table E.1: CSU HCCI Engine Valve Profiles

°ATDC	**intake valve lift [mm]**	**°ATDC**	**exhaust valve lift [mm]**
-369.5	0	0	0
-368	0.0254	140	0
-366.5	0.0508	146.5	0.0254
-362.5	0.127	148.5	0.254
-358.5	0.254	152.5	0.508
-356	0.381	156	0.635
-353.5	0.508	159	0.762
-351	0.635	162.5	1.016
-348.5	0.762	165.5	1.27
-347	0.889	168.5	1.524
-345	1.016	172.5	1.778
-343.5	1.143	176.5	2.159
-342	1.27	180.5	2.413
-340.5	1.397	183.5	2.667
-338.5	1.524	185.5	2.794
-337	1.651	188	2.921
-335.5	1.778	191	3.175

Continued on Next Page...

Table E.1 – Continued

°ATDC	intake valve lift [mm]	°ATDC	exhaust valve lift [mm]
-334	1.905	193.5	3.429
-333	2.032	195.5	3.556
-331	2.159	197	3.683
-330	2.286	199.5	3.81
-328.5	2.413	202.5	4.064
-327	2.54	204	4.191
-325.5	2.667	207.5	4.445
-323.5	2.794	210	4.572
-322.5	2.921	211	4.699
-321	3.048	213	4.826
-319.5	3.175	215.5	4.953
-318.5	3.302	218	5.08
-316.5	3.429	220	5.334
-315	3.556	223.5	5.461
-313.5	3.683	226.5	5.588
-312	3.81	228.5	5.715
-310	3.937	233	5.842
-308	4.064	237	5.969
-307.5	4.191	240.5	5.9944
-303.5	4.318	247	6.096

Continued on Next Page...

Table E.1 – Continued

°ATDC	**intake valve lift [mm]**	**°ATDC**	**exhaust valve lift [mm]**
-301.5	4.445	252.5	6.096
-300.5	4.572	261	5.969
-298.5	4.699	267	5.842
-296.5	4.826	268.5	5.715
-294.5	4.953	274.5	5.588
-292.5	5.08	277.5	5.334
-290.5	5.207	283.5	5.08
-288.5	5.334	287.5	4.826
-286.5	5.461	294	4.318
-283.5	5.588	298.5	4.064
-280.5	5.715	299	3.81
-276	5.842	302.5	3.556
-270	5.969	305.5	3.429
-264	5.9944	307.5	3.302
-259	5.969	310	3.048
-250	5.842	314	2.794
-247	5.715	317	2.54
-245	5.588	320	2.286
-243	5.461	323.5	2.032
-241	5.334	325	1.8288

Continued on Next Page...

Table E.1 – Continued

°ATDC	intake valve lift [mm]	°ATDC	exhaust valve lift [mm]
-238.5	5.207	327.5	1.5748
-235.5	5.08	332.5	1.397
-233.5	4.953	334.5	1.016
-231.5	4.826	339	0.762
-229.5	4.699	342	0.508
-227	4.572	346	0.254
-225	4.445	351	0.127
-223.5	4.318	356.5	0
-221.5	4.191	720	0
-220	4.064		
-218	3.937		
-217	3.81		
-215	3.683		
-214.5	3.556		
-214	3.429		
-213	3.302		
-211.5	3.175		
-210	3.048		
-209	2.921		
-207.5	2.794		

Continued on Next Page...

Table E.1 – Continued

°ATDC	intake valve lift [mm]	°ATDC	exhaust valve lift [mm]
-206	2.667		
-205	2.54		
-204.5	2.413		
-202.5	2.286		
-201	2.159		
-200	2.032		
-198	1.905		
-196.5	1.778		
-195	1.651		
-194	1.524		
-192	1.397		
-191	1.27		
-189	1.143		
-187.5	1.016		
-186	0.889		
-184.5	0.762		
-183	0.635		
-182	0.508		
-178	0.381		
-177	0.2032		

Continued on Next Page...

Table E.1 – Continued

°ATDC	**intake valve lift [mm]**	**°ATDC**	**exhaust valve lift [mm]**
-176	0.127		
-175	0.0508		
-172.5	0		
350.5	0		